Suspension Feeders as Biological Models to Develop Biomimetic Filter Modules and Reduce Microplastic Emissions

Dissertation

zur

Erlangung des Doktorgrades (Dr. rer. nat.)

der

Mathematisch-Naturwissenschaftlichen Fakultät

der

Rheinischen Friedrich-Wilhelms-Universität Bonn

vorgelegt von

M.Sc. Leandra Hamann

aus Bergisch Gladbach

Bonn, März 2023

Acknowledgements

Summary

With every wash cycle, microplastic fibres are released from textiles and enter the environment via the wastewater system. In order to develop an innovative washing machine filter, a biomimetic approach was employed. In biomimetics, biological working principles are analysed, abstracted models are created, and products and processes are developed that solve technical problems. The problem of microplastic release was studied for kitchen sponges by conducting a citizen science experiment. The results indicate that 58 - 355 t of microplastic particles are released annually from kitchen sponges into wastewater in Germany. The separation of microplastics from wastewater is a liquid-solid separation and the biological analogue to this was identified in suspension feeders. Suspension feeders are aquatic organisms that separate particles from the surrounding water for feeding. Within the framework of a literature study, 35 separation mechanisms were described on the basis of 18 biological and technical parameters and evaluated with regard to their biomimetic potential. Two filtration mechanisms were selected for more in-depth analysis: Mucus filtration and cross-flow filtration.

Mucus surfaces are formed by biofilms. Field and laboratory experiments showed that surfaces with biofilms absorb up to 12 times more microplastic particles than surfaces without biofilms. A biomimetic abstraction was not pursued due to the lack of technical materials that have the same particle-separating properties.

In cross-flow filtration, parallel flow is applied to the filter medium, preventing particle deposition and sebsequent clogging. In order to study this filtration mechanism, five ram-feeding fish species were selected. As ram-feeders swim forward, water flows into their mouths and food particles are retained by the gill arch system. Based on morphometric data, micro-CT scans, and behavioural experiments, three morphotypes were described that differ in terms of geometry, surface structuring, and materials. A modification of cross-flow filtration was identified as the underlying filtration mechanism, which is described for the first time as semi-cross-flow filtration. In further experiments, it was confirmed that the angle of attack of the filter medium to the fluid is decisive in semi cross-flow filtration in order to avoid the accumulation of particles. Subsequently, filter elements were created based on the conical geometry, the arrangement of the gill arches and the mesh size of the gill arch system. A filter housing generates a turbulent inflow and discharges the clean permeate and the particle-containing concentrate. Initial laboratory tests demonstrated a proof-of-concept of the biomimetic filter module that has an average filter efficiency of 97.3%.

Zusammenfassung

Mit jedem Waschgang werden Mikroplastikfasern aus Textilien freigesetzt, die über das Abwassersystem in die Umwelt gelangen. Um einen innovativen Waschmaschinenfilter zu entwickeln, wurde ein bionisches Vorgehen gewählt. In der Bionik werden biologische Funktionsprinzipien analysiert, abstrahierte Modelle erstellt und Produkte und Prozesse entwickelt, die technische Probleme lösen sollen. Zuerst wurde das Problem der Mikroplastikfreisetzung am Bespiel von Spülschwämmen im Rahmen eines Citizen-Science-Experiments untersucht. Die Ergebnisse zeigen, dass pro Jahr in Deutschland etwa 58 – 355 t an Mikroplastikpartikeln aus Spülschwämmen ins Abwasser freigesetzt werden. Die Abscheidung von Mikroplastik aus Abwasser ist eine flüssig-fest Trennung. Die biologische Analogie dazu wurde in Suspensionsfressern identifiziert. Suspensionsfresser sind aquatische Organismen, die Partikel zur Nahrungsaufnahme aus dem umgebenden Wasser trennen. Im Rahmen einer Literaturstudie wurden 35 Separationsmechanismen anhand von 18 biologischen und technischen Parametern beschrieben und hinsichtlich ihres bionischen Potentials bewertet. Zwei Filtrationsmechanismen wurden für eine tiefergehende Analyse ausgewählt: Schleimfiltration und Querstromfiltration. Schleimige Oberflächen werden durch Biofilm gebildet. In Feld- und Laborversuchen konnte gezeigt werden, dass Oberflächen mit Biofilm bis zu 12-mal mehr Mikroplastikpartikel aufnehmen als Oberflächen ohne Biofilm. Eine bionische Abstraktion wurde aufgrund von fehlender technischer Materialien, die über die gleichen partikelbindenden Eigenschaften verfügen, nicht weiterverfolgt. In der Querstromfiltration wird das Filtermedium parallel angeströmt, sodass Partikel nicht anlagern und zu Verstopfung führen können. Um diesen Filtrationsmechanismus zu untersuchen wurden fünf Fischarten ausgewählt, die als ‚ram-feeders' bezeichnet werden. Durch ihr Vorwärtsschwimmen wird Wasser ins Maul geströmt und Nahrungspartikel werden mit dem Kiemenreusensystem herausgefiltert. Basierend auf morphometrischen Daten, micro-CT Scans und Verhaltensversuchen wurden drei Morphotypen beschrieben, die sich hinsichtlich Geometrie, Oberflächenstrukturierung und Materialien unterscheiden. Als zugrunde liegender Filtrationsmechanismus wurde eine Abwandlung der Querstromfiltration identifiziert, die erstmals als Semi-Querstromfiltration beschrieben wird. In weiterführenden Versuchen bestätigte sich, dass der Ausrichtungswinkel des Filtermediums zum Fluid in der Semi-Querstromfiltration ausschlaggebend ist, um eine Anlagerung von Partikeln zu vermeiden. Anschließend wurden basierend auf der konischen Geometrie, der Anordnung der Kiemenbögen und der Maschenweite des Kiemenreusensystems Filterelemente erstellt. Ein Filtergehäuse erzeugt einen turbulenter Anstrom und leitet das saubere Permeat und das partikelenthaltende Konzentrat ab. In ersten Laborversuchen konnte ein Proof-of-Concept des bionischen Filters mit einer durchschnittlichen Filtereffizient von 97.3% gezeigt werden.

Contents

»Wir finden Partikelfresser in zwei Bezirken des Wassers: Als mobile, aktive Filtratoren durcheilen sie mehr oder weniger schnell das Wasser und gewinnen dabei jene Partikel (Pelagische Formen). Als sessile, aktive Filtratoren sitzen sie am Boden des Wassers fest und ernähren sich von den vorbeischwimmenden oder niederregnenden Kleinorganismen (Benthostiere).«

Jordan & Hirsch (1927), p. 25

Previous page:

Water colour drawings of suspension feeders (not to scale). Credits: Leandra Hamann 2021

1. General Introduction

1.1.   Microplastics in the Environment

Plastic particles and fibres smaller than 5 mm, so-called microplastics (MPs) (Hartmann *et al.*, 2019), are found in every environmental compartment: Soil (de Souza Machado *et al.*, 2018), air (Evangeliou *et al.*, 2020), and aquatic environments, such as beaches (Figure 1), Artic sea ice (Peeken *et al.*, 2018), deep-sea sediments (Zhang *et al.*, 2020), coral reefs (Huang *et al.*, 2021), or freshwater (Triebskorn *et al.*, 2019). MPs were found on beaches and in biological samples that date back to the 70s (Carpenter *et al.*, 1972; Gregory, 1977). In 2021, 1288 marine species were reported to ingest micro- and macroplastics (Santos, Machovsky-Capuska, & Andrades, 2021). Marine invertebrates ingested MPs (Wright, Thompson, & Galloway, 2013) and passed it on to higher trophic levels (Farrell & Nelson, 2013) so it was even found in the top predators in the marine food web (Nelms *et al.*, 2018, 2019). PET particles ingested as larvae were still present in the adults of *Chironomus riparius*, proving carry-along contamination through different life stages and an aquatic-terrestrial transfer (Setyorini *et al.*, 2021). MPs were identified in vascular plants (Yin *et al.*, 2021), changed the fungal pathogen abundance in terrestrial ecosystems (Gkoutselis *et al.*, 2021), and were retained by spiderwebs in urban areas (Goßmann, Süßmuth, & Scholz-Böttcher, 2022). Laboratory exposure tests showed that ingested MPs can decrease the feeding rate, survival rate, body length, oxidative stress, and reproduction (for example, GESAMP, 2016; Anbumani & Kakkar, 2018; de Sá *et al.*, 2018).

Humans were estimated to ingest around 5 g of MPs per week (Senathirajah *et al.*, 2021) that end up in the faeces (Yan *et al.*, 2021), the placenta (Ragusa *et al.*, 2021), or the blood (Leslie *et al.*, 2022). Exposure comes through inhalation, dermal contact, or ingestion (Prata *et al.*, 2020). MPs were found in several beverages and food products, such as tab and bottled water, the consumption of which leads to an estimated annual uptake of 4000 and 90000 particles, respectively (Cox *et al.*, 2019). Exposure to humans was higher through meals exposed to dust fallout than by consuming mussels contaminated with MPs (Catarino *et al.*, 2018). High concentrations of MPs in the air led to airway and interstitial inflammatory responses in workers in the synthetic textile and flock industry (Prata, 2018; Gasperi *et al.*, 2018). Especially particles larger than 5 µm are more likely to migrate to organs (Gruber *et al.*, 2022), a size range that has not been examined in field studies so far, as sampling and identification methods typically are limited to sizes larger than 10 µm (Zheng *et al.*, 2021; Rolf *et al.*, 2022). In the future, methods are still to be developed to understand the effects of MPs on organ, cellular, and protein level (Gruber *et al.*, 2022).

Figure 1: Macroplastics and microplastics collected on beaches at the French Atlantic coast: 1) Microplatic fragments, 2) plastic bottle, 3) parts of fishing gear, 4) balloon, 5) plastic foil (maybe from packaging), 6) bottle cap, 7) drinking straw, 8) plastic pieces of undefined sources. Credits: Leandra Hamann 2018

It is commonly agreed that a diverse combination of mitigation strategies is needed to reduce the release and effects of micro- and macroplastics in the environment (Rochman *et al.*, 2019; Santos *et al.*, 2021). Some measures have already been implemented, such as the legislation to ban MPs in cosmetics, policy framework directives, or involvement of stakeholders (Auta, Emenike, & Fauziah, 2017; Lam *et al.*, 2018; Anbumani & Kakkar, 2018; Clausen *et al.*, 2020). Other measures are long-term goals, such as the shift to a circular economy, the development of new materials and sustainable product design, and educational work to change the mindset in society (Steensgaard *et al.*, 2017; Turrell, 2020; Santos *et al.*, 2021; Munhoz *et al.*, 2022). Filtration mechanisms provide a short-term means to reduce MPs at their sources and entry paths (Rochman *et al.*, 2019; Zhang *et al.*, 2021).

While the source for macroplastics is often apparent (Figure 1), it is challenging to identify the sources of MPs based on environmental samples. This is because MPs emissions can originate from a variety of point or diffuse sources. Point sources include sources where the location, e.g., plastic recycling plants (Kallenbach *et al.*, 2022), or product type, e.g., cosmetics (Bashir *et al.*, 2021), is known. Diffuse sources refer to MPs of which the source is unknown, e.g., the presence of MPs in soil that might originate from urban dust or tyre and road wear particles (Campanale *et al.*, 2022). When MPs loss into the sewage system can be reduced

by waste water treatment plants. Wastewater treatment plants equipped with secondary and tertiary treatment stages retain 84% to 94% of MPs (Iyare, Ouki, & Bond, 2020). However, retained MPs accumulate in the sewage sludge is introduced into the environment when disposed of on agricultural fields (Corradini *et al.*, 2019; Iyare *et al.*, 2020). One of the major sources of MPs in sewage sludge is fibres released from washing machines with 63%-90% (Iyare *et al.*, 2020). Plastic fibres in clothing account for around 6% of the global use of polymers, which equaled around 28 million tonnes in 2022 (OECD, 2022). The amount of released MPs fibres from textiles in washing machines ranges between 10 and 120 g per person per year (Sherrington *et al.*, 2016; Boucher & Friot, 2017; Bertling, Bertling, & Hamann, 2018; Zhang *et al.*, 2021) and ranks as the 10th largest MPs source in Germany (Bertling *et al.*, 2018). On a global level, this equates to 320,000 to 960,000 tonnes per year (current world population: 8 billion). Washing machines have coarse filters to protect the pump by retaining stones or coins (Masselter *et al.*, 2022). In order to mitigate MPs emission into the environment, scientists and engineers are developing filters that separate MPs fibres from the effluent and meet the requirements to fit into washing machines (personal information and for example, Schöpel & Stamminger, 2019). These designs often apply established separation technologies, such as bag filters, hydrocyclones, or depth filters, and adapt them to washing machines. However, up to date, no market-ready, one-fits-all solution is available. Therefore, an innovative filter will be designed for washing machines to retain microplastic fibres from textiles and reduce MPs in wastewater treatment plants and the environment.

1.2.   Nature as Inspiration for Innovative Filters

In order to develop a filter that is designed outside conventional engineered solutions and optimised to retain MPs fibres in washing machines, a biomimetic approach was chosen. In biomimetics, functional principles and strategies in biological systems are identified, abstracted into models, and applied to technical product and processes to generate novel ideas or improve present technologies (Vincent *et al.*, 2006; Fayemi *et al.*, 2017; Wanieck *et al.*, 2022). Working processes in biomimetics are categorized as either problem-driven and solution based. The problem-driven process starts with a technical problem, to which biological solutions are found, abstracted and transferred. The solution-based process starts with the knowledge of a biological principle, which has the potential to be transferred and applied to technology when a suitable application is identified (Fayemi et al., 2017). Microplastic separation in washing machines classifies as a technical solid-liquid filtration process (Sutherland, 2005) and is the initial starting point for the problem-driven working process. According to Fayemi et al. (2017), it consists of the following steps: (1) the problem analysis, (2) abstraction of the technical problem, (3) transposition to biology, (4) identification of biological models, (5) selection of biological models of interest, (6) the abstraction of biological

strategies, (7) the transposition to technology, and (8) the implementation and the testing in the initial context (Figure 2).
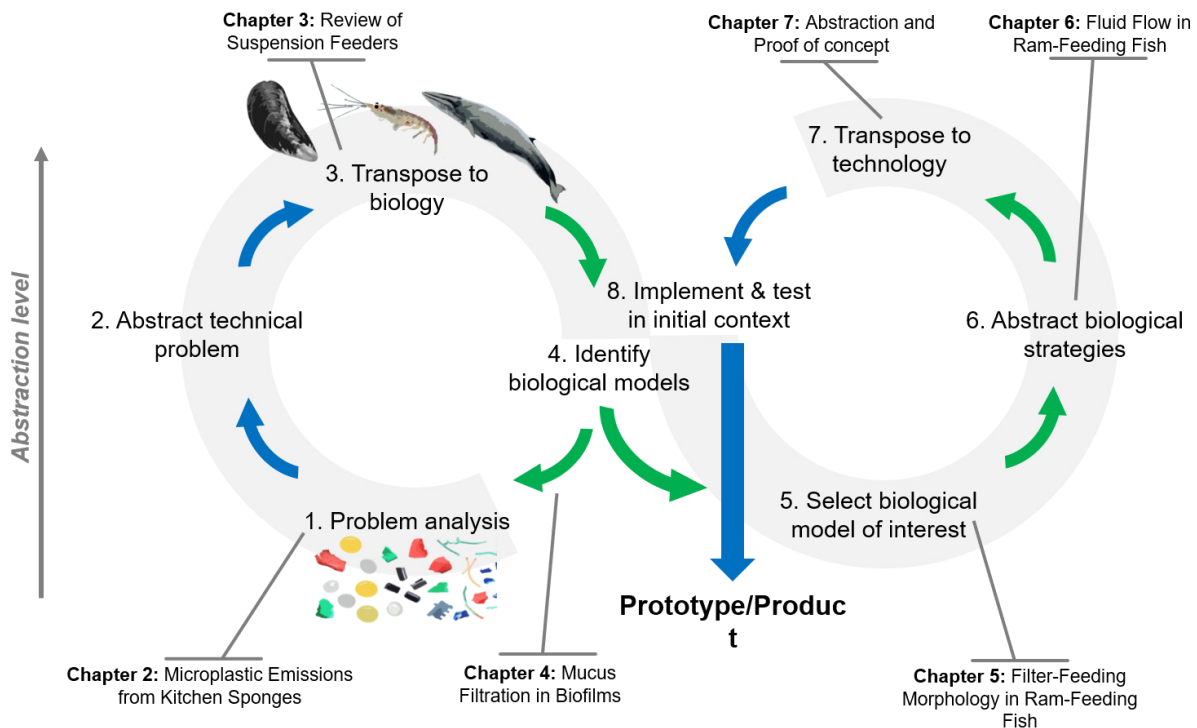
Figure 2: Biomimetic working process according to Fayemi et al. (2017) with eight steps from problem analysis to the implementation in the initial context. The corresponding chapters of this thesis are indicated along the steps.

In this thesis, I follow the steps of the problem driven process in order to design a biomimetic filter module (Figure 2). First, the problem of MPs release from anthropogenic sources is described and demonstrated by the example of kitchen sponges (Chapter 2). Afterwards, solid-liquid separation is identified in suspension feeders, which function as biological models. Suspension feeders (SFs) are organisms that separate food particles from the ambient water for nutrition (Jørgensen, 1966; Hentschel & Shimeta, 2008). A high diversity of suspension-feeding mechanisms (SFMs) has evolved by feeding on the highly heterogeneous seston. Also, it has been identified that this feeding type retains MPs (Germanov et al., 2018), proving their ability to retain MPs in principle. Therefore, these SFMs are reviewed and evaluated for their biomimetic potential (Chapter 3). Based on the results, two SFMs are selected for further analysis: mucus filtration using biofilms as a 'model organism' (Chapter 4) and cross-flow filtration of ram-feeding fishes based on their morphology (Chapter 5). As cross-flow filtration in ram-feeding fish shows promising results regarding transferability for the retention of MPs fibre from washing machine effluents, the fluid dynamics within the SFMs are studied to identify structure-function patterns and develop a deeper understanding of the filtration principles (Chapter 6). Finally, a selection of traits is abstracted into models that are manufactured and tested regarding their filtration performance under laboratory conditions (Chapter 7).

2. Microplastic Emissions from Kitchen Sponges

This chapter presents unpublished data.

Contributions:

Leandra Hamann: conceptualisation, formal analysis, investigation, methodology, visualisation, writing

Previous page:

Microplastics at a beach in Hossegor, France. Credits: Leandra Hamann 2019

2.1.   Introduction

Microplastics (MPs) are released during the extraction, production, usage, or end-of-life stage and reach the air, soil and water through different pathways (Maga *et al.*, 2021). In order to prioritise, develop, and implement general or product-based measurements to reduce MPs in the environment, it is necessary to gain reliable data on release and emission estimates (Hann *et al.*, 2018; Maga *et al.*, 2022). Several studies and regional reports have identified MPs point sources and pathways to quantify the released amounts based on a generic approach on a national (van Wezel, Caris, & Kools, 2016; Bertling *et al.*, 2018), regional (Hann *et al.*, 2018), or global level (GESAMP, 2016; Boucher & Friot, 2017). In a report by the Fraunhofer Institute of Environmental, Safety and Energy Technology UMSICHT in 2018, the authors identified and quantified 51 MPs sources that add up to around 4000 g/cap*a for Germany (Bertling *et al.*, 2018). The top ten of these quantified sources account for approximately 65% of the total released MPs, such as tyre wear abrasion, releases during waste management, pellet losses, losses from artificial turfs, or abrasion of MPs fibres from textiles, leaving 41 of minor sources for the remaining 35%. According to a recently published report by the Organisation for Economic Co-operation and Development that focused on these major sources, MPs releases will only be reduced by 9% by 2060 (OECD, 2022). Therefore, it is important to identify and quantify minor MPs sources to implement reduction measures.

In order to quantify MPs releases, data quality is of high importance. In most cases, quantifications are based on available stock data, models, and mass balances to calculate the range of MPs releases and emissions depending on different scenarios. For example, the data on MPs release from personal care products is based on the estimate that 10% of the ingredients are plastics multiplied by the production amounts and the population in a specific region (Essel *et al.*, 2015). These estimates often rely on public data and assumptions to fill in the missing information. By multiplying all these factors, the propagation of uncertainty increases, and the estimation accuracy will decrease (van Wezel *et al.*, 2016). A data quality assessment of MPs quantifications by the EU (Hann *et al.*, 2018) includes a scoring system with the following criteria: reliability (1 = verified based on measurements, 5 = non-qualified estimate), completeness (1 = representative data, 5 = representativeness unknown), temporal (1 = <3 years old, 5 = age unknown), and geography (1 = EU level data, 5 = unknown or very different geography). Applying this quality assessment, most published quantification of MPs releases achieve a medium data quality (Hann *et al.*, 2018).

I selected kitchen sponges as an example to quantify MPs emissions. A citizen science approach was chosen to ensure realistic handling and abrasion of the sponges and gain further information about usage routines through a survey because no experimental data on MPs release from kitchen sponges are available so far.

2.2. Materials and Methods

2.2.1. Determination of MPs Emissions using Citizen Science

Two different kitchen sponges were selected: a conventional and an alternative organic sponge. The conventional kitchen sponge has three layers: a cloth side (80% Viscose, 20% Polypropylene), foam in the middle (100% Polyurethane), and a scrubbing side (51% quartz, 24% resin, 17% Polyamide, 7% Polyester, 1% silicon carbide). It is one of the most common sponges found in German supermarkets and is the best-rated product on Amazon under the German term "Küchenschwamm" (engl. kitchen sponge). The organic kitchen sponge has two layers: a foam layer (100% Cellulose) and a scrubbing layer (60% sisal, 40% recycled Polyethylene terephthalate (PET)) (Figure 3A). Thirty sponges of each type were rinsed with clean tap water und dried for 24 hours in a heating cabinet (Binder GmbH) at 42°C for 24 h. Afterwards, they were numbered, weighted and handed out randomly to participants between March and May 2021. Each participant received a short survey regarding the daily usage of the sponge (see Supplement Information 10.1.1 Kitchen Sponge Survey). After the sponges were returned, each one was rinsed again with clean tap water, dried for 24 hours in a heating cabinet at 42°C for 24 h, and weighted again. The experiment was repeated in 2022 with again 30 sponges of the two types but other participants.

2.2.1. Statistics and Upscaling

The data is used to calculate the material loss of each sponge. For this study, we understand MPs releases as the material loss that arises from the source, i.e., at the start of the MPs pathway into the environment. The released MPs that reach the environment are termed as emission. A similar distinction was made by Maga *et al.* (2021). MPs release was calculated based on the material loss multiplied by the share of plastic used in each sponge layer, as 59.3% for the conventional sponge and 15.9% for the organic sponge (N = 3 each). Afterwards, the results were extrapolated to the MPs release per person and year (g/cap*a) to draw comparisons to other MPs sources. Furthermore, we used the mean of the data to extrapolate the total MPs releases from kitchen sponges for Germany (population: 84.3 million, Federal Statistical Office, January 2023), the European Union (EU population: 447.7 million, Eurostat, January 2020), and a global scale (population: 8 billion, United Nations, November 2022). Finally, we calculate annual MPs emissions for Germany by including a retention rate of 90% through waste water treatments (Iyare *et al.*, 2020).

The data was analysed and visualised using the R programming environment (R Core Team, R version 4.2.2, 2022). The data structure was visually checked for normality and heteroscedasticity (Zuur, Ieno, & Elphick, 2010). A two-sample t-test was used to identify significant differences between the sponge types. Linear models were used to test if the total days of usage significantly predicted the relative MPs release and the relative MPs release per day. Results are reported as mean with standard deviation. Finally, the results are compared to estimates of MPs releases and emissions from cosmetics based on estimates in the literature.

2.3.   Unpublished Results

By the end of the experiment, 31 plastic and 38 organic sponges were returned, which equals a return quote of 51.67% and 63.3%, respectively. Because of some incomplete surveys, 28 plastic and 32 organic sponges were used in further analysis (Table 1). Regarding persons per household (two-sampled t-test, p = 0.6445) and the number of households that used the sponge for rinsing with detergents, there were no significant differences between the groups using the two sponge types. A difference was found in the share of households that have a dishwasher. While 87.5% of the households testing an organic sponge had a dishwasher, only 67.9% of the households testing the plastic sponges had a dishwasher (Table 1). However, this had no significant effect on the average usage time per day, which was 8.21 ± 4.13 min/day for the plastic sponge and 11.25 ± 8.52 min/day for the organic sponge (two-sided t-test, p = 0.0915), or total days of usage (two-sampled t-test, p = 0.09474), even though the organic sponges were used on average 20 days longer than the conventional sponge.

One of the conventional sponges and five of the organic sponges gained weight after the end of usage by the participants. I assume these sponges have retained food wastes, oils, or other substances washed off the dishes during scrubbing and rinsing, and therefore removed them from the final analysis. On average, the conventional sponges lost 0.033 ± 0.016 g/day (N = 27) of material, significantly more than the organic sponges with 0.022 ± 0.019 g/day (N = 27, two-sampled t-test, p = 0.03399). When considering the plastic share in the sponges, this results in MPs releases of 0.019 ± 0.01 g/day for the conventional sponges and 0.004 ± 0.003 g/day for the organic sponges, and an annual MPs release of 4.212 ± 3.039 g/cap*a and 0.689 ± 0.576 g/cap*a, respectively, which is significant (two-sampled t-test, p = 2.583e-07, Figure 3B). The days in use do not correlate significantly with the relative MPs release after usage in the conventional sponge (p = 0.05193, Adjusted R^2 = 0.1086) or the organic sponge (p = 0.611, Adjusted R^2 = -0.02908, Figure 3C). There is a significant correlation between days in use and the relative MPs release per day for both sponge types (conventional sponge: p = 0.0022, Adjusted R^2 = 0.2904; organic sponge: p = 0.00238, Adjusted R^2 = 0.2863; Figure 3D).

However, homogeneity of variance was not given in the data and the R-squared value is low in all four linear models, with $R^2 < 0.3$.

Table 1: Overview of survey and weight results regarding the two sponge types, plastic and organic.

	Conventional	Organic
Number of participants with completed surveys	28	32
Persons per household	1.96 ± 0.79	2.06 ± 0.84
Household with dishwasher	19 (67.9 %)	28 (87.5%)
Usage "rinse"	28	30
Used with detergents	26	31
Average usage time (min/day)	8.21 ± 4.13	11.25 ± 8.52
Days of usage	43.71 ± 28.10	63.81 ± 81
Number of sponges that gained in weight	1	5
Weight loss per day [g/day]	0.033 ± 0.016	0.022 ± 0.019
MPs release per day [g/day]	0.019 ± 0.01	0.004 ± 0.003
MPs release per person and year [g/cap*a]	4.212 ± 3.039	0.689 ± 0.576
Total MPs releases in Germany [t/a]	355.1	58.05
Total MPs releases in EU [t/a]	1,885.85	308.29
Global total MPs releases [t/a]	33,698.51	5,508.95
Total MPs emissions in Germany [t/a]	319.59	52.25

The total MPs release for Germany is around 355 t/year if everyone uses conventional sponges and 58 t/a if everyone uses organic sponges (Table 1). This would increase to 1,886 t/a and 308 t/a for the EU and to 33,698 t/a and 5,508 globally. MPs from kitchen sponges are likely released into the sewage system, where wastewater treatment plants retain around 90% of MPs (Iyare *et al.*, 2020). Hence, the environmental emission would decrease to 319 t/a for the conventional sponge and 52 t/a for the organic sponges (Table 1). Estimates for MPs release from cosmetics vary between 2.4 g/cap*a and 11 g/cap*a depending on region, year, and method (Figure 3E). Only one estimate of MPs release from kitchen sponge was reported from Denmark with 8.57 g/cap*a (Lassen *et al.*, 2015).
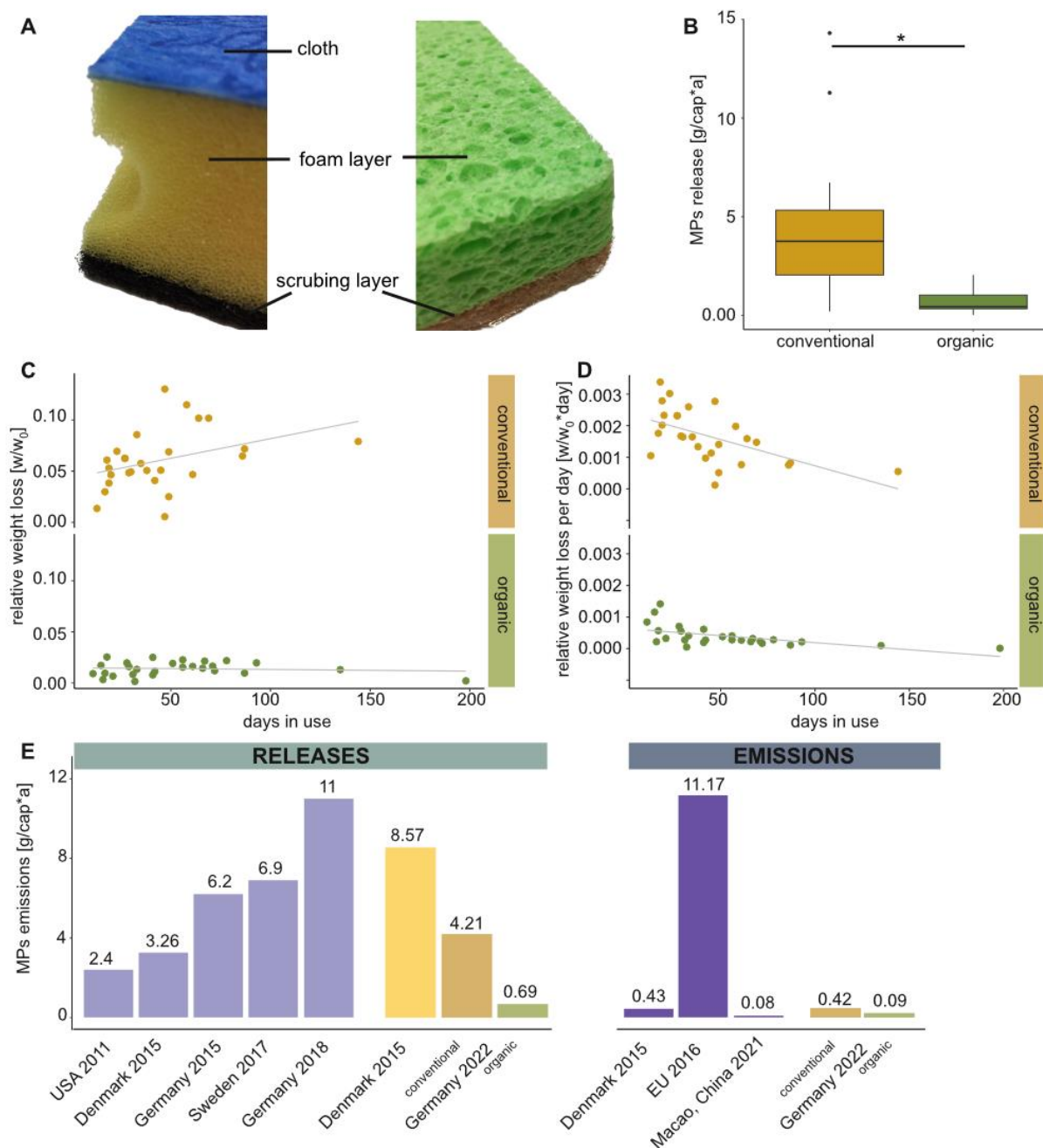
Figure 3: Results of the citizen science experiments in 2021 and 2022. A) Picture of the two sponge types and their different material layers. B) Comparison in weight loss of the two sponge types (two-sided t-test, N= 27 for each sponge type, p = 0.03399). C) Relative MPs release over days in use for the conventional (p = 0.05193, Adjusted R^2 = 0.1086) and the organic sponge (p = 0.611, Adjusted R^2 = -0.02908). D) Relative MPs release per day over days in use for the conventional (p = 0.0022, Adjusted R^2 = 0.2904) and organic sponge (p = 0.00238, Adjusted R^2 = 0.2863). E) Estimated MPs releases and emissions per head and year of cosmetics (purple) for the regions of the USA (Gouin *et al.*, 2011), Denmark (Lassen *et al.*, 2015), Germany (Essel *et al.*, 2015), Sweden (Magnusson *et al.*, 2016), EU (Sherrington *et al.*, 2016), Germany (Bertling *et al.*, 2018), Macao, China (Bashir *et al.*, 2021) at different years compared to available estimates of MPs emissions from kitchen sponges(yellow = conventional, green = organic) from literature and this study.

2.4.   Discussion

Kitchen sponges made from plastic polymers release MPs during daily use. Plastic content and material type play a significant role in material loss. The conventional sponge releases more MPs than the organic sponge, even though they were used on average 20 days longer than the conventional sponge. However, the high variance in the data limits statistical analysis and data quality. Even though the sponges were handed out to the participants randomly, the difference in the number of households equipped with a dishwasher might affect the usage time and, thus, the overall weight loss. Additionally, some sponges have gained weight during the experiment, which probably comes through the retention of food wastes, which strongly depends on individual use and cleaning behaviour. This process likely affects all sponges and leads to the conclusion that the actual material weight loss is higher than I have measured. Therefore, a set of laboratory experiments is required to measure weight loss under standardized conditions and complement the results from the citizen science project. There might also be a non-linear behaviour of material loss over days in use. I assume increased MPs release in the first days and less after several days of usage. Therefore, weight loss should be measured at regular intervals in future laboratory experiments.

MPs from kitchen sponges are likely to enter wastewater initially and, in Germany, a wastewater treatment plant. However, even if these retain 90% of MPs, 10% will still end up in freshwater systems as emissions and distributed to other environmental compartments (Iyare et al., 2020). MPs with a density >1 g/cm³ will sink and become part of the sediments, while MPs with a density <1 g/cm³ will float. Therefore, Polyurethane and Polyamide released from the conventional sponge and the recycled Polyethylene terephthalate (PET) from the organic sponges will be redistributed from freshwater environments to river sediments with an 89% chance and marine sediments with an 11% chance (Maga et al., 2022). Because of their low densities, Polypropylene and Polyester released into freshwater environments from the conventional sponges will float and be transported to marine waters. For fossil-based plastics, the degradation rates vary strongly with 0.001 up to 100 μm/a for the specific surface, which is influenced by polymer type, particle size, residence time in the environmental compartment, and degradation processes (Maga et al., 2022). Based on an average surface degradation rate of 1 μm/a and an initial particle size of 500 μm, MPs from kitchen sponges will persist for at least 250 years and might lead to various ecological effects now and in the future.

Despite unknown factors in the citizen science experiment, the calculated MPs releases are in a similar size range compared to the estimated data from Denmark and based on the EU data quality assessment of MPs quantifications (Hann et al., 2018), the present study's data can be evaluated as the second-best category with "likely to be good data quality". In order to increase the data quality, the number of distributed sponges should be increased, include more sponge

types or dish cleaning products, and represent a larger region, either within Germany or even the EU.

My data shows that kitchen sponges account for around 0.1% of the total estimated amount of MPs releases in Germany (Bertling *et al.*, 2018). Nonetheless, all MPs emissions in the environments should be reduced or completely avoided. A ban on kitchen sponges in general is unrealistic, as kitchen sponges are the second preferred method to clean dirty dishes, after dishwashers in Europe (Møretrø *et al.*, 2021). Therefore, I suggest a ban on plastic polymers in kitchen sponges. The organic sponge tested in this study proves that natural materials can replace plastic ingredients and still be used as long or even longer as the conventional sponge. Even though materials are still lost during dishwashing, they will have less effect on the environment and degrade faster. Similar to this study, more MPs sources should be quantified to identify suitable measures and reduce global MPs emissions.

3. Review of Suspension Feeders

This chapter is a summary of Manuscript I (Appendix, p. 121):

- Hamann, Leandra; Blanke, Alexander (2022) Suspension feeders: diversity, principles of particle separation and biomimetic potential, *J. R. Soc. Interface.*19202107412021074, https://doi.org/10.1098/rsif.2021.0741

Author Contributions:

Leandra Hamann: conceptualisation, formal analysis, investigation, methodology, visualisation, writing: original draft

Alexander Blanke: conceptualisation, funding acquisition, supervision, writing: original draft, writing: review and editing.

Previous page: Journal cover image of the Royal Society Interface, February 2022

The filaments of the gill crown in sabellid polychaetes are one of many particle capture mechanisms in the diversity of suspension feeders. Credit: Jens Hamann.

3.1.   Introduction and Review Approach

Suspension feeders (SFs) are defined as »[…] aquatic animals that have evolved special structures to process the surrounding water and to retain small suspended particles, […]« (Jørgensen, 1983, p. 89). These special structures are the focus for the biomimetic approach chosen in this thesis. For this purpose, suspension feeding mechanisms (SFMs) define all steps that enable the separation of particles from the first encounter to the ingestion into the oesophagus. The high diversity of SFMs in freshwater and marine habitats probably resulted from niche partitioning by adaption to specific particle sizes and types of seston, which mainly consists of plankton and detritus (Coma *et al.*, 2001; Wing & Jack, 2012; Sebens, Sarà, & Nishizaki, 2017). Already in the late Tonian Period, 1000-700 million years ago, the feeding activity of SFs mixed sediments, influenced particle fluxes, and moved high volumes of water, leading to deeper light penetration, changes in oxygen levels, and the distribution of dissolved organic carbon, forming the environment we know today (Ausich & Bottjer, 1991; Lenton *et al.*, 2014; Hölker *et al.*, 2015; Dohrmann & Wörheide, 2017).

Single SFs have been analysed for biomimetic abstraction before, such as filter-feeding fish or elasmobranches (Hung & Piedrahita, 2014; Divi, Strother, & Paig-Tran, 2018; Schroeder *et al.*, 2019). However, there has never been a systematic screening of SFMs to identify biological models for technical solutions. Therefore, 18 technical and biological parameters were developed to review metazoan taxa for SFMs. Literature on SFs was gathered until December 2020 from scientific search portals and biomimetic databases, i.e., SCOPUS, Google Scholar, and www.asknature.org, to extract information for each parameter and identify groups based on structure-function patterns. In order to include all variations of SFMs, all terms were adapted, e.g., filter medium was changed to separation medium. This review systematically describes and classifies 35 different SFMs (Figure 4) in a technical context and identifies their biomimetic potential (Table 2).

(1) Porifera

(2) Alcyonacea

(3) *Aurelia aurita*
Linnaeus 1758

(4) *Mnemiopsis leidyi*
Agassiz 1865

(5) Entoprocta

(6) Brachiopoda

(7) Phoronida

(8) Bryozoa

(9) Rotifera

(10) Sabellidae

(11) *Urechis caupo*
Fisher & MacGinitie 1928

(12) *Mytilus edulis*

(13) *Dendropoma maximum*
Sowerby 1825

(14) Daphnia

(15) *Euphausia superba*
Dana 1850

(16) Cirripedia

(17) Ephemeroptera

(18) Trichoptera

(19) Diptera

(20) Crinoidea

(21) Dendrochirotida

(22) Enteropneusta

(23) Amphioxiformes

(24) Ascidiacea

(25) Larvacea

(26) Petromyzontiformes

(27) Mobulidae

(28) *Rhincodon typus*
Smith 1828

(29) *Hypophthalmychthys molitrix*
LValenciennes 1844

(30) *Clupea harengus*
Linnaeus 1758

(31) Anura

(32) Anatidae

(33) Phoenicopteriformes

(34) *Balaena mysticetus*
Linnaeus 1758

(35) *Balaenoptera physalus*
Linnaeus 1758

Figure 4: Overview of the 35 SFMs represented by organisms or organism groups within the metazoans. Numbering of each SF is consistent with table 2. Adapted from Hamann & Blanke (2022)

3.2. Published Results

SFs live in marine and freshwater environments. Ducks and flamingos are terrestrial but still feed in aquatic environments. Most benthic SFs, such as sponges, barnacles, or dendrochirotid sea cucumbers (Figure 4), are sessile or remain stationary during feeding, while pelagic SFs are motile by active swimming or drifting (Bushek & Allen, 2005). Active SFs produce a feeding current by ciliary movement, pumping, or forward movement, while passive SFs retain particles from the ambient current that passes their SFMs (Wildish & Kristmanson, 1997; Hentschel & Shimeta, 2008; Riisgård & Larsen, 2010). SFs do not seize individual prey but feed on a range of particles sizes, which are 2 to 4 orders of magnitude smaller than the body length of the SFs (Hansen, Bjornsen, & Hansen, 1994; Conley, Lombard, & Sutherland, 2018). The smallest retained particles are determined by physical constraints, such as the mesh size or the physics of particle encounter (Rubenstein & Koehl, 1977; Shimeta & Koehl, 1997), while the upper limit can be given by the opening of incurrent canals or mouth opening (Moore & Mallatt, 1980; Yahel, Eerkes-Medrano, & Leys, 2006; Conley *et al*., 2018). Additionally, some SFs can actively select particles, such as bivalves (Ward & Shumway, 2004) or ducks (Brent Gurd, 2006).

The separation medium is usually permeable and in contact with the suspension to retain particles. In most SFs, it is flat or funnel-shaped (Table 2) and is enclosed in a pipe-like system that guides the suspension towards the separation medium, e.g., the funnel-shaped gill arch system in filter-feeding fishes (Cohen *et al.*, 2018), or in the open, e.g., the flat fan of barnacle appendages held across the ambient current (Trager, Hwang, & Strickler, 1990). Enclosed separation media come closest to technical filters, as they are defined as a device that typically holds the separation medium across the fluid so that all the suspension has to pass the separation medium (Sutherland, 2005). The separation medium can be formed by various body parts and thus consists of a variety of tissue and materials that retain particles, ranging from the epidermis, moving cilia, viscoelastic mucus or silk to rigid structures based on chitin or keratin (Table 2). On a larger scale, these materials form surfaces, meshes, or pores. For example, ctenophores have prey-capturing, adhesive surfaces within their inner lobes (Waggett, 1999), Atlantic krill has appendages that branch into secondary and tertiary setae to form fine meshes (McClatchie & Boyd, 1983), while sponges form three-dimensional structures with channels and filtering chambers (Witte *et al.*, 1997). The openings of the apertures in a separation medium, i.e., the mesh size, primarily determine the size of retained particles. However, other mechanisms than simple sieving might influence particle retention and capture (see hydrosol filtration theory by Rubenstein & Koehl, 1977 or Shimeta & Jumars, 1991), and it is difficult to predict the size of ingested particles solely on the morphology.

The fluid involved in suspension-feeding is water, which carries the particles towards the separation medium. Dead-end or cross-flow filtration can occur depending on the flow direction towards separation medium. Cross-flow filtration is found, for example, in the filter house of larvaceans, in suspension-feeding elasmobranches and fishes, and in bowhead whales. Brachiopods, lancelets, ascidians, or tadpoles use dead-end filtration (Table 2). Some SFs have evolved traits and mechanisms that do not find a technical analogy. For example, in bryozoans, the ciliated tentacles on the lophophore induce a water current to flick particles directly into the mouth in its middle (Riisgård & Goldson, 1997). Dendrochirotid sea cucumbers have ten to thirty highly branched tentacles around the mouth held upwards into the current. When enough particles are retained on the adhesive papillae, one arm after the other is inserted into the mouth, and particles are scraped off (Roberts *et al.*, 2000). All SFs need a driving force that pushes particles towards the separation medium and creates a high enough flow velocity to overcome its hydrodynamic drag. The driving force can be the ambient current, which is taken advantage of in passive SFs or actively induced through the movement of cilia or appendages, rhythmic pumping, or forward swimming. Because of the small dimensions of particles and separation medium structures, many SFs separate particles in an intermediate flow regime with a Reynolds number (inertial to viscous forces) between 0.5 and 50, where flow is primarily laminar. Faster flow with higher Reynolds numbers of around 300 can be

found, for example, in ram-feeding mobulid rays and whale sharks. Suspension-feeding fish and ducks were suspected of inducing vortices (Kooloos *et al.*, 1989; Brooks *et al.*, 2018). In order to maintain functioning SFMs, the separation medium needs to be cleaned in a continuous or discontinuous manner. If particles are not directly ingested, they can be removed through ciliary transport, mucus, feeding or scraping off, or back flushing (Table 2). In SFs that use cross-flow filtration, the tangential flow pushes particles along the separation medium to prolong or avoid clogging.

Table 2: The biological traits of each SFM are clustered and presented for each parameter (there is no relation between the columns). The numbers represent the SFs according to Figure 4. Subunits in SFs, e.g., choanocyte in sponges, polyps in gorgonians, zooid in bryozoans, are indicated by (*). Adapted from Hamann & Blanke (2022).

Separation medium	Geometry	Flat (2, 14, 16, 19)	Flat (in pipe) (12, 13)	Funnel (1*, 2*, 7, 8*, 9, 10, 18, 20)	Funnel (in pipe) (6, 11, 22, 23, 24, 26, 27, 28, 29, 30, 31, 32, 33, 34, 35)		Others (1, 3, 4, 9, 15, 17, 21, 25)
	Material of separation medium	Cell structures (1*)	Epidermis (2, 3, 20, 21, 27, 28, 29, 30)	Cilia (5, 6, 7, 8*, 9, 10, 12, 22, 23)	Mucus (3, 4, 11, 13, 22, 23, 24, 25, 26, 31)	Silk (18)	Chitin (14, 15, 16, 17, 19) / Horn/ keratin (32, 33, 34, 35)
	Mesh design	Flat surface (3, 4)	First level of organisation (1*, 2*, 3, 5, 9, 22, 32, 33, 34, 35)	Second level of organisation (2*, 6, 7, 8*, 10, 12, 14, 16, 17, 19, 27, 31)	Third level of organisation (14, 15, 20, 28, 30)	Net (11, 13, 18, 23, 24, 25, 31)	"Spongy"/ 3D (1, 2, 21, 29)
	Particle size	<1 µm (1*, 11, 14, 19, 23, 25)	1-100 µm (1, 2, 4, 5, 6, 7, 8, 9, 10, 11, 12, 14, 15, 17, 18, 19, 20, 22, 23, 24, 25, 26, 27, 29, 31, 32)	100-1000 µm (1, 3, 20, 21, 25, 26, 27, 28, 30, 32, 33)	1-10 mm (21, 38, 32, 33, 34)		>10 mm (35)
Separation type		No Filtration (2, 3, 4, 5, 7, 8, 9 10, 14, 19, 20, 21)	Filtration				
			Dead-end filtration (1, 7, 11, 12, 13, 15, 16, 17, 18, 22, 23, 24, 31, 32, 33, 35)		Cross-flow filtration (7, 8, 25, 27, 28, 29, 30, 34)		
Fluid dynamics	Driving force	None (passive) (1, 2, 4, 13, 16, 17, 18, 19, 20, 21)	Ciliary (+flagellar) Movement (1*, 4, 5, 6, 7, 8*, 9, 10, 12, 22, 23, 24, 25)	Movement of appendages (14, 15, 16, 17, 19, 25)	Pumping (11, 22, 26, 28, 29, 31, 32, 33,)	Forward movement (3, 27, 28, 30, 34, 35)	
	Water velocity (inflow)	<0.1 cm/s (1, 5, 10, 12, 22)	0.1-1 cm/s (2*, 4, 7, 8*, 11, 14, 23, 24, 25)	1-10 cm/s (2, 3, 6, 15, 16, 17, 20, 25)	>10 cm/s (16, 18, 19, 27, 28, 30, 34, 35)		
	Flow regime (at mesh)	Creeping flow (Re <1) (1*, 2*, 8*, 9, 10, 12, 14, 15, 19, 22, 24,)	Laminar flow (Re 1-50) (2, 3, 4, 6, 8*, 16, 17, 19, 20, 22, 25, 27, 28, 29, 30, 34, 35)		Turbulent flow (Re >50 (27, 33, 34, 35)		
Cleaning	Working mode	Continuous (1, 2, 3, 4, 6, 7, 8, 9, 10, 12, 14, 15, 16, 17, 19, 20, 21, 22, 23, 24, 25, 27, 28, 29, 30, 31, 32, 33, 34)	Discontinuous (11, 13, 18, 25, 35)				
	Cleaning	Direct ingestion/ phagocytosis (1, 5, 11, 13, 25)	Ciliary transport (3, 4, 5, 6, 7, 8, 9, 10, 12, 20, 22, 31)	Mucus (10, 12, 22, 23, 24, 26, 31)	Feeding, scraping, combing off (2, 14, 15, 16, 17, 18, 19, 21, 32, 33, 35)	Back flush (24, 28, 34)	Non-clogging mechanism (25, 27, 28, 29, 30 34)

3.3. Discussion

In many regards, separation processes in SFs are similar to technical filtration processes because they face the same 'design challenges': high particle retention, overcoming the

hydrodynamic resistance of the separation medium, cleaning mechanism to reduce clogging, and reduction of energetic costs. For example, the setules on the appendages in daphnids or the gill structure in bivalves are angled, similar to pleated filter media, which are used in technical filters to increase the filtration area (Brendelberger & Geller, 1985; Chen, Pui, & Liu, 1995; Beninger, St-Jean, & Poussart, 1995). These similarities could be used in a biomimetic approach to optimise technical filters. However, there are also differences, and some mechanisms that are widespread in nature are somewhat rare in technical applications and vice versa. For example, particles in the range of 1 mm down to 5 µm are usually retained in solid-liquid filtration through dead-end filters, while smaller particles are often separated by cross-flow filtration in ultra- or nanofiltration (Sutherland, 2008). In SFs, cross-flow filtration can be especially found in large organisms that feed on particles up to 5 cm, as observed in the bowhead whale (Werth, 2019). Then again, centrifugal separation is not common in SFs but in technical applications.

Another difference is that filters are often static, consist of several parts, and are designed for one specific separation process. SFMs are integrated mechanisms, often multifunctional, that come with an inherent cleaning mechanism, and can adjust to their environment, e.g., temperature, flow velocity, or particle concentration. This needs to be considered during a biomimetic working process. The abstraction into theoretical and physical models can facilitate an in-depth understanding of the function and be the next step towards developing a product for a technical application. However, 'abstraction' always includes a reduction of traits (Helms, Vattam, & Goel, 2009). Therefore, it needs to be taken great care that relevant traits are not lost during the abstraction process when taking an adapted trait out of its ecological context (Broeckhoven & du Plessis, 2022). Besides transferability, scalability is another crucial aspect. Depending on the scale, physical and chemical properties can change, e.g., the Reynolds number. Optimisation or innovation, this review provides a systematic overview of 35 SFMs (Table 2) and can guide biologists and engineers to appropriate biological models during their biomimetic working process to develop biomimetic filters.

4. Mucus Filtration in Biofilms

This chapter gives a summary of Manuscript II (Appendix, p. 172),

- Hamann, Leandra; Werner, Jennifer; Haase, Felicia; Thiel, Massimo; Scherwaß, Anja; Laforsch, Christian; Löder, Martin G.J.; Blanke, Alexander; Arndt, Hartmut (in prep.) Retention of microplastics by biofilms and ingestion by protists

and presents additional unpublished data.

Author Contributions:

Leandra Hamann: conceptualization and methodology, experimental investigation, data analysis and visualization, formal analysis, writing: original draft, writing: review and editing

Jennifer Werner: conceptualization and methodology, experimental investigation, formal analysis, writing: original draft

Felicia Haase (master thesis*): experimental investigation of biofilms in large flow tank

Massimo Thiel (bachelor thesis): experimental investigation of ingestion by protists

Anja Scherwaß: conceptualization and methodology

Christian Laforsch: MPs analytic, writing: review and editing

Martin G.J. Löder: MPs analytic, writing: review and editing

Alexander Blanke: Writing: review and editing, supervision, project administration and funding acquisition

Hartmut Arndt: Conceptualization and methodology, Writing: review and editing, supervision, project administration and funding acquisition

*daily supervisor: Leandra Hamann and Jennifer Werner

Previous page:

Watercolour drawing of biofilm organisms (not to scale). Credits: Leandra Hamann 2023

4.1.   Introduction

During the biomimetic working process, biological working principles are transferred from biology to technology. One way to identify potentiall working principles is the identification of similar traits that have evolved independently in distant taxonomic groups, i.e., convergent evolution, which allow to describe them detached from phylogenetic constraints (Broeckhoven & du Plessis, 2022). In twelve of the reviewed suspension feeding mechanisms, particles are retained or transported by mucoid meshes or surfaces (Chapter 3). In ascidians, particles are caught with a mucus net continuously produced by the endostyle within the branchial basket (Figure 5A). The mesh size is smaller than 1 µm (Pennachetti, 1984). The medusae of the moon jelly *Aurelia aurita* have mucus-covered external surfaces on the bell margin (Figure 5B) that retain particles in addition to particle retention with their tentacles (Stoecker, Michaels, & Davis, 1987). Outside of suspension feeders, mucus serves different functions in biology, such as in the defence mechanism of the hagfish (Böni, 2018), the locomotion of snails (Gutow *et al.*, 2019), or in the biochemical processes of organs, e.g., respiratory tracts, gastrointestinal tracts, or reproductive tracts (Bansil & Turner, 2018; McShane *et al.*, 2021).

Figure 5: Particle retention with mucus: A) the ascidian *Ciona intestinalis* retains particles with a mucus net (white arrow) inside its pharyngeal basket (credits: Jens Hamann 2018), B) the moon jelly *Aurelia aurita* retains particles with tentacles and transports the particles with the help of mucus along the bell margin (white arrow, credits: Jens Hamann 2021), and C) biofilms form a heterogeneous, mucoid structure (white arrow) on submersed substrates (credits: Leandra Hamann 2018).

In mammalians, mucus secretes from specialised goblet and mucous cells, and can have distinct rheological properties, e.g., vary in viscoelasticity, depending on the function of the epithelial surfaces (Lai *et al.*, 2009; Bansil & Turner, 2018). It consists of many components, such as electrolytes, lipids, various proteins, and water, which serve as the solvent and can make up to 95% of the mucus (Bansil & Turner, 2018). Mucins or mucin proteins are the major functional component of mucus and influence its viscoelastic properties (Bansil & Turner, 2018). Secreted mucins can remain as small, non-polymeric glycoproteins or form chains of polymers with complex cross-linking (McShane *et al.*, 2021). In ascidians, these mucin polymers form filaments of 10 to 40 nm width that build the mucus mesh (Flood & Fiala-Medioni, 1981). There is limited data available about the specific chemical or physical properties of mucus involved in particle retention. Mucus is highly adhesive to different

substrates and can bind particles by electrostatic interaction, von der Waals forces, hydrophobic forces, hydrogen bonding, and chain entanglement (Mikos & Peppas, 1990; Liu *et al.*, 2015; Bansil & Turner, 2018). In technical terms, mucus, i.e., materials based on cross-linked, hydrophilic polymer chains, are called hydrogels and are applied in tissue engineering, cosmetics, drug delivery, soft electronics, and actuators (Zhang & Khademhosseini, 2017).

In order to investigate the retention mechanism of MPs by mucoid surfaces, biofilms were used as naturally grown mucoid surfaces (Figure 5C). Biofilms are microbial communities of bacteria, algae, and protists living in a matrix of extracellular polymeric substances (EPS) on organic and inorganic substrates (Branda *et al.*, 2005; Böhme, Risse-Buhl, & Küsel, 2009). Several factors influence particle retention in biofilms: 1) passive interception by biofilm surface morphology, 2) agglomeration of particles to the EPS matrix, and 3) grazing activities of ciliates at the surface biofilm (Eisenmann *et al.*, 2001), that account for around 10% of particle retention (Roche *et al.*, 2017). In technical applications, biofilms are already used in micro- and ultrafiltration to form dynamic and permeable membranes (Sprouse & Rittmann, 1990; Drury, Characklis, & Stewart, 1993; Huang *et al.*, 2019).

Through a combination of methods, the three retention mechanisms were investigated to, on one hand, study the relevance of biofilms in the context of the environmental problem of MPs, and, on the other hand, investigate the retention mechanisms of mucoid surfaces for a biomimetic application. The retention of MPs by biofilms was studied in field and laboratory experiments. Naturally grown biofilms in the River Rhine were analysed for their MPs content and exposed to artificial MPs in flow channels. Additionally, the ingestion of MPs by a typical biofilm-associated ciliated was investigated under varying ambient MPs concentrations. In another set of flow channel experiments under laboratory conditions, biofilms were compared to materials and surface structures that represent the different physical and chemical properties of biofilms, ranging from adhesives to solids with a complex surface structure.

4.2.   Methods

Biofilms were grown under natural conditions on clay tiles within the River Rhine on the Ecological Rhine Station boat of the University of Cologne (Figure 6A), permanently anchored in Cologne-Bayenthal (Rhine-km 684.5). Four experiments were conducted, of which the first three focus on the retention of MPs by biofilms and protists with regard to the environmental problem of MPs, and the fourth, in which the retention properties of the EPS matrix in comparison to other surface materials and structures was investigated.
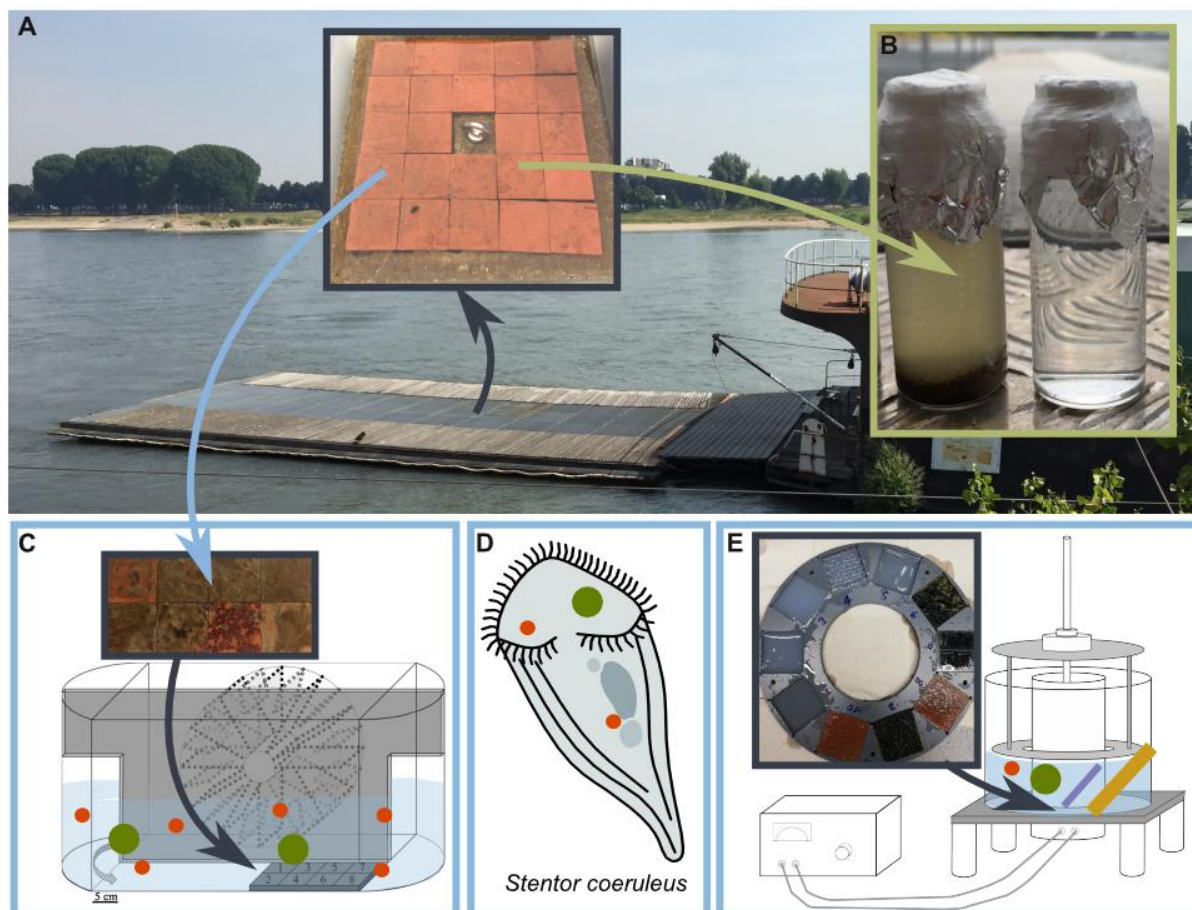
Figure 6: Experimental setups to investigate MPs retention in biofilms in field (green) and laboratory (blue) experiments. A) The float behind the Ecological Rhine station boat contains channels in which biofilms grow under natural conditions on clay tiles (4.9 x 4.9 x 0.5 cm). B) Natural MPs concentrations were measured in biofilm samples (left) and pure Rhine Water as controls (right) after 6, 12, and 18 months. C) Biofilms were set in flow channels and exposed for 24 h to different MPs sizes and flow velocities, which were adjusted with a paddle wheel. D) Graphic of the ciliate *Stentor coeruleus* that was exposed to varying MPs concentration and sizes. E) Circular flow tank with the control unit to adjust the flow velocity of the rotating wheel. A disc with ten cut-outs positions the materials and surface properties in the tank.

4.2.1. Microplastic Retention by Biofilms and Protists (published)

MPs concentration was analysed in biofilm samples that were exposed to the natural conditions of the River Rhine after 6, 12, and 18 months. Each time, biofilms of 12 tiles were carefully removed using a wooden brush with natural fibres, filled up to 40 ml with unfiltered River Rhine water, and stored in glass bottles covered with aluminium foil. In addition, three control samples of Rhine water were taken in the same manner, including stirring with the brush but without the biofilms (Figure 6B). The samples were stored in a -18 °C freezer until analysis at the University of Bayreuth. Sadly, during the transportation of the frozen samples by a transportation company, several samples were destroyed, which led to varying numbers of replicates and the total loss of the control samples after 12 months. After sample preparation, µFTIR was used to identify MPs, i.e., polymer type, particle size, and shape.

For the first set of laboratory experiments, clay tiles with naturally grown biofilms were removed from the River Rhine and positioned into four flow channels (Figure 6C) in addition to rough and smooth clay tiles and rough and smooth acrylic tiles. Fluorescent, red microbeads (6 µm) were added to the tanks in a concentration of 500 MPs/ml, and the flow velocity was set to 0.1 m/s or 0.2 m/s. In a second set, biofilms were only compared to rough clay tiles, but three sizes of MPs were added, 1 µm, 6 µm, and 10 µm. After 24 hours, the samples were removed carefully with a brush and rinsed with water. MPs concentration of samples was counted manually using a fluorescence microscope.

The uptake of MPs by a biofilm-associated ciliate was studied in *Stentor coeruleus* (Stentoridae, Figure 6D), a stalked, omnivorous filter-feeder (Fenchel, 1987). *S. coeruleus* individuals were exposed to 6 µm and 10 µm particles with varying ambient MPs concentration (500 MPs/ml, 1250 MPs/ml, 2500 MPs/ml, 5000 MPs/ml) for one hour in a plankton wheel. All specimens were immediately examined alive after the experiment for MPs ingestion under the fluorescence microscope.

4.2.2. Comparison of Materials and Surface Structures (unpublished)

In the last set of experiments, the retention capability of MPs by biofilms was compared to eight other materials and surface properties, each presenting chemical and/or physical properties of biofilms. The EPS is a cross-linked network of polymers made from polysaccharides, nucleic acids, proteins, and other macromolecules with typical viscoelastic properties (Kundukad *et al.*, 2016). Agar was chosen to represent the viscoelastic and adhesive properties of the EPS matrix. Agar is a polysaccharide that forms hydrogen bonds between its polymers and builds an internal network when in contact with water (Armisén & Galatas, 2009). It is used as a gelling agent in the food industry and is readily available. Three different concentrations of agar were used to study the effect of gel viscosity with 0.5 wt%, 1.0 wt%, and 1.5 wt%. The higher the weight share of agar, the higher the shear viscosity (Ellis *et al.*, 2017). A smooth acrylic plate, sandpaper, and the hooked side of Velcro mimicked the surface structure of the heterogeneous biofilm morphology. A combination of viscoelastic material and surface structure was achieved by imprinting two different surface patterns into agar of 1.5 wt%.

Eight circular flow channels were available, each with a motor unit to adjust the rotational speed of the rotating wheel, which was set to 0.2 m/s for all experiments (Figure 6D). A disc with cut-outs for ten tiles was placed at the bottom of the tank. These cut-outs were filled with the selected substrates (Figure 6E). The agar powder was weighted according to the three different concentrations and dissolved in boiled-up water. The liquid agar was poured into the detected disc positions and cured for 24 hours at 6°C. The surface structure of agar 1,5% P1 was modified by adding a silicone embossed mat during the curing process. Agar P2 1,5% was modified after the curing process by pressing the hooked-side of Velcro onto the gelled

surface. Sandpaper and the hooked side of Velcro were glued onto acrylic tiles and positioned into the cut-outs. A clean acrylic plate was added as the eights sample. Because biofilms can grow very heterogeneous, two biofilm tiles were implemented in each experiment. The positions of the ten substrates were chosen randomly.

Before the experiment, each basin was filled with 10 litres of water, 5 litres of filtered Rhine water, and 5 litres of tap water. Four of the flow channels were used to test 6 µm (500 MPs/ml) and 10 µm (300 MPs/ml) particles, and the other four were used to test 1 mm (100 MPs/ml) and 2 mm fibres (15 MPs/ml). After 24 hours, the motor was stopped and the disc with the substrates were carefully removed. The biofilms, acrylic and sandpaper surfaces were brushed and rinsed with 40 ml of tap water. The Velcro was detached from the tile and vortexed in a Falcon tube, diluted with 40 ml of water. The different concentrated and surface-modified types of agar were removed from the disc using a plastic card and filled into falcon tubes. The falcon tubes were heated in a water bath at 90°C for 20 minutes until the agar was liquid and the samples could be counted. 200 µl of each sample were manually counted using a McMaster counting chamber. The fibres were counted using a light microscope (ZEISS Axioskop 2), while the microbeads were counted with a fluorescence microscope (ZEISS Axioskop HXP 120). Due to their comparatively large size, the fibres were easy to recognise and distinguish. If fibres overlapped the edge of the counting strips, they were counted to the strip that contained the largest part.

4.2.3.   Data Analysis and Statistics

The data was analysed and visualised using the R programming environment (R Core Team, R version 4.2.2, 2022). Based on subsampling and dilution factors, MPs concentration was extrapolated to concentration per 1 ml of water volume or 1 cm of surface area. In the field experiments, height of the biofilms were assumed to have an average height of 1 mm to transfer MPs concentration per area to MPs concentration per volume. Before data analysis, the data structure was checked for normality, heteroscedasticity, and outliers (Zuur *et al.*, 2010). Mean concentrations between samples were tested for significance using ANOVA as a parametric test or alternatively a Kruskal-Wallis-Test as a non-parametric test. Data is reported as mean with standard deviation. Controls that included no MPs were not included in the statistical tests.

4.3.   Published Results

After 6 months in the River Rhine, biofilms contain 240 ± 143 MPs per tile (n = 5, Figure 7A), corresponding to 10 MPs/cm² of biofilms. This is significantly more than in the control samples with 24 ± 30 MPs in 40 ml of river water (n = 4, $p < 0.5$, Kruskall-Wallis and post-hoc dunn test (method 'holm')). The 12-month-old biofilms contain 147 ± 88 MPs per tile (n = 4), while in 18-

month-old biofilms have 93 MPs per tile (n = 4), which is not significantly more than in the river water controls with 48 ± 18 MPs/ml (n = 3). MPs size distribution is similar in all biofilms and control samples after 6, 12, and 18 months. Between 70 % and 78 % of MPs are smaller than 50 µm, and between 11 % and 36 % are smaller than 11 µm (Figure 7B).
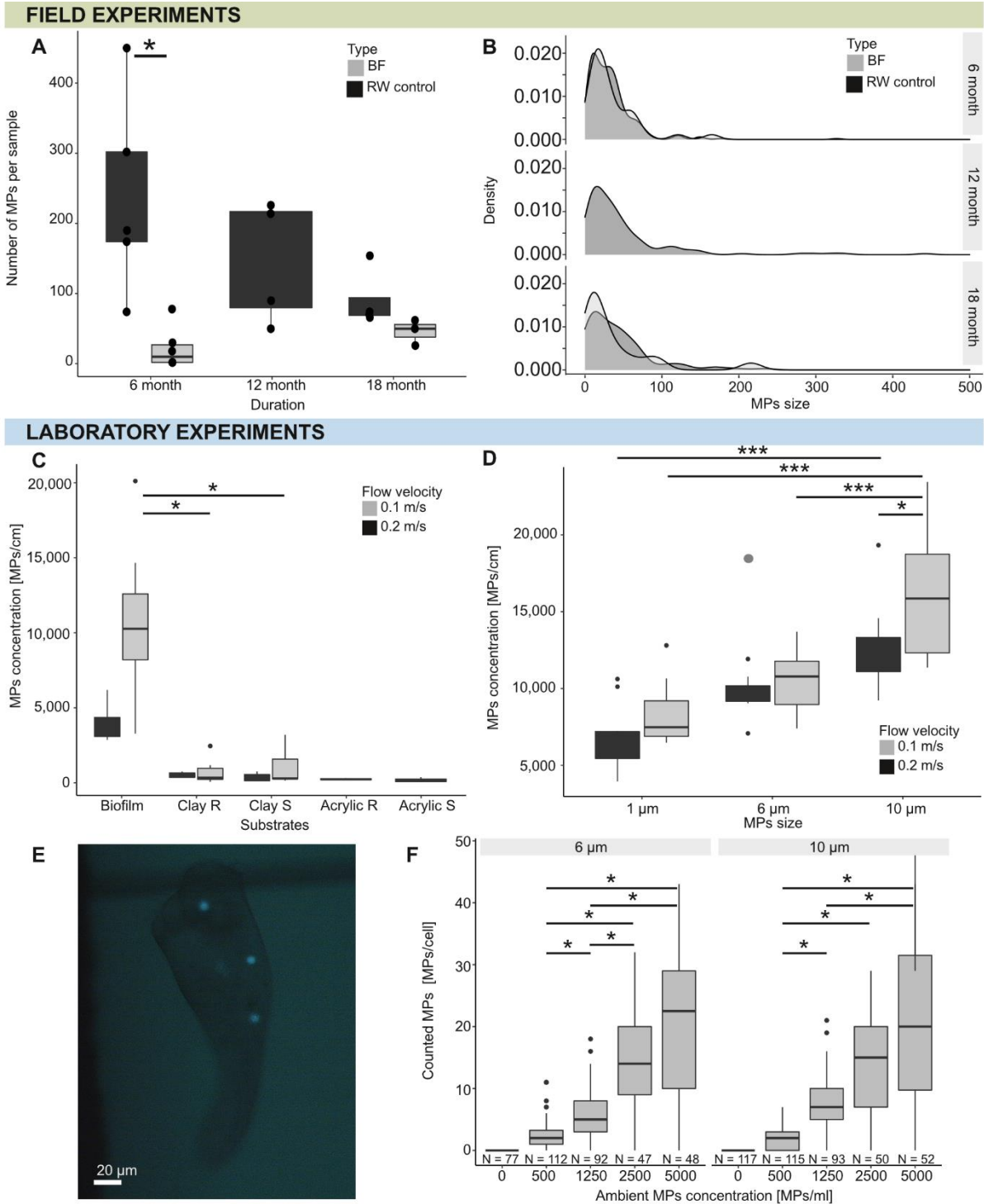
Figure 7: Results of the field and first two laboratory experiments. A) Number of MPs found in each sample (black points) for biofilms and the river water (RW) controls (Kruskall–Wallis * <0.05, post-hoc Dunn test method 'holm'). B) Density plot of MPs sizes found in biofilms and RW controls for particles <500 µm. C) MPs retention of 6 µm particles by biofilms, rough clay tiles (R), smooth clay tiles (S), rough acrylic (R), and smooth acrylic (S) for two different flow velocities: 0.1 m/s (black) and 0.2 m/s

(grey) after 24 hours (Kruskal–Wallis–Test, * = p < 0.05, post–hoc Dunn–Test, method 'holm'). D) Concentration of MPs in biofilms for according to MPs sizes (1 µm, 6 µm, 10 µm) and two flow velocities (0.1 m/s (black) and 0.2 m/s (grey)) after 24 hours. One outlier was removed from statistics (grey circle), (ANOVA p < 0.05, post–hoc TukeyHSD, *< 0.05, ***< 0.001). E) *S. coeruleus* with ingested green MPs (10 µm). F) Ingestion of MPs for 6 µm and 10 µm MPs by *S. coeruleus* in presence of varying ambient concentrations (Kruskal–Wallis–Test, post–hoc Dunn–Test, *= p < 0.05). The control (concentration of 0 MP/ml) was significantly different from all other groups (not indicated).

In the lab experiments, MPs concentration in biofilms is 6 - 8 times (velocity of 0.1 m/s) and 9 - 12 times (velocity of 0.2 m/s), significantly higher than on rough and smooth clay tiles resembling natural stone surfaces (Kruskal-Wallis-Test, p < 0.05, post-hoc Dunn-Test, method 'holm'). The acrylic tiles retain the least amount of MPs. There are no significant differences of MPs retention between the two flow velocities (0.1 m/s, 0.2 m/) for each of these substrates (Figure 7C). The number of MPs trapped in biofilms significantly increases with particle size (ANOVA, p < 0.05, post-hoc TukeyHSD; Figure 7D). The concentration of the retained particles is at least twice as high for the 10 µm particles as for the 1 µm particles. The highest concentrations of particles in the biofilms are found for the 10 µm particle size, and it differs significantly between the two flow velocities with 12,639 MPs/cm for 0.1 m/s and 16,164 MP/cm for 0.2 m/s (ANOVA, p < 0.05, post-hoc TukeyHSD). After one hour of exposure, *Stentor coeruleus* contains more MPs if the ambient MPs concentration is higher (Figure 7). Almost every increase in the exposure concentration leads to a significant increase in particle concentration in the cell (Kruskal-Wallis-Test, post-hoc Dunn-Test, *= p < 0.05). The maximum number of ingested MPs is present at an exposure concentration of 5000 MPs/ml with a mean of 21 MPs/Ind for the 6 µm and 10 µm particles. There are no significant differences related to particle sizes; both are ingested in the same amount.

4.4.   Unpublished Results

Biofilms contain between 0.041 ± 0.007 %/cm of 2 mm fibres and 0.162 ± 0.052 %/cm of 10 µm particles (each N = 8) after the experiment (Figure 8). There is no significant difference in the amount of retained MPs between the particle types. Because of that, only the 10 µm particles were used for statistical data analysis between the substrates. All agar substrates, even with surface structures, retain very few MPs particles and fibres, and are not significant compared to biofilms, the acrylic tile or the sandpaper surface. Only the Velcro surface retains significantly more MPs than the other substrates (Figure 8, Kruskal-Wallis-Test p < 0.05. post-hoc Dunn-Test, method 'holm') and contains 0.422 ± 0.054 %/cm of 10 µm particles (N = 4).
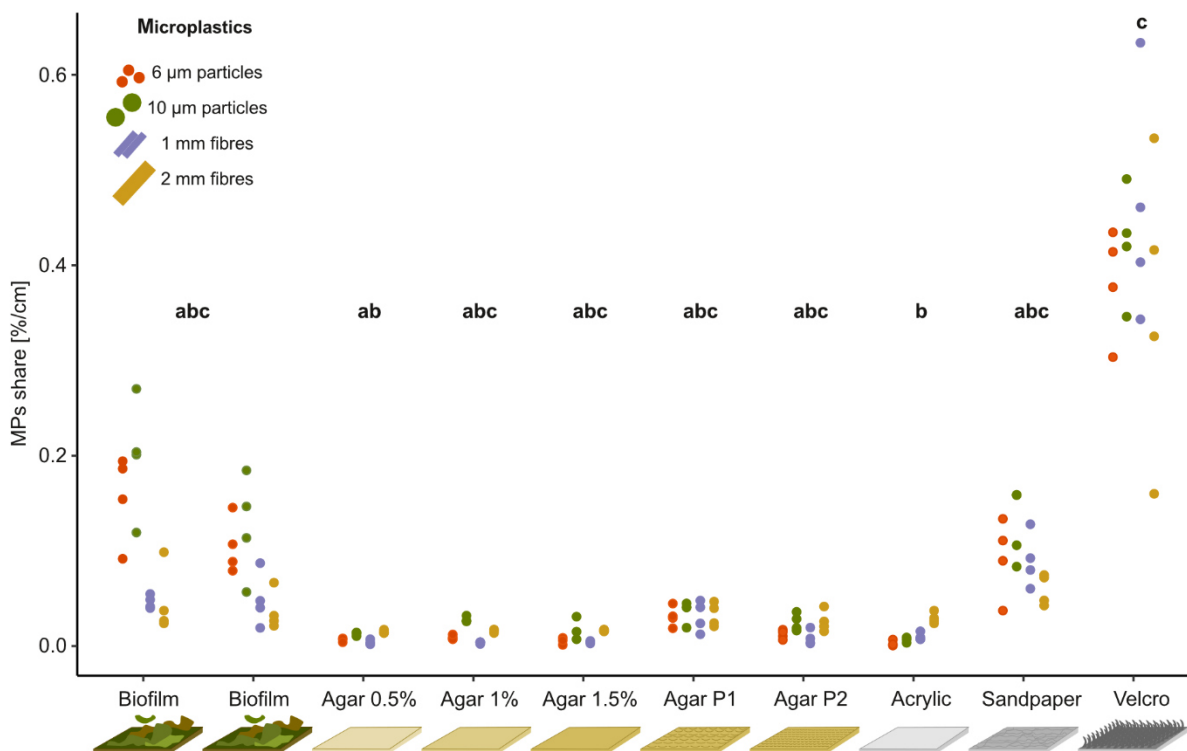
Figure 8: Comparison of MPs retention by biofilms in comparison to different viscosities of agar (0.5 wt%, 1 wt%, 1.5 wt%), agar with two different surface structures (P1, P2), and hard substrates with varying surface structure: smooth acrylic, sandpaper, and Velcro (each N = 4, Kruskal–Wallis–Test p < 0.05. post–hoc Dunn–Test, method 'holm', significances are displayed as compact letters). The retention is given as the MPs share of the initial concentration per area.

4.5.   Discussion

Biofilms retain and accumulate MPs from the ambient river water in size of 5.9 to 300 µm. These are the first results of MPs concentrations in biofilms in field experiments. In combination with the laboratory studies, it can be seen that MPs retention is influenced by environmental factors, such as MPs concentration and size, seasonal changes, flow velocity, and by the biofilms itself through their morphology and the presence of protists. This align with previus studies (Mikos & Peppas, 1990; Drury *et al.*, 1993; Okabe, Yasuda, & Watanabe, 1997; Böhme *et al.*, 2009; Ackermann *et al.*, 2011; Roche *et al.*, 2017).

Once captured within biofilms, MPs have several pathways: long-term storage (with degradation), redistribution, ingestion by protists and trophic transfer as demonstrated in earier studies. Particles were found in the depth of biofilms within 90 min of experiments and can remain there for 20 days or longer (Stoodley, DeBeer & Lewandowski, 1994; Okabe *et al.*, 1997). Biofilms become increasingly dense as pores become significantly smaller towards the substrate (Zhang & Bishop, 1994). Long-term presence and accumulation of particles was associated with the clogging of pores, which might alter the local flow field that is essential for mass transfer and oxygen flux (De Beer, Stoodley, & Lewandowski, 1996; Reichert & Wanner,

1997). Another natural process of biofilms during growth is sloughing. Mature biofilms often reach a thickness that cannot withstand the forces of river flow velocities and parts of the biofilms can tear off (Wanner & Gujer 1986; Okabe *et al.*, 1997). This causes the biofilm and its organisms to disperse and reattach to other substrates in the river (Drury *et al.*, 1993; Risse-Buhl & Küsel, 2009). This also might lead to MPs redistribution, which means that biofilms only act as temporary sinks.

The ingestion of MPs down to a size of 6 µm by protists proves that plastics are likely to enter the food web in lower trophic levels than suggested in previous studies. This can have negative effects, because particles smaller than 20 µm are more likely to translocate into tissues and cause inflammation or necrosis (Triebskorn *et al.*, 2019). To date, there is a lack of information on the exposition and effects of MPs in biofilms and protists (Rillig & Bonkowski, 2018; Langlet *et al.*, 2020). Rivers play a significant role in transporting and distributing MPs and plastic litter from inland to shores and oceans (Lebreton *et al.*, 2017), and more information is needed to evaluate ecological risks in freshwater environments and establish biofilms as assessable, natural MPs sink or monitoring system (More *et al.*, 2014; Li *et al.*, 2018).

In technical applications, biofilms have been used for particle separation processes or for removing carbon and nitrogen, such as wastewater treatment (Martin & Nerenberg, 2012). However, the use of hydrogels to mimic mucus is limited so far. Intermediate filaments were separated from hagfish mucins and used to produce mucus films to verify their biomimetic potential for technical applications such as implants, scaffolds for cell culture or contact lenses (Böni, 2018). Bio-inspired cellulose-based hydrogel were tested to capture uranium from seawater (Gao *et al.*, 2020). However, hydrogels are expensive, require specific lab environments and are often petro-based polymers (for example, Laftah, Hashim, & Ibrahim, 2011; Thomas, Cipriano, & Raghavan, 2011), which is not in the sense of finding a technical solution for the environmental problem of MPs.

Our results indicate that the surface structure is more relevant in particle separation than the viscoelastic and adhesive properties of the material. However, agar did not turn out to be a representative hydrogel of the biofilm EPS matrix. In order to fix the agar within the positions of the disc and reduce disintegration by the permanent current in the flow channel, the viscosity had to be relatively high, which made the surface smooth and probably reduced its 'stickiness'. Additionally, the hooked side of the Velcro does not resemble the natural surface structure of biofilms but rather a comb that sieves out MPs. More experiments are needed to evaluate if these materials can mimic biofilms in technical applications. In the future, engineered hydrogels with controlled architecture, activity and functionality might function in various applications (Zhang & Khademhosseini, 2017).

For this thesis, the abstraction of mucus ends here.

5. Filter-Feeding Morphology in Ram-Feeding Fishes

This chapter gives a summary of Manuscript III (Appendix, p. 211),

- Hamann, Leandra; Hagenmeyer, Jan; Eduardo, Santiago; Spanke, Tobias, Blanke, Alexander (in prep) Morphological Diversity of Filter-Feeding Structures in Five Ram-Feeding Fish Species (Clupeidae, Scombridae),

and presents the state of the art of washing machines and MPs filters (not published).

Author Contributions:

Leandra Hamann: conceptualization and methodology, analysis of the state of the art of wahing machines and waschine machine filters, experimental investigation of gill arch system morphology and filter-feeding behaviour, data analysis and visualization, formal analysis, writing: original draft, writing: review and editing

Jan Hagenmeyer (bachelor thesis*): experimental investigation of GAS morphology

Santiago Eduardo (bachelor thesis*): experimental investigation of GAS morphology

Tobias Spanke: PTA staining and micro-CT scans at ZFMK

Alexander Blanke: review and editing, supervision, project administration and funding acquisition

*Supervisor: Leandra Hamann

Other Contributions:

Christian Grünewald: analysis of the state of the art of wahing machines and waschine machine filters

Previous page:

*Filter-feeding pilchards (*Sardina pilchardus*) and Allis shads (*Alosa alosa*) at the Aquarium de la Rochelle, France. Credits: Leandra Hamann 2020.*

5.1.   Introduction

An alternative way to find suitable biological models besides the identification of common traits due to convergent evolution (Chapter 4), is the selection based on similarities. The requirements of the initial technical problem are matched to the solutions identified in nature, i.e., the technical requirements of washing machines are matched to suspension feeding mechanisms. Therefore, it was first necessary describe the state-of-the-art of washing machines, the composition of the effluent, and available washing machine filters.

5.1.1.   State of the Art: Washing Machines and MPs Filters

The use of washing machines is common in the European Union (Lasic, 2014). In Germany, 96% of the households owned one in 2007 and washed 164 to 234 times annually (Lasic, 2014). The typical European washing machine is front loading (Figure 9A) and has a standardized size of 85 cm in height, 60 cm in width, and 60 in depth. A large part of the inner space of washing machines is used for the drum and additional room for it to swing during the spinning cycle. The remaining space is used for valves, pipes, the detergent drawer, and a coarse filter to protect the pump by retaining stones or coins (Masselter *et al.*, 2022). This leaves an available space of an averaged 34 cm in height, 21 cm in width, and 16 cm in depth for an additionl filter (own measurements in four models).

During washing, fresh water is let through the detergend drawer into the drum. Depending in the washing programme, it takes usually two to three washing cycling. Afterwards, the implemented pump transports the effluent out of the drum and into the waste water system with a pressure of around 0.1 to 0.15 bar (for example, Miele PWM 908 DV/DP). Depending on the washing load, type of programme, and washing machine model, the amount of water varies between 20 l and 120 l but is around 60 l in most washing programmes in Germany (Pakula & Stamminger, 2010). There are typically two to three pumping cycles in one washing programme, of which each can have a maximum volume flow of up to 5 l/min and a maximum flow velocity of 0.5 m/s (pipe diameter of 20 mm; own measurements). The washing temperature is usually between 30°C and 60°C, with a maximum of 95°C (Lasic, 2014)

Fibre release from textiles (Figure 9C) into the effluent depends on factors, such as the textiles' composition, age and structure, washing machine type, and washing machine programme (Schöpel & Stamminger, 2019; Zhang *et al.*, 2021). Textile fibres are made from natural sources, e.g., cotton, flax, wool, silk, cellulose, and viscose, or made from plastics, e.g., polyester, polyamide, or polypropylene (Zhang *et al.*, 2021). MPs fibres have a maximum length of 15 mm and a length-to-diameter ratio of >3 (Zhang *et al.*, 2021). Washing machines remove stains, oils, greases, and dirt, such as sand, dust, pollen or hair from clothing and other textiles. Dirt that ends up in the effluent could affect the MPs filter performance by blocking the

filter mesh. Additionally, detergents can increase clogging because they contain insoluble ingredients, such as zeolites. This is not a problem for liquid or gel detergents, but powders can contain up to 20% of zeolites (Schöpel & StammINGER, 2019).
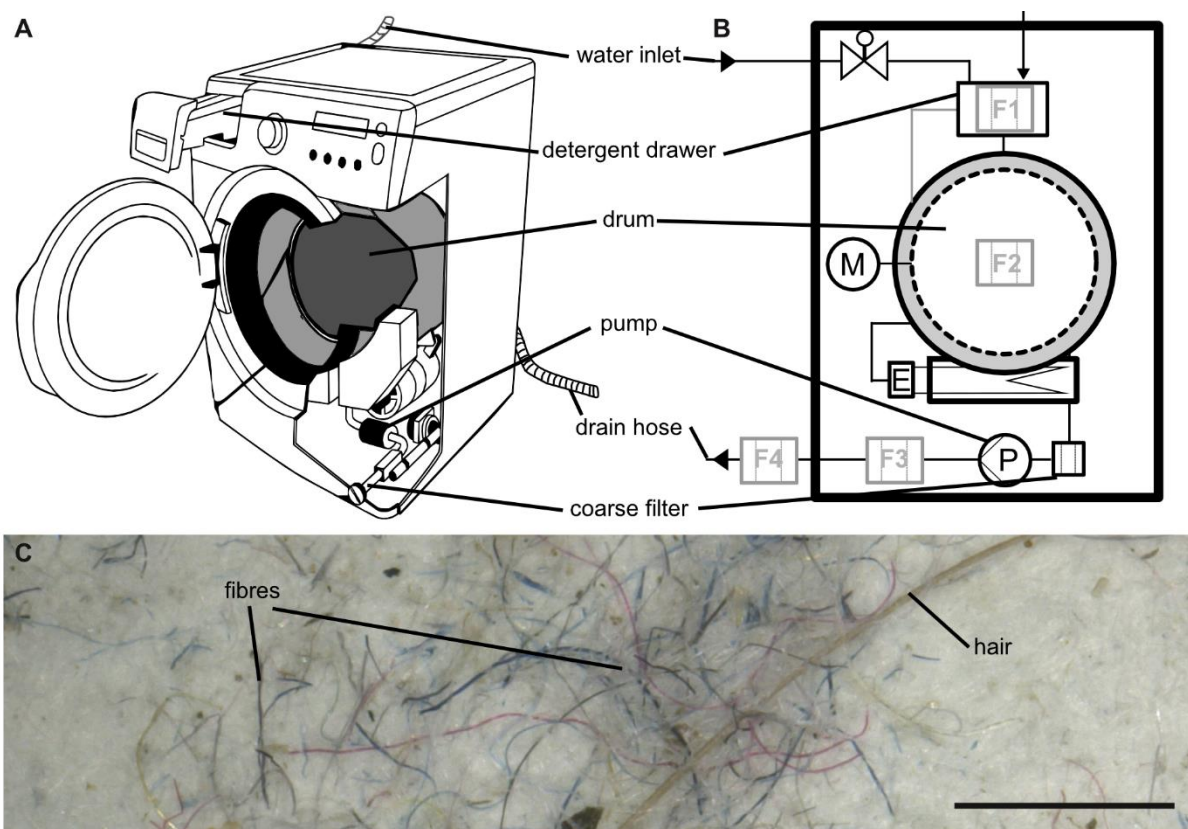
Figure 9: Washing machines are the application for the biomimetic filter module. A) Schematic drawing of a front–loader washing machine (adapted from HOMETIPS®). B) Simplified process flow sheet of a washing machine with the position of the coarse filter and possible installation positions for MPs filters, such as in the detergent drawer (F1), within the drum (F2), after the pump inside the housing (F3), or connected to the drain hose outside the housing (F4, compare to Table 3). C) Filtered washing machine effluent with fibres and other dirt, such as hair (scale = 1 mm).

Scientists, engineers, and product developers have started designing MPs filters for washing machines with nine products currently available (Table 3). The Cora Ball® and GuppyFriend® are atypical filtration devices because both are used in the drum together with the laundry (Figure 9B, F2). The others are dead-end filters that retain the fibres on the surface of a filter medium. Dead-end filtration is one of the two major surface filtration mechanisms in technical solid-liquid separation (Sutherland, 2005, 2008). The filter medium of dead-end filters is positioned perpendicular to the feed of particles within a liquid, i.e., a suspension. All particles that are larger than the mesh size are retained at the surface. This mass fraction is called the retentate, while smaller particles and the clean fluid pass through the filter medium. This is called the permeate (Figure 10A). Cleaning is required to remove the retentate from the filter medium to prevent clogging. In cross-flow filtration, the feed flows parallel to the filter medium.

The crossflow induces a shear force close to the filter medium that move particles along the surface and decreases particle deposition (Di, Martin, & Dunstan, 2021). This reduces the amount of retentate, delays clogging, and increases particle concentration in the concentrate, retrieved at the end of the cross-flow filtration process (Figure 10B).

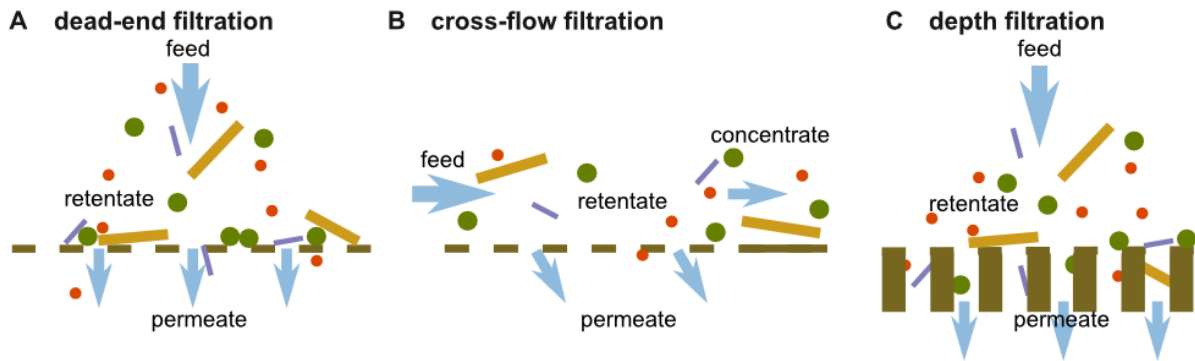Figure 10: Comparison of fluid flow and particle retention in two types of surface filtration methods, A) dead-end filtration and B) cross-flow filtration, and C) depth filtration.

The Planet Care filter utilizes a combination of dead-end and depth filtration in which the fibres are retained within the porous filter medium (Figure 10C). The mesh size ranges between 100 μm and 1.8 mm. Six filters are designed to be connected to the drain hose outside the washing machines (Figure 9B, F4) and can be retrofitted to all models. Cleaning intervals of the filters range from every 3 washes up to every 15-20 washes. The AEG Microplastic Filter is designed to fit two models by AEG and sits in the detergent drawer (Figure 9B, F1). It gives a light signal when manual cleaning is required. The maximum filtration efficiency is around 90% in the Filtrol 160 Lint Filter and the FiberCatcher™. However, this information is provided by the manufacturers and has not yet been confirmed by independent institutions. The price for the retrofit solutions varies between 30€ and 282€ (Table 3).

User acceptance is an relevant factor that might influence product design, handling, and therefore the effectiveness of MPs filters. Four filters were tested privately during the thesis (Table 3). The Cora Ball® and the Guppyfriend® require consequent and correct usage because they must be added to the drum before each wash and require manual cleaning afterwards. Additionally, the Cora Ball® has a relatively low filtration efficiency that might lower the long-term motivation of the user. The first two versions of the Planet Care filter seemed to be made from cheap material, which led to the impression that the filter itself might release MPs and not contribute to an overall positive effect. Even though the Planet Care filter has a comparable long service time until the filter medium is clogged, it must be replaced every few weeks to months. Therefore, the manufacturer offers to refurbish and recycle filter media that are sent back to Ljubljana through the subscription for a return-and-reuse service. This system is advantageous regarding a circular economy but requires high user commitment. The AEG

Microplastic Filter was observed to have a fine mesh, which led to a built-up of effluent in the drain hose. It did not work with powder detergent, fibres seemed to stick to the cleaned clothes and were not washed off, which led to frustration for the user.

At the start of this thesis, no biomimetic approach existed to develop MPs filters for washing machines specifically. In 2022, the cross-step filtration process inspired from the American paddlefish, initially described by Sanderson et al. in 2016 (Sanderson *et al.*, 2016), has been adapted by Masselter *et al.* (2022) to improve the coarse filter for MPs fibre retention in washing machines. In their study, two filter types were 3D-printed and tested with ground pepper particles (N = 5) to observe particle behaviour in the filter and determine filtration efficiency. As far as I know, the filter is still in the concept phase, and problems need to be solved, such as removing particles from the filter element.

A biomimetic filter will have to separate MPs fibres from other waste particles and water, or separate all particles from water. It should be small to fit into the washing machine housing (Figure 9B, F3), not add additional drag for the pump, and withstand a specific volume flow and flow velocity. It should retain >80% of fibres larger than 100 µm to be able to compete with other washing machine filters (Table 3 and Anthony *et al.*, 2020). It is estimated that washing machine filters must work in the presence of around 30 g of potential solids when using powder detergents and around 10 g when using liquid or gel detergents (Schöpel & Stamminger, 2019). These quantities are relevant for the size of the filter, its 'dirt-holding' capacity, and cleaning intervals (Sutherland, 2008). If powder detergents are to be used, the filter needs to be three times larger or cleaned three times more often. In later design stages, the biomimetic filter should also sustain temperatures up to 90°C, alkaline detergents, and a wet or moist environment. The filter would need to be in a position which is easy to reach for the user when the disposal of MPs is required. Ideally, the filter could be added to the position of the already installed coarse filter (Figure 9A) to retrofit old washing machine models. A marked-ready product should be cost-efficient, user-friendly, and eco-friendly.

Table 3: Products for MPs reduction in washing machines that are currently available. Installation positions within a washing machine (F1–F4) refer to Figure 9. The filtration efficiency is retrieved by the product homepages respectively or by the study of De Falco *et al.*, (2021), indicated by *. Remarks based from own experience are from Leandra Hamann and Christian Grünewald.

Name	Description	Filtration efficiency	Remarks based on own experience
Cora Ball® (ca. 39 €)	Ball with hooks that catches fibres in the drum (F2), cleaning required after each wash	26%* of fibres >100 µm, 31%	Does not 'feel' effective, users might not regularly use it
Guppyfriend® (ca. 30€) by Langbrett	Clothes are in a washing bag that retains fibres in drum (F2), cleaning required after each wash	54%*, 79% - 86%	Requires high user interaction
Planet Care (ca. 60€)	Cartridge filter with porous filter medium installed at drain hose (F4), clogged after 15-20 washes	31-64%* depending on filter type and pore size, best retention for fibres > 771 µm, 90%	Cheap material, separation medium itself might release fibres, subscription system to recycle the cartridge
Microfiber Filter (ca. 42€) By girlfriend collective	Mesh steel filter with 200 µm mesh size installed at drain hose (F2), cleaning required after 3 washes	na	-
Filtrol 160 Lint Filter (ca. 150€) by Fa. Wexco	Bag filter with 100 µm mesh size installed at drain hose (F4), cleaning required after 8-10 washes	89%	-
Lint LUV (ca. 178€) By Environmental Enhancements	Mesh steel filter with 1.8 mm mesh size installed at drain hose (F4), cleaning required after 10-15 washes	85%* of fibres >100 µm; 65%* of cotton fibres, 74%* of synthetic fibres, 65-100%	-
FiberCatcher™ (ca. 12€) By Grundig	Mesh 'basket' in detergent drawer (F1), only available for two Grundig models	90%	-
Gulp® (ca. 282€)	NA, installed at drain hose (F4), cleaning required after 10-15 washes	na	-
AEG Microplastic Filter (ca. 89€)	Cartridge filter with mesh installed at drain hose (F4), light signal if cleaning is required	90% for particles >45 µm	Water builds up, does not work with powder detergents, fibres stick to clothes

5.1.2.   Selection of a Biological Model

I matched the technical requirements of the washing machine to the SFMs presented in Chapter 3 (Table 2) and identified analogue traits to select a biological model. The geometry should be flat or funnel-shaped in a pipe, the desired retained particle size should be 100 µm to 10 mm, the driving force should be passive, pumping, or forward movement, and SFMs should work with a water velocity of >1 cm/s. I found ram-feeding fish meet all those criteria. Their gill arch system (GAS) is composed of gill arches (GA) with elongated gill rakers (GR) and denticles, and forms a cone-shaped separation medium within the buccal cavity (Figure 12). While swimming forward with an open mouth, a tangential flow transports the food particles towards the oesophagus, and the cleared water exists between the GA and under the opercula. The underlying filtration principle in these fishes was described as cross-flow filtration (Sanderson & Wassersug, 1993; Storm *et al.*, 2020). Even though the general principle of technical cross-flow filtration and the SFMs in ram-feeding fish have similarities, details of the functional morphology and its influence on fluid dynamics and particles separation are still lacking. Therefore, we used digital microscopy, micro-CT scans and conducted a video analysis of five ram-feeding fish species within Scombridae and Clupeidae to describe the filter-feeding morphology, calculate filtration parameters, and identify function-specific traits that are relevant in cross-flow filtration.

5.2.   Methods

We analysed Atlantic herrings (*Clupea harengus*, N = 7), Atlantic pilchards (or sardines *Sardina pilchardus*, N = 11, Figure 11A), Atlantic anchovys (*Engraulis encrasicolus*, N = 11, Figure 11B), Atlantic mackerels (*Scomber scombrus*, N = 7), and Indian mackerels (*Rastrelliger kanagurta*, N = 7, Figure 11C). The fishes were ordered fresh from a local delicatessen shop and immediately frozen one day after capture.

5.2.1.   Morphometric Analysis

A set of 20 parameters was used to describe fishes standard length, head length, and details of the GAS, i.e., length of the five GA and each branchial, length, width, height and distance of GR, and position, length and distance of denticles (Figure 11D). Additionally, the open area ratio was determined in a black-white image by measuring the area occupied by GR and denticles compared to the open area where water flows through. Larger structures were photographed with a Nikon D850 (Macro lens Nikon AF-S Micro NIKKOR 60 mm 1:2.8G ED), while smaller structures were analysed with a digital microscope (Keyence VHX-700F, Ver 2.3.8.2, lens VH-Z20R RZx20-x200, Software Version 1.93). After dissection, the GAs were fixed in 5% formaldehyde and dehydrated in increasing ethanol concentration up to 70 % ethanol for long-term fixation.
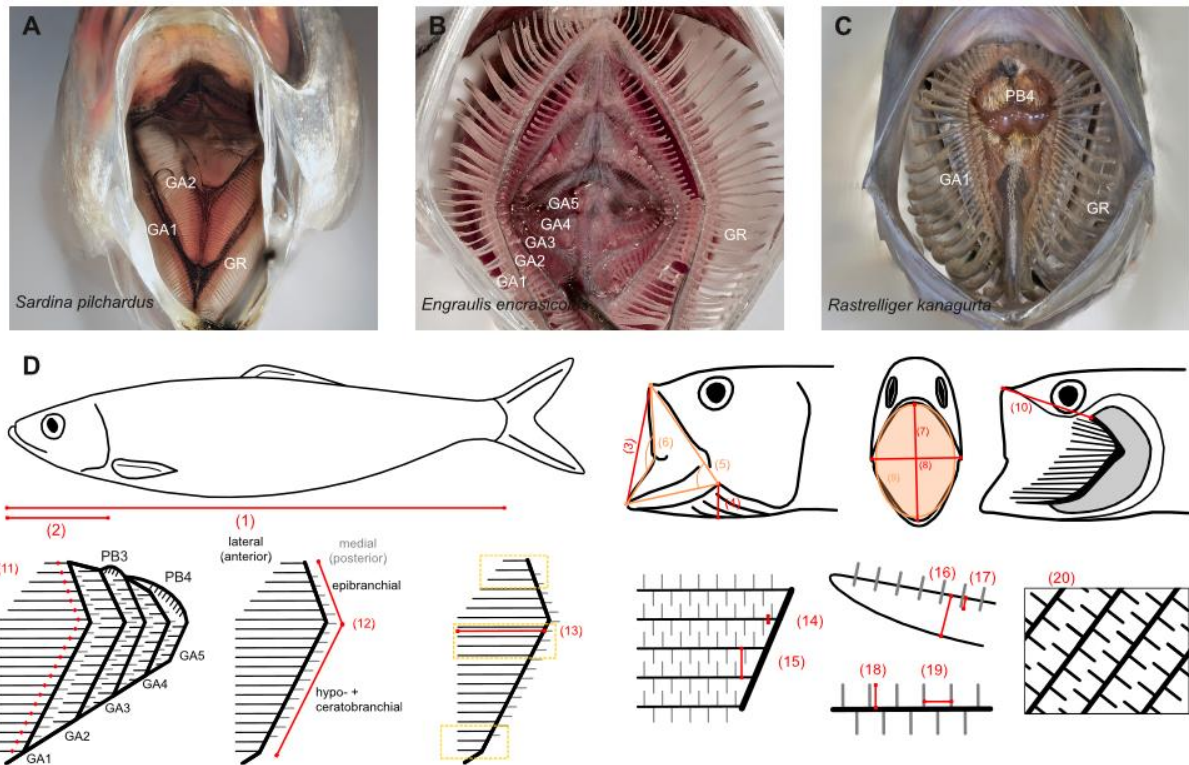
Figure 11: Morphology of ram–feeding fish and morphometric parameters. Frontal view into the mouth showing the gill arches (GAs) and gill rakers (GRs) of A) Atlantic pilchard (*Sardina pilchardus*, Walbaum 1792, B) Atlantic anchovy (*Engraulis encrasicolus*, Linnaeus 1758), C) Indian mackerel (*Rastrelliger kanagurta*, Cuvier 1816). Images not to scaled. Credits: Jens Hamann. Morphometric parameters: 1) standard length with open and closed mouth, 2) head length, 3) open mouth height (lateral), 4) branchiostegal height, 5) jaw angle, 6) lip angle, 7) open mouth height frontal, 8) open mouth width frontal, 9) open mouth area, 10) upper lip to epibranchial, 11) number of GR, 12) length of GA and pharyngobranchials (PB, only in Scombridae), 13) length of GR, 14) width of GR, 15) distance between GR, 16) height of GR, 17) vertical position of denticles on the GR, 18) length of denticles, 19) distance between denticles, 20) open area ratio.

5.2.1. Micro-CT Scans

One individual for each of the five selected ram-feeding species, was selected for micro-CT scanning to visualise the three-dimensional arrangement of the GAS in an open-mouth position. Before dissection, they were thawed in cold water for one hour. The head was cut from the body and pinned upwards in an open-mouth position onto Styrofoam. The samples were then fixed in 5 % formaldehyde, dehydrated in a series of ethanol concentrations up to 70 %, and stained with PTA. Afterwards, each head was scanned with the Bruker SkyScan 1173 at the Leibniz-Institute for the Analysis of Biodiversity Change in Bonn, Germany. The scans were reconstructed with NRecon (Version 1.7.5.9), and volume renders were created with Drishti (Version 2.6.4). Virtual cross-sections of the fish heads were made in the sagittal plane along the hyoid bone and in the frontal plane close to the epi-ceratobranchial joint on GA1 with view on the dorsal side of the GAS.

5.2.2. Video Analysis

Only four of the five species are currently held in public aquaria across Europe. On location, *S. scombrus*, *C. harengungs,* and *S. pilchardus* were filmed several minutes before and during feeding. Their usual food was reduced in size to increase the chance of filter-feeding (Crowder, 1985; Garrido *et al.*, 2007). Due to the travel restrictions during the Covid-19 pandemic, *E. encrasicolus* was filmed underwater by the aquarium curator with a GoPro. *R. kanagurta* is not held in captivity, so field footage in the Red Sea was obtained from amateur divers. The videos were only used for further analysis if the quality was good and the camera position fixed. The videos were analysed using ImageJ (Version 2.3.0) to measure head morphometrics in relation to standard length, swimming speed, and feeding behaviour.

5.2.3. Data Analysis and Statistics

The morphometric and video data were used to calculate the total filtration area, the open area ratio (open area divided by total filtration area), the leakiness for each GA (volume flow through the open area of one GA divided by the total open area), the fluid exit ratio (open filtration area divided by open mouth area), the minimum and maximum mesh size, the Reynolds number (inertial divided by viscous forces), and the volume flow rate through the open mouth. The data was analysed and visualised using the R programming environment (R Core Team, R version 4.2.2, 2022) and Scribus (Version 1.5.6.1). In addition to descriptive statistics of untransformed data, a principal component analysis (PCA) was performed on 19 selected traits to investigate their relationship (log-transformation of measurements, correction of size based on standard length, extraction of residuals). The first three principle components (PCs) described >75% of the variation and were chosen for further analysis. Their loadings were extracted and a the correlation matrix (based on Spearman rank test) was analysed to identify essential morphological traits that contribute most to PC1 to PC3. The difference of the jaw angle in the dissected individuals to the measurements in the videos, as well as the comparison of the swimming speed before and during feeding was tested for significance with a Kruskal-Wallis rank sum test (chi-squared) and a posthoc dunn test (method 'Holm').

5.3. Published Results

S. scombrus is the largest species of the analysed fishes with 169.4 ± 4 mm standard length and *E. encrasicolus* is the smallest with 97.9 ± 2.4 mm. Accordingly, GA1 is the longest in *S. scombrus* and the shortest in *E. encrasicolus* (Figure 12A+B). GA length decreases from anterior to posterior, i.e., from GA1 to GA5. In *S. pilchardus*, GA2 is longer than GA1. The two mackerel species *S. scombrus* and *R. kanagurta* have anterior and posterior GR on every GA except GA5. *C. harengus* and *E. encrasicolus* have posterior GR only on GA4 and GA5, and *S. pilchardus* has posterior GR only on GA4. GR are longest on GA1 in all five species. Within

one GA, the longest GR are on the ceratobranchial and the smallest are at the distal ends of the epi- and hypobranchial. The GR are extended towards the next anterior or posterior GA to close the gap between the GA and form a separation medium with the denticles. The denticles in *S. scombrus* and *R. kanagurta* are positioned on top of the anterior, blade-shaped GR on GA1. They are at regular distance, thin, and measure around 0.59 mm in length. On the shorter posterior GR of GA1 and GR on GR2, GR3, and GR4, the denticles vary strongly in size, and are irregularly arranged. Because GA5 has no GR, we assume that the hairy structures are teeth (Figure 12E). Additionally, two pharyngobranchials with teeth are visible at the scombrid species' dorsal side of the GAS (Figure 12C). The denticles of *C. harengus*, *S. pilchardus*, and *E. encrasicolus* are at regular distances, and denticle length remains similar across all GA. The calculated minimum and maximum mesh sizes (Figure 12C) are smallest in *S. pilchardus* with 0.007 mm² and 0.014 mm² and largest in *S. scombrus* with 0.113 mm² and 0.148 mm². In the clupeid species, the minimum mesh size is smaller than the maximum mesh size on all GA. In the scombrid species, this is only true for the anterior and posterior GR on GA1 and the posterior GR on GR2. Otherwise, the minimum mesh size is larger than the maximum mesh size (Figure 12D). During the dissection of the fish, mucus formation was observed close to the oesophagus in the scombrid species *S. scombrus* and *R. kanagurta* (Figure 12E).

The first three PCs explain 78.5% of the variance in the data with PC1 relating to overall geometry and size (highest loadings: GAS length, GR length on GA1, the length ratio of GA1 to GA5 (GA1-5 ratio), GR height to width ratio, filtration area, and head length), PC2 relating to filter medium and fluid flow (highest loadings: GR number, mesh size max, mesh size min, leakiness of GA1 and MO ratio), and PC3 relating to GAS symmetry (highest loadings: symmetry, mesh size ratio, fluid exit ratio, weight, and leakiness at GA1). The individuals of one species cluster into distinct groups with little overlap in the morphospace. While PC1 distributes the groups evenly, PC2 clusters the species into two groups that consist of *R. kanagurta*, *S. scombrus* and *E. encrasicolus*, and *C. harengus* and *S. pilchardus*. PC3 shows a higher spread of the individuals within each group and separates the two scombrids, *R. kanagurta* and *S. scombrus*, with the clupeid species in between them.

Because of the high number of combinations in the correlation matrix, only significant correlations with a correlation coefficient of $\rho > 0.70$ are described. For example, weight correlates positively with GAS length ($\rho = 0.7$), GAS length is positively correlated with GR length of GA1 ($\rho = 0.92$), and head length correlates positively with denticle length ($\rho = 0.83$). This shows that despite the correction for standard length, size plays a significant role in the feeding morphology. Additionally, the longer the GAS, the larger is the filtration area ($\rho = 0.7$), and the more cone-shaped and less cylindrical is the GAS ($\rho = 0.81$). The mouth opening is more oval-shaped in *C. harengus* and *S. pilchardus* and round in the other three species. The

more oval the mouth shape, the higher the GR number on GA1 (ρ = 0.73). GR number on GA1 negatively correlates with minimum (ρ = -0.74) and maximum mesh size (ρ = -0.80).

In the video analysis, the swimming velocity was measured in 20 *S. scombrus* (Figure 12F), five *R. kanagurta*, nine *C. harengus*, 15 *S. pilchardus*, and 24 *E. encrasicolus* indiviuals during feeding with an open mouth position. The mean swimming velocity ranges between 0.34 m/s in *C. harengus* up to 0.5 m/s in *S. scombrus*. Based on the standard length, the Reynolds number around the fish ranges between 35,000 in *E. encrasicolus* and 137,000 in *S. scombrus*. At the mouth opening, the Reynolds number ranges between 4,100 in *S. pilchardus* and 15,600 in *R. kanagurta* and around the denticles, the Reynolds number ranges between 30 in *E. encrasicolus* and 300 in *S. scombrus.* Based on open-mouth area and swimming velocity, the volume flow rates range between 1.9 l/min in *S. pilchardus* and 23.5 l/min in *R. kanagurta*.
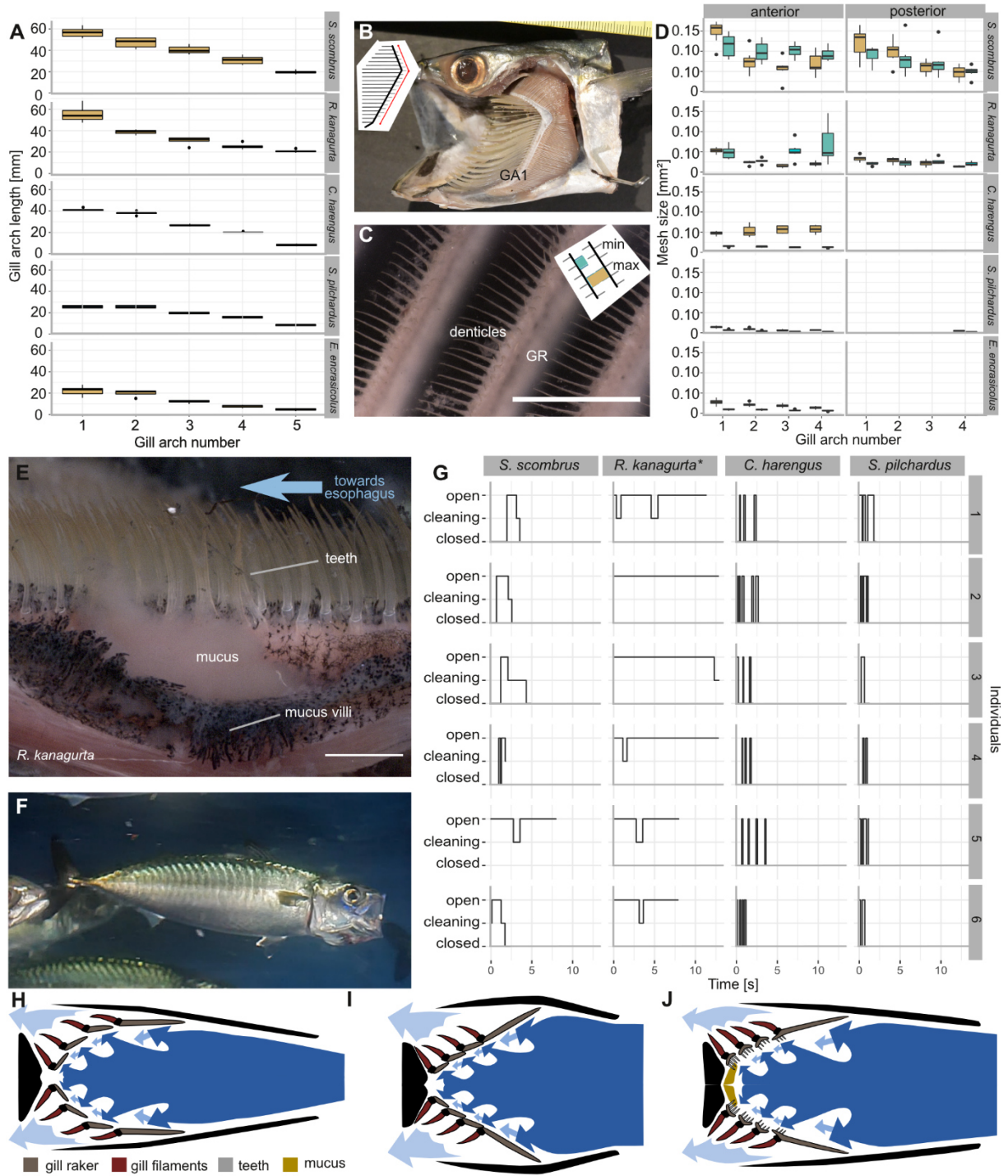
Figure 12: Results of morphometric and behavioural analysis of five ram–feeding fish species. A) Morphometric data of gill arch length. B) Picture of gill arches in *R. kanagurta*. GA length was measured as depicted by the red line. C) Picture of denticles in *R. kanagurta*. Minimum mesh was calculated based on denticle length and denticle distance, maximum mesh size was calculated based on GR distance and denticle distance. D) Morphometric data of mesh sizes. E) Mucus, mucus villi and teeth in front of the oesophagus of *R. kanagurta*. F) Filter-feeding *S. scombrus* in an aquarium. G) Results of filter-feeding behaviour of *R. kanagurta* in the field (*) and the other three species in the aquaria. Schematic drawing of three identified morphotypes that represent: H) *C. harengus* and *S. pilchardus*, I) *E. encrasicolus*, and J) *R. kanagurta* and *S. pilchardus*.

The feeding behaviour was observed in six individuals of *S. scombrus*, *R. kanagurta*, *C. harengus*, and *S. pilchardus* (Figure 12G). *C. harengus* and *S. pilchardus* show frequent mouth opening and closing with an average opening time of 0.17 s and 0.27 s, respectively. The average opening time in *S. scombrus* and *R. kanagurta* is 0.53 s and 3.7 s. In both species, cleaning was observed after the mouth was held open. Cleaning lasted 0.25 s in *S. scombrus* and 0.71 s in *R. kanagurta*.

5.4.   Discussion

Three morphotypes are described based on the GAS and buccal cavity in the five ram-feeding species (Figure 12). Within the clupeid species, *S. pilchardus* and *C. harengus* are similar, with an oval-shaped mouth opening and a narrow buccal cavity leading towards the GAS (Figure 12H). In *E. encrasicolus*, the mouth is wide open with a short distance from the round mouth opening to the cone-shaped GAS (Figure 12I). The two scombrid species (Figure 12J) have a round mouth opening, and the distance from mouth opening to the GAS is longer than in *E. encrasicolus.* Teeth and mucus were only identified in these two scombrid species. In all three morphotypes, the GAS system is cone-shaped and angled towards the incoming flow, a typical characteristic for cross-flow filtration in ram-feeders (Cheer, Ogami, & Sanderson, 2001; Paig-Tran *et al.*, 2011; Hamann & Blanke, 2022). However, as the water flows posteriorly and exits through the permeable filter medium, the angle of the GAS becomes more perpendicular, which suggests a transition to dead-end filtration close to the oesophagus. Therefore, we hypothesise that these ram-feeding fish use a combination of cross-flow and dead-end-filtration, which was also suggested for the ram-feeding American shad (Storm *et al.*, 2020). This is also supported by the fact that we observed frequent cleaning, which disagrees with the hypothesis that cross-flow filtration is the only mechanism in the fish mouth.

Based on our results, we can identify morphological adaptations to decrease hydrodynamic drag. The protruded lips and the open operculum form a pipe-like structure to guide the water towards and through the cone-shaped GAS system. We assume that the pipe structure of the buccal cavity directs the flow towards the separation medium, breaks down large vortices from the turbulent environment, and induces a laminar flow regime at the filter medium, which might be more efficient in overcoming its hydrodynamic resistance (Werth, 2004). Hence, the mesh size could evolve smaller and denser in fishes with a longer pipe to retain smaller particles. All GR in the clupeid species and the GR on GA1 in the scombrid species are blade-shaped with length-to-width and height-to-width ratios similar to other filter-feeding species (Gibson, 1988; Storm *et al.*, 2020). The height-to-width ratio of the GR cross-section is also described as the fineness ratio, which describes the geometry of streamlined bodies to minimise drag (Vogel, 1996) and ranges between 2 and 8 (Blake, 1983; Williams & Kooyman, 1985; Ahlborn, Blake, & Chan, 2009). The fineness ratio of the GR on GA1 in the ram-feeding species is between

2.6 and 7.2 and lies within the optimal range for streamlined bodies. High open area ratios and large filtration areas also reduce the resistance to flow. The filtration area is larger than the mouth opening area (fluid exit ratio), which indicates that there is no increased drag within the mouth that would lead to a pronounced bow wave in front of the fish (Brooks et al., 2018). However, we did not include the drag posed by the gill filaments during gas exchange as each GA has two rows of gill filaments (Strother, 2013), or the friction drag of surfaces, which becomes more relevant at lower Reynolds numbers and should be included in more complex models (Cheer et al., 2001).

It remains unclear if the different denticle shapes influence mesh size. Mesh size is calculated based on the assumption of evenly distributed, rectangular, stiff meshes (Sutherland, 2008; Collard et al., 2017). However, denticles from neighbouring GR do not touch and form closed meshes. The role of denticles in mesh formation is even more unclear in the two scombrid species. Their denticles and teeth are directed into the buccal cavity, differ in length, and are not evenly spaced, except on GR on GA1. Particles might be retained within this brushy structure or mucus, which is more typical for depth filtration (Figure 10). Alternatively, the surface structures could form vortices, thereby inducing particle capture more similarly to cross-step filtration in paddlefish (Sanderson et al., 2016) or to the ricochet filtration in manta rays (Divi, Strother, & Paig-Tran, 2018).

In the biomimetic working process, the morphological diversity described in the morphotypes can be used to design parametric models and identify the best solution to retain MPs fibres in washing machines. Compared to the market-ready products (Table 3), a cross-flow filter would be unique and might have advantages because it reduces clogging of the filter medium. However, more morphological traits need further investigation to determine their function and whether they have to be integrated into biomimetic filter modules to increase MPs fibre retention.
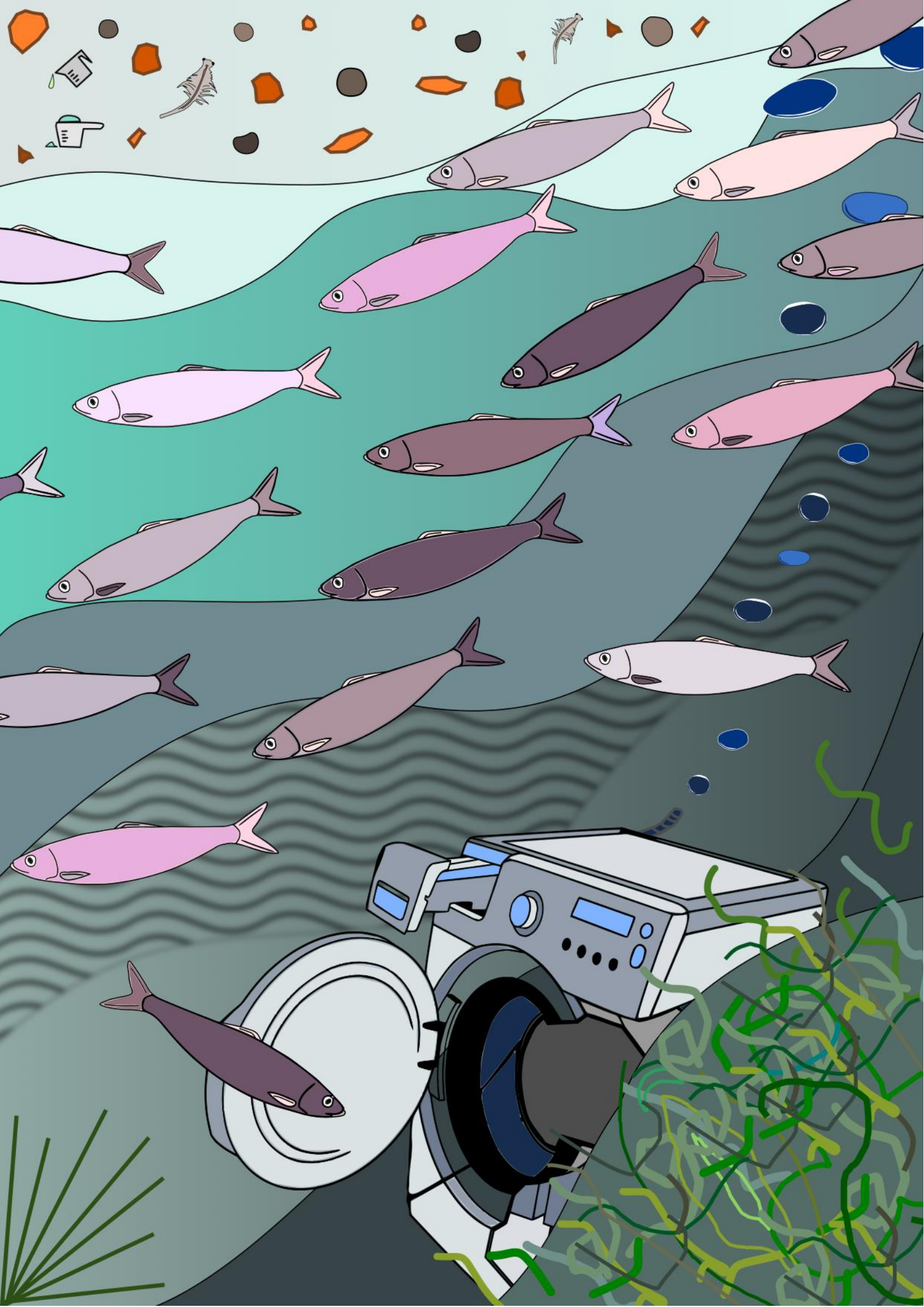
6. Fluid Flow in Ram-Feeding Fish

This chapter presents unpublished data.

Contributions:

Leandra Hamann: conceptualization and methodology, sample preparation, conduction of experiments in the small and large water tunnel, data analysis and visualization

Kristina Schreiber (master thesis*): water tunnel assembly, conduction of experiments in the large water tunnel

Christian Grünewald: water tunnel assembly

Hendrik Herzog: Water tunnel design and assembly, programming of Python scripts for semi-automatic particle tracking

*daily supervisor: Leandra Hamann

Previous page:

Collage of the graphics used in figures in this thesis. Credits: Leandra Hamann 2023

6.1.   Introduction

Based on GAS morphology, we assume that the filtration mechanism in ram-feeding fish combines cross-flow and dead-end filtration. The parallel inflow towards the anterior gill arches (GA) and gill rakers (GR) induces cross-flow filtration. The perpendicular flow towards the posterior GAS close to the oesophagus is characteristic for dead-end filtration (Figure 13A). In technical filtration processes, the angle of the filter medium towards the flow, which we define as the angle of attack α, is typically 90° in dead-end filtration and 0° in cross-flow filtration (Sutherland, 2008). The conically tapered geometry of the GAS from anterior to posterior suggests a transition from dead-end to cross-flow filtration. For the purpose of this thesis, I will define the filtration process with 0°< α <90° as semi-cross-flow filtration (Figure 13A). In models for particle deposition in cross-flow filtration, it was found that the probability of particle rolling increases with increasing lateral crossflow velocity parallel to the filter medium and vice versa (Di *et al.*, 2021). Similarily, I hypothesize that a decrease in the angle of attack increases the chance of particle rolling. At higher angles, the crossflow velocity is less parallel to the filter medium and the force in direction of the permeate increases, which increases the change of particle deposition (Figure 13). Similar to cross-flow filtration, the particles in semi-cross-flow filtration can either be retained on the surface of the filter medium as retentate, collected in the concentrate, or pass the filter medium and end up in the permeate. The volume flow is diverted into the clean permeate and particle-loaded concentrate.
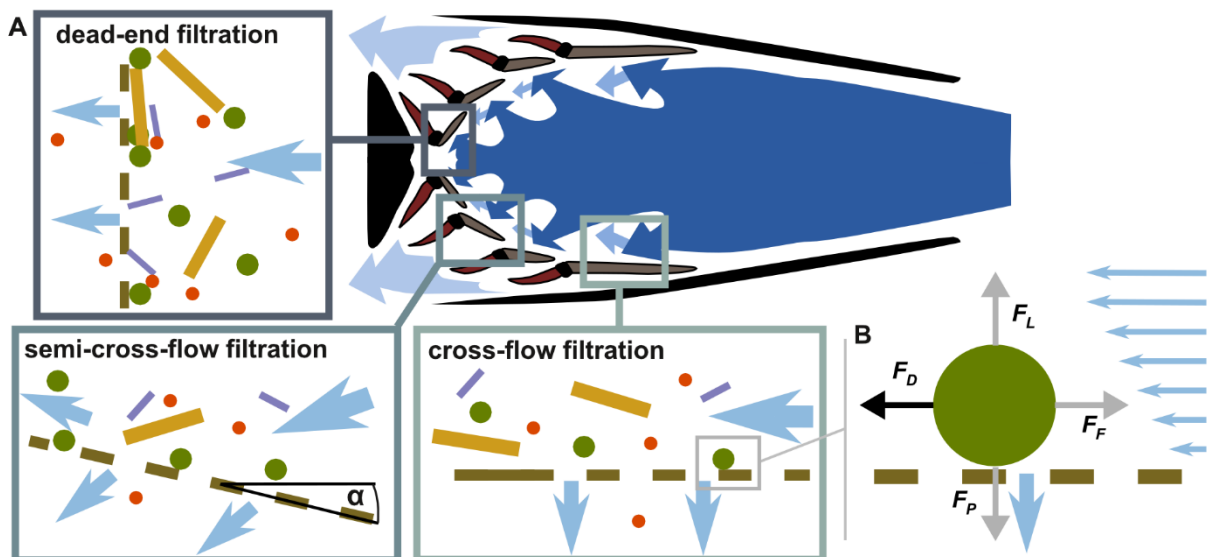
Figure 13: Types of filtration process within the buccal cavity as suggested based on the morphotypes, here based on *C. harengus* and *S. pilchardus*. A) In the anterior part of the GAS, the separation medium is parallel to the inflow, which induces cross-flow filtration. Towards the posterior GAS, the angle of attack α of the separation medium increases towards 90°, indicating dead-end filtration. We describe the filtration process at angles between 0° and 90° as semi-cross-flow filtration. B) Simplified models of forces acting on a particle in cross-flow filtration: drag force (F_D), lift force (F_L), friction force (F_F), and force in direction of the permeate (F_P). Blue arrows indicate the magnitude of crossflow velocity

close to the filter medium. The larger the lateral velocity, the higher the probability of rolling in direction of F_D. Modified from Di *et al.*, (2021).

Ram-feeding fish are large shoaling fish (Alder *et al.*, 2008) that use their forward motion to induce a volume flow through the GAS (Sanderson & Wassersug, 1993). Factors, such as particle size and concentration, influence feeding behaviour and, as observed in the behavioural experiments, the environment of the aquaria pose an additional influence (Chapter 5.4). This makes it challenging to investigate the natural feeding position of the GAS and measure the angle of attack α, which is crucial to identify cross-flow, semi-cross-flow, or dead-end filtration. Therefore, we used a combination of methods to investigate our hypothesis of semi-cross-flow filtration in the GAS of five ram-feeding fish species. First, we used micro-CT scand to describe the three-dimensional arrangement of the GAS and approximate α of the GR. The same fish heads were positioned in a water tunnel to visualize streamlines with black ink and observe particle behaviour. In order to test our hypothesis that a smaller α leads to particle rolling of the filter medium, we analysed the behaviour of natural and artificial particles after contact with a filter mesh with different mesh sizes.

6.2.   Materials and Methods

6.2.1.   Micro-CT Scans and Angle of Attack

The frontal cross-section of the Micro-CT scans (Chapter 5.2.1) were used to measure α in ImageJ (Version 2.3.0). The two sides of the angle were set parallel to the GR of each GA, and the hyoid bone as the centre line of the fish. The measurements of each side were added and divided by two to account for asymmetries in the head due to preparation artefacts.

6.2.2.   Visualization of Streamlines in a Water Tunnel

The same fish heads that were prepared for micro-CT scanning were also used to analyse the flow through the GAS under laminar flow conditions in a water tunnel (Supplementary Information 10.1.2). Therefore, they were mounted on a streamlined holder in the test section facing the incoming flow (Figure 14). The flow velocity was set to 6.5 cm/s because this shows the best laminar conditions in this water tunnel. The black ink was injected at the middle axis of the fish's mouth opening. A camera (Nikon D850, Macro lens Nikkor AF-S 24-120 mm 1:4 G ED) was mounted outside the tank to film the right side of the fish. Four dissection steps were proceeded: 1) intact head, 2) removal of right operculum and replacement with a transparent foil, 3) removal of left operculum and replacement with a transparent foil, and 4) removal of the right GA1 to be able to look inside the buccal cavity (Figure 14C-F). For each dissection step, three videos were taken for each position. The ink streamline was checked for laminarity between each video without the fish. A zoom body tube (Navitar 1-60135) combined with a coupler (Navitar 1-6010) and a c-mount (LMScope) to fit the Nikon D850 camera were

used to take close-up videos of the GAS at the entrance of the mouth opening, the outside of the GR of the right GA1, and the inside of the GR of the left GA1. Additionally, fluid flow around the teeth of GA5 and pharyngobranchial in front of the oesophagus was recorded for the two scombrid species. Except for the outside of the GR on the left GA1, all positions were also filmed when brine shrimp eggs (*Artemia salina*, 1.09 g/cm³) were introduced in the water tunnel to analyse their velocity in comparison to the velocity when no fish was in the tank and identify different particle behaviours: free (no contact with surfaces), out (particles leaves the GAS through the mesh), roll (contact with a surface and particle keeps moving), or stop (contact with a surface that leads to no further movement).
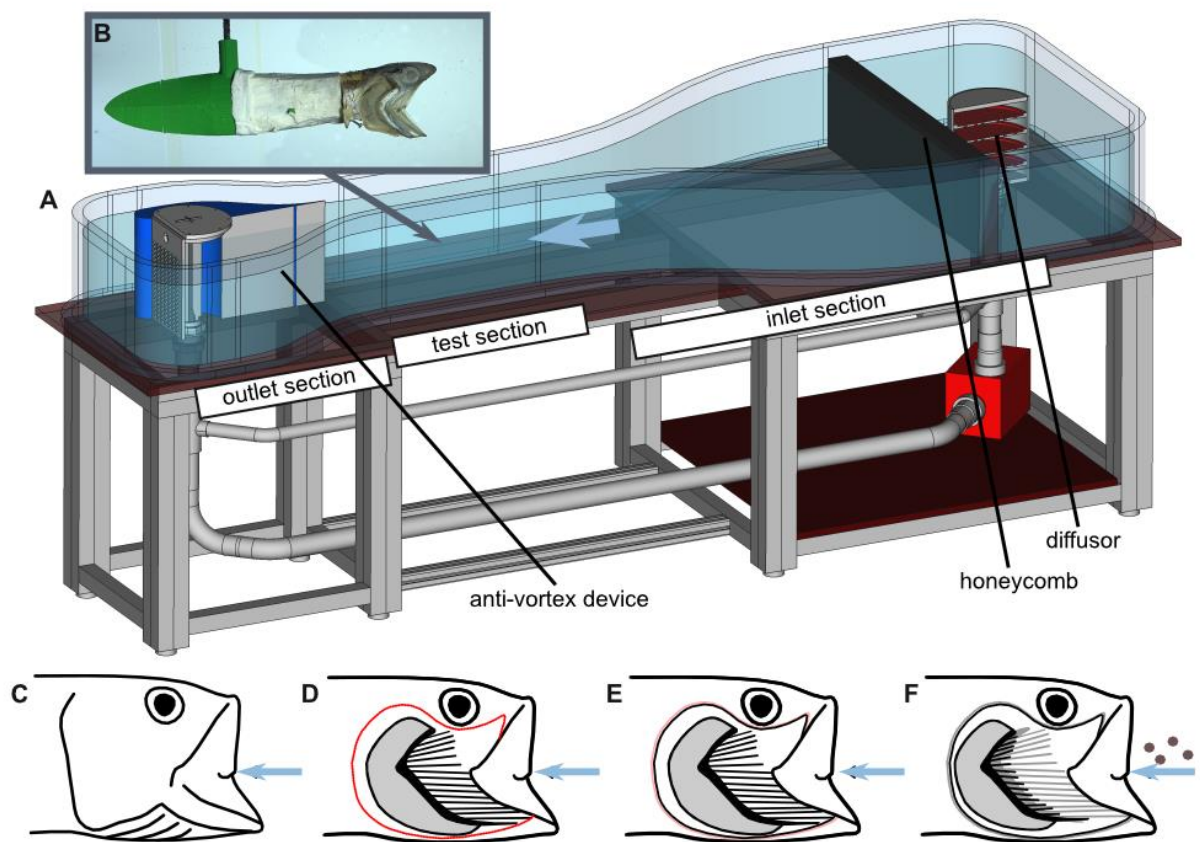
Figure 14: Water tunnel set up. A) General design of the circular water tunnel with inlet, test and outlet section (for detailed setup, see Supplementary Information 10.1.2). Direction of flow is indicated by the blue arrow. B) Fish head of *E. encrasicolus* positioned on a streamlined object holder in an open mouth position. Videos were taken of the ink flowing into C) the intact fish head, D) the head with removed right operculum and replacement with a transparent foil, E) the head with removed left operculum and replacement with a transparent foil, and F) removal of the right GA1. After the last dissection step, brine shrimp eggs were introduced into the tank to observe particle behaviour.

The videos were visually analysed, and the ink streamlines were described by direction, distribution, and diffusion for each dissection step of each species. For the presentation in this thesis, single frames were extracted that are exemplary for the recorded videos and show all aspects of pbserved ink motion. The close-up videos of brine shrimp eggs were analysed using

ImageJ (Version 2.3.0) and the Manual Tracking plugin. The average egg size (0.242 mm) was used to set the scale in the videos and approximate the velocity of the moving eggs. The velocity was only measured for particles within the focal plane to ensure that the interaction with the focused structures was tracked.

6.2.3.   Influence of Angle of Attack on Particle Retention

In order to test the influence of α on particle retention, an experimental setup was designed in which a filter medium can be positioned at angles from 0° (parallel) to 90° (perpendicular) in increments of 10° towards the unidirectional flow in a small, circular water tunnel (Figure 15A+B). Only angles from 10° to 60° were studied because this is the range measured in the micro-CT scans of the GAS. Three filter media with a mesh size of 53 µm, 100 µm, and 300 µm were selected, and four types of particles were tested: brine shrimp eggs (0.242 ± 0.019 mm) and adults (6.112 ± 0.993 mm) to represent natural food sources, and polyamide particles (median diameter 130 µm,) and flock fibres (2 mm length, polyamide) to represent MPs particles (Figure 15C, see Supplementary Information 10.1.3 for specifications of the test particles). The flow velocity was set to around 11 cm/s, and a camera (Nikon D850, Macro lens Nikkor AF-S 24-120 mm 1:4 G ED) was positioned outside the tank to film the particle encounter on the filter medium. After each rotation, the camera's focal plane was adjusted, and the scale was recorded by filming a ruler close to the filter medium.
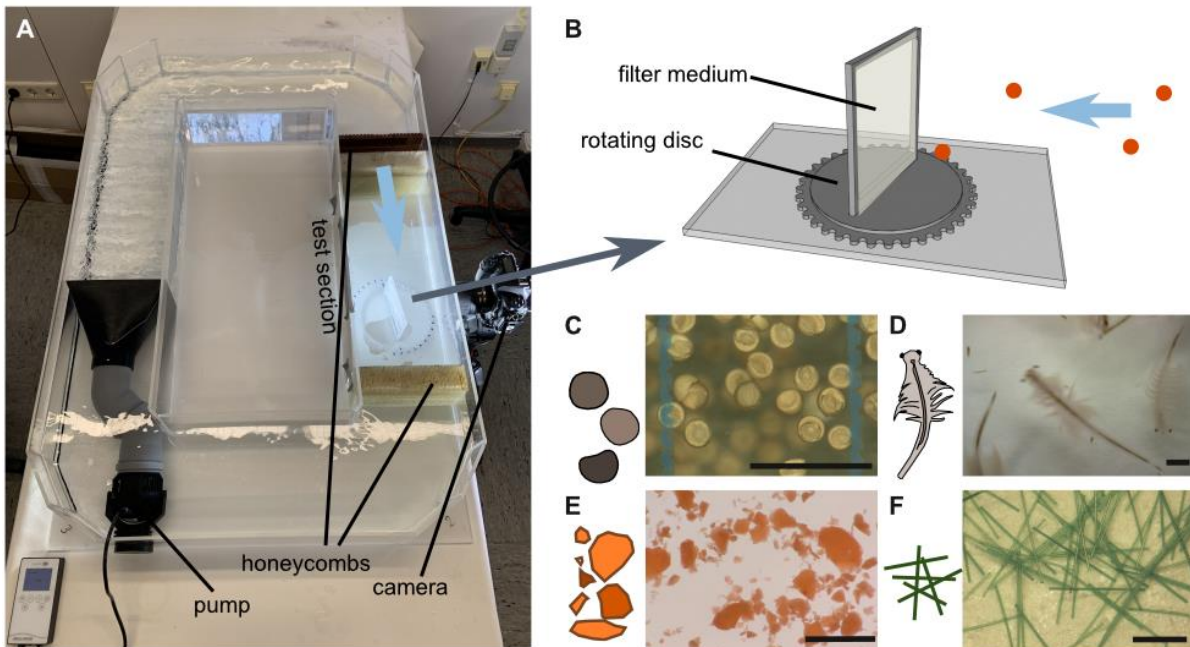
Figure 15: Experimental setup to study the interaction of particles and filter medium with varying α. A) Small circular flow tank with a pump, honeycombs before and after the test section, and the holder for the filter medium. B) The holder consists of a plate with a rotating disc with 10° increments and a frame that holds the filter media with mesh sizes of 53 µm, 100 µm, and 300 µm across the passing fluid. Four particle types were tested: C) brine shrimp eggs, D) brine shrimp adults, E) polyamide particles, and 2 mm flock fibres (for specifications, see Supplementary Information 10.1.3). Scale = 1 mm.

The videos of the brine shrimp eggs, adults, and fibres were analysed manually with ImageJ (Version 2.3.0) and the Manual Tracking plugin. A fixed point was selected on the particles to track their motion. Each particle that came in contact with the mesh was tracked when it entered the recorded video section and ended when it was out of frame. The frame in which the particles touched the mesh was noted as "contact". Before further analyses, the number of frames was reduced to a maximum of 20 frames before and after the contact frame. The MPs particles were semi-automatically analysed. Therefore, only the frame of contact and the position of the particle within the frame were noted. Afterwards, Python (Python Software Foundation, Version, script by Dr. Hendrik Herzog) was used to automatically track the pre-identified particles and extract the particle velocity in each frame to a maximum of 20 frames before and after the contact frame.

6.2.4. Data Analysis and Statistics

Based on the extracted particle velocity in a maximum of 40 frames for all four particle types, a Boltzmann sigmoidal curve (Motulsky & Christopoulos, 2003) was fitted to the data using Python (Python Software Foundation, script by Dr. Hendrik Herzog). Based on the fit, the average velocity before contact, average velocity after contact, and R^2 of the fit were extracted for further analysis in the R programming environment (R Core Team, R version 4.2.2, 2022). The mean of R^2 was calculated to compare the quality of the fits of each particle type and describe the steadiness of particle motion. A threshold value was set to 0.3 cm/s (20% of the average minimum velocity of all observed particles after contact with the filter medium) to distinguish rolling particles (>0.3 cm/s) and particles that stopped on the filter medium (<0.3 cm/s). The ratio of the number of rolling particles to all particles gives the probability of rolling for each angle, mesh size, and particle type. Polynomial regression was fitted to the data to describe the influence of α on probability of rolling. Because only six points are available for the fit, linear to cubic polynomial regression (degree 1 to 3) was applied to prevent an overfitted high-polynomial regression that includes every data point. The Akaike's Information Criterion (AIC) was used to identify the best fit (Burnham & Anderson, 2002).

6.3. Unpublished Results

6.3.1. Micro-CT Scans

The micro-CT scans of the fish heads show the three-dimensional arrangement of the GAS within the buccal cavity in an open mouth position (Figure 16). The cross-sections in the middle of the sagittal and frontal plane show similarities between the species that align with the three morphotypes (Chapter 5.4). In *S. scombrus* (Figure 16A) and *R. kanagurta* (Figure 16B), GA1 is prominent in the anterior part of the buccal cavity. GA5 and the fourth pharyngobranchial narrow down the buccal cavity towards the oesophagus. The angle of attack α increases from

anterior to posterior and ranges between 15° and 45° for GA2 to GA5. However, the GR in *R. kanagurta* spread outwards with α equal 16° and only touch the operculum with their distal tip, whereas the GR in *S. scombrus* are directed inwards with negative α.
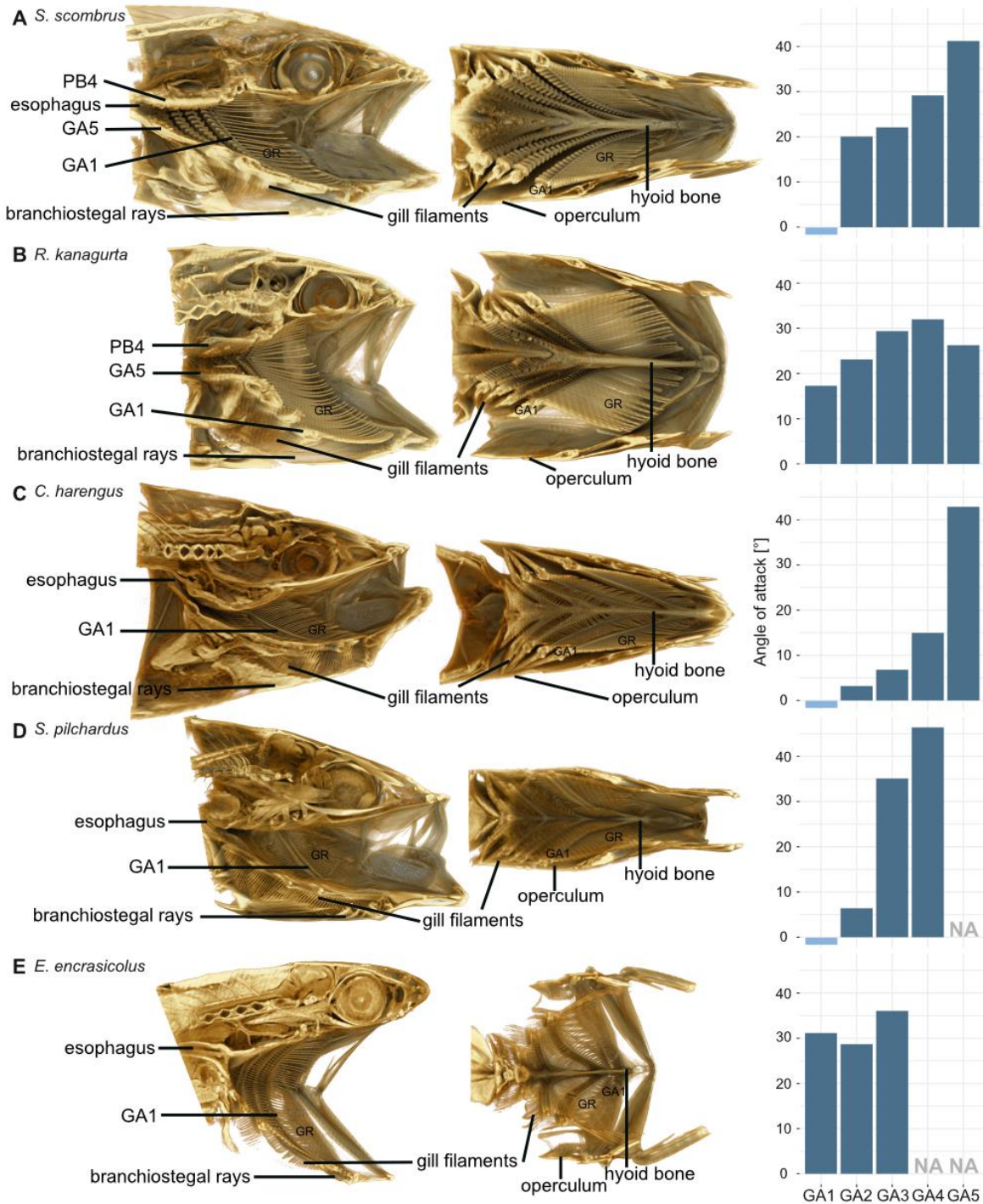
Figure 16: Sagittal cross-section with lateral view in the right size and frontal cross-sections with dorsal view on the ventral side of the buccal cavity of Micro-CT scans for each species: A) *S. scombrus*, B) *R. kanagurta*, C) *C. harengus*, D) *S. pilchardus*, and E) *E. encrasicolus*. Organisms not to scale. The angle of attack α was measured for each GA in the frontal cross-section between the GR and the hyoid bone and is given as the mean of the left and right GAS side.

Even though the jaw angle of the head in this *S. scombrus* specimen is 56.3° and lays within the range of jaw angles during feeding (see morphometric measurements in Chapter 5), we assume that the mouth was not fully opened sideways, so the opercula did not open, and the GAS could not expand to a natural feeding position. In the lateral view of *C. harengus* (Figure 16C) and *S. pilchardus* (Figure 16D), the buccal cavity has a narrow, cylindrical shape that bends upwards towards the oesophagus. In the frontal cross-section with the view on the dorsal side, the buccal cavity is narrow at the mouth opening and opens up at the GAS. The angle of attack also reflects this. GA1 and GA2 have low α that rapidly increase to over 30° in GA5 in *C. harengus* and GA3 in *S. pilchardus*. In *S. pilchardus*, GA1 is in contact with the inner sides of the opercula, which again might indicate that the GAS is not fully expanded. The buccal cavity, the opercula, and the GAS in *E. encrasicolus* (Figure 16E) are shorter in an anterior-posterior direction compared to the other species. From both views, the GAS has a conical, symmetric shape with α ranging between 30° and 47° in GA1 to GA3.

6.3.2. Fluid Flow through the GAS

The ink flows in a straight line through the test section until it comes close to the fish's open mouth (Figure 17). In the intact fish heads of *R. kanagurta* and *C. harengus*, the ink flows into the open mouth and exits from the operculum in a ventral direction. At the open mouth of *R. kanagurta*, the ink diffuses into a stable vortex that rotates downwards (Figure 17B). The ink in the mouth entrance of *C. harengus* is directed upwards but remains in a steady line (Figure 17C). In *S. pilchardus* and *E. encrasicolus*, most ink passes outside the fish's head. When the opercula are removed, a higher fraction of the ink flows into the buccal cavity and through the GAS. Thereby, the ink is distributed along GA1 and the gill filaments. Even though the opercula were replaced by transparent foil, the vortex formation at the open gape in *R. kanagurta* and *E. encrasicolus* is less stable and remains a steady line in the last dissection step (Figure 17, D4).
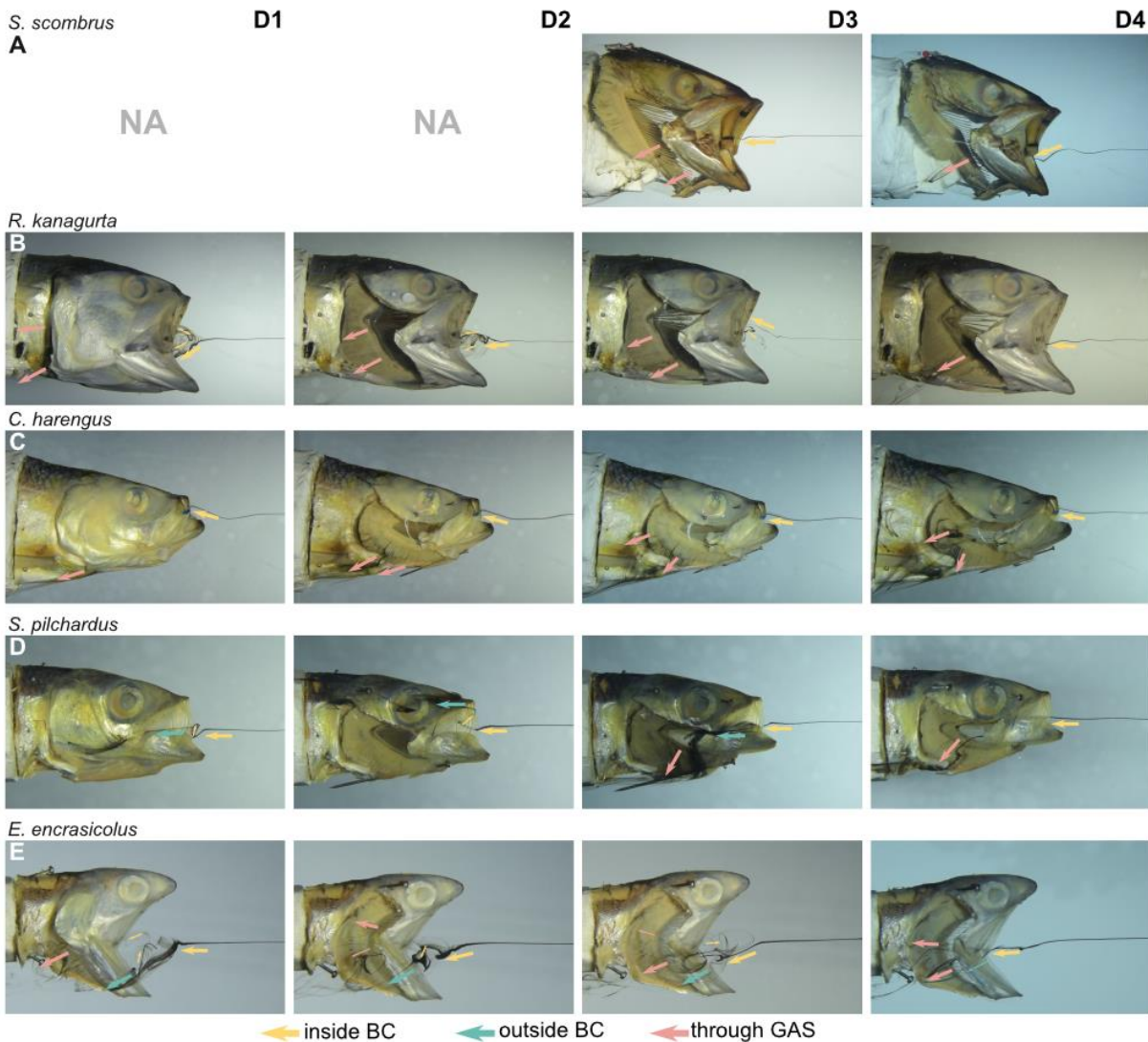
Figure 17: Flow analysis in the water tunnel with streamlines visualized by black ink for the four dissection steps D1 to D4 for reach species: A) *S. scombrus*, B) *R. kanagurta*, C) *C. harengus*, D) *S. pilchardus* and E) *E. encrasicolus*. Arrows indicate the direction and type of flow. NA indicates missing videos. Fish not to scale.

In the closeups of GR and denticles on GA1, it is observed that the ink streamlines brake up into small streamlines, and the ink becomes more diffused. Between neighbouring GR and denticles, the ink flows slower at the surface and faster in the middle between these two structures, leading to arch-shaped flow patterns (Figure 18A+B). The ink flows parallel to the gill filaments that extend laterally from GA1 (Figure 18C). In the perpendicular view of GR and denticles in *C. harengus*, the ink is not directly in contact with the surfaces of opposing denticles and GR that form the meshes might indicate boundary layers (Figure 18D).
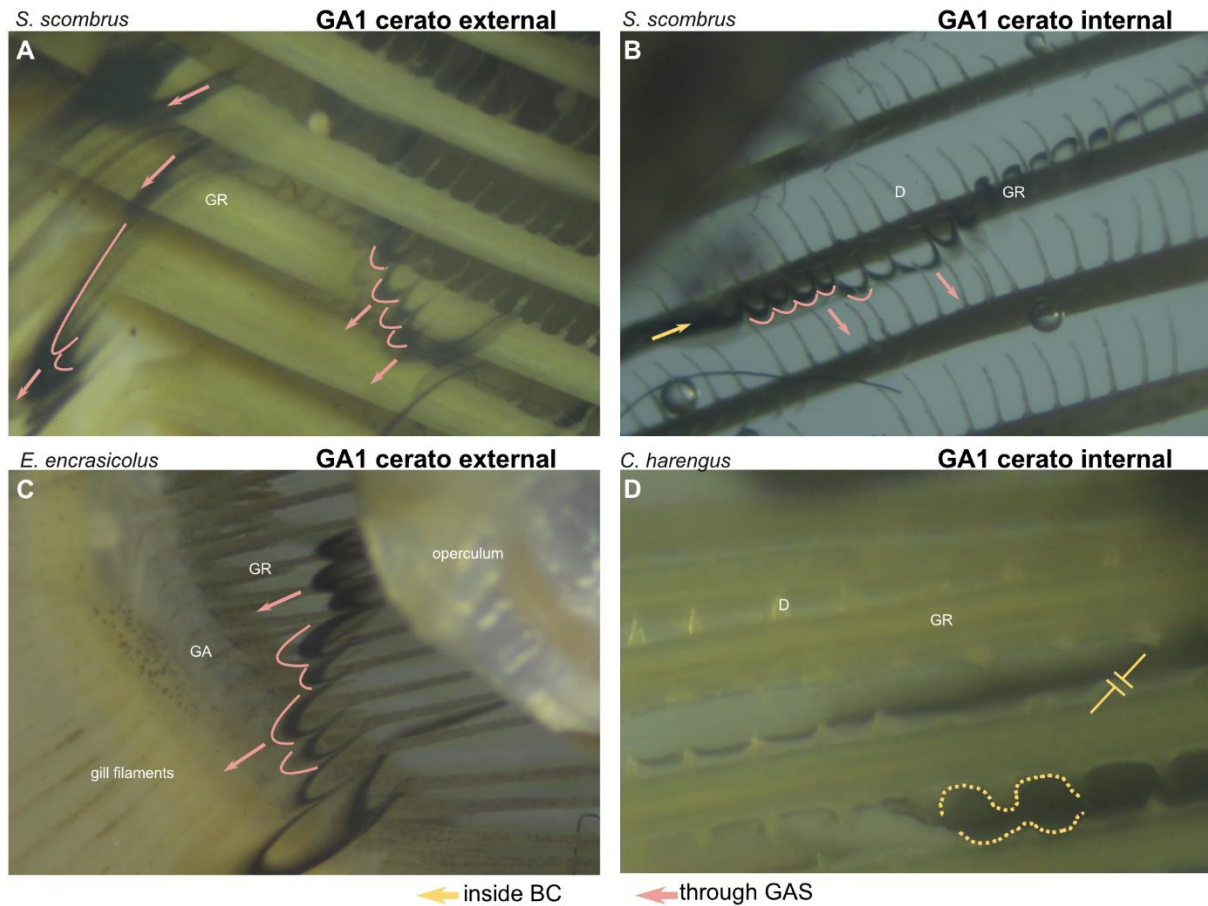
Figure 18: Flow visualized by black ink through the GR and denticles at GA1 (ceratobranchial) seen from an external (A, C) and internal perspective (B, D). Arrows indicate flow direction. Coloured lines highlight arch-shaped flow patterns. Dotted lines outline the mesh size. T-lines indicate the boundary layer around the structures.

With no fish in the water tunnel, the brine shrimp eggs move at an average velocity of 66.5 ± 0.7 mm/s (N = 49). With the fish in the water tunnel, the velocity of free-moving brine shrimp eggs decreases the further they move posteriorly within the buccal cavity (Figure 19A). At the open mouth, the velocity ranges between 43.9 ± 3 mm/s in *R. kanagurta* and 62.7 ± 4.3 mm/s in *C. harengus*, which equals a reduction of 66% and 94.3%, respectively. At GA1, the velocity decreases to 19.2 ± 7.2 mm/s (28.9%) in *E. encrasicolus* and 40.4 ± 12.7 mm/s (60.7%) in *C. harengus*. At the pharyngobranchials in the two mackerel species, the velocity of the brine shrimp egg is 13.5 ± 5.8 mm/s (20.6%) in *R. kanagurta* and 26.3 ± 9.8 mm/s (39.6%) in *S. scombrus*. The particle trajectories at the mouth entrance show a relatively straight line into the mouth in *R. kanagurta* and *C. harengus* (Figure 19B). At GA1, between 50% of the particles in *E. encrasicolus* and 83.3% in *C. harengus* move freely in a posterior direction and have no contact with GR or denticles (Figure 19C). Particle rolling along the surface of GR and denticles is observed in 3.3% of the particles in *C. harengus* and 16.7% in *S. pilchardus*. The share of particles that stop on the surface of the mesh at GA1 ranges between 5% in *C. harengus* and 20% in *E. encrasicolus*. Between 8.3% of the particles in *C. harengus* and 32.7% in *R.*

kanagurta move through the meshes of GA 1and out of the GAS. No particles are lost in *S. pilchardus*. At the pharyngobranchial, all brine shrimp eggs move freely in *R. kanagurta*. In *S. scombrus*, 92.5% of the brine shrimp eggs move freely, 5% roll, and 2.5% stop (Figure 19C).
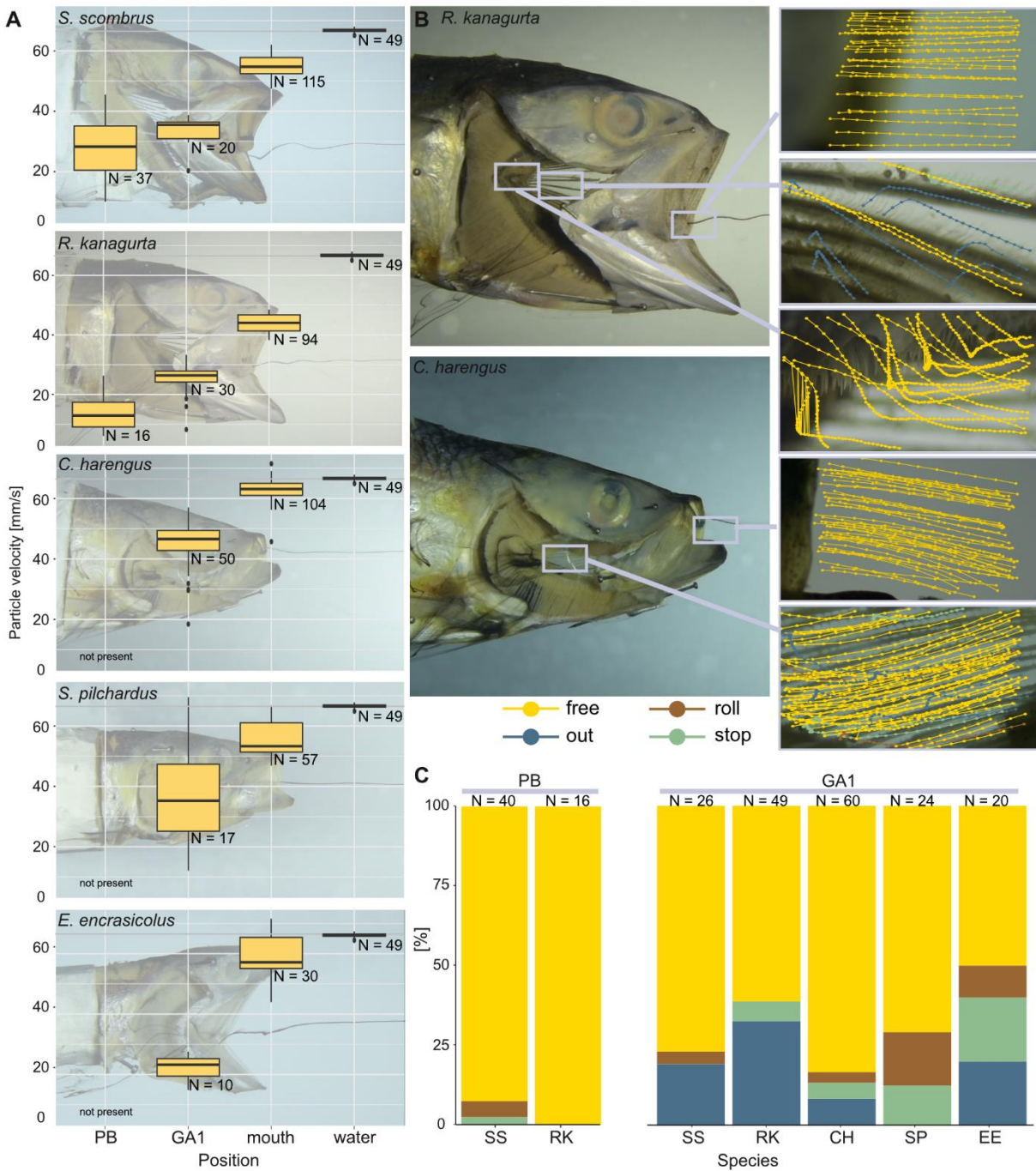
Figure 19: Velocity of brine shrimp eggs in ram-feeding fish in an open-mouth position in the water tunnel. The opercula are replaced by transparent foil, and GA1 is removed (dissection step 4). Particle behaviour is divided into free (yellow), out (blue), roll (brown), and stop (green). A) Velocity of the free moving brine shrimp eggs (mm/s) in the water without the fish, at the mouth entrance, at the left ceratobranchial of GA1, and the pharyngobranchials (PB) if present. B) Examples for the detailed sections filmed in *R. kanagurta* and *C. harengus* with particle movement plotted over the image. C) Share [%] of particle behaviour at the positions GA1 and PB for the five ram-feeding species: *S. scombrus* (SS), *R. kanagurta* (RK), *C. harengus* (CH), *S. pilchardus* (SP), and *E. encrasicolus* (EE).

6.3.3. Influence of Angle of Attack on Particle Retention

When particles come in contact with the filter medium, they can either stop or roll. When the brine shrimp eggs roll along the surface of the filter medium, the motion is steady, and the velocity is relatively constant (Figure 20A, $\alpha = 10°$). For rolling brine shrimp adults, we observed that the organism's active movement leads to an unsteady motion and flow velocity. These two different behaviours are reflected in the R^2 value that describes the quality of the curve fit, which was used to extract the average velocity before and after contact of the particles with the filter medium (Figure 20B). Over all mesh sizes and angles, the average R^2 is similarly high for brine shrimp eggs with 0.95 ± 0.03, polyamide particles with 0.07 ± 0.05, and flock fibres with 0.98 ± 0.06. For the brine shrimp adults, the average R^2 is 0.60 ± 0.34. When the particles stop after contact with the filter medium, the velocity is zero or close to zero when it alternates between rolling and stopping (Figure 20A, compare $\alpha = 60°$).

In general, the probability of particle rolling decreases with an increasing angle of attack α (Figure 20C). Depending on particle type and mesh size, the relation cannot be described with linear but polynomial regression. At α of $10°$, the brine shrimp eggs have a 100% chance of rolling with the 53 µm and the 100 µm mesh size. The relation between α and the probability of rolling is cubic. It remains close to 100% until it drops to 35% and 85% at $60°$, respectively. The probability of rolling in the brine shrimp adults decreases linearly from 100% at $10°$ to 40% at $60°$ with the 53 µm mesh size and from 100% at $10°$ to 70% at $60°$ with the 100 µm mesh size. With the 300 µm mesh size, a quadratic relation describes the decrease in the probability of rolling with increasing mesh size. It is 100% at $10°$ and 40% at $60°$. The probability of rolling for the polyamide particles decreases in a cubic relation from 81.3% at $10°$ to 0% at $50°$ with the 53 µm mesh size and from 88.3% at $10°$ to 1.7% at $60°$ with the 100 µm mesh size. The probability of rolling is overall the smallest for the flock fibres compared to the other particles. At $10°$, the probability of rolling drops from 20% at $10°$ to 0% at $40°$ with the 53 µm mesh size and from 37.5% at $10°$ to 0% at $50°$ with the 100 µm mesh size. With the 300 µm mesh size, the probability of rolling first increases from 50% at $10°$ to 70% at $20°$ and $30°$ and then decreases to 20% at $60°$. The particle velocity before and after contact with the filter medium tends to decrease with increasing α up to $40°$ for the brine shrimp eggs, the polyamide particles, and the flock fibres. At higher α, the velocity after contact decreases while the velocity before contact increases again. For the brine shrimp adults, the pattern is not as regular as in the other particles types because, at low angles, the velocity after contact is sometimes higher than before contact. This might indicate repulsion behaviour (Rashid *et al.*, 2012).
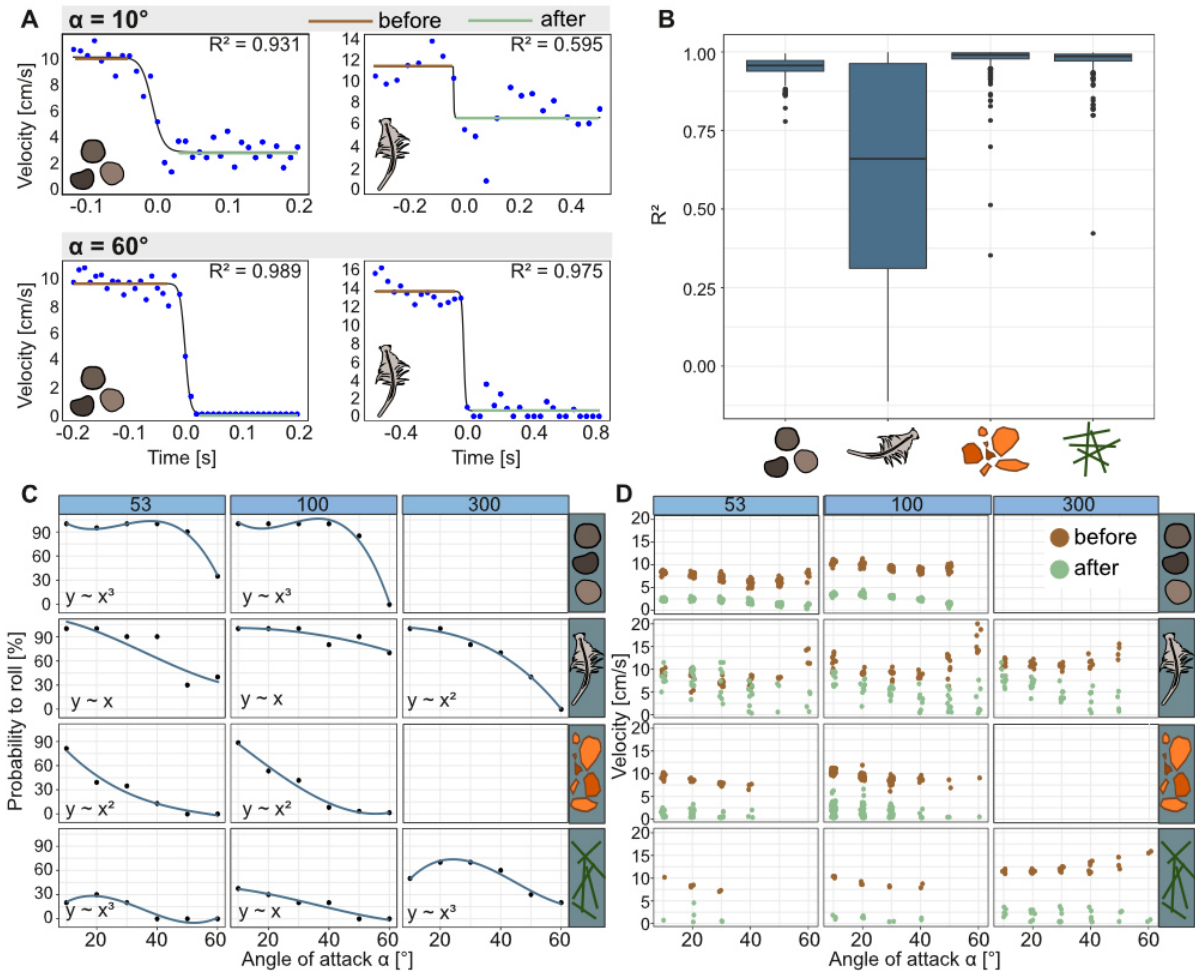
Figure 20: Influence of the angle of attack α on particle behaviour. A) Exemplary graphs of the sigmoidal curve fit on particle velocity of brine shrimp eggs and adults with the 100 μm mesh for α = 10° and α = 60°. R² and particle velocity before (brown) and after (green) the contact with the filter medium were extracted from the curve fit to describe particle motion and behaviour. B) Box plots of R² for rolling particles for each particle type over all mesh sizes and angles of attacks. C) Probability to roll for each α, particle type, and mesh size. Polynomial regression as y on x was used to describe the influence of α on the probability of rolling. There are no results for the brine shrimp eggs and polyamide particles because the mesh size was too big to retain particles on the surface. D) Particle velocity before (brown) and after (green) contact with the filter medium for each α, particle type, and mesh size.

6.4.　Discussion

The angle of attack α in the GAS towards the incoming flow ranges between 0° in the anterior part and 50° in the posterior part of the GAS. In the range of these angles, the experiments of particle interaction show that the probability of particle rolling is higher at lower angles of attack. This supports my initial hypothesis of semi-cross-flow filtration and the relation of α and probability of rolling. This regard to the fish, this means that particles that come into contact with the anterior part of the GAS will likely roll towards the oesophagus, where they stop before being swallowed. The observation of brine shrimp eggs inside the buccal cavity in fixated fish shows that the majority of particles move free or roll along the surface of the GA1 in the GAS

(Figure 19). The sum of the share of free and rolling particles accounts for 80.8% in *S. scombrus*, 61.2% in *R. kanagurta*, 86.7% in *C. harengus*, 87.5% in *S. pilchardus*, and 60% in *E. encrasicolus*. Free moving particles were also observed in Nile tilaoia and linked to cross-flow filtration (Smith & Sanderson, 2007).

Once the particles are in contact with the filter medium of the GAS, we assume that a smooth surface increases the chance of rolling. Surface structures, such as teeth, will probably pose an obstacle that leads the particles to stop. As expected, the clupeid species with a smooth show a higher share of rolling particles with 9.8 ± 6.4% than *S. scombrus* with 3.8% and *R. kanagurta* 0% in, which both have teeth. However, this hypothesis is contradicted by the fact that the share of free and rolling particles at the pharyngobranchial in the two scombrid species is still above 90% (Figure 10). We suspect that the removal of GA1 in the fourth dissection step manipulated flow and keeps the particles suspended because we observed that particles exited the buccal cavity towards the side with the removed GA1 without touching the GAS (Figure 19). Therefore, the setup is limited in the representation of natural conditions, especially at the posterior pharyngobranchials.

Based on the morphotypes identified in the ram-feeding fish species (Chapter 5.4), we assumed unidirectional and relatively laminar flow inside the buccal cavity. The Reynolds number around the denticles was calculated as 30 in *E. encrasicolus* and 300 in *S. scombrus*. Additionally, we suggested that the pipe like buccal cavity might break down large turbulences. However, we observe a stable vortex in the mouth opening of *R. kanagurta* and diffusion of the ink when it passes the GR and denticles in all species. In technical cross-flow filtration, turbulences are desired because they increase the crossflow velocity close to the filter medium and decrease particle deposition. Turbulence can be induced by rotors (Bott, Langeloh, & Ehrfeld, 2000) or by rotating or vibrating the filter medium, and is often referred to as dynamic cross-flow filtration (Sutherland, 2008). This filtration process requires additional energy. Therefore, the generation of turbulent flow by geometries might advantageous and should be part of further studies on suspension feeders.

We observed fluid flow in the water tunnel at a set flow velocity of around 0.067 m/s to study the ink streamlines under laminar conditions. This is slower than the swimming speed measured for the fish during feeding, which was measured as 0.34 m/s in *C. harengus* up to 0.5 m/s in *S. scombrus* (Chapter 5). If we apply the relative velocity decrease measured in the water tunnel to the natural swimming velocities, we can refine our previous calculation of the Reynolds numbers. Particle velocity decreases to around 83.2 ± 10.7% at the mouth entrance and 42.3 ± 11.8% at GA1 across all five species compared to the particle velocity without the fish heads in the water tunnel (Figure 19). This equates to a flow velocity between 0.29 m/s and 0.41 m/s at the mouth entrance and between 0.14 m/s and 0.21 m/s at GA1. This results

in Reynolds numbers between 2454 in *S. pilchardus* to 6225 in *S. scombrus* at the mouth (with equivalent spherical diameter of the mouth opening) and between 9.1 in *E. encrasicolus* and 91.2 in *S. scombrus* at the denticles (with denticle width, compare to Manuscript III in the Appendix, p. 211). At Reynolds numbers >10, other particle encounter mechanisms than sieving become more relevant in particle retention in suspension feeders, such as direct interception, inertial impaction, motile particle deposition, and gravitational deposition, which was shown for smaller suspension feeders than filter-feeding fish (Rubenstein & Koehl, 1977; Shimeta & Jumars, 1991).

The measured decrease in flow velocity inside the buccal cavity of ram-feeding fish are in a similar size range reported in other studies. Flow velocity reduction based on models in whale sharks was estimated at around 86.1 – 93.5% at the mouth opening compared to the swimming velocity (Motta *et al.*, 2010) and the flow velocity at the ceratobranchial of GA1 inside the buccal cavity in fixed specimen of the pump-feeding American paddlefish was 60-85% of the flow velocity at the rostrum tip (Brooks *et al.*, 2018). However, it must be taken into account that the fixation process has stiffened the flexible structures and soft tissue of the GAS and gill filaments, which might have reduced the open area of the filter medium and led to an increase in drag. The fluid exit ratio, i.e., the ratio open area of the filter medium to the open mouth area, was identified as a significant predictor of flow speed in the mouth of preserved paddlefish (Brooks *et al.*, 2018). Additionally, we noticed in the micro-CT scans that the opercular of *S. scombrus* and *S. pilchardus* did not open sideways, the GAS is not fully expanded, and the gill filaments stick together (Figure 16). We observe that most of the ink flows outside of the buccal cavity in *S. pilchardus* and *E. encrasicolus*, which might indicate increased drag. On the other hand, removing structures might have decreased drag even though we replaced the opercula with transparent foil. The stable vortex we observe in the intact head of *R. kanagurta* is not present in the last dissection step, and when we introduced the brine shrimp eggs, they did not show a rotational movement but a straight line into the mouth.

As mentioned in the introduction, studying fluid flow and particle behaviour inside the buccal cavity in living ram-feeding fish under natural conditions is challenging, if not impossible. The combination of the fluid flow and particle behaviour analysis in fixated fish heads in a water tunnel and the study of α on particle behaviour allowed us to approach the problem from different directions and gain valuable data supporting our hypothesis of semi-cross-flow filtration. Thereby we were able to report particle velocities and observed fluid flow around GR and denticles in ram-feeding fish for the first time.

Even though the brine shrimp eggs and polyamide particles are of similar size, the fragments with irregular shapes and edges seem to get stuck in the meshes, whereas the round brine shrimp eggs roll along the surface. The motility of the prey organisms leads to particle

behaviour that differs from artificial particles. This factor must be considered in the analysis and models of filter-feeding because most organisms feed on motile organisms. Based on the three morphotypes identified within these five species (Chapter 5), it seems as if the narrow and pipe-like buccal cavity in *C. harengus* and *S. pilchardus* allows a steady and laminar inflow, while larger open mouth angles induce a vortex and lead to ink diffusion. However, a more extensive study is required to analyse flow patterns for each morphotype. Computational fluid dynamics (CFD) pose an additional methodology to study fluid flow around GR and denticles, the influence of boundary layers in mesh size formation, and particle trajectories.

For the development of a biomimetic filter module based on semi-cross-flow filtration, the angle of attack of the filter medium is a relevant trait in the abstraction process to design functioning models. We identified that small α increases particle rolling on filter meshes. However, depending on the particle type, the optimal range of angles is limited. For example, α should be smaller than 30° to increase the probability of rolling in flock fibres. Generated turbulences and vortices might pose an additional parameter to change particle behaviour.

7. Abstraction and Proof of Concept

This chapter presents unpublished results. The design of here described filter element and filter housing was filed as a patent on the 30th March, 2023. Inventors:

- University of Bonn: Leandra Hamann, Christian Grünewald, Hendrik Herzog, Alexander Blanke
- Fraunhofer Institute for Environmental, Safety and Energy Technology UMSICHT: Christian Geitner, Jan Blömer, Ilka Gehrke

Contributions:

Leandra Hamann: conceptualization and methodology, biomimetic abstraction, experimental investigation, data analysis and visualization, formal analysis,

Kristina Schreiber (master thesis*): experimental investigation

Christian Grünewald: conceptualization and methodology, test stand design and assembly, CAD modelling and 3D-printing, experimental investigation

Hendrik Herzog: CAD modelling, test stand design and assembly, conceptualization and methodology

*daily supervisor: Leandra Hamann

Previous page:

Selection of some filter elements that were designed, build, and tested during the FishFlow project (Oct 2021 – Dec 2022). Credits: Leandra Hamann 2022.

7.1.   Introduction

During the biomimetic working process, the abstraction of biological principles is crucial (step 6, Figure 2). The aim is to design functional models based on principles independent of the living system (Fayemi *et al.*, 2017). Often, only a selection of traits is transferred to models because an exact replication of the biological system is not feasible (Helms *et al.*, 2009). We abstracted three main aspects of the ram-feeding fish into models: 1) the geometry of the GAS to design the filter element, 2) the denticles and teeth as surface structures in the filter element, and 3) the inflow and the cleaning behaviour that is mimicked by the filter housing that holds the filter element.

7.1.1.   Abstraction into Models

The basic shape of the filter element is a cone. The base of the cone is the fish mouth opening and was set to have a diameter of 50 mm. The apex of the cone was designed as the concentrate outlet to resemble the oesophagus and has a diameter of 10 mm (Figure 21A). Based on observation that low angles of attack increase particle rolling, 11° and 22° angles of attacks were selected, and the length of the filter elements scaled accordingly. Four curved struts that resemble the GA were implemented to support the filter mesh. The filter mesh mimics GR and denticles (Figure 21B). We selected a filter mesh made from Polyamide 6.6 with a mesh size of 100 µm and an open area ration of 44% (Bückmann PA6.6-100/51-44). It has a mesh similar to the ones calculate for the ram-feeding fish, which ranges from 0.007 mm² to 0.148 mm², and as recommended in studies to retain MPs fibres in washing machines (Browne *et al.*, 2020; De Falco *et al.*, 2021). Additionally, the filter mesh is temperature resistant up to 140-180°C and stable in soapy waters. The support structures of the filter element were 3D-printed (PolyJet multi-material 3D Printer, StrataSys J35™ Pro) with a polyacrylate polymer resin (VeroUltra, StrataSys). Afterwards, the filter mesh was glued inside the support structures using acrylic super glue. In total, three biomimetic filter elements were designed and built, i.e., Small-11, Small-22, and Large-11, which differ in length, filtration area, and angle of attack α (Figure 21A, Supplementary Information 10.1.4). A dead-end filter element with the same filtration area as the Large-11 filter element was designed and built to represent market-ready filters. The dead-end filter element has a cylindrical shape with α of 0°, which resembles the cartridge filter design of the Planet Care filter (Table 3). It is closed at the end, so the retentate cannot be cleaned during filtration.

The hyoid bone, the short GR, denticles, and teeth form a structured surface in the two scombrid species (Figure 21). The function of these structures is not clear yet, but the hair and denticles might capture particles. Alternatively, we assume that the surface structures could create additional turbulences to keep the filter medium clean, similar to the d-type structure

found in pump-feeding fish (Brooks *et al.*, 2018) or dynamic cross-flow filtration (Bott *et al.*, 2000).
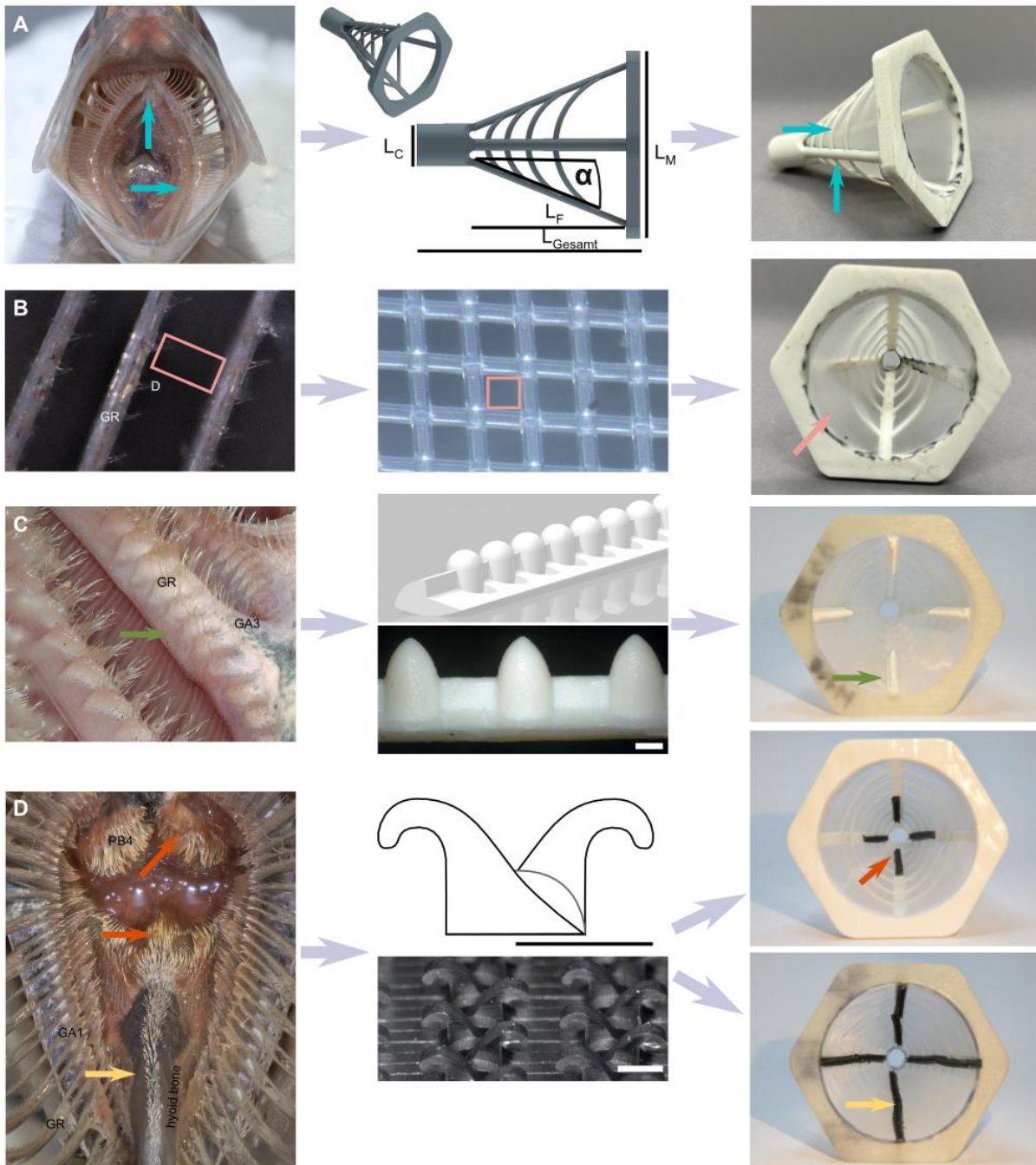
Figure 21: Abstraction of morphological traits of the GAS into CAD-models and physical models. A) The cone-shaped GAS with a given angle of attack α is abstracted into the supporting structures of the filter element. B) The GR and denticles are mimicked with a ready-made filter mesh that is glued onto the support structures. C) A row of ellipsoids was designed to mimic the short GR in the two scombrid species and glued into the Large-11 filter element. D) Hooked tape (VELCRO® HTH820) mimics the denticles and teeth and was glued in the full and half length of the Large-11 filter element.

In order to observe the influence of surface structures and study their effect on the filter performance, a line with ellipsoids was designed, 3D-printed (PolyJet multi-material 3D Printer, StrataSys J35™ Pro), and glued onto the first half of the lengthways supporting structures of

the Large-11 filtering element to mimic the short GR and hyoid bone in the scombrid species (Figure 21C). The teeth and denticles were mimicked by hooked tape (VELCRO® HTH820) consisting of rows with hooks facing opposite directions. In one Large-11 filter element, the hooked tape was glued in the posterior half of the filter, and in another, it was glued on the entire length (Figure 21D).

The filtering chamber is modular and consists of an inlet, a flange, a transparent pipe, and an outlet (Figure 22A+B). The inlet leads the suspension towards the filter element. Based on our study of the fluid flow (Chapter 5), the inflow into the buccal cavity might be unidirectional or turbulent. Therefore, we designed and tested four different inlets: 1) a short inlet with unidirectional flow (Figure 22C), 2) a long, conical inlet with an inner wall to distribute the unidirectional flow evenly onto the filter mesh (Figure 22D), 3) a long, conical inlet with an inner screw-shaped wall to create a rotational flow (Figure 22E), and 4) an asymmetric, snail-shaped inlet to further induce rotational flow within the filter element (Figure 22F).

The brass flange connects the inlet, transparent pipe, and outlet with four stainless steel screws. A small screw in the flange allows to release air from the filter housing. The transparent pipe allows us to observe the filtration process in and around the filter element and comes in two sizes to test different filter element lengths. The outlet has two separate outputs for concentrate and permeate, which can be connected to pipes and containers. In the first setup, two manual valves were implemented in the outlet pipes to control the outflow and mimic the cleaning behaviour in the fish. Later, the manual valves were replaced by automatic valves to set the cleaning to reproducible intervals. The valve at the permeate outflow was normally open (EPK-1502-NO, 24V, Takasago, BMT Fluid Control Solutions GmbH), and the valve at the concentrate outflow was normally closed (EPK-1502-NC, 24V, Takasago, BMT Fluid Control Solutions GmbH). Both valves were connected in parallel and adjustable with a control unit. During cleaning, the valve at the concentrate opens, and the valve at the permeate closes simultaneously. The cleaning interval can be set to durations between 13 s and 86 s, and the cleaning process itself can be set to 0.6 s to 6.5 s.

Due to the complex design of the inlet, flange, and outlet section, they had to be custom-made. The flange was manufactured in the workshop at the University of Bonn. The inlet and outlet were 3D-printed (PolyJet multi-material 3D Printer, StrataSys J35^{TM} Pro) using a waterproof acrylate resin polymer (VeroUltra, StrataSys). The filter housing with the filter element is termed filter module.
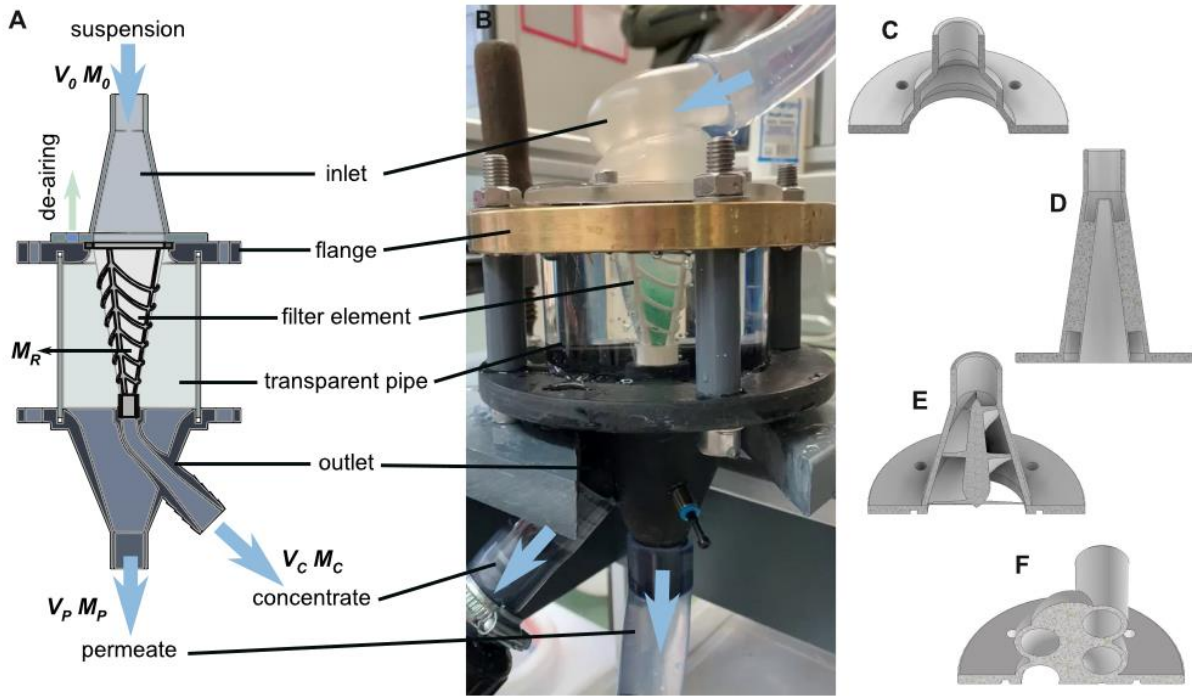
Figure 22: Design of the filter module consisting of filter housing and filter element. A) The modular filter housing consists of an inlet with a screw to de-air the system, a flange, a transparent pipe, and the outlet. The filter module separates the suspension, which consists of a fluid volume (V_0) and a particle mass (M_0) into a concentrate volume (V_C) with a particle mass fraction (M_C) and the clean permeate (V_P) with a second particle mass fraction (M_P). The particle mass fraction that remains in the filter element is called the retentate (M_R). B) Set-up of the filter module with the snail inlet and the Small-11 filter element. Four different inlets were designed and tested: C) small conical inlet, D) long conical inlet with inner wall, E) long conical inlet with inner screw, and F) snail inlet.

7.1.2. Performance Criteria of Filter Modules

The transposition of biological working principles to technology requires knowledge about the biological function but also the technical application (Fayemi *et al.*, 2017). In order to demonstrate the functionality of abstracted filter modules, the filtration process will be evaluated with a set of established filtration performance criteria.

In solid-liquid separation, filters separate solid particles from a fluid. Therefore, a major filter requirement is the specification of a cut-off point, which describes the size of the largest particle that passes through the filter (Sutherland, 2008). Selecting a filter medium with an appropriate mesh size and permeability is an important step in fulfilling the separation task, but it also determines the volume flow through the filter (Sutherland, 2008). High permeability represents a low resistance to flow and vice versa. It is directly proportional to flow rate, fluid viscosity, filter medium thickness, and inversely proportional to filter area and fluid density (Sutherland, 2008). During the filtration process, particle deposition on the filter medium increases the hydrodynamic drag, and the flow rate will decrease and eventually stop when the filter is clogged. In order to maintain a constant flow rate, the pumping pressure has to be increased (energy and cost investment), or the filter medium needs to be cleaned (Richardsons, Harker,

& Backhurst, 2002). Another critical factor is the particle concentration in the suspension, which determines the filter medium's "dirt-holding capacity" and influences operating cycle time and cleaning frequencies. The ratio of upstream particle concentration to the downstream particle concentration of the filter medium determines the filtration efficiency. It is applied over the whole particle size range down to the cut-off value and is often expressed in per cent (Sutherland, 2008).

In the first performance tests of the biomimetic filter module, two performance criteria will be analysed: volume flow rate and particle filtration efficiency. The volume flow rate is determined by the time required for a given volume to flow through the filter module. The filtration efficiency is determined in several steps and adapted from membrane cross-flow filtration (PS Prozesstechnik GmbH, 2023). First, the concentrating factor X is calculated, which is the ratio of the volume in the concentrate to the starting volume in the water reservoir prior to the experiment (Equation 1). The aim is to keep the concentrating factor as low as possible so that post-filtration treatment of the concentrate is kept minimal.

with
X = concentrating factor
V_0 = starting volume [l]
V_c = concentrate volume [l]

1) $$X = \frac{V_0}{V_c}$$

Afterwards, two filtration efficiencies are calculated. E_R is the share of particles that are retained in the filtration system, i.e., the concentrate and retentate (Equation 2), which can also be expressed as the subtraction of the share found in the permeate and is a typical performance criterion for filters, also in washing machines (Browne *et al.*, 2020). If all particles were retained within the filter and none were lost to the permeate, E_R would be 100%. E_C is the share of particles that is retained in the concentrate (Equation 3). E_C should be as high as possible because the biomimetic filter is designed to accumulate most of the particles in the concentrate to avoid clogging.

with
E_R = Filtration efficiency in concentrate and retentate
E_C = Filtration efficiency in concentrate
M_C = Particle mass in concentrate [g]
M_P = Particle mass in permeate [g]
M_R = Particle mass in retentate [g]
M_{C+P+R} = Sum of particle masses in concentrate, permeate and retentate [g]

2) $$E_R = \left(\frac{M_C + M_R}{M_{C+P+R}}\right) = 1 - \left(\frac{M_P}{M_{C+P+R}}\right)$$

3) $$E_C = \left(\frac{M_C}{M_{C+P+R}}\right)$$

Another option to describe the performance of the filter is the yield in concentrate η_C, which includes the particle mass in the concentrate M_C and the concentrate volume V_C (Equation 4). A high value indicates a good-performing cross-flow filter.

4) $$\eta_C = X^{(E_R-1)} * 100$$

with
η_C = yield in concentrate [%]
X = concentrating factor
E_R = filtration efficiency

The aim is to show a proof of concept of the filter module with the filter elements based on semi-cross-flow filtration. We want to achieve constant volume flow and high filtration efficiency in the concentrate and retentate (E_R) of >80% to be competitive with other products on the market (compare with Table 3). We test the influence of the angle of attack, filtration area, mesh size, particle type, inflow through the inlets, and surface structures on filter performance and compare this to a dead-end filter element. Based on the yield in concentrate, we identify the best-performing biomimetic filter module.

7.2.   Materials and Methods

7.2.1.   Fluid Flow in Filter Elements

The four filter elements, i.e., Small-11, Small-22, Large-11 and dead-end, were positioned in the flow tank, similar to the fish heads (Chapter 6.2.2). The concentrate outlet was observed open and closed for each filter element with three repetitions. Black ink was directed towards the rotational middle axis and filmed for 30 seconds (Nikon D850, Macro lens Nikkor AF-S 24-120 mm 1:4 G ED). The recordings were analysed qualitatively by describing ink direction, dilution, and the occurrence of stable vortices around the filter elements and compared to the fish heads.

7.2.2.   Test Stand

Similar to the company Hengst SE, a manufacturer of filters, a test stand was built to test the filter module's volume flow and particle filtration efficiency. The basic setup consists of a water reservoir (FastBrewing Starter Kid, 30 L Volume) with a mixer, a pipe that leads the suspension towards the filter module, a pipe for the concentrate, a pipe for the permeate, and two containers to collect both fractions (Figure 23). The simple setup prevents dust and dirt from influencing mass fraction measurements (personal information from Hengst SE), has steady flow conditions, and the volume flow will naturally decrease due to the decrease of hydrostatic pressure.
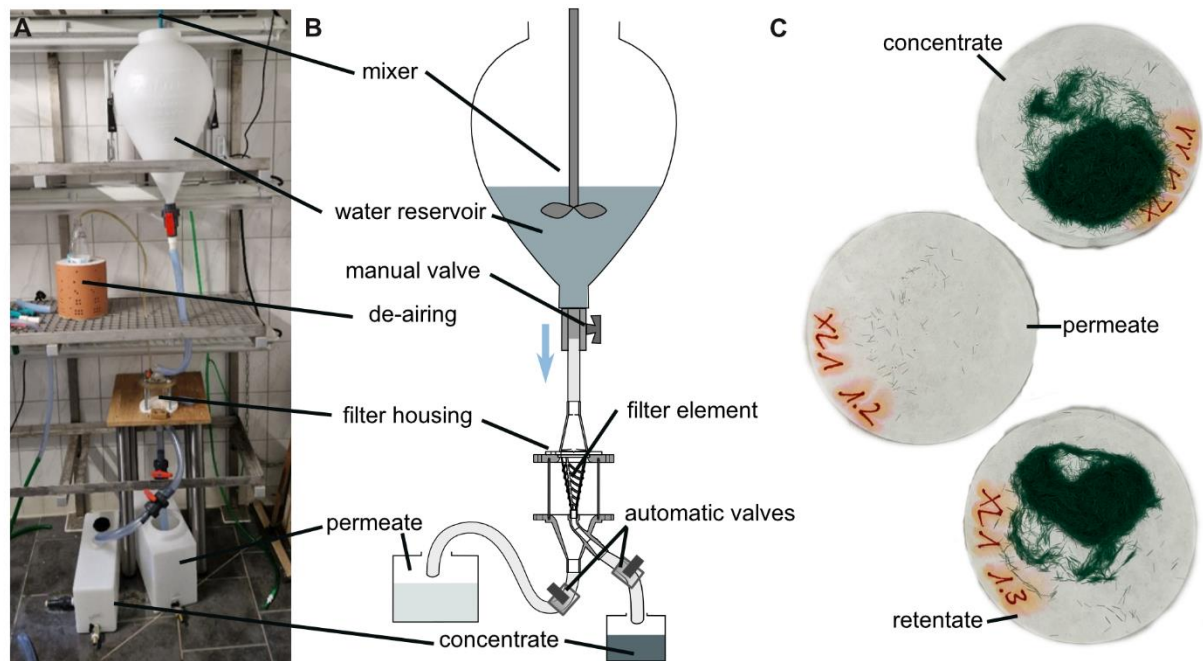
Figure 23: Test stand to analyse volume flow and filtration efficiency of the biomimetic filter module.
A) Setup of the test stand in the lab without siphon and automatic valves (credits: Christian Grünewald).
B) Overview of the test stand with all components, including siphon and automatic valves. C) Filter papers (diameter 45 mm) with flock fibres (2 mm) after concentrate, permeate, retentate samples of the Large-11 filter were filtered with the vacuum pump, dried, and weighted.

7.2.3. Volume Flow through the Filter Module

Before each experiment, the water reservoir was filled with 25 l. Wwe tested cotton fibres, polyamide particles, and flock fibres (2 mm) and added 5 ml of liquid detergent to the suspension to reduce the adherence of fibres to the walls of the teststand. As tested in preliminary experiments, the liquid detergent does not influence the sample analytics (see Supplementary Information 10.1.6). The volume flow was recorded with a camera (Nikon D850, Macro lens Nikkor AF-S 24-120 mm 1:4 G ED) directed towards the water reservoir to monitor the water level over time. The experiment ended after 20 l passed the filter module.

The four inlets, i.e., short, long, swirl, and snail (Figure 22C-F), were tested in all combinations with the four filter elements and no filter element in the filter housing. No particles, siphons or valves were used. The influence of different particle types on volume flow was tested with three different particle types: cotton fibres, 2 mm flock fibres, and polyamide particles (see Supplementary Information 10.1.3 for particle specifications). The particle concentration was set to 0.1 g/l. In order to achieve the highest effect, the Small-11 filter element was chosen because it has the smallest filtration area, in combination with the small and snail inlet. No siphons and valves were used in this setup. In order to implement the cleaning mechanism by the automated valves, the setup was changed. A siphon was formed with the pipe of the permeate outlet and the valves were implemented in the concentrate and permeate outlet. The volume flow through the new setup was tested with the snail inlet but no filter element and no

particles. Two automatic valves were implemented in the concentrate and permeate pipe to clean the filter element at set intervals. The concentrate outlet opened and the permeate outlet closed for 0.6 s for the Small filter elements and 1.3 s for the Large filter elements when 10 l and 20 l passed the filter module. The cleaning effect on volume flow was tested with the Small-11 filter element and cotton fibres (0.1 g/l), as this combination has the highest chance of clogging. The snail inlet was used, and a siphon was formed in the permeate outlet pipe. The volume flow through the Large-11 filter element with the biomimetic surface structures were compared to the Large-11 filter element with no surface structures and the dead-end filter. The snail inlet was used, flock fibres were added (0.025 g/l), and the siphon was present. Only 10 l were filtered and the filter element was cleaned after 5 l and 10 l. Each combination was repeated five times. Between each trial, the test stand was rinsed with clean water, and the filter element was washed manually to remove retained particles. The recorded videos were anyseld for the time when 5 l, 10 l, 15 l, and 20 l passed the filter module. We noticed that the valves increasingly leaked over the course of the experiments. Therefore, only the experiments that were carried out on the same day were compared. The data was analysed and visualised using the R programming environment (R Core Team, R version 4.2.2, 2022). Measurements that were identified as outliers were removed when something unusual was observed during the experiment, e.g., a kink in the hose. We performed no statistical analysis because of the low replication number. For the volume flow experiments, the filtered volume was plotted against time to analyse the volume flow during the experiment. The time to filter 15 l was extracted and presented in boxplots.

7.2.4. Particle Retention of the Filter Module

Because we observed agglomeration of cotton fibres in the volume flow experiments, we used polyamide particles and 2 mm flock fibres to test the filtration efficiency. However, the recovery of the polyamide particles (0.025 g/l) were low with 47.9 ± 14.8 % (N = 3) compared to 85.9 ± 15.0% with the flock fibres (0.025 g/l) over all experiments (N = 40), which is a good quality recovery rate (personal information from Hengst SE). The recovery *R* of the particles in the particle retention experiments is determined by the sum of the particle mass fractions collected within the concentrate, the permeate (extrapolated to total permate volume) and the filter in relation to the total particle mass in the feed (Equation 5).

5) $$R = \left(\frac{M_C + (M_P * (V_0 - V_K)) + M_R}{M_0} \right) * 100$$

with
R = recovery [%]
M_C = Particle mass in concentrate [g]
M_P = Particle mass in permeate [g]
V_0 = starting volume [l]
V_C = concentrate volume [l]
M_R = Particle mass in retentate [g]
M_0 = Total particle mass in the starting volume [g/l]

We observed that the orange polyamide particles stuck to the inner walls of the water reservoir and pipes even though 5 ml of liquid detergent was added to reduce particle adhesion. Therefore, we decided to proceed with flock fibres only.

Before each trial, the valves were closed, the filter module was filled with clean water and de-aired, and 20 l of tap water, 0.5 g of flock fibres, and 5 ml of liquid detergent were mixed in the water reservoir. The valve in the permeate pipe was opened to start the experiment. Cleaning was automatically set when 5 l and 10 l passed the filter module. After the second cleaning, the experiment was stopped, and the valves closed. We tested the influence of filter size (Small-11 and Large-11), MPs type (polyamide particles and 2 mm flock fibres), mesh size (53 µm and 100 µm), inlet type (long and swirl), and filter type with different surface structures on filter performance. The test stand and filter module were rinsed with clean water between each trial. The order of the experiments was chosen at random.

Three samples were taken after each experiment: 1) the total volume of the concentrate, 2) one litre of the permeate, and 3) all the fibres that remained within the filter, i.e., the retentate (M_R) resuspended in a maximum of one litre (Figure 22). The MPs mass fractions were separated from the water using a suction filter (Nalgene Reusable Bottle Top Filter) with round filtering papers (ROTILABO Type 11A, ø 45 mm, retention range 12-15 µm) and a vacuum pump (Vaccubrand MZ 2C, 1.7 m³/h = 28.3 l/min). Prior to the vacuum filtration, the filtering papers were labelled, dried in a heating cabinet (minimum 30 min), cooled down in a desiccator (minimum 30 min), and weighted with a precision scale (Sartorius ED153-CW, weighing capacity 150 g, readability 0,001 g, repeatability (std. deviation) ≤± 0.001 g). After the samples were poured onto the suction filter, the bottle, bottle cap, and walls of the suction filter were rinsed with deionized water, so all fibres were collected on the filtering paper. Afterwards, the filtering papers with the fibres (Figure 23C) were dried in the heating cabinet and desiccator and weighted again. The weight difference determined the fibre mass fraction of each sample.

In order to test the lab contamination and the scale's accuracy, three control samples were treated with the analytical procedure but filtered with 1000 ml of clean tap water and weighted three times. The weight difference of the filter papers without experimental samples are 0.00107 g, 0.00010 g, and 0.00010 g. Additionally, we ran three blank trials after rinsing the test stand and without adding flock fibres to determine the contamination of the test stand and the influence of previous trials. The weight difference of the filter papers with the blank samples are 0.00082 g, -0.00029 g, and -0.00059 g for the concentrate samples and -0.00667 g, -0.01148 g, and -0.01574 g for the permate samples. Due to the high contamination in the permeate samples, all results are rounded to two decimal places.

7.3.   Unpublished Results

7.3.1.   Fluid Flow in the Filter Elements

In all three biomimetic filter elements, the ink streamlines became turbulent and diffused at the entrance of the filter elements. However, we did not observe a stable vortex such as observed in *R. kanagurta* (Supplementary Information 10.1.5). In the Large-11 filter element, the ink flows through the filter element and exits in the first half through the filter mesh. When the concentrate outlet is open, some of the ink flows through it, but most exits through the filter mesh. The direction of flow that goes through the filter mesh differs depending on the angle of attack α. At α of 22°, the ink exits more in a downstream direction compared to the Small-11 filter element. In the dead-end filter element with the same filter area as the Large-11 filter element, some of the ink passes outside the filter element. The outflow through the filter mesh is perpendicular to the incoming flow. Both aspects indicate that the cylindric geometry has a higher hydrodynamic drag induced by the closed end of the filter elements that forces the fluid into a 90° turn.

7.3.2.   Volume Flow through Filter Elements

The time to filter 20 l through the filter module increases linearly in all filter elements when no particles are filtered, showing a steady volume flow (Figure 24A). The different inlets have little influence on the time to filter 15 l. Across all combinations, the long inlet with the Large-11 filter element has the fastest volume flow with 60.8 ± 4.4 s to filter 15 l, and the slowest is the snail inlet and no filter element with 64.8 ± 1.3 s, a difference of 0.27 s/l. When particles are introduced, the flock fibres are the fastest to be filtered with the Small-11 filter element in combination with the small inlet and snail inlet (Figure 24B). The suspension with particles takes the longest in combination with the small inlet, and the cotton fibres take the longest with the snail inlet. The implementation of the valves does not influence volume flow. The siphon in the permeate outlet increases the time to pass the filter module by around 160% (Figure 24C). The cleaning of the filter element after 10 l and 20 l does not influence the volume flow when no particles are present. When cotton fibres are filtered, the volume flow decreases from 4.04 s/l for the first 5 l and 9.92 s/l for the last 5 l (Figure 24D). After 15 l, the filtering process of cotton fibres is 125% slower compared to no cotton fibres. The cleaning of the filter element after 10 l and 20 l reduces the time to filter 15 l to 93%. The surface structures in the Large-11 filter element do not influence the volume flow compared to the Large-11 filter element with no surface structures or the dead-end filter (Figure 24D).
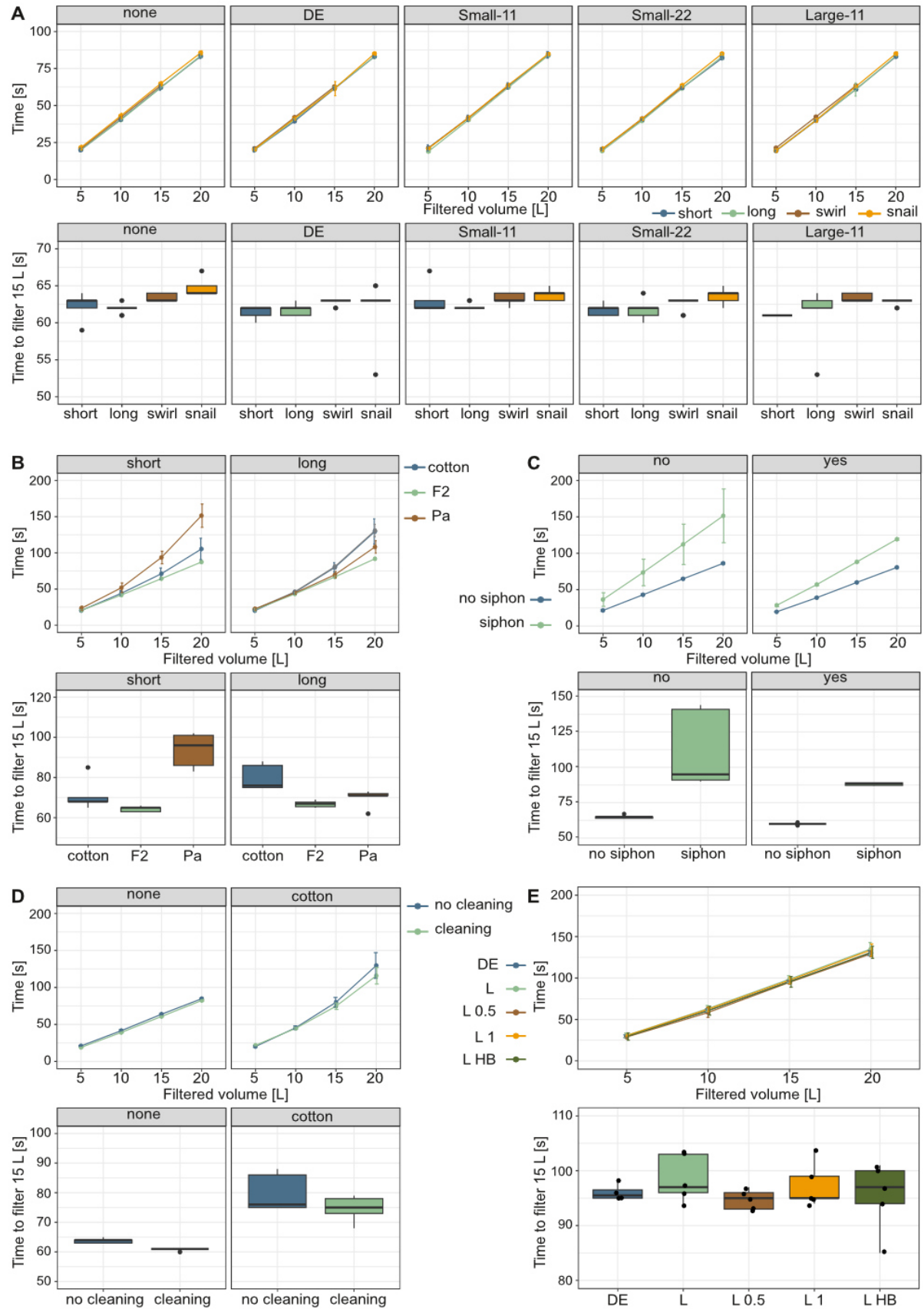
Figure 24: Volume flow through the biomimetic filter module and comparison of the time to filter 15 l for each tested factor. A) Comparison of the four inlets with each filter element (N= 5, no particles, no siphon, no valves). B) Comparison of three particle types: cotton fibres, flock fibres (F2), and polyamide

particles (PA) with the Small–11 filter element (no siphon, no valves). C) Influence of siphon and valves on the setup (no filter, no particles, snail inlet). D) Influence of cleaning on volume flow (Small–11 filter element, cotton fibres, snail inlet, siphon). E) Comparison of the Large–11 filter element (L) with biomimetic surface structures (0.5 = half length with Velcro, 1 = full length with Velcro, HB = ellipsoids) and the dead–end filter (snail inlet, siphon).

7.3.3. Particle Filtration Efficiency

During the experiments, we observed in the Large-11 filter element that the fibres partly remain suspended and partly roll along the surface of the filter medium (Figure 25A). The fibres distribute over the whole length of the filter element before cleaning. In the Small-11 filter element, more fibres remain suspended and accumulate closer to the concentrate outlet than in the Large-11 filter element (Figure 25B). After cleaning, only the lower half of the Large-11 filter element was free of flock fibres, while in the Small-11 filter element, all fibres seemed to be washed into the concentrate. This influence of filter element size in particle retention is also reflected in the share of fibres in the permeate and concentrate (E_R), respectively (Figure 25C). The concentrate contains 68.8 ± 19.5% of the fibres with the Small-11 filter element and 41.8 ± 10.1% with the Large-11 filter element. Only 11.2 ± 4.6% of the polyamide particles end up in the concentrate, compared to 41.8 ± 10.1% of flock fibres (Figure 25D). In the comparison of the 53 µm and 100 µm mesh size, more fibres are retained in concentrate and retentate with the 100 µm (Figure 25E). However, 78.7 ± 5.8% of the fibres end up in the concentrate with the 53 µm mesh size compared to 68.6 ± 19% with the 100 µm mesh size (E_C). The swirl and long inlet comparison shows no influence on E_C, with 68.6 ± 19.5% and 67.7 ± 11.1%, respectively (Figure 25F). In the dead-end filter, 98.8 ± 5.7% of the fibres are retained in the filter element (Figure 25G). The comparison of different surface structures in the Large-11 filter elements shows that the most fibres are retained in the concentrate of the filter element (E_C) without surface structures with 86.2 ± 2.8% (Figure 25G). The least fibres are retained in the concentrate of the filter element with the hooked tape over the whole length with 65.7 ± 4.9%. In all experiments with flock fibres (N = 43), the particle share is 64.1 ± 24.1% in the concentrate and 33.2 ± 24.4 % in the retentate. On average, only 2.7 ± 3.2% of the fibres are not retained by the filter filter module and end up in the permeate. This means that the goal of retaining more than 80% of the fibres has been achieved. Based on the yield in concentrate η_C , which considers the filtration efficiency and the water volume in the concentrate, the best-performing filter element is the Small-11 filter element (Figure 25G).
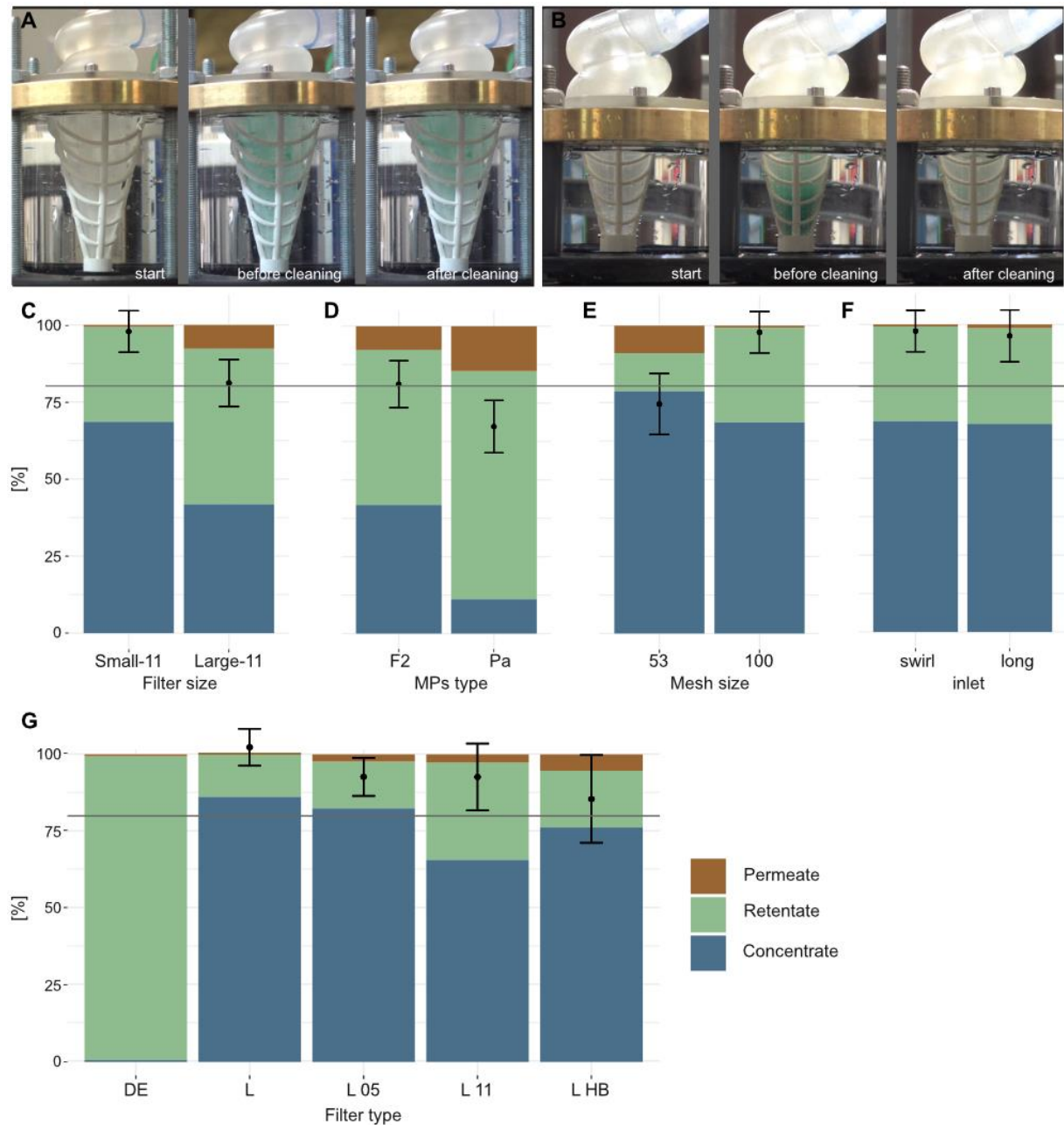
Figure 25: Analysis of particle filtration efficiency [%] of the filter module. Observations during the filtration of flock fibres at the start of the experiment, before cleaning and after cleaning with A) the Large-11 and B) Small-11 filter element (Credits: Leandra Hamann, Christian Grünewald). Share of MPs masses in permeate (brown), retentate (green), and concentrate (blue) were measured to test the influence of C) filter size (N = 3, swirl inlet, flock fibres), D) MPs type (N = 3, swirl inlet, Large-11 filter element), E) mesh size (N = 3, snail inlet, Small-11 filer element, flock fibres), F) inlet (N = 3, Small-11 filer element, flock fibres), and G) filter types (N = 5, snail inlet, flock fibres). The yield in concentrate [%] η_C is displayed on the same axis and given as the mean with standard deviation (black). A grey line indicates the desired filtration efficiency E_R of 80%.

7.4. Discussion

The biomimetic filter module can filter 20 l of particle suspensions with cotton fibres, polyamide particles, or flock fibres without clogging, which demonstrates the proof of concept. All filter

elements reach a filtration efficiency (E_R) that is larger than the 80% threshold. However, the filter performance varies regarding the share of particle in the concentrate (E_C) and depends on filter size, MPs type, mesh size, and surface structures. All three surface structures lead to a lower share of fibres in the concentrate and lower yield in concentrate. The mesh size of 53 µm has the higher share of fibres in the concentrate, but the yield in concentrate is lower compared to the same filter element with a 100 µm mesh size. The fluid volume in the concentrate seems to increase with smaller open area of the filter mesh, due to small meshes. Another factor that might lead to an increase in fluid volume in the concentrate is clogging. When particles block the meshes, less fluid can pass through it. This was observed with the polyamide particles that led to a decrease in volume flow and yield in concentrate compared to the flock fibres. We assumed that the sharp edges get stuck in the meshes, which decreases the probability of rolling (Chapter 6.4) and reduces the volume flow. The comparison of 11° and 22° angles of attack has no influence in volume flow. However, the observations of streamlines in the water tunnel show that the ink exits the filter mesh more perpendicular to the incoming flow when the angle of attack is low or even 0°, as seen in the dead-end filter. The turn in flow direction might induce additional hydrodynamic drag. Therefore, it might be beneficial to optimise the outflow through an optimised shape of the filter housing that guides the flow away from the filter medium similar to the opercula in the fish.

We observed that all inlets induced turbulent flow, with a rotational direction in the swirl and snail inlet. We expected that a rotational flow would reduce the angle of flow towards the filter medium and lead to a more noticeable difference in the fibre share in the concentrate, but all inlets seem to have the same effect. In cross-flow filtration, turbulent flow is preferred over laminar flow, because it increases the shear rate and prevents particle deposition on the filter mesh (Richardsons *et al.*, 2002). We assume that the Small-11 filter element shows the highest yield in concentrate, because the suspended particles could be removed over the whole length during cleaning. This was surprising, because a smaller filtration area is more prone to clogging than a larger one (Sutherland, 2008), but through the periodic cleaning we could prevent clogging. Cleaning increases the volume flow of a fibre suspension compared to when no cleaning is applied. The effect could be even stronger of the cleaning frequency is increased. However, this might go to the expense of high fluid volume in the concentrate. Additionally, we noticed that the cotton fibres accumulate and form aggregates that clog the inlet, especially the inlet with the inner wall and screw. Therefore, the snail inlet might be the best choice for suspensions where particle or fibre agglomeration is expected.

We were able to demonstrate that several factors influence volume flow and filtration efficiency of the biomimetic filter module. Some combinations were tested, but even more should be studied with higher replicates to perform statistical analysis. Nevertheless, we could show that factors besides the filter module itsels, such as the siphon and valves, influence its

performance. This needs to be considered during the fitting/installation of the biomimetic filter module in the washing machine. As shown in the angle of attack experiments, the particle shape influences the probability of rolling and filtration efficiency, which is not considered in models that are solely based on spherical particles (Di *et al.*, 2021). This is of high relevance to the filter design for washing machines. In the next step, the biomimetic filter module should be tested with real washing machine effluent that consists of a heterogeneous particle mixture. Standardised test procedure (for example as proposed by De Falco *et al.*, 2021) then allow to draw comparison to marked-ready products (Table 3) and test if the biomimetic filter module based on semi-cross-flow filtration outperforms dead-end filters in the application of washing machines.

Previous page:

View of the Atlantic Ocean through a littered, broken, and degraded plastic bottle at a beach in Portugal. Credits: Leandra Hamann 2017

8. General Discussion

Within this doctoral thesis, I reviewed 35 suspension-feeding mechanisms for their biomimetic potential, selected two for an in-depth analysis, described and analysed a new variation of cross-flow filtration in ram-feeding fish, and finally abstracted a selection of traits into functioning filter modules. The biomimetic filter module based on ram-feeding fish is unique in its combination of a cone-shaped filter element that positions the filter medium at a set angle of attack to induce semi-cross-flow filtration, a filter housing that allows a rotational inflow and a separated extraction of permeate and concentrate, and a regular cleaning mechanism that delays clogging. A patent for the new biomimetic filter module was filed at the German Patent and Trade Mark Office in March 2023.

The technology readiness level (TRL) is a metric to asses the maturity of a technology based on nine steps (Mankins, 1995). In the first step, the basic principle is observed and reported. In the last step, the technology is proven in the operational environment. The biomimetic filter module is currently at TRL 4, which means that the technology is validated in a laboratory environment (Mankins, 1995). This is similar to biomimetic filter designs based on other suspension feeders. The particle separator by Piedrahita *et al.* (2015) is inspired by cross-flow filtration in pump-feeding fish. In simulations, a maximum of about 70% (Hung, Piedrahita, & Cheer, 2012) and in experiments with prototypes, a maximum of 43% of particles were retained (Hung & Piedrahita, 2014). Even though a patent (US 2015/0143784A1) was published in 2015, as far as I know, no active research or product development has followed up. The principle of "cross-step filtration" is based on pump-feeding fish and was first described and published by Sanderson et al. in 2016 (patent WO 2015/123300 A1). Afterwards, the filtration mechanism was abstracted into models to collect harmful algae (Schroeder *et al.*, 2019). In 2022, the filtration mechanism was adapted to test models for the application in washing machines (Masselter *et al.*, 2022). To my knowledge, the filter models have not yet been tested with fibres or real washing machine effluent. The concept of "ricochet filtration" was discovered in manta rays by Divi *et al.* in 2018 (US 11,161,067 B2) that describes a mechanism in which particles bounce off the specific surface structures and accumulate close to the oesophagus. The mechanism was abstracted into models and further tests are currently underway (personal information). The specific geometries involved in ricochet filtration were used to manufacture surface patterning on membranes to manipulate local flow fields and inhibit particle deposition (Li *et al.*, 2022). These efforts show that scientists and engineers see an innovation potential in the analysis of suspension feeding mechanisms. However, marked-ready biomimetic filters still need to be developed.

Vertebrates are currently in the focus of above mentioned studies to develop biomimetic filters. Among these, only filtration mechanisms in a few species of pump-feeding and ram-feeding

fish, elasmobranches, and whales are analysed and abstracted into models. This is in contrast to our review of suspension feeders in which we identified 35 different suspension feeding mechanisms (Chapter 3). Invertebrates represent 25 of those. On species level, the share of invertebrate suspension feeder would be even higher. There are alone around 10,000 sponge species, 4,500 bryozoan species, 15,000 bivalve species, and 2,000 ascidian species, which are all suspension feeders (Westheide & Rieger, 2013). A likely reason that the majority of investigations is focused on vertebrates is that they are larger and scalability is less of an issue during the abstraction process. Additionally, all vertebrate suspension feeders have an internal suspension feeding mechanism, that more resembles technical filters that are enclosed in pipes or housings. In my anaylsis of biofilms, I experienced that the abstraction process was limited by the availability of comparable materials, because the manufacturing of hydrogels is still in its infancy and highly complex. The availability of technical material also poses a challenge during the abstraction of invertebrate suspension feeding mechanisms as they use cell, epidermis, and cilia as separation medium. However, other traits than the materials bear biomimetic potential in invertebrates. In a small study in ascidians and lancelets using computational fluid dynamics (CFD), I was able to show that the morphology and orientation towards flow influence the passive fluid flow through these two benthic suspension feeders. This might lead to a reduction of the energy expenditure during filter-feeding (Supplementary Information 10.1.7).

For the here developed biomimetic filter module based on ram-feeding fish, it was very useful that I intensively studied the morphology and function of specific traits in the biological model. Only through a combination of methods it was possible to describe an innovative filtration mechanism, identify relevant parameters and be aware of ecological constraints. Future studies on ram-feeding fish should also investigate functional contraints. Tor example, the gill arch system forms the filter medium for the retention of food particles but is also involved in gas exchange and needs to ensure a constant flow along the gill filaments. This poses a trade-off, which might limit the performance of both traits (Broeckhoven & du Plessis, 2022). The study of several species enabled us to compare morphological variations and design parametric models accordingly. Biomimetic working processes that are solely based on previous publications might be faster in the proposition of models but are limited to the provided information (Broeckhoven & du Plessis, 2022). Therefore, I recommend to do a systematic overview of biological models with a wide taxonomic range, select the best suitable biological principle, do a multi-species comparison to gain knowledge about biological diversity and parametric variation, and experimentally investigate form-function relations.

In the future, the cleaning mechanism will be one of the major challenges to improve the biomimetic filter module and reach TRL 5, which describes technologies validated in a relevant environment (Mankins, 1995). This includes the further reduction of the fluid volume in the

concentrate, drying, and disposal of retained MPs and dirt. Therefore, it could be beneficial to further analyse the inherent cleaning mechanisms in the fishes or combine a cleaning mechanism from another suspension feeder, such as the whale shark that uses backflushing for cleaning (Motta *et al.*, 2010). Computational methods, such as finite element modelling (FEM) and computational fluid dynamics (CFD) can complement physical experiments and reveal the nature of form-function relation, e.g., the stability and hydrodynamics of GR or the role of boundary layers around denticles in mesh formation.

My motivation for this thesis was the retention of microplastics to prevent negative ecological effects in the environment. As such, it is necessary for both the application of the biomimetic filter module to be environmentally friendly, but also its construction. Therefore, manufacturing processes and material selection should be based on renewable resources, designed for recycling, and have a minimal ecological footprint. Through a life cycle assessments (LCA), in which the contribution of MPs fibre reduction is included (Maga *et al.*, 2022) potential environmental impacts of the biomimetic filter module can be estimated and compared to other products. The market for MPs filters in washing machine is likely to increase on a global scale in the future due to legal requirements (e.g., expected obligation to retain microplastics in washing machines in France from 2025) and the increasing awareness of customers. In 2021, an estimated 3.35 million washing machines were sold in Germany (Statista, 2023). Besides washing machines, the biomimetic filter module could be implemented in sewage systems to retain MPs losses from tyre wear or artificial turfs. Additional applications of the filter, other than the retention of MPs, dewatering of suspensions in a multi-step process, harvesting of biomass, processing of mineral slurries, or to reduce waste during filtration processes in winemaking may also be possible.

9. References

Ackermann, B., Esser, M., Scherwaß, A. & Arndt, H. (2011) Long-Term Dynamics of Microbial Biofilm Communities of the River Rhine with Special References to Ciliates. *International Review of Hydrobiology* **96**, 1–19.

Ahlborn, B.K., Blake, R.W. & Chan, K.H.S. (2009) Optimal fineness ratio for minimum drag in large whales. *Canadian Journal of Zoology* **87**, 124–131.

Alder, J., Campbell, B., Karpouzi, V., Kaschner, K. & Pauly, D. (2008) Forage Fish: From Ecosystems to Markets. *Annual Review of Environment and Resources* **33**, 153–166.

Anbumani, S. & Kakkar, P. (2018) Ecotoxicological effects of microplastics on biota: a review. *Environmental Science and Pollution Research* **25**, 14373–14396. Environmental Science and Pollution Research.

Armisén, R. & Galatas, F. (2009) Agar. In *Handbook of Hydrocolloids: Second Edition* pp. 82–107.

Ausich, W.I. & Bottjer, D.J. (1991) History of tiering among suspension feeders in the benthic marine ecosystem. *Journal of Geological Education* **39**, 313–319.

Auta, H.S., Emenike, C.U. & Fauziah, S.H. (2017) Distribution and importance of microplastics in the marine environmentA review of the sources, fate, effects, and potential solutions. *Environment International* **102**, 165–176. Elsevier Ltd.

Baker, R.J., Fane, A.G., Fell, C.J.D. & Yoo, B.H. (1985) Factors affecting flux in crossflow filtration. *Desalination* **53**, 81–93.

Bansil, R. & Turner, B.S. (2018) The biology of mucus: Composition, synthesis and organization. *Advanced Drug Delivery Reviews* **124**, 3–15. Elsevier B.V.

Bashir, S.M., Kimiko, S., Mak, C. & Fang, J.K. (2021) Personal Care and Cosmetic Products as a Potential Source of Environmental Contamination by Microplastics in a Densely Populated Asian City Market Survey for PCCPs **8**, 1–11.

De Beer, D., Stoodley, P. & Lewandowski, Z. (1996) Liquid flow and mass transport in heterogeneous biofilms. *Water Research* **30**, 2761–2765.

Beninger, P.G., St-Jean, S.D. & Poussart, Y. (1995) Labial palps of the blue mussel Mytilus edulis (Bivalvia: Mytilidae). *Marine Biology* **123**, 293–303.

Bertling, J., Bertling, R. & Hamann, L. (2018) Kunststoffe in der Umwelt: Mikro- und Makroplastik. Oberhausen.

BLAKE, R.W. (1983) Functional design and burst-and-coast swimming in fishes. *Canadian Journal of Zoology* **61**, 2491–2494.

BÖHME, A., RISSE-BUHL, U. & KÜSEL, K. (2009) Protists with different feeding modes change biofilm morphology. *FEMS Microbiology Ecology* **69**, 158–169.

BÖNI, L.J. (2018) Biophysics and Biomimetics of Hagfish Slime. ETH Zürich.

BOTT, R., LANGELOH, T. & EHRFELD, E. (2000) Dynamic cross flow filtration. *Chemical engineering journal* **80**, 245–249.

BOUCHER, J. & FRIOT, D. (2017) Primary microplastics in the oceans: A global evaluation of sources. IUCN International Union for Conservation of Nature, Gland, Switzerland.

BRANDA, S.S., VIK, Å., FRIEDMAN, L. & KOLTER, R. (2005) Biofilms: The matrix revisited. *Trends in Microbiology* **13**, 20–26.

BRENDELBERGER, H. & GELLER, W. (1985) Variability of filter structures in eight Daphnia species: mesh sizes and filtering areas. *Journal of Plankton Research* **7**, 473–486.

BRENT GURD, D. (2006) Filter-feeding dabbling ducks (Anas spp.) can actively select particles by size. *Zoology* **109**, 120–126.

BROECKHOVEN, C. & DU PLESSIS, A. (2022) Escaping the Labyrinth of Bioinspiration: Biodiversity as Key to Successful Product Innovation. *Advanced Functional Materials* **2110235**, 1–8.

BROOKS, H., HAINES, G.E., LIN, M.C. & SANDERSON, S.L. (2018) Physical modeling of vortical cross-step flow in the American paddlefish, Polyodon spathula. *PLOS ONE* **13**, e0193874.

BROWNE, M.A., ROS, M. & JOHNSTON, E.L. (2020) Pore-size and polymer affect the ability of filters for washing-machines to reduce domestic emissions of fibres to sewage, 1–17.

BURNHAM, K.P. & ANDERSON, D.R. (2002) *Model Selection and Multimodel Inference: A Practical Information-Theoretic Approach*, 2nd edition. Springer New York.

BUSHEK, D. & ALLEN, D.M. (2005) Motile Suspension-Feeders in Estuarine and Marine Ecosystems. In *The Comparative Roles of Suspension-Feeders in Ecosystems* pp. 53–71. Springer-Verlag, Berlin/Heidelberg.

CAMPANALE, C., GALAFASSI, S., SAVINO, I., MASSARELLI, C., ANCONA, V., VOLTA, P. & URICCHIO, V.F. (2022) Microplastics pollution in the terrestrial environments: Poorly known diffuse sources and implications for plants. *Science of The Total Environment* **805**, 150431.

CARPENTER, E.J., ANDERSON, S.J., HARVEY, G.R., MIKLAS, H.P. & PECK, B.B. (1972) Polystyrene Spherules in Coastal Waters. *Science* **178**, 749–750.

CATARINO, A.I., MACCHIA, V., SANDERSON, W.G., THOMPSON, R.C. & HENRY, T.B. (2018) Low levels of microplastics (MP) in wild mussels indicate that MP ingestion by humans is minimal compared to exposure via household fibres fallout during a meal. *Environmental Pollution* **237**, 675–684. Elsevier Ltd.

CHEER, A.Y., OGAMI, Y. & SANDERSON, S.L. (2001) Computational fluid dynamics in the oral cavity of ram suspension-feeding fishes. *Journal of Theoretical Biology* **210**, 463–474.

CHEN, D.R., PUI, D.Y.H. & LIU, B.Y.H. (1995) Optimization of pleated filter designs using a finite-element numerical model. *Aerosol Science and Technology* **23**, 579–590.

CLAUSEN, L.P.W., HANSEN, O.F.H., OTURAI, N.B., SYBERG, K. & HANSEN, S.F. (2020) Stakeholder analysis with regard to a recent European restriction proposal on microplastics. *PloS one* **15**, e0235062.

COHEN, K.E., HERNANDEZ, L.P., CRAWFORD, C.H. & FLAMMANG, B.E. (2018) Channeling vorticity: Modeling the filter-feeding mechanism in silver carp using μcT and 3D PIV. *Journal of Experimental Biology* **221**. Company of Biologists Ltd.

COMA, R., RIBES, M., GILI, J. & HUGHES, R. (2001) The ultimate opportunists: consumers of seston. *Marine Ecology Progress Series* **219**, 305–308.

CONLEY, K.R., LOMBARD, F. & SUTHERLAND, K.R. (2018) Mammoth grazers on the ocean's minuteness: a review of selective feeding using mucous meshes. *Proceedings of the Royal Society B: Biological Sciences* **285**, 20180056.

CORRADINI, F., MEZA, P., EGUILUZ, R., CASADO, F., HUERTA-LWANGA, E. & GEISSEN, V. (2019) Evidence of microplastic accumulation in agricultural soils from sewage sludge disposal. *Science of The Total Environment* **671**, 411–420.

COX, K.D., COVERNTON, G.A., DAVIES, H.L., DOWER, J.F., JUANES, F. & DUDAS, S.E. (2019) Human Consumption of Microplastics. *Environmental Science and Technology* **53**, 7068–7074.

CROWDER, L.B. (1985) Optimal foraging and feeding mode shifts in fishes. *Environmental Biology of Fishes* **12**, 57–62.

DI, H., MARTIN, G.J.O. & DUNSTAN, D.E. (2021) Characterization of particle deposition during cross fl ow fi ltration as in fl uenced by permeate fl ux and cross fl ow velocity using a micro fl uidic fi ltration system **15**, 552–561.

DIVI, R. V., STROTHER, J.A. & PAIG-TRAN, E.W.M. (2018) Manta rays feed using ricochet separation, a novel nonclogging filtration mechanism. *Science Advances* **4**, eaat9533.

DOHRMANN, M. & WÖRHEIDE, G. (2017) Dating early animal evolution using phylogenomic data. *Scientific Reports* **7**, 1–6.

DRURY, W.J., CHARACKLIS, W.G. & STEWART, P.S. (1993) Interactions of 1 µm latex particles with pseudomonas aeruginosa biofilms. *Water Research* **27**, 1119–1126.

EISENMANN, H., LETSIOU, I., FEUCHTINGER, A., BEISKER, W., MANNWEILER, E., HUTZLER, P. & ARNZ, P. (2001) Interception of Small Particles by Flocculent Structures, Sessile Ciliates, and the Basic Layer of a Wastewater Biofilm. *Applied and Environmental Microbiology* **67**, 4286–4292.

ELLIS, A.L., NORTON, A.B., MILLS, T.B. & NORTON, I.T. (2017) Stabilisation of foams by agar gel particles. *Food Hydrocolloids* **73**, 222–228. Elsevier Ltd.

ESSEL, R., ENGEL, L., CARUS, M. & AHRENS, R.H. (2015) Quellen für Mikroplastik mit Relevanz für den Meeresschutz in Deutschland. In *Gutachten* p. Dessau-Roßlau.

EVANGELIOU, N., GRYTHE, H., KLIMONT, Z., HEYES, C., ECKHARDT, S., LOPEZ-APARICIO, S. & STOHL, A. (2020) Atmospheric transport is a major pathway of microplastics to remote regions. *Nature Communications* **11**, 3381.

DE FALCO, F., DI PACE, E., AVELLA, M., GENTILE, G., ERRICO, M.E., KRZAN, A., ELKHIAR, H., ZUPAN, M. & COCCA, M. (2021) Development and Performance Evaluation of a Filtration System for Washing Machines to Reduce Microfiber Release in Wastewater. *Water, Air, & Soil Pollution* **232**. Springer International Publishing.

FARRELL, P. & NELSON, K. (2013) Trophic level transfer of microplastic: Mytilus edulis (L.) to Carcinus maenas (L.). *Environmental Pollution* **177**, 1–3.

FAYEMI, P.E., WANIECK, K., ZOLLFRANK, C., MARANZANA, N. & AOUSSAT, A. (2017) Biomimetics: process, tools and practice. *Bioinspiration & Biomimetics* **12**, 011002.

FENCHEL, T. (1987) *Ecology of Protozoa*, 1st edition. Springer Berlin Heidelberg, Berlin, Heidelberg.

FLOOD, P.R. & FIALA-MEDIONI, A. (1981) Ultrastructure and Histochemistry of the Food Trapping Mucous Film in Benthic Filter-Feeders (Ascidians). *Acta Zoologica* **62**, 53–65.

GAO, J., YUAN, Y., YU, Q., YAN, B., QIAN, Y., WEN, J., MA, C., JIANG, S., WANG, X. & WANG, N. (2020) Bio-inspired antibacterial cellulose paper-poly(amidoxime) composite hydrogel for highly efficient uranium(vi) capture from seawater. *Chemical Communications* **56**, 3935–

3938. Royal Society of Chemistry.

GARRIDO, S., MARÇALO, A., ZWOLINSKI, J. & VAN DER LINGEN, C. (2007) Laboratory investigations on the effect of prey size and concentration on the feeding behaviour of Sardina pilchardus. *Marine Ecology Progress Series* **330**, 189–199.

GASPERI, J., WRIGHT, S.L., DRIS, R., COLLARD, F., MANDIN, C., GUERROUACHE, M., LANGLOIS, V., KELLY, F.J. & TASSIN, B. (2018) Microplastics in air: Are we breathing it in? *Current Opinion in Environmental Science & Health* **1**, 1–5.

GESAMP (2016) Sources, fate and effects of microplastics in the marine environment: part 2 of a global assessment.

GIBSON, R.N.N. (1988) Development, morphometry and particle retention capability of the gill rakers in the herring, Clupea harengus L. *Journal of Fish Biology* **32**, 949–962.

GKOUTSELIS, G., ROHRBACH, S., HARJES, J., OBST, M., BRACHMANN, A., HORN, M.A. & RAMBOLD, G. (2021) Microplastics accumulate fungal pathogens in terrestrial ecosystems. *Scientific Reports* **11**, 1–13. Nature Publishing Group UK.

GOßMANN, I., SÜßMUTH, R. & SCHOLZ-BÖTTCHER, B.M. (2022) Plastic in the air?! - Spider webs as spatial and temporal mirror for microplastics including tire wear particles in urban air. *Science of The Total Environment* **832**, 155008.

GOUIN, T., ROCHE, N., LOHMANN, R. & HODGES, G. (2011) A thermodynamic approach for assessing the environmental exposure of chemicals absorbed to microplastic. *Environmental Science and Technology* **45**, 1466–1472.

GREGORY, M.R. (1977) Plastic pellets on New Zealand beaches. *Marine Pollution Bulletin* **8**, 82–84.

GRUBER, E.S., STADLBAUER, V., PICHLER, V., RESCH-FAUSTER, K., TODOROVIC, A., MEISEL, T.C., TRAWOEGER, S., HOLLÓCZKI, O., TURNER, S.D., WADSAK, W., VETHAAK, A.D. & KENNER, L. (2022) To Waste or Not to Waste: Questioning Potential Health Risks of Micro- and Nanoplastics with a Focus on Their Ingestion and Potential Carcinogenicity. *Exposure and Health*. Springer Netherlands.

GUO, C. YU, XU, P., WANG, C. & KAN, Z. (2019) Numerical and Experimental Study of Blockage Effect Correction Method in Towing Tank. *China Ocean Engineering* **33**, 522–536.

GUTOW, L., BARTL, K., SABOROWSKI, R. & BEERMANN, J. (2019) Gastropod pedal mucus retains microplastics and promotes the uptake of particles by marine periwinkles. *Environmental Pollution* **246**, 688–696. Elsevier Ltd.

HAMANN, L. & BLANKE, A. (2022) Suspension feeders: diversity, principles of particle separation and biomimetic potential. *Journal of The Royal Society Interface* **19**.

HANN, S., SHERRINGTON, JAMIESON, C., HICKMAN, O., KERSHAW, M., BAPASOLA, P.A. & COLE, G. (2018) Investigating options for reducing releases in the aquatic environment of microplastics emitted by (but not intentionally added in) products - Interim Report. *Report for DG Env EC* **Vol. 62**, **N**, 1596–1605.

HANSEN, B., BJORNSEN, P.K. & HANSEN, P.J. (1994) The size ratio between planktonic predators and their prey. *Limnology and Oceanography* **39**, 395–403.

HARTMANN, N.B., HÜFFER, T., THOMPSON, R.C., HASSELLÖV, M., VERSCHOOR, A., DAUGAARD, A.E., RIST, S., KARLSSON, T., BRENNHOLT, N., COLE, M., HERRLING, M.P., HESS, M.C., IVLEVA, N.P., LUSHER, A.L. & WAGNER, M. (2019) Are We Speaking the Same Language? Recommendations for a Definition and Categorization Framework for Plastic Debris. *Environmental Science and Technology* **53**, 1039–1047.

HELMS, M., VATTAM, S.S. & GOEL, A.K. (2009) Biologically inspired design: process and products **30**, 606–622.

HENTSCHEL, B.T. & SHIMETA, J. (2008) Suspension Feeders. In *Encyclopedia of Ecology* pp. 3437–3442. Elsevier Science Ltd, Amsterdam.

HÖLKER, F., VANNI, M.J., KUIPER, J.J., MEILE, C., GROSSART, H.-P., STIEF, P., ADRIAN, R., LORKE, A., DELLWIG, O., BRAND, A., NÜTZMANN, G. & LEWANDOWSKI, J. (2015) Tube-dwelling invertebrates: Tiny ecosystem engineers have large effects in lake ecosystems. *Ecological Monographs* **85**, 333–351.

HUANG, J., WU, X., CAI, D., CHEN, G., LI, D., YU, Y., PETRIK, L.F. & LIU, G. (2019) Linking solids retention time to the composition, structure, and hydraulic resistance of biofilms developed on support materials in dynamic membrane bioreactors. *Journal of Membrane Science* **581**, 158–167. Elsevier B.V.

HUANG, W., CHEN, M., SONG, B., DENG, J., SHEN, M., CHEN, Q., ZENG, G. & LIANG, J. (2021) Microplastics in the coral reefs and their potential impacts on corals: A mini-review. *Science of The Total Environment* **762**, 143112.

HUNG, T.-C., PIEDRAHITA, R.H. & CHEER, A. (2012) Bio-inspired particle separator design based on the food retention mechanism by suspension-feeding fish. *Bioinspiration & Biomimetics* **7**, 046003.

HUNG, T. & PIEDRAHITA, R.H. (2014) Experimental validation of a novel bio-inspired particle separator. *Aquacultural Engineering* **58**, 11–19.

IYARE, P.U., OUKI, S.K. & BOND, T. (2020) Microplastics removal in wastewater treatment plants: a critical review. *Environmental Science: Processes and Impacts* **6**, 2664–2675. Royal Society of Chemistry.

JØRGENSEN, C. (1983) Fluid mechanical aspects of suspension feeding. *Marine Ecology Progress Series* **11**, 89–103.

JØRGENSEN, C.B. (1966) *Biology of Suspension Feeding*. Pergamon Press, Oxford.

KALLENBACH, E.M.F., ERIKSEN, T.E., HURLEY, R.R., JACOBSEN, D. & LARSEN, C.S. (2022) Plastic recycling plant as a point source of microplastics to sediment and macroinvertebrates in a remote stream. *Microplastics and Nanoplastics*. Springer International Publishing.

KALYANKAR, H., MELWANKI, R., CHOUDHARY, D., JETHWA, S. & CHAUDHARI, D. (2015) Design and Analysis of Low Speed Water Tunnel for Flow Visualization of Bluff Body. *2nd International Conference on Advances in Mechanical Engineering and its Interdisciplinary Areas*, 49–57.

KOOLOOS, J.G.M., KRAAIJEVELD, A.R., LANGENBACH, G.E.J. & ZWEERS, G.A. (1989) Comparative mechanics of filter feeding in Anas platyrhynchos, Anas clypeata and Aythya fuligula (Aves, Anseriformes). *Zoomorphology* **108**, 269–290.

KULKARNI, V., SAHOO, N. & CHAVAN, S.D. (2011) Simulation of honeycomb–screen combinations for turbulence management in a subsonic wind tunnel. *Journal of Wind Engineering and Industrial Aerodynamics* **99**, 37–45.

KUNDUKAD, B., SEVIOUR, T., LIANG, Y., RICE, S.A., KJELLEBERG, S. & DOYLE, P.S. (2016) Mechanical properties of the superficial biofilm layer determine the architecture of biofilms. *Soft Matter* **12**, 5718–5726. Royal Society of Chemistry.

LAFTAH, W.A., HASHIM, S. & IBRAHIM, A.N. (2011) Polymer hydrogels: A review. *Polymer - Plastics Technology and Engineering* **50**, 1475–1486.

LAI, S.K., WANG, Y.-Y., WIRTZ, D. & HANES, J. (2009) Micro- and macrorheology of mucus. *Advanced Drug Delivery Reviews* **61**, 86–100.

LAM, C.S., RAMANATHAN, S., CARBERY, M., GRAY, K., VANKA, K.S., MAURIN, C., BUSH, R. & PALANISAMI, T. (2018) A Comprehensive Analysis of Plastics and Microplastic Legislation Worldwide. *Water, Air, and Soil Pollution* **229**.

LANGLET, D., BOUCHET, V.M.P., DELAETER, C. & SEURONT, L. (2020) Motion behavior and metabolic response to microplastic leachates in the benthic foraminifera Haynesina germanica. *Journal of Experimental Marine Biology and Ecology* **529**, 151395.

LASIC, E. (2014) Sustainable use of washing machine : modeling the consumer behavior related resources consumption in use of washing machines. University of Bonn.

LASSEN, C., HANSEN, S.F., MAGNUSSON, K., NOREN, F., HARTMANN, N.B., REHNE JENSEN, P., NIELSEN, T.G. & BRINCH, A. (2015) Microplastics - Occurrence, effects and sources of release to the environment of Denmark.

LEBRETON, L.C.M., VAN DER ZWET, J., DAMSTEEG, J.W., SLAT, B., ANDRADY, A. & REISSER, J. (2017) River plastic emissions to the world's oceans. *Nature Communications* **8**, 1–10. Nature Publishing Group.

LENTON, T.M., BOYLE, R.A., POULTON, S.W., SHIELDS-ZHOU, G.A. & BUTTERFIELD, N.J. (2014) Co-evolution of eukaryotes and ocean oxygenation in the Neoproterozoic era. *Nature Geoscience* **7**, 257–265.

LESLIE, H.A., VELZEN, M.J.M. VAN, BRANDSMA, S.H., GARCIA-VALLEJO, J.J. & LAMOREE, M.H. (2022) blood. *Environment International*, 107199. Elsevier LTD.

LI, H., RAZA, A., YUAN, S., ALMARZOOQI, F., FANG, N.X. & ZHANG, T.J. (2022) Biomimetic on-chip filtration enabled by direct micro-3D printing on membrane. *Scientific Reports* **12**, 1–9. Nature Publishing Group UK.

LI, L., XU, G., YU, H. & XING, J. (2018) Dynamic membrane for micro-particle removal in wastewater treatment: Performance and influencing factors. *Science of the Total Environment* **627**, 332–340.

LIU, M., ZHANG, J., SHAN, W. & HUANG, Y. (2015) Developments of mucus penetrating nanoparticles. *Asian Journal of Pharmaceutical Sciences* **10**, 275–282. Elsevier.

LUMLEY, J.L. (1964) Passage of a Turbulent Stream Through Honeycomb of Large Length-to-Diameter Ratio. *Journal of Basic Engineering* **86**, 218–220.

MAGA, D., GALAFTON, C., BLÖMER, J., THONEMANN, N., ÖZDAMAR, A. & BERTLING, J. (2022) Methodology to address potential impacts of plastic emissions in life cycle assessment. *The International Journal of Life Cycle Assessment*, 469–491. Springer Berlin Heidelberg.

MAGA, D., THONEMANN, N., STROTHMANN, P. & SONNEMANN, G. (2021) Resources , Conservation & Recycling How to account for plastic emissions in life cycle inventory analysis ? *Resources, Conservation & Recycling* **168**, 105331. Elsevier B.V.

MAGNUSSON, K., ELIASSON, K., FRÅNE, A., HAIKONEN, K., HULTÉN, J., OLSHAMMAR, M., STADMARK, J. & VOISIN, A. (2016) Swedish sources and pathways for microplastics to the marine environment. A review of existing data. *IVL report*, 1–89.

MANKINS, J.C. (1995) Technology Readiness Levels.

MARTIN, K.J. & NERENBERG, R. (2012) The membrane biofilm reactor (MBfR) for water and wastewater treatment: Principles, applications, and recent developments. *Bioresource Technology* **122**, 83–94. Elsevier Ltd.

MASSELTER, T., SCHAUMANN, U., KAMPOWSKI, T., ULRICH, K., THIELEN, M., BOLD, G. & SPECK, T. (2022) Improvement of a microfiber filter for domestic washing machines. *Bioinspiration & Biomimetics* **18**, 22408–22418.

MCCLATCHIE, S. & BOYD, C.M. (1983) Morphological Study of Sieve Efficiencies and Mandibular Surfaces in the Antarctic Krill, Euphausia superba. *Canadian Journal of Fisheries and Aquatic Sciences* **40**, 955–967.

MCSHANE, A., BATH, J., JARAMILLO, A.M., RIDLEY, C., WALSH, A.A., EVANS, C.M., THORNTON, D.J. & RIBBECK, K. (2021) Mucus. *Current Biology* **31**, R938–R945.

MIKOS, A.G. & PEPPAS, N.A. (1990) Bioadhesive analysis of controlled-release systems. IV. An experimental method for testing the adhesion of microparticles with mucus. *Journal of Controlled Release* **12**, 31–37.

MOORE, J.W. & MALLATT, J.M. (1980) Feeding of Larval Lamprey. *Canadian Journal of Fisheries and Aquatic Sciences* **37**, 1658–1664.

MORE, T.T., YADAV, J.S.S., YAN, S., TYAGI, R.D. & SURAMPALLI, R.Y. (2014) Extracellular polymeric substances of bacteria and their potential environmental applications. *Journal of Environmental Management* **144**, 1–25. Elsevier Ltd.

MØRETRØ, T., MOEN, B., ALMLI, V.L., TEIXEIRA, P., FERREIRA, V.B., ÅSLI, A.W., NILSEN, C. & LANGSRUD, S. (2021) Dishwashing sponges and brushes: Consumer practices and bacterial growth and survival. *International Journal of Food Microbiology* **337**.

MOTTA, P.J., MASLANKA, M., HUETER, R.E., DAVIS, R.L., DE LA PARRA, R., MULVANY, S.L., HABEGGER, M.L., STROTHER, J.A., MARA, K.R., GARDINER, J.M., TYMINSKI, J.P. & ZEIGLER, L.D. (2010) Feeding anatomy, filter-feeding rate, and diet of whale sharks Rhincodon typus during surface ram filter feeding off the Yucatan Peninsula, Mexico. *Zoology* **113**, 199–212.

MOTULSKY, H. & CHRISTOPOULOS, A. (2003) *Fitting Models to Biological Data using Linear and Nonlinear Regression*, 4th edition. GraphPad Software Inc., San Diego.

MUNHOZ, D.R., HARKES, P., BERIOT, N., LARRETA, J. & BASURKO, O.C. (2022) Microplastics: A Review of Policies and Responses. *Microplastics* **2**, 1–26.

NELMS, S.E., BARNETT, J., BROWNLOW, A., DAVISON, N.J., DEAVILLE, R., GALLOWAY, T.S., LINDEQUE, P.K., SANTILLO, D. & GODLEY, B.J. (2019) Microplastics in marine mammals stranded around the British coast: ubiquitous but transitory? *Scientific Reports* **9**, 1–8. Springer US.

NELMS, S.E., GALLOWAY, T.S., GODLEY, B.J., JARVIS, D.S. & LINDEQUE, P.K. (2018) Investigating microplastic trophic transfer in marine top predators. *Environmental Pollution* **238**, 999–1007. Elsevier Ltd.

NOWELL, A.R.M. & JUMARS, P.A. (1987) Flumes: theoretical and experimental considerations for simulation of benthic environments. In *Oceanography and Marine Biology* p. 573.

OECD (2022) Global Plastics Outlook: Policy Scenarios to 2060. Paris.

OKABE, S., YASUDA, T. & WATANABE, Y. (1997) Uptake and release of inert fluorescence particles by mixed population biofilms. *Biotechnology and Bioengineering* **53**, 459–469.

PAIG-TRAN, E.W.M., BIZZARRO, J.J., STROTHER, J.A. & SUMMERS, A.P. (2011) Bottles as models: Predicting the effects of varying swimming speed and morphology on size selectivity and filtering efficiency in fishes. *Journal of Experimental Biology* **214**, 1643–1654.

PAKULA, C. & STAMMINGER, R. (2010) Electricity and water consumption for laundry washing by washing machine worldwide, 365–382.

PEEKEN, I., PRIMPKE, S., BEYER, B., GÜTERMANN, J., KATLEIN, C., KRUMPEN, T., BERGMANN, M., HEHEMANN, L. & GERDTS, G. (2018) Arctic sea ice is an important temporal sink and means of transport for microplastic. *Nature Communications* **9**, 1505.

PENNACHETTI, C.A. (1984) Functional morphology of the branchial basket of ascidia paratropa (Tunicata, Ascidiacea). *Zoomorphology* **104**, 216–222.

PIEDRAHITA, R.H. & HUNG, T.C. (2015) Crossflow Filtration Particle Separator. USA.

PRATA, J.C. (2018) Airborne microplastics: Consequences to human health? *Environmental Pollution* **234**, 115–126. Elsevier Ltd.

PRATA, J.C., DA COSTA, J.P., LOPES, I., DUARTE, A.C. & ROCHA-SANTOS, T. (2020) Environmental exposure to microplastics: An overview on possible human health effects. *Science of the Total Environment* **702**, 134455. Elsevier B.V.

PS PROZESSTECHNIK GMBH, N. (2023) Pressure driven membrane processes: Calculations. Https://www.ps-prozesstechnik.com/en/membrane-technology/membrane-process-development/membrane-process-calculation.html.

RAGUSA, A., SVELATO, A., SANTACROCE, C., CATALANO, P., NOTARSTEFANO, V., CARNEVALI, O., PAPA, F., RONGIOLETTI, M.C.A., BAIOCCO, F., DRAGHI, S., D'AMORE, E., RINALDO, D., MATTA, M. & GIORGINI, E. (2021) Plasticenta: First evidence of microplastics in human placenta. *Environment International* **146**, 106274. Elsevier Ltd.

RASHID, M.T., FRASCA, M., ABDULKAREEM, A., ALI, R.S., FORTUNA, L. & XIBILIA, M.G. (2012) Artemia swarm dynamics and path tracking, 555–563.

REICHERT, P. & WANNER, O. (1997) Movement of solids in biofilms: Significance of liquid phase transport. *Water Science and Technology* **36**, 321–328. International Association on Water Quality.

RICHARDSONS, J.F., HARKER, J.H. & BACKHURST, J.R. (2002) *Coulson and Richardson's Chemical Engingeering: Particle Technology and Separation Processes*.

RIISGÅRD, H. & GOLDSON, A. (1997) Minimal scaling of the lophophore filter-pump in ectoprocts (Bryozoa) excludes physiological regulation of filtration rate to nutritional needs. Test of hypothesis. *Marine Ecology Progress Series* **156**, 109–120.

RIISGÅRD, H. & LARSEN, P. (2010) Particle capture mechanisms in suspension-feeding invertebrates. *Marine Ecology Progress Series* **418**, 255–293.

RILLIG, M.C. & BONKOWSKI, M. (2018) Microplastic and soil protists: A call for research. *Environmental Pollution* **241**, 1128–1131.

RISSE-BUHL, U. & KÜSEL, K. (2009) Colonization dynamics of biofilm-associated ciliate morphotypes at different flow velocities. *European Journal of Protistology* **45**, 64–76.

ROBERTS, D., GEBRUK, A., LEVIN, V. & MANSHIP, B.A.D. (2000) Feeding and digestive strategies in deposit-feeding Holothurians. *Oceanography and marine biology: an annual review.* **38**, 257–310.

ROCHE, K.R., DRUMMOND, J.D., BOANO, F., PACKMAN, A.I., BATTIN, T.J. & HUNTER, W.R. (2017) Benthic biofilm controls on fine particle dynamics in streams. *Water Resources Research* **53**, 222–236.

ROCHMAN, C.M., BROOKSON, C., BIKKER, J., DJURIC, N., EARN, A., BUCCI, K., ATHEY, S., HUNTINGTON, A., MCILWRAITH, H., MUNNO, K., FROND, H. DE, KOLOMIJECA, A., ERDLE, L., GRBIC, J., BAYOUMI, M., ET AL. (2019) Rethinking microplastics as a diverse contaminant suite. *Environmental Toxicology and Chemistry* **38**, 703–711.

ROLF, M., LAERMANNS, H., KIENZLER, L., POHL, C., MÖLLER, J.N., LAFORSCH, C., LÖDER, M.G.J. & BOGNER, C. (2022) Flooding frequency and floodplain topography determine abundance of microplastics in an alluvial Rhine soil. *Science of the Total Environment*

836, 155141. The Authors.

ROLLING HILLS RESEARCH CORPORATION (2015) University Desktop Water Tunnel Model 0710. *Water Tunnels*, 3–5.

RUBENSTEIN, D.I. & KOEHL, M.A.R. (1977) The Mechanisms of Filter Feeding: Some Theoretical Considerations. *The American Naturalist* **111**, 981–994.

DE SÁ, L.C., OLIVEIRA, M., RIBEIRO, F., ROCHA, T.L. & FUTTER, M.N. (2018) Studies of the effects of microplastics on aquatic organisms: What do we know and where should we focus our efforts in the future? *Science of the Total Environment* **645**, 1029–1039.

SANDERSON, S.L., ROBERTS, E., LINEBURG, J. & BROOKS, H. (2016) Fish mouths as engineering structures for vortical cross-step filtration. *Nature Communications* **7**, 11092. Nature Publishing Group.

SANDERSON, S.L.L. & WASSERSUG, R.J. (1993) Convergent and Alternative Designs for Vertebrate Suspension Feeding. In *The skull* (eds J. HANKEN & B.K. HALL), pp. 37–112. University of Chicago Press, Chicago and London.

SANTOS, R.G., MACHOVSKY-CAPUSKA, G.E. & ANDRADES, R. (2021) Plastic ingestion as an evolutionary trap: Toward a holistic understanding. *Science* **373**, 56–60.

SCHEIMAN, J. & BROOKST, J.D. (1981) Comparison of experimental and theoretical turbulence reduction from screens, honeycomb, and honeycomb-screen combinations. *Journal of Aircraft* **18**, 638–643.

SCHÖPEL, B. & STAMMINGER, R. (2019) A Comprehensive Literature Study on Microfibres from Washing Machines **56**, 94–104.

SCHROEDER, A., MARSHALL, L., TREASE, B., BECKER, A. & SANDERSON, S.L.L. (2019) Development of helical, fish-inspired cross-step filter for collecting harmful algae. *Bioinspiration & Biomimetics* **14**, 056008.

SEBENS, K., SARÀ, G. & NISHIZAKI, M. (2017) Energetics, particle capture, and growth dynamics of benthic suspension feeders. In *Marine Animal Forests: The Ecology of Benthic Biodiversity Hotspots* pp. 813–854. Springer, New York.

SENATHIRAJAH, K., ATTWOOD, S., BHAGWAT, G., CARBERY, M., WILSON, S. & PALANISAMI, T. (2021) Estimation of the mass of microplastics ingested – A pivotal first step towards human health risk assessment. *Journal of Hazardous Materials* **404**, 124004. Elsevier B.V.

SETYORINI, L., MICHLER-KOZMA, D., SURES, B. & GABEL, F. (2021) Transfer and effects of PET

microfibers in Chironomus riparius. *Science of the Total Environment* **757**, 143735. Elsevier B.V.

SHERRINGTON, C., DARRAH, C., HANN, S., COLE, G. & CORBIN, M. (2016) Study to support the development of measures to combat a range of marine litter sources. Report for European Commission DG Environment, 429.

SHIMETA, J. & JUMARS, P.A. (1991) Physical mechanisms and rates of particle capture by suspension- feeders. *Oceanography and marine biology: an annual review* **29**, 191–257.

SHIMETA, J. & KOEHL, M.A.R. (1997) Mechanisms of particle selection by tentaculate suspension feeders during encounter, retention, and handling. *Journal of Experimental Marine Biology and Ecology* **209**, 47–73.

SHTERN, V., BORISSOV, A. & HUSSAIN, F. (1998) Vortex sinks with axial flow: Solution and applications. *Physics and Fluids* **9**.

SMITH, J.C. & SANDERSON, S.L. (2007) Mucus function and crossflow filtration in a fish with gill rakers removed versus intact. *Journal of Experimental Biology* **210**, 2706–2713.

DE SOUZA MACHADO, A.A., KLOAS, W., ZARFL, C., HEMPEL, S. & RILLIG, M.C. (2018) Microplastics as an emerging threat to terrestrial ecosystems. *Global Change Biology* **24**, 1405–1416.

SPROUSE, G. & RITTMANN, B.E. (1990) Colloid Filtration in Fluidized Beds. *Journal of Environmental Engineering* **116**, 299–313.

STATISTA (2023) Absatz von Waschinen in Deutschland. Https://de.statista.com/statistik/daten/studie/556824/umfrage/absatz-von-waschmaschinen-in-deutschland/.

STEENSGAARD, I.M., SYBERG, K., RIST, S., HARTMANN, N.B., BOLDRIN, A. & HANSEN, S.F. (2017) From macro- to microplastics - Analysis of EU regulation along the life cycle of plastic bags. *Environmental Pollution* **224**, 289–299.

STOECKER, D.K., MICHAELS, A.E. & DAVIS, L.H. (1987) Grazing by the jellyfish, Aurelia aurita, on microzooplankton. In *Journal of Plankton Research* p.

STOODLEY, P., DEBEER, D. & LEWANDOWSKI, Z. (1994) Liquid flow in biofilm systems. *Applied and Environmental Microbiology* **60**, 2711–2716.

STORM, T.J., NOLAN, K.E., ROBERTS, E.M. & SANDERSON, S.L. (2020) Oropharyngeal morphology related to filtration mechanisms in suspension-feeding American shad (Clupeidae). *Journal of Experimental Zoology Part A: Ecological and Integrative*

Physiology **333**, 493–510.

SUTHERLAND, K. (2005) *The A-Z of Filtration and Related Separations*. In *Filtration & Separation* p. Elsevier Science Ltd, Surrey.

SUTHERLAND, K. (2008) *Filters and Filtration Handbook*Fifth Edit. Elsevier.

THOMAS, P.C., CIPRIANO, B.H. & RAGHAVAN, S.R. (2011) Nanoparticle-crosslinked hydrogels as a class of efficient materials for separation and ion exchange. *Soft Matter* **7**, 8192–8197.

TRAGER, G.C., HWANG, J.-S. & STRICKLER, J.R. (1990) Barnacle suspension-feeding in variable flow. *Marine Biology* **105**, 117–127.

TRIEBSKORN, R., BRAUNBECK, T., GRUMMT, T., HANSLIK, L., HUPPERTSBERG, S., JEKEL, M., KNEPPER, T.P., KRAIS, S., MÜLLER, Y.K., PITTROFF, M., RUHL, A.S., SCHMIEG, H., SCHÜR, C., STROBEL, C., WAGNER, M., ET AL. (2019) Relevance of nano- and microplastics for freshwater ecosystems: A critical review. *TrAC - Trends in Analytical Chemistry* **110**, 375–392.

TURRELL, W.R. (2020) Estimating a regional budget of marine plastic litter in order to advise on marine management measures. *Marine Pollution Bulletin* **150**, 110725. Elsevier.

VINCENT, J.F.V., BOGATYREVA, O.A., BOGATYREV, N.R., BOWYER, A. & PAHL, A.K. (2006) Biomimetics: Its practice and theory. *Journal of the Royal Society Interface* **3**, 471–482.

VOGEL, S. (1996) *Life in Moving Fluids: The Physical Biology of Flow - Revised and Expanded Second Edition*. Princeton University Press, Princeton.

WAGGETT, R. (1999) Capture mechanisms used by the lobate ctenophore, Mnemiopsis leidyi, preying on the copepod Acartia tonsa. *Journal of Plankton Research* **21**, 2037–2052.

WANIECK, K., HAMANN, L., BARTZ, M., UTTICH, E., HOLLERMANN, M., DRACK, M. & BEISMANN, H. (2022) Biomimetics Linked to Classical Product Development: An Interdisciplinary Endeavor to Develop a Technical Standard, 1–11.

WARD, J.E. & SHUMWAY, S.E. (2004) Separating the grain from the chaff: Particle selection in suspension- and deposit-feeding bivalves. *Journal of Experimental Marine Biology and Ecology* **300**, 83–130.

WERTH, A.J. (2004) Models of hydrodynamic flow in the bowhead whale filter feeding apparatus. *Journal of Experimental Biology* **207**, 3569–3580.

WERTH, A.J. (2019) Variable Porosity of Throughput and Tangential Filtration in Biological and 3D Printed Systms. In *Advances in Engineering Research.* (ed V.M. PETROVA), pp. 571–

582. Hampden-Sydney, VA.

WESTHEIDE, W. & RIEGER, G. (2013) *Spezielle Zoologie. Teil 1: Einzeller und Wirbellose Tiere*. Springer Berlin Heidelberg, Berlin, Heidelberg.

VAN WEZEL, A., CARIS, I. & KOOLS, S.A.E. (2016) Release of primary microplastics from consumer products to wastewater in the Netherlands. *Environmental Toxicology and Chemistry* **35**, 1627–1631.

WILDISH, D. & KRISTMANSON, D.D. (1997) *Benthic suspension feeders and flow*. Cambridge University Press.

WILLIAMS, T.M. & KOOYMAN, G.L. (1985) Swimming Performance and Hydrodynamic Characteristics of Harbor Seals Phoca vitulina. *Physiological Zoology* **58**, 576–589.

WING, S. & JACK, L. (2012) Resource specialisation among suspension-feeding invertebrates on rock walls in Fiordland, New Zealand, is driven by water column structure and feeding mode. *Marine Ecology Progress Series* **452**, 109–118.

WITTE, U., BRATTEGARD, T., GRAF, G. & SPRINGER, B. (1997) Particle capture and deposition by deep-sea sponges from the Norwegian-Greenland Sea. *Marine Ecology Progress Series* **154**, 241–252.

WRIGHT, S.L., THOMPSON, R.C. & GALLOWAY, T.S. (2013) The physical impacts of microplastics on marine organisms: a review. *Environmental pollution (Barking, Essex : 1987)* **178**, 483–492.

YAHEL, G., EERKES-MEDRANO, D.I. & LEYS, S.P. (2006) Size independent selective filtration of ultraplankton by hexactinellid glass sponges. *Aquatic Microbial Ecology* **45**, 181–194.

YAN, Z., LIU, Y., ZHANG, T., ZHANG, F., REN, H. & ZHANG, Y. (2021) Analysis of Microplastics in Human Feces Reveals a Correlation between Fecal Microplastics and Inflammatory Bowel Disease Status. *Environmental Science & Technology*.

YIN, L., WEN, X., HUANG, D., DU, C., DENG, R., ZHOU, Z., TAO, J., LI, R., ZHOU, W., WANG, Z. & CHEN, H. (2021) Interactions between microplastics/nanoplastics and vascular plants. *Environmental Pollution* **290**, 117999.

ZHANG, D., LIU, X., HUANG, W., LI, J., WANG, C., ZHANG, D. & ZHANG, C. (2020) Microplastic pollution in deep-sea sediments and organisms of the Western Pacific Ocean. *Environmental Pollution* **259**, 113948.

ZHANG, T.C. & BISHOP, P.L. (1994) Density, porosity, and pore structure of biofilms. *Water Research* **28**, 2267–2277.

ZHANG, Y.-Q., LYKAKI, M., ALRAJOULA, M.T., MARKIEWICZ, M., KRAAS, C., KOLBE, S., KLINKHAMMER, K., RABE, M., KLAUER, R. & STOLTE, S. (2021) Microplastics from textile origin – emission and reduction measures. *Green Chemistry* **23**, 5247–5271. Royal Society of Chemistry.

ZHANG, Y.S. & KHADEMHOSSEINI, A. (2017) Advances in engineering hydrogels. *Science* **356**.

ZHENG, Y., LI, J., SUN, C., CAO, W., WANG, M., JIANG, F. & JU, P. (2021) Comparative study of three sampling methods for microplastics analysis in seawater. *Science of The Total Environment* **765**, 144495.

ZUUR, A.F., IENO, E.N. & ELPHICK, C.S. (2010) A protocol for data exploration to avoid common statistical problems. *Methods in Ecology and Evolution* **1**, 3–14.

10.   Appendix

10.1. Supplementary Information

10.1.1. Kitchen Sponge Survey

(Original in German)

Dear participants,

I am pleased that you want to participate in my study on microplastic emissions from kitchen sponges. I would like to measure how much weight a sponge loses in material during normal use, which then ends up as microplastics in the wastewater.

Procedure: Two different types of sponges will be tested (classic vs. organic). The sponges will be drawn by lot. Please use the sponge as you do normally in the kitchen from the moment you receive it.

End point: The test ends when you feel that the sponge should be discarded. Please contact me and return the sponge to me or my colleagues (do not throw it away!).

In order for me to assess how the sponge is being used, you will need to answer a few questions. The results will be published, but your data will of course remain anonymous.

Sponge number_____   Start date: _____

                                                End date: _____

1)   How many persons live in your household? _____

2)   Do you have a dishwasher?   O Yes   O No

3)   How is the sponge used?

   O Rinsing

   O Cleaning

   O In combination with rinsing detergent

   O In combination with cleaning detergent

   Comments_____

4)   How often do you use the sponge?

   O Several times per day

   O Once per day

   O Less than once per day

   Comments_____

5)   How long on average is the sponge used per day?

O up to 5 min

O 5-15 min

O 15-25 min

O 25-35 min

O 35-45 min

O more than 45 min

       Comments

O   I am voluntarily participating in the study. The personal data will be deleted after completion of the study. I agree that the study results may be published anonymously.

Date, Signature

10.1.2. Water Tunnel Setup

Based on a manuscript in preparation:

Herzog, Hendrik; Schreiber, Kristina; Grünewald, Christian; Hamann, Leandra; Blanke, Alexander (in prep), Compact water tunnel to study fluid flow around objects

During the course of our scientific study in which we investigated flow patterns around fish, we designed a water tunnel that compromises general design guidelines and a reduction in size and costs but still achieves laminar flow in the test section. Therefore, we developed an inlet and outlet section that breaks down vortices induced by the 90° turns of the circular design and distributes the water equally along the flow tank. In order to visualise streamlines, we developed ink mixtures with suitable properties to observe single streamlines over the distance of the test section. Additionally, we provide information about design, manufacturing, and handling during the experiments. This water tunnel design allows students and scientists to study diverse flow phenomena around solid objects and validate CFD simulations.

Design of the tank

One of the most critical aspects when designing a water tunnel is the distance of the test objects to the tunnel walls and the blocked area of the cross-section by the test object. Flow around objects that are too near to the tunnel walls is influenced by the wall-effect and thus would show artificial flow conditions (Guo *et al.*, 2019). Therefore, blocked area by the test object should be as small as possible. As a consequence, object size should be planned before the water tunnel design, as all parts have to be scaled accordingly. We planned to investigate round objects with a maximum diameter of 5 cm and allowed a maximum blocked area of the cross-section of 5%, so our test section has a cross-section of 20 x 20 cm². The inlet length of our flow tank is one metre long, resulting in a length-to-width-ratio of 5, the "practical lower limit" according to Vogel & LaBarbera (1978). Additionally, the inlet region has a four times larger width than the examination section (constriction-ratio of 4) to ensure that water slowly passes the honeycombs. In total, the tank's overall size ended up being 2.5 m in length and 0.8 m in width and a total weight of about 400 kg (85 kg tank + 260 l water + additional equipment) that is supported by a rig. In order to achieve this small size by maintaining laminar and uniform flow within the test section, we present a new design of the inlet and outlet section.

Reducing turbulence by new inlet and outlet section

We decided for a vertical circular design with four sharp directional changes by 90°: inside the pump, inlet and outlet in the tank, and one below the tank. A custom-built diffuser was added to the inlet to settle the incoming turbulent flow from the pump and the 90° turn, which 1) redirects the flow horizontally, 2) distributes the flow equally along the vertical axis, i.e., with similar velocity bottom to top, and 3) distribute the flow in five horizontal planes such that equal velocities along the honeycomb wall were achieved. The diffuser was positioned centrally

above the inlet, weighted down for testing and later glued to the bottom of the flow tank by means of PDMS silicone. Because the momentum of the water results in higher flow velocities at the water surface than at the walls, four sieve-like plates (relevant thickness equal to wall thickness of outer hollow cylinder) each featuring 120 holes (diameter of 8.5 mm) were manufactured by means of a CNC mill. These plates separate the diffuser into five horizontally-stacked chambers, each featuring additional holes (diameter of 8.5 mm) to release water into the settling tank. The water level must be at least 1 cm above the highest row of holes in the diffuser, and the water flow within the diffuser needs to be distributed in such a way that the water flow released from each chamber is the same (similar flow velocity in all vertical sheets of the flow tank). As a consequence of the passage of subsequent chambers, fewer holes are needed in the lowest chamber to compensate for the added hydrodynamic resistance along the diffuser.

Due to the equal distribution of flow velocity along the vertical axis, the settling area within the inlet section can be shorter and has a constriction ratio of 4. Additionally, the tapered inlet section reduces the build-up of a boundary layer at the tank walls (this is a simplified description, details, e.g., in Prandtl 1904, Schlichting 1979) and increases the honeycomb wall cross-section area, which reduces pressure loss. Honeycombs are placed downstream of the inflow area to create a uniform and laminar flow in the study area. Our honeycombs consist of single cells with a diameter of 4 mm. This results in a length-to-diameter-ratio of 12.5, slightly higher than the suggested optimum for wind tunnels of 8 to 10 (Kulkarni, Sahoo, & Chavan, 2011). Since the reduction in the tangential component of the velocity is proportional to the length-to-diameter ratio of the length of the single cell (Lumley, 1964), larger length-to-diameter-ratios result in straighter flow at the expense of higher friction. Alternatively, further laminarisation of flow while maintaining a high flow velocity could be achieved by combining honeycombs with a downstream screen (Scheiman & Brookst, 1981). We experimentally determined the optimal position of the 3-4 honeycomb walls during calibration of the flow tank.

In the outlet region of the water tunnel, the water is sucked down into the pipeline system by the pump. Although the outlet is often considered less relevant than the inlet, it can also induce non-uniform and asymmetric flow conditions in the test section, lead to vortex formation, generation of gurgling noise, or air in-take that may damage the pump in the long-term (Nowell & Jumars, 1987; Shtern, Borissov, & Hussain, 1998). Therefore, the sink should be placed at a considerable distance downstream of the test section, e.g., 45 cm in the case of our water tunnel. We also implemented a flow splitter to distribute the flow equally to the left and right sides. Vortex formation above the pipeline was reduced by adding a cross-shaped vortex breaker made from two thin acrylic plates fitted inside the flow splitter and a perforated plate was slid into the downstream side of the flow divider to ensure that flow velocity in all vertical

layers was equa. We tested different hole patterns and found the best results for a plate featuring 245 holes, each 8.5 mm in diameter. In addition to the vortex reduction by the vortex breaker, air intake is avoided by plates covering the water surface above the sink. Thereby, we avoided two sinks in the outlet section that form two swirls of opposite rotation direction (Kalyankar *et al.*, 2015; Rolling Hills Research Corporation, 2015), reducing manufacturing complexity.

We injected the ink into the water by a custom-built apparatus featuring 1) an ink reservoir, 2) a mounting rod to place the reservoir at a defined height, 3) a regulator to adjust the flow rate of the ink, 4) a tubing, and 5) a small brass pipe to guide the ink into the tank.

10.1.3. Specifications of Test Particles

Particles	Length [mm]	Material	Density	Additional information	Source/ fabrication
Brine shrimp eggs	0.242 ± 0.019	NA	1.09 g/cm³	-	University of Bonn
Brine shrimp adults	6.112 ± 0.993	NA	1.09 g/cm³	-	Breeding by Sea Life Oberhausen
Cotton fibres	0.2 - 4	Cotton, white	1.51 g/cm³	DMT Prüfstaub Typ 8	Provided by Hengst SE
Polyamide particles	0.00002 – 2	Polyamide, orange	1.08 g/cm³	*see manufacturing process	VESTAMID® LX9057 orange E20081 by Evonik
Flock fibres	2 mm (dtex 3.3)	Polyamide, green	1.08 g/cm³	Dtex = 22	Borchert + Moller GmbH & Co. KG

*The orange polyamide polymer (VESTAMID® LX9057 orange E20081) was selected because its density is close to water and to be able to observe the particles during the experiments. The polymer came in pellets and was reduced in size through a cryogenic grinding process at Fraunhofer UMSICHT. The particle size distribution in the obtained powder was characterised by a Malvern Mastersizer 2000 (Hydro2000S). Particle size ranges between 0.020 µm and 2000 µm with a median of around 130 µm (Figure 26).
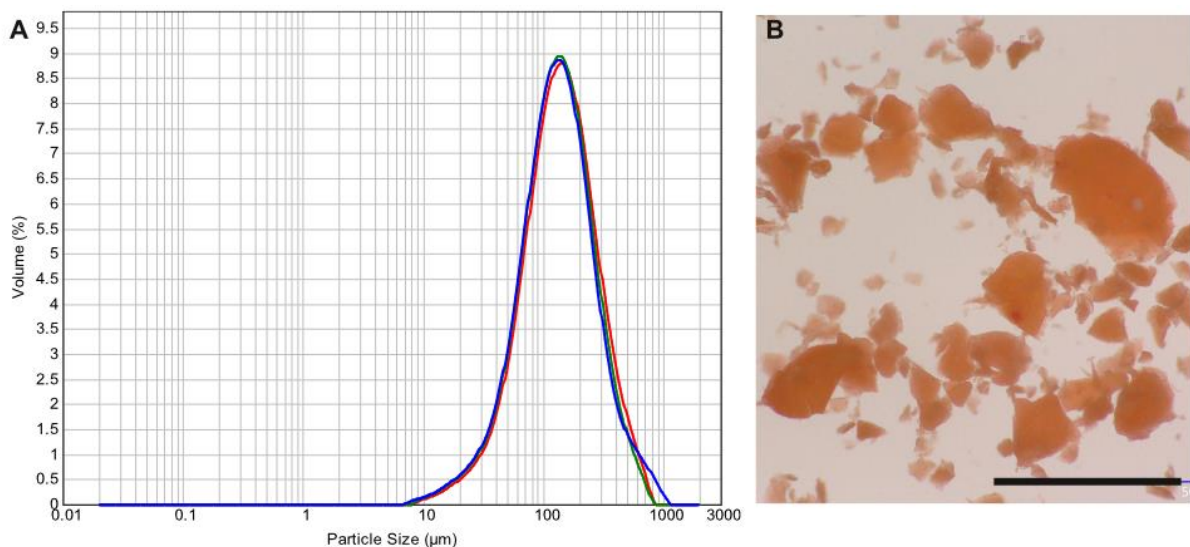
Figure 26: Polyamide particles as artificial MPs. A) Particle size distribution measured with a Mastersizer. **B)** The orange polyamide particles are of irregular shape. Scale = 500 µm.

10.1.4. Dimensions of Filter Elements

Table 4: Overview of three biomimetic filter elements and a dead–end filter for comparison.
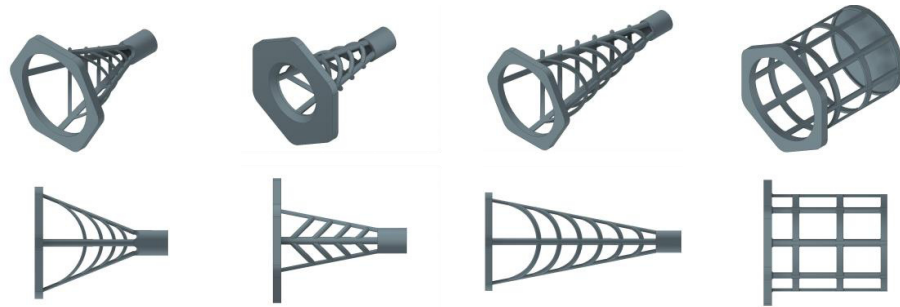
	Small-22	Small-11	Large-11	Dead-end
Filter length L_F [mm]	62.6	52.7	102.7	60.8
Angle of attack α [°]	22	11	11	0
Inner diameter at inlet d_M [mm]	50	30.5	50	50
Inner diameter of outlet d_C [mm]	10	10	10	50
Filtration area A_F [mm²]	5075.4	3415.5	9861.1	9860.0
Mesh size [µm]	100	100	100	100
Open area A0 [%]	44	44	44	44

10.1.5. Flow through filter elements
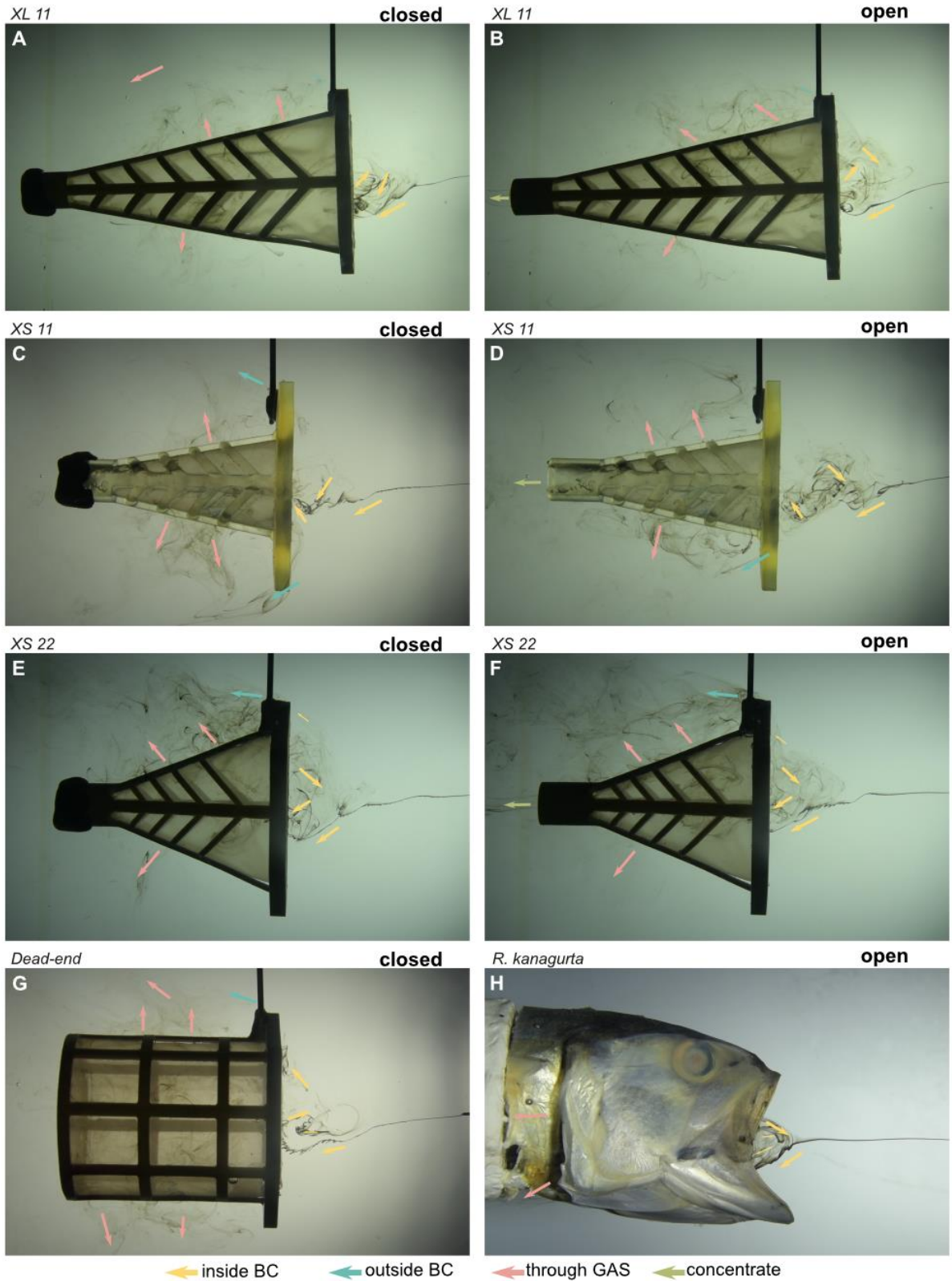
Figure 27: Exemplary pictures of flow through the four filter elements in a water tunnel with streamlines visualized by black ink: XL 11 filter with A) closed and B) open concentrate exit, XS 11 filter with C) closed and D) open concentrate exit, XS 2 filter with C) closed and D) open concentrate exit, G) dead-end filter and H) the head of *R. kanagurta* in an open mouth position. Direction and type of flow is indicated by arrows.

10.1.6. Influence of Washing Detergents on Analytical Procedure

Washing machine effluent usually contains detergents, either as a liquid or powder (Schöpel & Stamminger, 2019). In previous studies, it was shown, that the powder can cause clogging of the filtering papers in the analytical process of effluent analysis, because it contains small particles, so called zeolites. To test the influence of detergents on the analytical procedure and decide on a final effluent mixture for the experiments, we tested two powder detergents (P1: Persil Universal Color Pulver, P2: Frosch Voll-Waschpulver), one liquid detergent (FL: Frosch Sensitiv-Waschmittel Aloe Vera), and a liquid fabric softener (WS: Sodasan Weichspüler Lavendel). We combined them with 2 mm microfibres and fibres collected from dryers, and as control, no fibres. Additionally, we collected the washing machine effluent (RW) and compared it to the other combination of the experimental plan (Table 5).

Table 5: Experimental plan to determine the influence of detergents on the analytical procedure, with K = none, F2 = 2 mm flock fibres, FL = liquid detergent, P = powder detergent, TF = dryer fibres.

Detergent/fibres	None	Flock fibres	Dryer fibres	WM effluent
None	K-K	F2-K	TF-K	
Powder 1	K-P1	F2-P1	TF-P1	RW
Powder 2	K-P2	F2-P2	TF-P2	
Liquid 1	K-FL	F2-FL	TF-FL	
Softener 1	K-WS	F2-WS	TF-WS	

Based on the manufacturer's specification, we weighted 3 g/l of the powder detergents, 2 ml/l of the liquid detergents and 50 mg/l of the flock fibres. Each combination was added to one litre of water four hours prior to the experiment and shaken to dissolve the detergents in the water. One litre was extracted from the washing machine effluent and tested as the 16th combination. The analytical procedure to analyse the suspensions followed the standard set for this thesis (Chapter 7). Weight difference and volume of filtered suspension were measured to determine the influence of the analytical procedure.

The results show that the type of detergent has a high influence on clogging of the filtering paper. When powder detergent is used, on average 218.33 ml (N = 6) can be filtered. At the same time, 991 ml (N = 6) of the samples with the liquid detergent or softener can be filtered. Foaming appears during the vacuum filtration of the liquid detergents, which might explain the slight volume loss. Based on the experiments in which all of the suspension is filtered, 97.8% (N = 6) of the particles are recovered, which means that 2.2% of the fibres are lost during the analytical procedure. In order to further reduce fibres loss, we optimised the handling in the petri dishes. In this experiment, the petri dish cover was leaned against the petri dish bottom to allow air circulation. Afterwards, we drilled a hole in the covers and closed it with a filter

mesh with a mesh size of 20 µm. This allowes air circulation and drying, while keeping the fibres inside. Only 140 ml of washing machine effluent can be filtered until the filter paper is clogged.
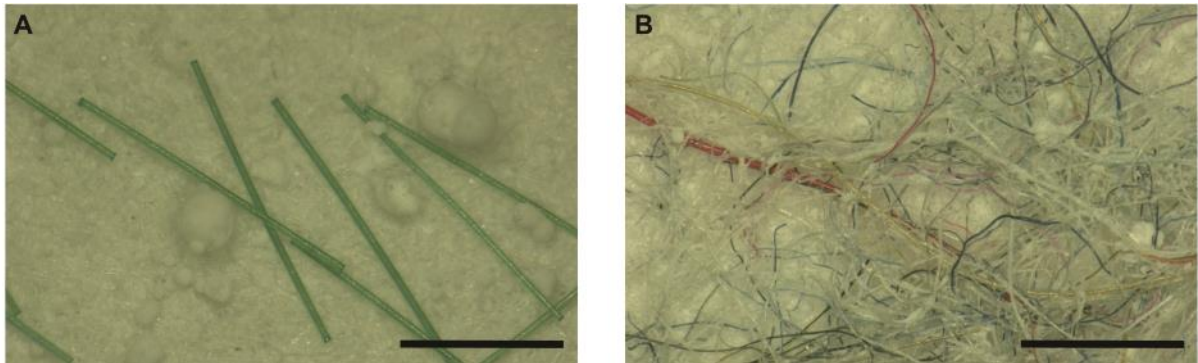

Figure 28: Powder detergents in combination with A) 2 mm flock fibres and B) fibres from a dryer. Scale bar: 1 mm.

10.1.7. Fluid Flow through Two Benthic Suspension Feeders

Next page: Poster presented at the Annual Meeting of the German Zoological Society (DZG) 2022

GO WITH THE FLOW
Passive flow in two benthic suspension feeders

Leandra Hamann[1], Raffaella Frank[2], Lukas Török[2], Alexander Blanke[1]

[1] Institute of Evolutionary Biology and Animal Ecology, University of Bonn, An der Immenburg 1, 53121 Bonn, Germany
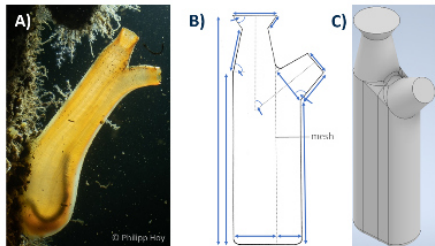[2] Westphalian University of Applied Sciences, Münsterstraße 265, 46397 Bocholt, Germany

Introduction

Suspension feeders separate food particles from the surrounding water. Ascidians and lancelets are active, benthic suspension feeders that produce a feeding current through ciliary activity. We assumed that an additional passive flow through the filtering structures is induced by the specific morphology. We analysed the fluid-shape interactions with computational fluid dynamics (CFD) to determine the effects of ambient flow, morphology, and orientation of the suspension feeders.

Labels (Ciona diagram): inhalant siphon; exhalant siphon; branchial basket with gill bars and mucus net; atrium; gut

Labels (Branchiostoma diagram): mouth with buccal tentacles; notochord; atrium; pharynx with gill bars and mucus net; atriopore

Ciona intestinalis

- Up to 14 cm in size
- feed on of 0.3 - 50 µm sized plankton
- sessile

A) B) C) mesh

From organism to model:
A) Photographs of specimen
B) Morphometric measurement describe the filter-feeding morphology
C) Abstraction into simplified models

Branchiostoma lanceolatum

- 30-60 mm in size
- feed on 4 - 100 µm sized plankton
- Buried partly in the sand while feeding

A) B) C) mesh
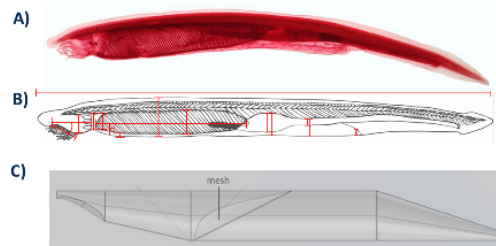
Implementation in COMSOL
- The mucus net was represented by a screen function with given solidity
- The virtual flow resembled natural conditions above the sediments with 0.1 to 0.2 m/s
- Volume flow was determined to evaluate passive flow

Results of CFD

When tilted 15° towards the flow, the volume flow was highest with around 2 l/h and a laminar flow regime within the branchial basket.

- Increasing ambient flow → increase volume flow
- Open area ratio of the mesh → no influence on volume flow
- Vertical rotation → reversed flow
- Angle between inhalant and exhalant siphon →no influence on volume low
- Branchial basket length → no influence on volume flow

Results of CFD

When tilted 45° towards the flow with the ventral side facing downwards, the volume flow was highest with 0.004 l/h..

- Increasing ambient flow → increase volume flow
- Open area ratio of the mesh → no influence on volume flow
- Pharynx length → volume flow is constant
- Variation of mouth geometry → decrease of volume flow
- Depth in sediments → protrusion increases volume flow
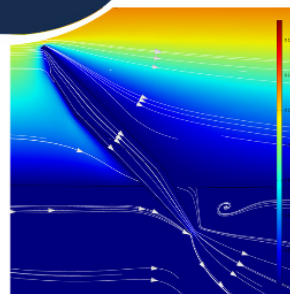
Conclusion

→ Orientation towards the flow increases passive volume flow relative to other parametric changes
→ Passive flow might reduce energy expenditure during active filter-feeding
→ Flow patterns of living individuals will be investigated to verify the results

References:
- DU CLOS (2017). Model-assisted measurements of suspension-feeding flow velocities. Journal of Experimental Biology
- MACGINITIE (1939). The method of feeding of tunicates. The Biological Bulletin
- NIELSEN et al. (2007). On particle filtration by amphioxus (Branchiostoma lanceolatum). Journal of the Marine Biological Association of the United Kingdom
- RIISGÅRD & SVANE (1999). Filter Feeding in Lancelets (Amphioxus), Branchiostoma lanceolatum. Invertebrate Biology

Are you working in the area of fluid dynamics? Please reach out to me:
lhamann@evolution.uni-bonn.de
LinkedIn: Leandra Hamann

Want to know more about the particle separation mechanisms in suspension feeders, their diversity, and biomimetic potential?
Scan this QR-Code:

UNIVERSITÄT BONN   IEZ

10.2. Manuscripts

10.2.1. Manuscript I

THE ROYAL SOCIETY PUBLISHING

Suspension feeders: diversity, principles of particle separation and biomimetic potential

Leandra Hamann and Alexander Blanke

Institute of Evolutionary Biology and Animal Ecology, University of Bonn, An der Immenburg 1, 53121 Bonn, Germany

LH, 0000-0002-5564-7755; AB, 0000-0003-4385-6039

Suspension feeders (SFs) evolved a high diversity of mechanisms, sometimes with remarkably convergent morphologies, to retain plankton, detritus and man-made particles with particle sizes ranging from less than 1 µm to several centimetres. Based on an extensive literature review, also including the physical and technical principles of solid–liquid separation, we developed a set of 18 ecological and technical parameters to review 35 taxa of suspension-feeding Metazoa covering the diversity of morphological and functional principles. This includes passive SFs, such as gorgonians or crinoids that use the ambient flow to encounter particles, and sponges, bivalves or baleen whales, which actively create a feeding current. Separation media can be flat or funnel-shaped, built externally such as the filter houses in larvaceans, or internally, like the pleated gills in bivalves. Most SFs feed in the intermediate flow region of Reynolds number 1–50 and have cleaning mechanisms that allow for continuous feeding. Comparison of structure–function patterns in SFs to current filtration technologies highlights potential solutions to common technical design challenges, such as mucus nets which increase particle adhesion in ascidians, vanes which reduce pressure losses in whale sharks and changing mesh sizes in the flamingo beak which allow quick adaptation to particle sizes.

1. Introduction

Suspension feeders (SFs) are a group of organisms with the common ability to separate food particles from suspension for nutrition [1,2], which includes organisms ranging from sponges to birds [3,4]. Since the late Tonian Period, 1000–720 Ma, SFs form habitats by mixing sediments, influencing particles fluxes, and moving high volumes of water [5,6]. Consequently, SFs altered light penetration depths, oxygenation levels and the distribution of dissolved organic carbon [7–9].

Suspension-feeding mechanisms (SFMs), which we define as all steps that enable separation of particles from the surrounding water, from the first encounter to the ingestion into the oesophagus, show a high diversity today. This diversity most likely resulted from niche partitioning, i.e. positive selection for the retention of certain particle size ranges from the heterogeneous seston [10,11]. Due to the high ratio of particle size to SF size, SFs provide small particles to higher trophic levels in aquatic ecosystems, e.g. products of primary production in the water column reach benthic habitats through the production of faecal pellets, subsidence of mucus and other biomass, and thus is an important linkage in the food web, known as benthic–pelagic coupling [12,13]. The diversity and species richness of SFs affect ecosystems because of their influence on plankton abundance, filtration rates and nutrient fluxes [14–16]. SFs also impact human living: Suspension-feeding herring, sardines and anchovies are
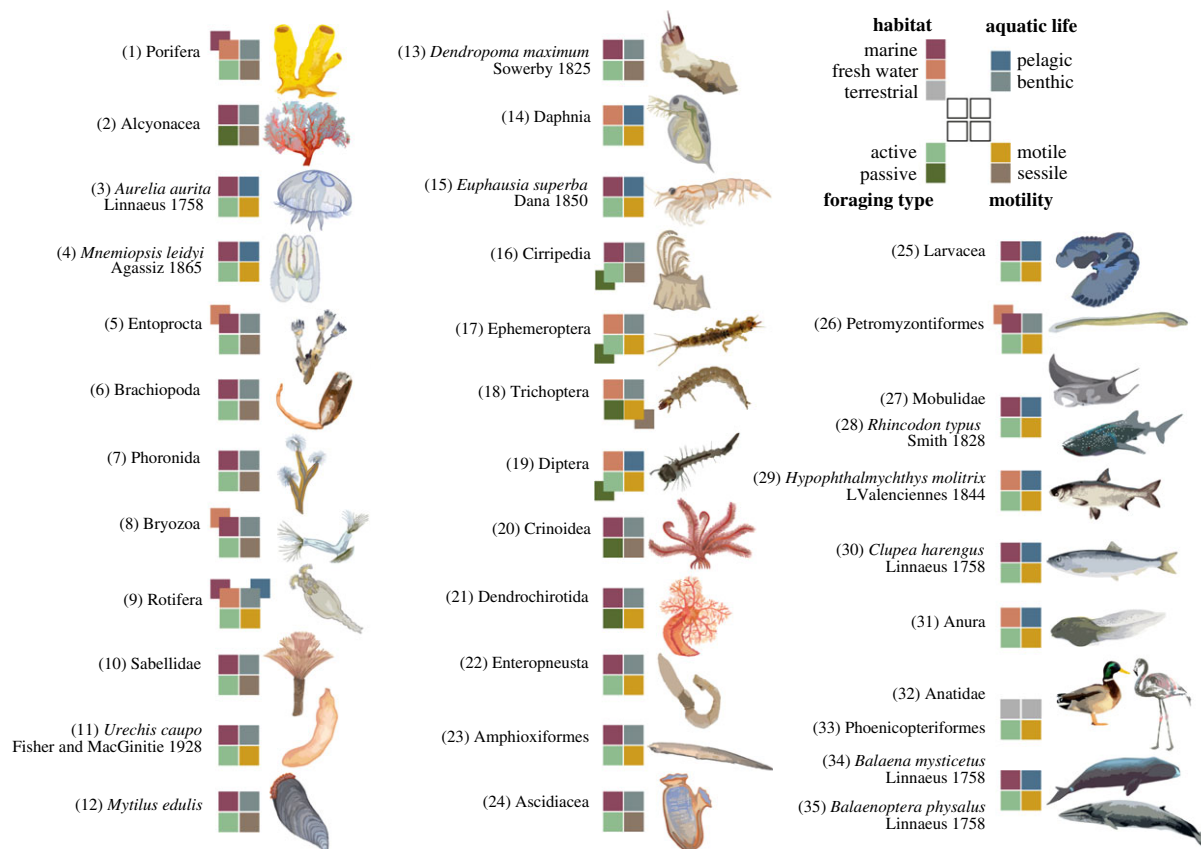
Figure 1. Overview of the selected SFs within the Metazoa with a focus on functional aspects. Each selected organism or organism group represents one SFM. Coloured squares indicate characteristics of biological parameters for each group: habitat (marine, freshwater, terrestrial), aquatic life (pelagic, benthic), foraging type (active, passive) and motility (motile, sessile). Numbering of each SF is consistent with table 1. A short description of each SFMs is in electronic supplementary material, table S2. For individual references, see electronic supplementary material, table S4.

relevant food sources [17] while bivalves and crustaceans are used as biofilters for water clarification [18–21].

Besides their ecological role, the separation mechanisms by which SFs separate food particles have also been of interest for engineers. The SFMs of manta rays inspired a nanofibrous membrane for oil–water separation [22] and led to the identification of a novel non-clogging filtration mechanism, called ricochet filtration [23], whereas suspension-feeding fish have inspired a helical, cross-step filter for collecting harmful algae [24].

Based on technical definitions [25], suspension-feeding processes are solid–liquid separations with particle recovery and the biological mechanisms show several similarities to technical ones. Natural and technical separation processes are divided into: (i) transport of the suspension to the separation medium, (ii) flow past the separation medium, (iii) separation of particles and (iv) particle removal from the separation medium.

Based on an extensive literature search, we developed a set of biological and technical parameters to systematically describe and classify SFMs and screened the animal kingdom for different SFMs.

2. A biomimetic approach to suspension feeders

The literature screening included scientific search portals (SCOPUS, Google Scholar) as well as biomimetic databases (www.asknature.org) up to December 2020 to identify as many SFs as possible and find SFMs that have not yet been considered in a biomimetic or technical context (electronic supplementary material, table S1). Because a detailed description of the SFM in each species would go beyond the scope of this review, species with a largely similar SFM within a taxonomic level (i.e. genus, family, order, class or phylum) were grouped and described briefly (electronic supplementary material, table S2). If sufficient data were available for one species to fully describe the SFM, it was chosen as a representative for the group, e.g. *Mytilus edulis* for all bivalves, otherwise the basic mechanism was described for the taxon, e.g. sponges. In the case of arthropods with their high diversity, only the groups with the best described SFMs were included.

Organisms were not considered for a detailed description if (i) they went extinct (e.g. pterosaurs), (ii) their feeding apparatuses have been mentioned only briefly thus far (e.g. sieve-like teeth in the crab-eater seal *Lobodon carcinophagus* [26]), (iii) they are mainly assigned to other feeding strategies (e.g. deposit-feeding cucumbers [27]), (iv) ciliary feeding larval stages [28] and (v) protists [29]. Filtration of molecules, such as in kidneys or aquaporins, was excluded as these mechanisms are not an aquatic feeding strategy [30]. Although not exhaustive regarding phylogenetic diversity, a total of 35 organisms and organism groups were selected (figure 1; electronic supplementary material, table S2) to cover the diversity of morphological principles, which we subsequently evaluate for their potential to inspire technical particle filters.

The technical process of *filtration* is best comparable to SF. It describes a separation process using a filter medium to remove

solid particles, microorganisms or droplets from a fluid [25]. Filters can remove particles from a fluid to receive a clean fluid (clarification), or they can retain valuable materials from a fluid (recovery) [31]. Based on these definitions, suspension-feeding processes are solid–liquid separations with particle recovery.

Because suspension-feeding, and especially filter-feeding, is similar to technical definitions of filtration, we propose the description of SFs using 12 technical parameters which are already established in particle separation processes such as particle properties, separation medium, fluid dynamics and cleaning of the separation medium (electronic supplementary material, tables S3 and S5) in addition to six ecological parameters (electronic supplementary material, tables S3 and S4) from previous biological descriptions (electronic supplementary material, table S6). Based on convergent SFMs, groups were clustered to each parameter (table 1) and corresponding literature presented for each SF (electronic supplementary material, tables S4 and S5). The groups also show the evolution of similar traits in response to the same boundary conditions that indicate structure–function relations and high biomimetic potential [27,28]. To account for the diversity of SFs that include typical filtration mechanisms but also other particle separation techniques, all technical terms including the term 'filtration' were changed to 'separation', i.e. 'filter medium' was changed to 'separating medium', 'particle filtration' to 'particle separation'. In technical terms, the retained particle mass is called the retentate, the clean fluid that passes the filter is called filtrate [25].

3. Ecological description

SFs live in marine and aquatic environments with SF birds as the only solely terrestrial SFs dependent on aquatic environments (figure 1; electronic supplementary material, table S4). Insect larvae and tadpoles are the only groups that live exclusively in freshwater environments. Species within bryozoans, rotifers, bivalves, crustaceans, ammocoetes and fishes are present in freshwater and marine environments.

Benthic SFs are mainly sessile and live epifaunal on substrates or infaunal in burrows within the sediments such as ammocoetes [32]. Benthic SFs, such as the spoon worm *Urechis caupo*, enteropneusts, the sea snail *Dendropoma maxima* or lancelets are motile (or hemisessile) but remain stationary while feeding [33–36]. Through the building of substrates by tube-dwelling worms, bivalves or suspension-feeding corals, some SFs also act as ecosystem engineers influencing biogeochemical processes [2,7].

Habitat depth ranges from intertidal zones for barnacles and ascidians [37,38] down to the deep sea for sponges or brachiopods [39,40]. Pelagic SFs are motile by active swimming or drifting [41] and feed in varying depths, with whale sharks also feeding at the water surface [42] and suspension-feeding whales diving down several hundred metres [43,44]. Suspension-feeding usually is developed throughout the life or in adult life stages, but can also occur only in the larval stage such as in freshwater insects [45], anurans [46], lamprey larvae [47] or marine, invertebrate larvae [28]. Juvenile fish switch to filter-feeding at a species-specific size during growth [48].

Active SFs can influence local flow fields producing a feeding current by ciliary movement, pumping or forward motion [2,49] while passive SFs, such as gorgonians, crinoids or dendrochirotid sea cucumbers, retain particles from the ambient current [3,50].

4. Seston: the diverse food particles for suspension feeders

SFs feed on seston, which includes all particles suspended in water regardless of their nature and origin, and mainly consists of plankton and detritus [15,51]. Plankton is commonly categorized by size (figure 2; electronic supplementary material, table S7) with the smallest size fraction consisting of viruses, followed by bacteria and protists. Protists range from 1 µm (flagellates) up to 1 cm (foraminifera) while phytoplankton ranges mainly between 2 µm and 200 µm. Macro- and mega plankton consists of invertebrate to vertebrate zooplankton including their life stages, among them are also SFs such as crustaceans [52]. Detritus and non-living matter ranges from dissolved or colloidal organic matter up to dead organic matter or marine snow several millimetres in size (figure 2; electronic supplementary material, table S7).

SFs do not seize individual prey but feed on a range of particle sizes (figure 2). Despite the relatively small size of seston, the ability to harvest small food particles in large amounts allows SFs to grow large with a particle to body length relation of about $1:10^2$ to $1:10^4$ [53,54]. SFs range from less than a millimetre (rotifers and bryozoans) up to 30 m for baleen whales and there is a positive correlation between SF size and food size (figure 2).

Small SFs, such as insect larvae, retain particle sizes down to colloidal particles [45], the spoon worm *U. caupo* can feed on 4 nm particles [55], corals and ascidians feed on bacteria [56], while larvaceans or bivalves retain viruses [57,58]. SFs feed on particles at least over two orders of magnitude in size, most of them in the range of 1–100 µm (figure 2). Data on preferred particle sizes are scarce for particles below 1 µm, which could be due to methodological detection difficulties [59].

SFs cope with varying seston concentrations and availability, which depend on habitat and local and seasonal dynamics [60,61]. Standing stocks of phytoplankton were calculated between 1 µg and 100 µm l^{-1} of oceanic waters, 5 µg and 1700 µg l^{-1} of coastal waters and 7 µg and 6800 µg l^{-1} of inshore waters [1]. Vertical migration of plankton changes daily seston concentrations in local areas and leads to behavioural changes in pelagic SFs, such as larvaceans [62], herrings [63], suspension-feeding sharks [42,64], bowhead or rorqual whales [43,65], the latter feeding at sites with prey concentrations up to 10^5 per m^{-3}, equivalent to around 170 g m^{-3} [66]. Several benthic SFs can change their feeding behaviour [67–69] or switch to other feeding strategies such as deposit feeding depending on particle flux and concentration [34,70,71].

Although being predominantly non-selective, particle selectivity can be determined by physical constraints. A lower limit of particle size are mesh size or the physics of particle encounter, i.e. hydrosol filtration [72,73]. An upper limit for particle size is the opening of incurrent canals, such as in sponges [74], tunicates [53,69] and ammocoetes [47]. Some SFs such as bivalves can actively select particles: the opening size of the inflow siphon regulates pre-capture while mucociliary transport in the four gut areas allows for post-capture selectivity before digestion [75]. Similar to bivalves,
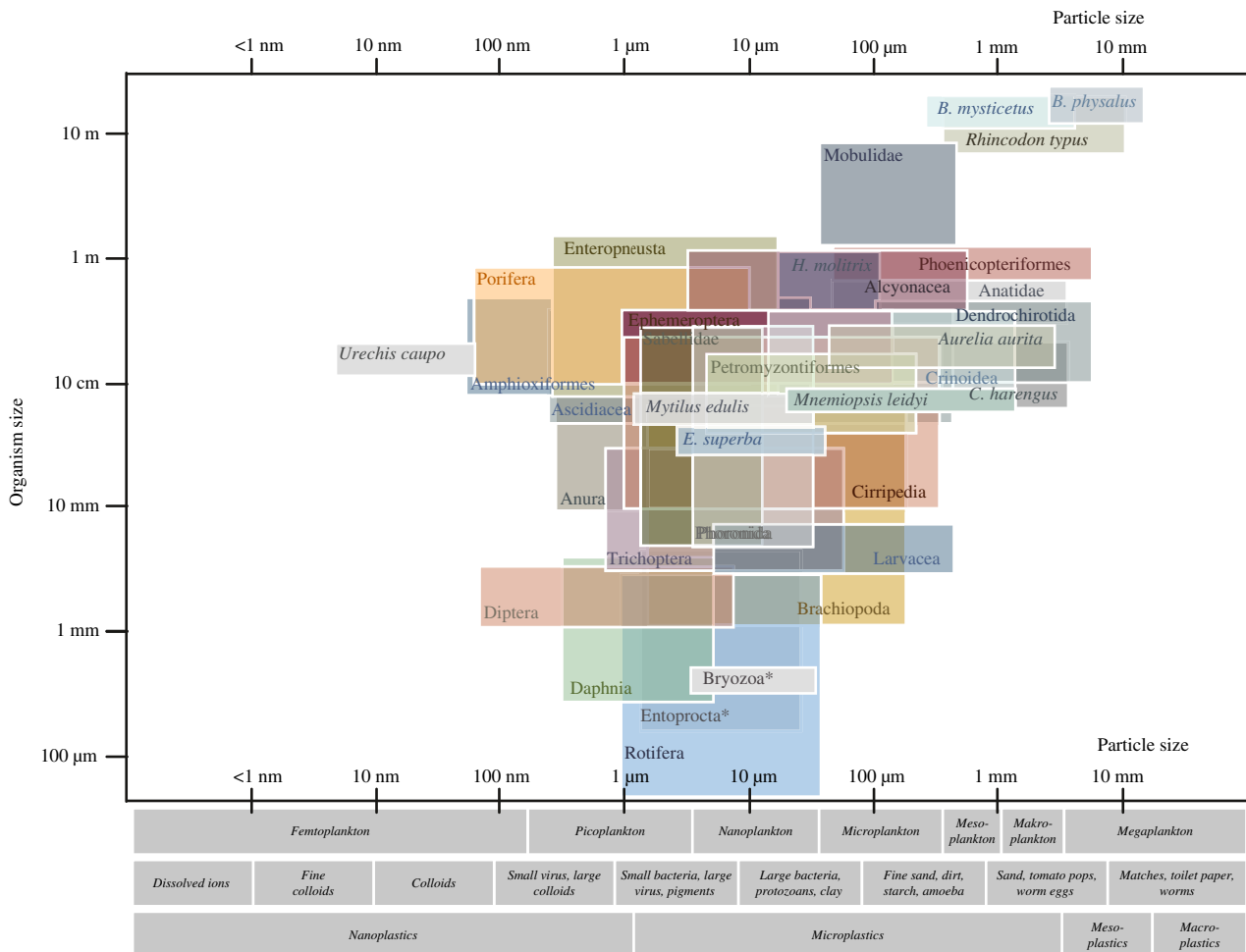
Figure 2. Size of the SFs (except *Dendropoma maximum*) and particle size of seston. Each box indicates the range of organism size and food particle size. For individual references, see electronic supplementary material, table S4. The colours are only used for visual reasons. Examples of seston particles are listed under the x-axis and compared to typical particle sizes found in waste water treatment and microplastics. For individual references of particle sizes, see electronic supplementary material, table S7.

brachiopods produce pseudofaeces with rejected particles [76]. Suspension-feeding ducks select particle sizes by the beak opening, thereby changing mesh size [77]. SFs that use mucus to increase adhesive forces might select particles based on their chemical composition [78,79]. Particles are retained on surfaces when adhesive forces are greater than the sum of drag and lift forces acting on the particle to remove it [73]. Other particle properties that might influence particle retention and selectivity are density, shape, chemical criteria or energy content [75,80,81]. Each SF is adapted to a specific particle size range optimum for which the retention efficiency and ingestion rate are highest [82,83].

5. Separation medium

The separation medium is usually permeable and serves as a barrier to components in the suspension [31]. Geometry, physical dimensions and the separation medium's chemical properties influence water flow and particle retention in SFs (figure 3).

5.1. Geometry

The separation medium is formed by body parts, such as appendages, inner structures like the pharyngeal basket, the body or external structures like excreted mucus nets

(table 1; electronic supplementary material, table S5). The geometry of separation media has been described as funnel-shaped [86,87] or flat [88]. It can be extended in the open water stream or enclosed by the SF's body, burrows or other sorts of casing. This differentiation is not trivial because, in technical terms, a filter is a device that typically holds the separation medium across the fluid in such a way that all the fluid has to pass the separation medium [31]. Thus, we suggest that only enclosed separation media in SFs are filters (figure 4a), and, hence, filter-feeding is a particular case of suspension-feeding [2].

Separation media in SFs can be described by geometry and the open or enclosed position (figure 4a). The calcareous or gorgonin-based skeletons of gorgonians grow perpendicular to the fluid flow and they are an example for an open and flat separation medium [89]. Water flows through or around the space between the skeleton branches and particles are caught with the tentacles of the polyps. Suspension-feeding arthropods sweep their flat feeding appendages through the water [90–92]. The setules on the appendages in daphnids [93] and the gill of the bivalve *M. edulis* [94] can be angled, similar to pleated filter media used in common technical filters [95]. This provides elasticity for the filtering apparatus, increases the filtering area and decreases flow velocity at the mesh [88,93]. The marine snail *D. maxima* builds meshes across the opening of its burrow to retain particles [33].

Table 1. The biological traits of each SFM are clustered and presented for each parameter (there is no relation between the columns). The numbers represent the SFs according to figure 1. Subunits in SFs, e.g. choanocyte in sponges, polyps in gorgonians, zooid in bryozoans, are indicated by (*). For individual references, see the numbers in electronic supplementary material, table S5.

separation media

geometry

flat	flat (in pipe)	funnel	funnel (in pipe)	others
(2, 14, 16, 19)	(12, 13)	(1*, 2*, 7, 9, 10, 18, 20)	(6, 11, 22, 23, 24, 26, 27, 28, 29, 30, 31, 32, 33, 34, 35)	(1, 3, 4, 9, 15, 17, 21, 25)

material of separation medium

cell structures	epidermis	cilia	mucus	chitin	silk	horn/keratin
(1*)	(2, 3, 20, 21, 27, 28, 29, 30)	(5, 6, 7, 8*, 9, 10, 12, 22, 23)	(3, 4, 11, 13, 22, 23, 24, 25, 26, 31)	(14, 15, 16, 17, 19)	(18)	(32, 33, 34, 35)

mesh design

flat surface	first level of branching	second level of branching	third level of branching	net	spongy/3D
(3, 4)	(1*, 2*, 3, 5, 9, 22, 32, 33, 34, 35)	(2*, 6, 7, 8*, 10, 12, 14, 16, 17, 19, 27, 31)	(14, 15, 20, 28, 30)	(11, 13, 18, 23, 24, 25, 31)	(1, 2, 21, 29)

particle size

<1 µm	1–100 µm	100–1000 µm	1–10 mm	>10 mm
(1*, 11, 14, 19, 23, 25)	(1, 2, 4, 5, 6, 7, 8, 9, 10, 11, 12, 14, 15, 17, 18, 19, 20, 22, 23, 24, 25, 26, 27, 29, 31, 32)	(1, 3, 20, 21, 25, 26, 27, 28, 30, 32, 33)	(21, 38, 32, 33, 34)	(35)

separation type

no filtration	dead-end filtration	cross-flow filtration
(2, 3, 4, 5, 7, 8, 9 10, 14, 19, 20, 21)	(1, 7, 11, 12, 13, 15, 16, 17, 18, 22, 23, 24, 31, 32, 33, 35)	(7, 8, 25, 27, 28, 29, 30, 34)

fluid dynamics

driving force

none (passive)	ciliary (+flagellar) movement	movement of appendages	pumping	forward movement
(1, 2, 4, 13, 16, 17, 18, 19, 20, 21)	(1*, 4, 5, 6, 7, 8*, 9, 10, 12, 22, 23, 24, 25)	(14, 15, 16, 17, 19, 25)	(11, 22, 26, 28, 29, 31, 32, 33)	(3, 27, 28, 30, 34, 35)

water velocity (inflow)

<0.1 cm s⁻¹	0.1–1 cm s⁻¹	1–10 cm s⁻¹	>10 cm s⁻¹
(1, 5, 10, 12, 22)	(2*, 4, 7, 8*, 11, 14, 23, 24, 25)	(2, 3, 6, 15, 16, 17, 20, 25)	(16, 18, 19, 27, 28, 30, 34, 35)

flow regime (at mesh)

creeping flow (Re <1)	laminar flow (Re 1–50)	turbulent flow (Re >50)
(1*, 2*, 8*, 9, 10, 12, 14, 15, 19, 22, 24)	(2, 3, 4, 6, 8*, 16, 17, 19, 20, 22, 25, 27, 28, 29, 30, 34, 35)	(27, 33, 34, 35)

cleaning

working mode

continuous	discontinuous
(1, 2, 3, 4, 6, 7, 8, 9, 10, 12, 14, 15, 1 6, 17, 19, 20, 21, 22, 23, 24, 25, 27, 28, 29, 30, 31, 32, 33, 34)	(11, 13, 18, 25, 35)

cleaning

direct ingestion/phagocytosis	ciliary transport	mucus	feeding, scraping, combing off	back flush	non-clogging mechanism
(1, 5, 11, 13, 25)	(3, 4, 5, 6, 7, 8, 9, 10, 12, 20, 22, 31)	(10, 12, 22, 23, 24, 26, 31)	(2, 14, 15, 16, 17, 18, 19, 21, 32, 33, 35)	(24, 28, 34)	(25, 27, 28, 29, 30 34)

Figure 3. Steps of a generalized suspension-feeding mechanism, from the first particle encounter to ingestion (inspired by Waggett [84]). Particles (brown) encounter the separation medium (yellow) in direction of flow (blue arrows). According to hydrosol filtration theory, particles encounter the separation medium based on at least one of five mechanisms: (i) direct interception, (ii) inertial impaction, (iii) gravitational deposition, (iv) diffusion or motile-particle deposition and (v) electrostatic attraction [72,85]. After contact, particles can be captured through sieving or adhesion, e.g. through mucus (green). Particles can escape from the separation medium at each step or be actively rejected by some SFs during cleaning and before ingestion. Ingestion is the point of entry of particles into the oesophagus.

The microvilli of choanocytes in sponges and the lophophores in entoprocts, bryozoans and phoronids are in the shape of open funnels (table 1; electronic supplementary material, table S5). The gill crown of sabellid worms extends as a spiralling funnel [96]. The arms of crinoids form a funnel and can be actively directed into the current [97]. The nets of trichopteran larvae are also funnel-shaped [98].

Deuterostomes such as hemichordates, cephalochordates, ascidians, ammocoetes, mobulid rays, tadpoles and species such as whale shark, silver carp, herring, fin whale or the bowhead whale, have funnel-shaped separation media within the pharynx (table 1; electronic supplementary material, table S5). The worm *U. caupo* builds a funnel-shaped net in its burrows [36]. The enclosed lophophore in brachiopods can vary in shape but is often funnel-shaped [99]. Ctenophores, sponges, the moon jelly *Aurelia aurita*, rotifers and mayfly larvae show other geometries of separation media, which do not fit the above classification. Examples for even more complex geometries are the highly branched arms of dendrochirotid sea cucumbers, the external filter house of larvaceans and the filtering basket formed by the legs of Antarctic krill (table 1; electronic supplementary material, table S5).

The total area of the separation medium exposed to the on-streaming fluid is called the *separation area* or *effective separation area* (effective filtration area in technical terms [31]). In gorgonians, the effective area is nearly equal to the skeleton area and therefore correlates with organism size [100]. By adding up all areas of the filtering pads in whale sharks, the filter area measures 10–12 m^2 in a 6 m individual [42]. However, the effective area can change dynamically, especially in changing flow fields: in sea lilies, the area decreases with increasing flow because the pinnules bend backwards with higher drag force [101]. The filter basket of Antarctic krill can be actively expanded and compressed by the organism to pump water through it [102].

5.2. Tissues and materials

Different tissues and materials influence particle capture in SFs (table 1; electronic supplementary material, table S5). The flagellum of the choanocytes in sponges creates a current towards the microvilli and the cell body, where particles are taken up by the cell through phagocytosis [103]. Epithelia and the epidermis of the tentacles of gorgonians and the

moon jelly *A. aurita*, the tube feed in crinoids, and the tentacle arms of dendrochirotid sea cucumbers have first contact with particles. In suspension-feeding Chondrichthyes, like mobulid rays and whale sharks, the separation medium consists of filter plates between the gill arches [104]. In bony fish, the gill arches are equipped with gill rakers (fuzed in silver carp), which build a screen for the water flowing through the mouth, towards the gills and out under the operculum [105].

Small SFs such as rotifers, entoprocts, lophophore-bearing brachiopods, bryozoans and phoronids predominantly use cilia to catch and retain particles [106]. Larger SFs with cilia are sabellid worms, the blue mussels *M. edulis*, enteropneusts and lancelets. Four different mechanisms of particle retention with cilia are distinguished based on the number of ciliary bands, the stiffness of the cilia and how the cilia move to interact with the particles: upstream collecting, ciliary sieving, cirri trapping and downstream collecting [107]. In the bivalve *M. edulis* and phoronids, different types of cilia are involved. While the lateral cilia create a current and trap the particles, the frontal cilia transport the particles towards the gut [106,108]. Bryozoans and rotifers can control the water current by cilia in such a way that particles are directly driven towards the mouth [109].

In various taxa, mucus is involved in suspension-feeding during retention, cleaning or transportation of the particles. Mucus used in separation media can be divided into three categories. (i) The ctenophore *Mnemiopsis leidyi*, the jelly fish *A. aurita* and dendrochirotid sea cucumbers cover surfaces to increase particle adhesion [71,110]. (ii) Lancelets, ascidians, ammocoetes and tadpoles have internal mucus nets. These nets are supported by structures, such as the pharyngeal basket, and transported with cilia. In ascidians, a continuously secreted mucus net covers the pharyngeal basket, which retains particles down to 1 μm and allows the water to pass the filter at low resistance [111]. (iii) The spoon worm *U. caupo* and the sea snail *D. maxima* build mucus nets externally within their burrows to catch particles and ingest the particle-laden mucus periodically [33,36]. Larvaceans secrete a complex filter structure around them, which is several times larger than the organism and consists of a coarse-meshed outer house and a fine-meshed inner house to concentrate the food particles towards the mouth [112].

Even though mucus has been recognized early as a relevant part of suspension-feeding [113], its physical and chemical
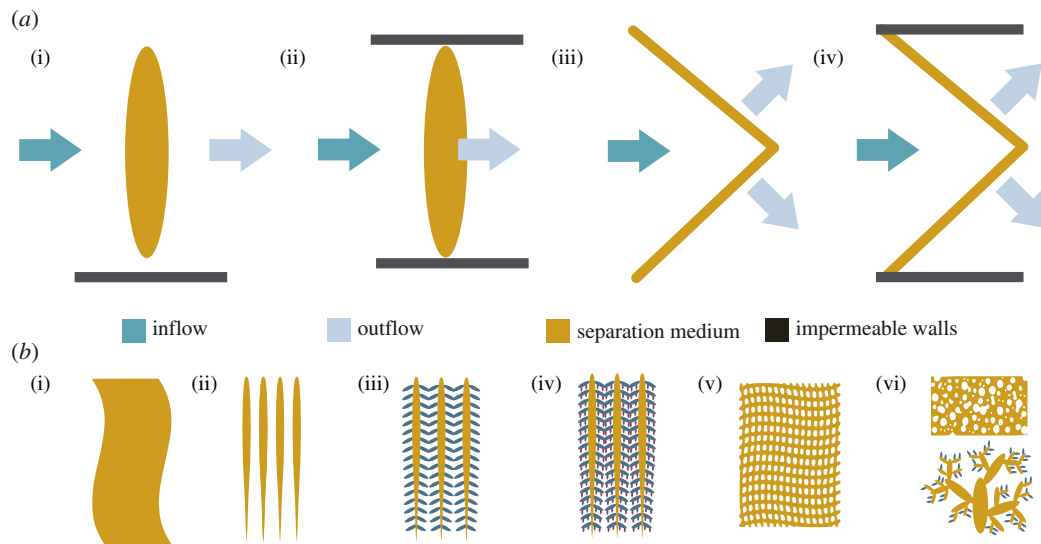
Figure 4. (*a*) Geometry of the separation medium (yellow) can be (i) flat and open, (ii) flat and enclosed, (iii) funnel-shaped and open or (iv) funnel-shaped and enclosed. Walls (grey) show if the separation medium is open or enclosed. Direction of flow is indicated by blue arrows. (*b*) Design of separation media to create surfaces, meshes and pores: (i) flat, (ii) first level of branching, (iii) second level of branching, (iv) third level of branching, (v) net structure and (vi) higher branching and porous media.

properties are not well understood compared to the information available for terrestrial organisms using mucus [114]. Generally, mucus is highly viscous and resembles an elastic gel with a high adsorption potential for particles. When particles touch a mucous surface, the mucus will engulf the particles and thereby retain them [114]. The spoon worm *U. caupo* [55] and larvaceans [78] retain particles down to 4 nm through the adhesive forces of mucus. Mucus properties, such as its electrical charging, can influence particle retention [115]. In SFs, the production of the mucus net and its physical and chemical properties were studied for ascidians [116], larvaceans [53], the blue mussel *M. edulis* [117,118] and salps [119].

Caddisfly larvae build nets with silk strands in rivers and streams to catch particles from the passing current [45]. A viscous liquid is drawn through a fine orifice to produce the protein fibres [120]. Each larva can secrete up to 70 strands simultaneously. The diameter of the strands in different species can vary between 0.34 μm and 47 μm [121]. Caddisfly silk can double in length before it breaks so that the larvae are able to build their nets between rocks and stones in flowing waters, where the silk needs to withstand fluctuations of flow velocity and impacts of larger particles [120].

Chitin is the material for separation media in suspension-feeding crustaceans and insects. Daphnids, the Antarctic krill *Euphausia superba*, barnacles and mayfly larvae use legs with bristle-like setae on them to retain particles, while dipterans have bristle-like mouthparts (electronic supplementary material, table S5).

Compared to other keratinous structures, the α-keratin in whale baleen hanging as bristles from the upper jaw has a higher degree of calcification, which increases abrasion resistance, enhances fraying into bristles and increases strength and flexibility [123,124]. Keratinized structures also form fine lamellae at the rim of the upper and lower beak in suspension-feeding birds [125,126].

5.3. Media design and meshes

The design of separation media ranges from flat surfaces, over different degrees of branching and net-forming screen-like meshes, to spongy and highly branched structures forming porous media to create surfaces, meshes and pores (figure 4*b*).

Ctenophores and the moon jelly *A. aurita* have flat, prey-capturing surfaces. Because the separation medium has no meshes, the water does not flow through the separation medium but around it. Particles that encounter the surface are retained with adhesive surfaces, sometimes covered with mucus [110,127].

Several levels of branching form apertures, so water can flow through the separation medium (figure 4*b*). The microvilli of choanocytes in sponges, the tentacles of the moon jelly *A. aurita*, the cilia of lophophores or the lamellae in the beaks of ducks and flamingos are examples of the first level of branching (table 1; electronic supplementary material, table S5). Barnacles, where setae are equipped with smaller setulae [92], or mobulid rays, where the filtering lobes divide up into smaller structures [104], are examples for the second level of branching. Atlantic krill, where the primary setae have secondary setae with even smaller tertiary setae on them [102], have a third level of branching. In herrings, the gill arches have gill rakers which themselves have denticles to create almost rectangular meshes [128]. By contrast, whale sharks have the same level of branching, but irregular-sized meshes [42].

Different to branching structures that develop through growth processes, nets are formed by, for example, spinning processes [120]. The larvae of caddisflies can build food-capturing nets in flowing waters and act as a trade-off between processing large volumes of water and the water pressure [129]. The net design ranges from being elongated, sac-like, disc-like or branching into tubes. Nets tend to be larger in faster flows, and mesh sizes can be altered by the organism for the retention of specific particle sizes [130,131]. Other net spinning and mucus-secreting SFs are the spoon worm *U. caupo*, the sea snail *D. maxima*, lancelets, ascidians, larvaceans and tadpoles (table 1; electronic supplementary material, table S5).

In engineering, the retention of particles on a two-dimensional mesh is called surface filtration, while the retention within a three-dimensional structure, i.e. pore, is distinguished as depth filtration or deep bed filtration [25,31]. In sponges, the water streams into the channels, where particles

are retained by archaeocytes on the sides in addition to the particle retention by choanocytes in the filtering chambers [132]. During the ontogeny of silver carps, the gill rakers fuse and form a porous medium [133]. The highly branched skeleton of gorgonians and the arms of dendrochirotid sea cucumbers form a three-dimensional structure in the open flow [71,134].

5.4. Mesh size and particle size

Mesh size is the size of apertures in a screen or mesh [31] or the distance between structures that retain particles. The distance between the cilia in the entoproct lophophore is around 0.1 μm [135], the smallest mesh size of ascidian mucus nets is 0.2 μm by 0.5 μm [69] and the mesh sizes in mobulid rays range from 0.27 mm^2 to 3.34 mm^2 depending on species [136]. The ratio of apertures to effective area is called the open area ratio, the ratio of pore volume to total volume in porous separation media is the porosity [31]. The open area ratio of the feeding appendages in daphnids ranges from 0.5 to 0.7 [137]; it is 0.46–0.6 in whale sharks [42] and the porosity in mucus nets in ascidians is 90–98% [69].

Mesh or pore size can be changed by passive forces, e.g. the distance between baleen fringes changes with the flow velocity [44,138]. Depending on the food source, flamingos and ducks can alternate the distance between the upper and lower jaw and hence adjust the mesh size actively between the upper and lower lamellae [125]. Because of these dynamic changes of the mesh or pore size, retention mechanisms other than sieving [72] and the fact that not all physical properties are known, it is not possible to predict the size of particles that are retained by a specific SFM, as is the case for technical filters by the cut-off point [31]. Thus, we suggest that the particle sizes, which have been ingested by SFs, are a better indicator for the sizes which can be retained by the SFMs (figure 2).

6. Fluid dynamics

In nature, the fluid of suspension-feeding is water, but in technical filters other liquids or even gases are treated in separation processes [31]. Flow velocity and flow regime of the fluid play a major role in particle motion towards the separation medium and the final encounter with the separation medium (figure 3) [3,4].

6.1. Type of separation

SFs are distinguished into filter feeders (FFs), which have a filter comparable to technical designs where all fluid has to pass the filter medium, and non-FFs [2]. Based on the direction of flow, dead-end and cross-flow filtration can occur. In dead-end filtration, the fluid flows orthogonally towards and through the filter medium; in cross-flow filtration, the flow streams tangentially along the separation medium [25,31]. Cross-flow filtration is present in SFs, such as in the external filter houses of larvaceans, and the internal SFMs in mobulid rays, whale sharks, suspension-feeding fish, such as silver carps and herrings, and bowhead whales (table 1; electronic supplementary material, table S5). The tangential flow pushes the particles across the surface of the filter medium towards the oesophagus. Thus, particles are

constantly removed and increased in concentration by fluid flow before being swallowed or ingested [112,139].

Brachiopods, the spoon worm U. caupo, the blue mussel M. edulis, the sea snail D. maxima, the Antarctic krill E. superba, barnacles, ephemeropterans, trichopterans, enteropneusts, lancelets, ascidians, tadpoles, flamingos and Anatidae have enclosed separation media, in which particles are deposited upstream in the dead-end filter (table 1; electronic supplementary material, table S5). The flow around the separation medium, and its geometry, distinguishes dead-end from cross-flow FFs. In entoprocts, the separation medium is funnel-shaped, but the flow is very slow and not tangential [34]. Daphnids form a flat mesh with the setulae on the feeding appendages, but the flow streams across it instead of through it [140].

Ctenophores, gorgonians, moon jellies, rotifers, entoprocts, bryozoans, phoronids, sabellid worms, larvae of dipterans, crinoids, dendrochirotid sea cucumbers and daphnids are non-FFs (table 1; electronic supplementary material, table S5) because their separation medium is not enclosed, and the fluid can stream around it. However, the separation medium might still form meshes or pores to retain particles by sieving.

6.2. Driving force

Passive, benthic SFs often grow large, are stalked, or extend away from the sediments and the benthic boundary layer to reach into faster flows and collect particles with higher energetic content [85,141]. The caddisfly larvae of Macronema, which build their nets within tubes, use the pressure difference of incurrent and excurrent openings to drive the fluid through the net within the tube, a similar mechanism to a pitot tube [142].

Within technological applications, suspensions are transported by hydraulic pumps, vacuums or gravity towards and through the filter [25,31]. The 'pumps' of SFs are ciliary and flagellar movement, movement of appendages, oscillatory pumping and forward motion.

Small SFs, which use cilia to catch particles, often induce a feeding current with their cilia. This includes rotifers, entoprocts, brachiopods, bryozoans, phoronids, sabellid, bivalves, enteropneusts and lancelets (table 1; electronic supplementary material, table S5). The activity of cilia to induce a flow is also referred to as ciliary pump [143]. Despite the small size of the flagella of the choanocytes, sponges can induce relatively fast flows. The area of the flagellated chamber with the choanocytes is around 6000 times greater than the profile area of the excurrent canal. Thus, the flow velocity is multiple times slower around the flagella and increases in speed up to 0.2 m s^{-1} with decreasing area of the excurrent canals [142].

Suspension-feeding crustaceans and insect larvae sweep their feeding appendages through the water [1]. The feeding behaviour of barnacles is influenced by ambient flow conditions and can change direction and between active and passive [144]. In slow currents, barnacles actively move the feeding cirri through the water, while in fast currents, the cirri are held up because flow velocity is high enough to be filtered passively and thus save energy. To be able to extend the cirri in fast water currents, the cirri are mechanically robust to withstand the pressure without buckling or bending [92,145]. Larvaceans move their tail to pump water through their external filter houses [112].

Rhythmic contractions of the pharyngeal wall in lamprey larvae or buccal pumping in tadpoles induce a flow into the buccal cavity [4]. Flamingos open and close their bill while their tongue moves like a piston to suck in the water at the tip of the beak and expel it at the sides [125]. Lamprey larvae pump against sediment resistance and obtain suspended food particles from the water above and within the sediments [32].

Ram feeders, such as suspension-feeding fishes, whale sharks and bowhead whales, feed while swimming and take advantage of the forward motion to stream water towards their separation media [4]. Because their separation medium lies within the oral cavity, ram feeders might benefit from the continuity effect and the pressure drop to reinforce flow through the mouth, as shown for bowhead whales [146]. Ram feeding is characterized by a unidirectional flow, as opposed to bidirectional flow, e.g. in fin whales [4]. Fin whales accelerate and open their mouth fully to engulf their prey with a big gulp. Water flow is then reversed through the baleen plates, where particles are retained [147].

6.3. Flow velocity and pressure difference

Sponges, rotifers, sabellid worms, blue mussels and enteropneusts induce flow velocities smaller than $0.1 \, \text{cm s}^{-1}$. Ctenophores, gorgonians, bryozoans, phoronids, the spoon worm *U. caupo*, daphnids, lancelets and ascidians stream water between $0.1 \, \text{cm s}^{-1}$ and gorgonians, the moon jellies *A. aurita*, brachiopods, the Antarctic krill *E. superba*, barnacles, Ephemeropterans and crinoids induce flows between $1 \, \text{cm s}^{-1}$ and $10 \, \text{cm s}^{-1}$. Ammocoetes, larvae of trichopterans and dipterans, mobulid rays, whale sharks, herrings, bowhead whales and fin whales induce flows higher than $10 \, \text{cm s}^{-1}$ (table 1; electronic supplementary material, table S5).

Flow velocity can change depending on individual organism size or spatial and temporal conditions. In larvaceans, the flow velocity varied between 0.37 and $12.2 \, \text{mm s}^{-1}$ within 23 measured individuals with an allometric exponent of trunk length to the power of 2.5 [148]. The flow velocity in sponges is $0.009 \, \text{mm s}^{-1}$ at the collar slit of the choanocytes while being $2.9 \, \text{mm s}^{-1}$ in large excurrent canals of the same species [149]. Passive SFs in ambient, oscillatory flows are exposed to flow velocities ranging from no flow up to $15 \, \text{cm s}^{-1}$ [67,92].

The separation medium in the fluid flow creates resistance, a drag, which is expressed as the pressure difference across the separation medium [25]. It depends on the specific resistance of the separation medium and the fluid velocity: the higher the flow rate per unit area, the higher the pressure difference. A whale shark swimming at $1.1 \, \text{m s}^{-1}$ creates a pressure difference of 113 Pa at the filtering plates [42]. Bowhead whales induce a pressure difference between 1200 Pa and 4000 Pa depending on swimming velocity [146]. The driving force and thus flow velocity must be high enough to move fluid towards the separation medium and overcome the pressure drag [85].

6.4. Flow regime

The flow regime describes the flow structure and is expressed by the dimensionless Reynolds number (Re), i.e. the relation of inertial to viscous forces within a fluid [31,142]. In low Reynolds numbers of less than 0.1 (sometimes Re < 1 [150]), the flow is creeping, viscous forces dominate and the streamlines are parallel around a body [72]. With higher Reynolds number, inertial forces become more relevant, and the flow regime changes from laminar to turbulent [150].

The flow velocity and the characteristic length of particles or separation medium structures influence the local flow regime [150–152]. In most SFs, the characteristic length of the feeding element varies between 0.1 μm and 1 mm, and the flow regime is in the intermediate flow region between Re 0.5 and 50, where inertial forces are almost equal to viscous forces and streamlines begin to compress around a body [3,85,151,153,154]. Numerical models of the particle encounter in this flow regime show that with increasing particle radius and increasing Reynolds number at the collector, the encounter rates increase nonlinearly [73,151]. Within the pharynx in enteropneusts [34], between the lobes of ctenophores [155], and at the lophophore in brachiopods [156] the flow regime is around Re 1, i.e. inertial forces equal viscous forces.

Creeping flow at the separation medium has been calculated as Re 5.6×10^{-4} down to 6.09×10^{-5} for single cilia in rotifers [157], Re 0.00057 around choanocytes in sponges [103], Re 0.2 and lower at the ciliary bands of sabellid worms [158] and Re 0.0002 at the cilia in blue mussels [159]. These low Reynolds numbers indicate that particles are not removed through sieving because viscous forces are dominant, and thus it is energetically too expensive [140]. Due to high shear forces at low Reynolds numbers, particles are often individually directed by cilia along path lines towards the mouth [85,157].

Higher Reynolds numbers indicate turbulent flow and the formation of eddies [142]. The Reynolds number at which laminar flow becomes turbulent in size classes relevant for SFs is at Re > 200 [85] or as high as Re > 1000 [150] and depends on environmental conditions and geometries [142,160]. In large pelagic SFs, Reynolds numbers at the mesh have been determined up to 300 for mobulid rays [136], whale sharks [42], bowhead whales and fin whales. Dissipating energy caused by turbulence increases the energetic costs of SFs [156]. Thus, even large SFs are likely to induce a laminar flow regime to reduce energetic costs. Vanes on the downstream side of the whale shark have been assumed to act as collimators to remove turbulent eddies larger than the grid size [42,85].

A vortex-based mechanism was identified in suspension-feeding fish [161] and is suspected to occur in bowhead whales [162], both being cross-flow FFs. Ducks have been suggested to use turbulence to induce cyclonic vortices that separate particles by density [126]. The jelly fish *A. aurita* creates vortices with Reynolds numbers changing between 0 and up to 150 during the power stroke, which brings particles towards the bell margin [110].

The ambient flow of SFs is typically turbulent due to wind, tides and currents [85,155]. For benthic SFs, an ambient turbulent flow regime leads to particle mixtures and fluid exchange in the benthic boundary layers [85], which increases the particle capture rate [163]. However, the Reynolds number for benthic bivalves and ascidians ranges between 8 and 520 at the inhalant siphon. Hence, flow is laminar when entering the organism [164]. In colonial SFs, such as bryozoans, the morphology and packing of single units influence the overall flow field to induce excurrent flows to vent the colony [163].

7. Cleaning of separation media

After particles are retained by the separation medium, the particles have to be removed to maintain the function of

the separation process. In technology, this process is referred to as cleaning and can be further distinguished as continuous or discontinuous cleaning, depending on the mechanism and frequency. An increase of particles that become stuck in a pore or mesh leads to increased drag and higher energy expenditure [25,31]. Sponges directly take up particles by phagocytosis when encountering the microvilli or the cell surface of choanocytes, and particles are engulfed by pseudopodial extensions if at a distance of several micrometres from the cell [165]. The spoon worm *U. caupo* and the snail *D. maxima*, which build external mucus nets, periodically eat their nets along with the retained particles [33,36].

In ciliary SFs, alteration of ciliary movements and reversed strokes lead to transport towards the gut, such as in rotifers [109], brachiopods [76] or phoronids [106]. Tentacle flicking pushes single particles towards the mouth [106,166]. In moon jellies, ciliated grooves transport particles towards the gut after being caught by tentacles and nematocysts [110]. Crinoids catch particles with their tube feet and pinnules. By flicking of the pinnules, the particles are moved to the food grooves, where cilia transport the particles towards the mouth [97].

Moon jellies [1], ctenophores [84], sabellid worms [158] or blue mussels [108] are transporting particles by cilia in combination with mucus. The continuous mucus net in ascidians, which aligns the pharyngeal basket, is transported by cilia towards the oesophagus, where it is rolled up into a string and digested with the attached particles [69,167]. Enteropneusts, lancelets, Petromyzontiformes and tadpoles entrap particles with mucus within their pharyngeal basket or buccal cavity and swallow the aggregation afterwards (table 1, electronic supplementary material, table S5).

Particles can be fed off, scraped off or combed off the separation medium mechanically. During the retraction of polyps in gorgonians [168] and bending of the arms towards the mouth in dendrochirotid sea cucumber [71], particles are wiped off within the mouth and ingested. Suspension-feeding crustaceans and insect larvae use legs or mouthparts as cleaning brushes to swipe off particles and pass them towards the mouth [92,102,121,169]. The tongues of flamingos [170] and suspension-feeding ducks [171] are covered with spines sweeping off the particles from the lamellae on the inner sides of the beak and transport them towards the oesophagus. Lunge feeding whales, e.g. fin whales, also mainly use their tongue to remove captured prey from the baleen fringes combined with other mechanisms [172,173].

In FFs that use cross-flow filtration, the tangential flow constantly removes particles from the separation medium and increases particle concentration near the oesophagus opening [112,162]. Larvaceans, mobulid rays, whale sharks, silver carp, herrings and bowhead whales use this non-clogging mechanism (table 1, electronic supplementary material, table S5).

In response to environmental conditions, such as high particle concentrations, some SFs can switch between cleaning mechanisms or adapt their cleaning behaviour. Whale sharks [42] and bowhead whales [43] use a mechanism that is known as back-flushing or back-washing in filtration technologies. The flow is reversed backwards through the separation medium to clear plugged or clogged particles from the meshes [31]. Back-flushing interrupts the feeding process and is only used by SFs when their usual cleaning techniques are unsuccessful [42,69].

If undisturbed, most of the selected SFs feed continuously (30 of 35 SFs). Only a few organisms interrupt the feeding process because particles need to be removed from the separation medium, including all SFs that build external mucus and silk nets. While the spoon worm *U. caupo*, the sea snail *D. maxima* and trichopterans eat their nets along with the retained particles, larvaceans repel their nets (table 1; electronic supplementary material, table S5). All have to rebuild their nets afterwards. Fin whales feed discontinuously because they catch their food in big gulps [172,173].

8. Biomimetic potential

Most SFs use filtration, i.e. the separation medium is held into the fluid so that all fluid passes it, as the mechanism of separation. Similar to filtration technologies, the type of flow is dead-end or cross-flow filtration. However, while cross-flow filtration in industrial applications retains small particles in ultra- and nanofiltration [174], SFs such as mobulid rays, whale sharks or baleen whales also retain particles up to 10 mm with this mechanism [23,42,175]. These organisms use varying material properties and/or fluid flows within their cross-flow filtration to influence the interaction of particles and the separation medium. In the ricochet mechanism of manta rays, the particles bounce off the filtering lobes towards the oesophagus [23], in pump-feeding fishes, the gill arches induce the formation of vortices known as cross-step filtration [24] and in bowhead whales, the flow is diverted by the tongue and pressed along the baleen fringes that change in porosity depending on flow speed [175]. In all of these mechanisms, particles smaller than the mesh size are retained and the tangential flow reduces the clogging rate.

Centrifugal separations in technical applications, that separate particles based on rotating baskets or sedimentation, are not common in nature. Even though some SFs influence fluid flow specifically and create vortices, they mostly rely on particle–material interactions. Therefore, the chemical and physical properties of the separation media are specifically adapted to increase the chances of retention after encounter (figure 3). For example, the addition of surfactants to change the surface charge of the particles in feeding experiments led to a decrease in retention of small particles in daphnids [122], which shows that the material properties of chitin increase particle retention. Mucus as separation medium has evolved convergently in several taxa of the SFMs (13 of 35) and aids in particle retention and transport. Even though the filter materials used in technology are highly diverse and include natural and synthetic, organic and inorganic materials [31], to our knowledge, mucus-like filter media that use adhesive forces to retain particles are rarely used in solid–liquid filtration technologies. For example, a hydrogel was inspired by plant tissue to absorb uranium from seawater [176] and membrane surfaces were manufactured with super-hydrophobicity for bioinspired oil–water separation [22]. Filtration media in industry are manufactured independent of the filter housing, with woven fibres, perforated sheets or sintered metals as common filter designs [174]. Most of the SFs built their separation media from one or several body parts by branching or bristling (figure 4). Filter and filtration media are thus inseparable and sometimes multifunctional, thus providing stability, or aid in locomotion or gas exchange. The external filter house of larvaceans is built from mucus, which gives stability

and acts as the separation medium itself. The geometry of the separation media ranges from allegedly simple surfaces to complex spinned three-dimensional geometries, but it is in most cases funnel-shaped (figure 4), which, we assume, is one of the more efficient ways of increasing the filtration area. The setules on the appendages in daphnids [93] and the gill of the bivalve *M. edulis* [94] can be angled, similar to pleated filter media used in common technical filters to increase the filtration area [95,96]. The combination of several functions and the construction of complex filters could be made possible in the future through additive manufacturing or spinning technologies [175,177]. However, parametric studies on filtration efficiency which determine the influence of geometries found in SFs have not been carried out to date.

SFs require energy to cover the metabolic costs of growth, reproduction and feeding, i.e. foraging, the formation of separation media and creating a feeding current [10,80,178–180]. Therefore, SFs evolved along several of these fitness gradients [85,181]. An elongate rectangular mesh design can save up to 18% of silk material and requires less spinning movement in trichopteran larvae [98]. Ascidians grow in the shape of a pitot tube which induces a passive flow that relieves their ciliary pumping activity [37]. Because the energetic costs of filtration are proportional to hydrodynamic resistance under a constant flow rate, whale sharks and manta rays have vanes to reduce the pressure difference at the separation medium [23,42]. These SFs are large and their structures to optimize flow could be used to improve large filters with high throughput, such as industrial and public waste water treatments plants.

In SFs and technical filters, the particles are usually retained upstream of the separation medium. Exeptions are sabellid worms, which use cilia to collect particles after the water has passed the filaments of the gill crown [96]. All SFs evolved SFMs together with an inherent cleaning mechanism to remove the retained particles from the separation medium. Clogged filter media increase pressure differences and energy expenditure, and also negatively affect filtration rates. Cleaning and transport of particles is often achieved by the structures of the separation medium such as cilia, mucus or cell surfaces but SFs also use combing or back-flushing. Non-clogging mechanisms are also combined with cross-flow filtration: the fluid flows tangentially towards the separation medium, the particles are constantly removed and directed towards the oesophagus. This is in contrast to technical filters in which a cake is formed on the filtration medium by the layers of retained particles [174]. Cake removal is a problem, for example, in filter presses where the filtration process has to be interrupted to remove the cake [182]. By contrast, the majority of SFs have cleaning mechanisms that allow a continuous working mode (table 1) and take up the particles for nutrition at the same time.

Because most SFs are non-selective within the particle size range their SFMs are adapted for, this leads to an uptake of a heterogenic particle mixture, including anthropogenic particles, such as carbon fibres [183], metals [184] and microplastics. Microplastic uptake was reported for sponges, gorgonians, jelly fish, rotifers, sabellid worms, blue mussels, daphnids, Antarctic krill, barnacles, mayfly larvae and caddisfly larvae, crinoids, dendrochirotid sea cucumbers, tunicates, whale sharks, suspension-feeding fishes, tadpoles, suspension-feeding birds such as prions, and baleen whales (electronic supplementary material, table S4). Secondary and

tertiary waste water treatment plants only retain 88% and 90% of microplastics and the rest is released into the environment, where they accumulate [185,186]. Seston and plastic particles have similar dimensions (figure 2) so that SFs feeding in a similar size range might be suitable biological models for microplastics filtration. Additionally, SFs have mechanisms that are selective for specific particle properties such as shape, size or chemical properties, which might be useful for applications to extract specific particles from a heterogeneous mixture, such as microplastics from waste water. Generally, appropriate biological models for technical applications can be identified based on similar boundary conditions found through the parameters presented here (table 1). Subtle variations within similar SMFs, e.g. within the 10 000 species of sponges, could then inform parametric studies. In environmentally relevant applications such as the retention of microplastics, aspects of sustainable product development also should be considered at an early design stage [187,188].

Within this review, we studied traits individually, but evolution leads to trade-offs and development with phenotypic and/or phylogenetic constraints on multiple traits. Examples in SFs are the jet propulsion of the moon jelly *A. aurita* that propels the organism forward and also streams particles towards the separation media. In filter-feeding fishes or manta rays, the gill arches are modified for nutrition, but they also serve gas exchange. Comparison and transfer-of-principles from nature to technology need to consider such multifunctional constraints when taking SFMs out of their natural context [189].

The abstraction into numerical or physical models enables testing and verification of the biological principles outside the environmental context and allows a first check of transferability and scalability. Filtration technologies can work with vacuum, high pressures or steam, to which biological systems might not be applicable because they work at ambient temperature, are adapted to water, and low pressure differences. Drum filters can operate up to pressure differences of 10 bar (1 MPa). Whale sharks as one of the largest SFs induce a pressure difference of around 113 Pa (pressure head) at a swimming speed of 1.1 m s^{-1} [42]. These systems could inspire designs which work at lower pressures. Recent technical developments are hydrophilic membranes with capillary entry pressure to replace vacuum or filtrate pumps [182]. An example besides SFs are bioinspired membranes with embedded aquaporins developed for ultrafiltration [30].

Filtration technologies change depending on the scale due to physical or chemical restrictions. Coarse particles greater than 10 µm are retained by vacuum disc filters whereas small particles are retained by gas overpressure filtration. SFs range from several hundred micrometres to 25 m in size (figure 2) and also here the separation principles change. On smaller scales and Reynolds number up to 50, cilia and mucus are more common to retain small particles. Large ram-feeding fishes, sharks and whales use cross-flow filtration in which high amounts of particles are retained from water velocities higher than 10 cm s^{-1}. SFs often have an optimal range were particle retention is close to 100% [82,83,190]. When an application of a bioinspired filter is outside its original scale, a check for scalability is necessary. Dimensionless numbers such as the Reynolds number offer a good approximation of fluid dynamical aspects [189].

Engineered solutions result from decision-making to predefined problems, whereas an organism has evolved under natural selection [182,191]. SFs are well-integrated into their

ecological environment, and they show species-specific phenotypic plasticity enabling them to react to environmental changes during their lifetime. They can adapt to changes in their environment and adjust their feeding behaviour to temperature, flow velocity and particle concentration, whereas technical filters are static [69,182]. Recent developments in filtration technologies are so-called smart filters. These include filter media designed by artificial intelligence to plan tailored membranes for applications such as the selective retention of salt ions in drinking water purification [192] or surface modified filters to detect toxic polar molecules in real time [193]. Adaptive changes to the surrounding flow are active and passive in SFs. Separation media are flexible to avoid buckling or bending, in general described as reconfiguration [142]. In strong currents, the pinnules and tube feet in crinoids bend downstream, resulting in a decreased filter area, thus reducing speed-specific drag and allowing crinoids to hold their posture and continue feeding [101]. The branching patterns in gorgonians depend on ambient flow conditions, trading-off between increasing filtration area and decreasing drag force [194,195]. The baleen plates have variable porosity that changes in response to flow velocity; the higher the flow velocity the higher the porosity [175].

A limiting factor for a successful transfer is the availability of data about the SFMs, which varies strongly between the reviewed SFs. While the SFM of the blue mussel *M. edulis* is well understood, there is only one reference about the feeding mechanism in the Antarctic krill *E. superba*, despite its ecological relevance. When looking at the three main aspects, namely particles, separation medium and fluid dynamics that are involved in particle separation, it is notable that the fewest studies are on fluid dynamics, i.e. water velocity and flow regime (electronic supplementary material, table S5). It might be beneficial to first analyse the interaction of two aspects at a time, such as the interaction of particles and different separation medium materials, the influence of different geometries on fluid flow or the flow regime around different types of particles, i.e. spheres, fibres, irregular shapes.

In a biomimetic working process, we propose to focus on single traits and functions instead of transferring the complete mechanism. For example, the technology to build artificial cilia has yet to be invented, so the mucus net transported by cilia in ascidians is challenging to mimic, but the fluid flow through the pharyngeal basket might show some new insights into how changes of direction of fluids in pipes might be accomplished without high pressure losses. Progress in manufacturing processes such as additive manufacturing [196] and increasing use of numerical simulations in addition to physical models to test and verify fluid dynamics [160,164], particle encounter [151] or retention mechanisms [197] will make a technical application of SFMs more feasible in the future.

References

1. Jørgensen CB. 1966 *Biology of suspension feeding*. Oxford, UK: Pergamon Press.

2. Hentschel BT, Shimeta J. 2008 Suspension feeders. In *Encyclopedia of ecology*), pp. 3437–3442. Amsterdam, The Netherlands: Elsevier Science Ltd.

3. Riisgård H, Larsen P. 2010 Particle capture mechanisms in suspension-feeding invertebrates. *Mar. Ecol. Prog. Ser.* **418**, 255–293. (doi:10.3354/meps08755)

4. Sanderson SLL, Wassersug RJ. 1993 Convergent and alternative designs for vertebrate suspension feeding. In *The skull* (eds J Hanken, BK Hall), pp. 37–112. Chicago, IL/London, UK: University of Chicago Press.

5. Lenton TM, Boyle RA, Poulton SW, Shields-Zhou GA, Butterfield NJ. 2014 Co-evolution of eukaryotes and ocean oxygenation in the Neoproterozoic era. *Nat. Geosci.* **7**, 257–265. (doi:10.1038/ngeo2108)

6. Dohrmann M, Wörheide G. 2017 Dating early animal evolution using phylogenomic data. *Sci. Rep.* **7**, 3599. (doi:10.1038/s41598-017-03791-w)

7. Hölker F *et al.* 2015 Tube-dwelling invertebrates: tiny ecosystem engineers have large effects in lake ecosystems. *Ecol. Monogr.* **85**, 333–351. (doi:10.1890/14-1160.1)

8. Ostroumov SA. 2005 Some aspects of water filtering activity of filter-feeders. *Hydrobiologia* **542**, 275–286. (doi:10.1007/s10750-004-1875-1)

9. Ausich WI, Bottjer DJ. 1991 History of tiering among suspension feeders in the benthic marine ecosystem. *J. Geol. Educ.* **39**, 313–319. (doi:10.5408/0022-1368-39.4.313)

10. Sebens K, Sarà G, Nishizaki M. 2017 Energetics, particle capture, and growth dynamics of benthic suspension feeders. In *Marine animal forests: the ecology of benthic biodiversity hotspots*, pp. 813–854. New York, NY: Springer.

11. Wing S, Jack L. 2012 Resource specialisation among suspension-feeding invertebrates on rock walls in Fiordland, New Zealand, is driven by water column structure and feeding mode. *Mar. Ecol. Prog. Ser.* **452**, 109–118. (doi:10.3354/meps09588)

12. Heinonen KB, Ward JE, Holohan BA. 2007 Production of transparent exopolymer particles (TEP) by benthic suspension feeders in coastal systems. *J. Exp. Mar. Biol. Ecol.* **341**, 184–195. (doi:10.1016/j.jembe.2006.09.019)

13. Malmqvist B, Wotton RS, Zhang Y. 2001 Suspension feeders transform massive amounts of seston in large northern rivers. *Oikos* **92**, 35–43. (doi:10.1034/j.1600-0706.2001.920105.x)

14. Whalen MA, Stachowicz JJ. 2017 Suspension feeder diversity enhances community filtration rates in different flow environments. *Mar. Ecol. Prog. Ser.* **570**, 1–13. (doi:10.3354/meps12133)

15. Coma R, Ribes M, Gili J, Hughes R. 2001 The ultimate opportunists: consumers of seston. *Mar. Ecol. Prog. Ser.* **219**, 305–308. (doi:10.3354/meps219305)

16. Valdivia N, de la Haye KL, Jenkins SR, Kimmance SA, Thompson RC, Molis M. 2009 Functional composition, but not richness, affected the performance of sessile suspension-feeding

assemblages. *J. Sea Res.* **61**, 216–221. (doi:10.1016/j.seares.2008.12.001)

17. FAO: Food & Agriculture Organisation. 2020 *FAO yearbook. Fishery and aquaculture statistics 2018/FAO annuaire. Statistiques des pêches et de l'aquaculture 2018/FAO anuario. Estadísticas de pesca y acuicultura 2018*. Rome, Italy: FAO.

18. Cranford PJ. 2019 Magnitude and extent of water clarification services provided by bivalve suspension feeding. In *Goods and services of marine bivalves*, pp. 119–141. Cham, Switzerland: Springer International Publishing.

19. Nepstad R, Størdal IF, Brönner U, Nordtug T, Hansen BH. 2015 Modeling filtration of dispersed crude oil droplets by the copepod *Calanus finmarchicus*. *Mar. Environ. Res.* **105**, 1–7. (doi:10.1016/j.marenvres.2015.01.004)

20. Letendre F, Mehrabian S, Etienne S, Cameron CB. 2020 The interactions of oil droplets with filter feeders: a fluid mechanics approach. *Mar. Environ. Res.* **161**, 105059. (doi:10.1016/j.marenvres.2020.105059)

21. Dvarskas A, Bricker SB, Wikfors GH, Bohorquez JJ, Dixon MS, Rose JM. 2020 Quantification and valuation of nitrogen removal services provided by commercial shellfish aquaculture at the subwatershed scale. *Environ. Sci. Technol.* **54**, 16 156–16 165. (doi:10.1021/acs.est.0c03066)

22. Li Z, Tan CM, Tio W, Ang J, Sun DD. 2018 Manta ray gill inspired radially distributed nanofibrous membrane for efficient and continuous oil–water separation. *Environ. Sci. Nano* **5**, 1466–1472. (doi:10.1039/C8EN00258D)

23. Divi RV, Strother JA, Paig-Tran EWM. 2018 Manta rays feed using ricochet separation, a novel nonclogging filtration mechanism. *Sci. Adv.* **4**, eaat9533. (doi:10.1126/sciadv.aat9533)

24. Schroeder A, Marshall L, Trease B, Becker A, Sanderson SLL. 2019 Development of helical, fish-inspired cross-step filter for collecting harmful algae. *Bioinspir. Biomim.* **14**, 056008. (doi:10.1088/1748-3190/ab2d13)

25. Walzel P. 2012 Filtration: fundamentals. In *Ullmann's encyclopedia of industrial chemistry*, pp. 25.1–25.40. Weinheim, Germany: Wiley-VCH.

26. Adam PJ, Berta A. 2001 Evolution of prey capture strategies and diet in pinnipedimorpha (Mammalia, Carnivora). *Oryctos* **4**, 83–107.

27. Schlichter D, Brendelberger H. 1998 Plasticity of the scleractinian body plan: functional morphology and trophic specialization of *Mycedium elephantotus* (Pallas, 1766). *Facies* **39**, 227–241. (doi:10.1007/BF02537018)

28. Pernet B. 2018 Larval feeding: mechanisms, rates, and performance in nature. In *Evolutionary ecology of marine invertebrate larvae* (eds TJ Carrier, AM Reitzel, A Heyland), pp. 87–102. Oxford, UK: Oxford University Press.

29. Fenchel T. 1987 *Ecology of protozoa*, 1st edn. Berlin, Germany: Springer.

30. Zhong PS, Chung T-S, Jeyaseelan K, Armugam A. 2012 Aquaporin-embedded biomimetic membranes for nanofiltration. *J. Membr. Sci.* **407–408**, 27–33. (doi:10.1016/j.memsci.2012.03.033)

31. Sutherland K. 2005 *The A-Z of filtration and related separations*. Oxford, UK: Elsevier Science Ltd.

32. Mallatt J. 1982 Pumping rates and particle retention efficiencies of the larval lamprey, an unusual suspension feeder. *Biol. Bull.* **163**, 197–210. (doi:10.2307/1541509)

33. Ribak G, Heller J, Genin A. 2005 Mucus-net feeding on organic particles by the vermetid gastropod *Dendropoma maximum* in and below the surf zone. *Mar. Ecol. Prog. Ser.* **293**, 77–87. (doi:10.3354/meps293077)

34. Cameron CBCB. 2002 Particle retention and flow in the pharynx of the enteropneust worm *Harrimania planktophilus*: the filter-feeding pharynx may have evolved before the chordates. *Biol. Bull.* **202**, 192–200. (doi:10.2307/1543655)

35. Nielsen SE, Bone Q, Bond P, Harper G. 2007 On particle filtration by amphioxus (*Branchiostoma lanceolatum*). *J. Mar. Biol. Assoc. U.K.* **87**, 983–989. (doi:10.1017/S0025315407053519)

36. Osovitz CJ, Julian D. 2002 Burrow irrigation behavior of *Urechis caupo*, a filter-feeding marine invertebrate, in its natural habitat. *Mar. Ecol. Prog. Ser.* **245**, 149–155. (doi:10.3354/meps245149)

37. Knott NA, Davis AR, Buttemer WA. 2004 Passive flow through an unstalked intertidal ascidian: orientation and morphology enhance suspension feeding in *Pyura stolonifera*. *Biol. Bull.* **207**, 217–224. (doi:10.2307/1543210)

38. Li NK, Denny MW. 2004 Limits to phenotypic plasticity: flow effects on barnacle feeding appendages. *Biol. Bull.* **206**, 121–124. (doi:10.2307/1543635)

39. Robertson LMLM, Hamel JFJ-F, Mercier A. 2017 Feeding in deep-sea demosponges: influence of abiotic and biotic factors. *Deep. Res. I Oceanogr. Res. Pap.* **127**, 49–56. (doi:10.1016/j.dsr.2017.07.006)

40. Kuzmina TV, Temereva EN. 2019 Organization of the lophophore in the deep-sea brachiopod *Pelagodiscus atlanticus* and evolution of the lophophore in the Brachiozoa. *Org. Divers. Evol.* **19**, 31–39. (doi:10.1007/s13127-018-0388-0)

41. Bushek D, Allen DM. 2005 Motile suspension-feeders in estuarine and marine ecosystems. In *The comparative roles of suspension-feeders in ecosystems*, pp. 53–71. Berlin, Germany: Springer-Verlag.

42. Motta PJ *et al.* 2010 Feeding anatomy, filter-feeding rate, and diet of whale sharks *Rhincodon typus* during surface ram filter feeding off the Yucatan Peninsula, Mexico. *Zoology* **113**, 199–212. (doi:10.1016/j.zool.2009.12.001)

43. Simon M, Johnson M, Tyack P, Madsen PT. 2009 Behaviour and kinematics of continuous ram filtration in bowhead whales (*Balaena mysticetus*). *Proc. R. Soc. B* **276**, 3819–3828. (doi:10.1098/rspb.2009.1135)

44. Goldbogen JA, Calambokidis J, Shadwick RE, Oleson EM, McDonald MA, Hildebrand JA. 2006 Kinematics of foraging dives and lunge-feeding in fin whales.

J. Exp. Biol. **209**, 1231–1244. (doi:10.1242/jeb.02135)

45. Yee DA, Kaufmann MG. 2019 Insect mouthparts. In *Insect mouthparts* (ed. HW Krenn), pp. 101–125. Cham, Switzerland: Springer International Publishing.

46. Seale DB, Wassersug RJ. 1979 Suspension feeding dynamics of anuran larvae related to their functional morphology. *Oecologia* **39**, 259–272. (doi:10.1007/BF00345438)

47. Moore JW, Mallatt JM. 1980 Feeding of larval lamprey. *Can. J. Fish. Aquat. Sci.* **37**, 1658–1664. (doi:10.1139/f80-213)

48. Sanderson SL, Cech JJJ, Laurie Sanderson S, Cech JJJ. 1992 Energetic cost of suspension feeding versus particulate feeding by juvenile Sacramento blackfish. *Trans. Am. Fish. Soc.* **121**, 149–157. (doi:10.1577/1548-8659(1992)121<0149:ecosfv>2.3.co;2)

49. Riisgård HU, Larsen PS. 2017 Filter-feeding zoobenthos and hydrodynamics. In *Marine animal forests*, pp. 787–811. Cham, Switzerland: Springer International Publishing.

50. Wildish D, Kristmanson DD. 1997 *Benthic suspension feeders and flow*. Cambridge, UK: Cambridge University Press.

51. Lenz J. 1977 Seston and its main components. In *Microbial ecology of a brackish water environment* (ed. G Reinheimer), pp. 37–60. Berlin, Germany: Springer.

52. Kiørboe T. 2011 How zooplankton feed: mechanisms, traits and trade-offs. *Biol. Rev.* **86**, 311–339. (doi:10.1111/j.1469-185X.2010.00148.x)

53. Conley KR, Lombard F, Sutherland KR. 2018 Mammoth grazers on the ocean's minuteness: a review of selective feeding using mucous meshes. *Proc. R. Soc. B* **285**, 20180056. (doi:10.1098/rspb.2018.0056)

54. Hansen B, Bjornsen PK, Hansen PJ. 1994 The size ratio between planktonic predators and their prey. *Limnol. Oceanogr.* **39**, 395–403. (doi:10.4319/lo.1994.39.2.0395)

55. MacGinitie GE. 1945 The size of the mesh opening in mucous feeding nets of marine animals. *Biol. Bull.* **88**, 107–111. (doi:10.2307/1538038)

56. Bak RPM, Joenje M, De Jong I, Lambrechts DYM, Nieuwland G. 1998 Bacterial suspension feeding by coral reef benthic organisms. *Mar. Ecol. Prog. Ser.* **175**, 285–288. (doi:10.3354/meps175285)

57. Lawrence J, Töpper J, Petelenz-Kurdziel E, Bratbak G, Larsen A, Thompson E, Troedsson C, Ray JL. 2018 Viruses on the menu: the appendicularian *Oikopleura dioica* efficiently removes viruses from seawater. *Limnol. Oceanogr.* **63**, S244–S253. (doi:10.1002/lno.10734)

58. Burge CA, Closek CJ, Friedman CS, Groner ML, Jenkins CM, Shore-Maggio A, Welsh JE. 2016 The Use of filter-feeders to manage disease in a changing world. *Integr. Comp. Biol.* **56**, 573–587. (doi:10.1093/icb/icw048)

59. Ribes M, Coma R, Gili J-M, Svoboda A, Julià A, Parera J. 2000 A 'semi-closed' recirculating system

for the in situ study of feeding and respiration of benthic suspension feeders. *Sci. Mar.* **64**, 265–275. (doi:10.3989/scimar)

60. Schartau M, Wallhead P, Hemmings J, Löptien U, Kriest I, Krishna S, Ward BA, Slawig T, Oschlies A. 2017 Reviews and syntheses: parameter identification in marine planktonic ecosystem modelling. *Biogeosciences* **14**, 1647–1701. (doi:10.5194/bg-14-1647-2017)

61. Vereshchaka A, Abyzova G, Lunina A, Musaeva E, Sutton TT. 2016 A novel approach reveals high zooplankton standing stock deep in the sea. *Biogeosciences Discuss.* **13**, 6261–6271. (doi:10.5194/bg-2016-145)

62. Bochdansky AB, Deibel D. 1999 Measurement of in situ clearance rates of *Oikopleura vanhoeffeni* (Appendicularia: Tunicata) from tail beat frequency, time spent feeding and individual body size. *Mar. Biol.* **133**, 37–44. (doi:10.1007/s002270050440)

63. Gibson RN, Ezzi IA. 1992 The relative profitability of particulate- and filter-feeding in the herring, *Clupea harengus* L. *J. Fish Biol.* **40**, 577–590. (doi:10.1111/j.1095-8649.1992.tb02607.x)

64. Sims DW, Southall EJ, Tarling GA, Metcalfe JD. 2005 Habitat-specific normal and reverse diel vertical migration in the plankton-feeding basking shark. *J. Anim. Ecol.* **74**, 755–761. (doi:10.1111/j.1365-2656.2005.00971.x)

65. Goldbogen JA, Hazen EL, Friedlaender AS, Calambokidis J, DeRuiter SL, Stimpert AK, Southall BL. 2015 Prey density and distribution drive the three-dimensional foraging strategies of the largest filter feeder. *Funct. Ecol.* **29**, 951–961. (doi:10.1111/1365-2435.12395)

66. van der Hoop JM, Nousek-McGregor AE, Nowacek DP, Parks SE, Tyack P, Madsen PT. 2019 Foraging rates of ram-filtering North Atlantic right whales. *Funct. Ecol.* **33**, 1290–1306. (doi:10.1111/1365-2435.13357)

67. Miller DC, Bock MJ, Turner EJ. 1992 Deposit and suspension feeding in oscillatory flows and sediment fluxes. *J. Mar. Res.* **50**, 489–520. (doi:10.1357/002224092784797601)

68. Miller LP. 2007 Feeding in extreme flows: behavior compensates for mechanical constraints in barnacle cirri. *Mar. Ecol. Prog. Ser.* **349**, 227–234. (doi:10.3354/meps07099)

69. Petersen JK. 2007 Ascidian suspension feeding. *J. Exp. Mar. Biol. Ecol.* **342**, 127–137. (doi:10.1016/j.jembe.2006.10.023)

70. Taghon GL. 1982 Optimal foraging by deposit-feeding invertebrates: roles of particle size and organic coating. *Oecologia* **52**, 295–304. (doi:10.1007/BF00367951)

71. Roberts D, Gebruk A, Levin V, Manship BAD. 2000 Feeding and digestive strategies in deposit-feeding Holothurians. *Oceanogr. Mar. Biol. Annu. Rev.* **38**, 257–310.

72. Rubenstein DI, Koehl MAR. 1977 The mechanisms of filter feeding: some theoretical considerations. *Am. Nat.* **111**, 981–994. (doi:10.1086/283227)

73. Shimeta J, Koehl MAR. 1997 Mechanisms of particle selection by tentaculate suspension feeders during encounter, retention, and handling. *J. Exp. Mar. Biol. Ecol.* **209**, 47–73. (doi:10.1016/S0022-0981(96)02684-6)

74. Yahel G, Eerkes-Medrano DI, Leys SP. 2006 Size independent selective filtration of ultraplankton by hexactinellid glass sponges. *Aquat. Microb. Ecol.* **45**, 181–194. (doi:10.3354/ame045181)

75. Ward JE, Shumway SE. 2004 Separating the grain from the chaff: particle selection in suspension- and deposit-feeding bivalves. *J. Exp. Mar. Biol. Ecol.* **300**, 83–130. (doi:10.1016/j.jembe.2004.03.002)

76. Thayer CW. 1986 Are brachiopods better than bivalves? Mechanisms of turbidity tolerance and their interaction with feeding in articulates. *Paleobiology* **12**, 161–174. (doi:10.1017/S0094837300013634)

77. Brent Gurd D. 2006 Filter-feeding dabbling ducks (Anas spp.) can actively select particles by size. *Zoology* **109**, 120–126. (doi:10.1016/j.zool.2005.10.002)

78. Conley KR, Gemmell BJ, Bouquet JM, Thompson EM, Sutherland KR. 2018 A self-cleaning biological filter: how appendicularians mechanically control particle adhesion and removal. *Limnol. Oceanogr.* **63**, 927–938. (doi:10.1002/lno.10680)

79. Lombard F, Selander E, Kiørboe T. 2011 Active prey rejection in the filter-feeding appendicularian Oikopleura dioica. *Limnol. Oceanogr.* **56**, 1504–1512. (doi:10.4319/lo.2011.56.4.1504)

80. DeMott WR. 1990 Retention efficiency, perceptual bias, and active choice as mechanisms of food selection by suspension-feeding zooplankton. In *Behavioural mechanisms of food selection*, pp. 569–594. Berlin, Germany: Springer.

81. Rosa M, Ward JE, Frink A, Shumway SE. 2017 Effects of surface properties on particle capture by two species of suspension-feeding bivalve molluscs. *Am. Malacol. Bull.* **35**, 181–188. (doi:10.4003/006.035.0212)

82. Strohmeier T, Strand T, Alunno-Bruscia M, Duinker A, Cranford PJ. 2012 Variability in particle retention efficiency by the mussel *Mytilus edulis*. *J. Exp. Mar. Biol. Ecol.* **412**, 96–102. (doi:10.1016/j.jembe.2011.11.006)

83. Sumerel AN, Finelli CM. 2014 Particle size, flow speed, and body size interactions determine feeding rates of a solitary ascidian *Styela plicata*: a flume experiment. *Mar. Ecol. Prog. Ser.* **495**, 193–204. (doi:10.3354/meps10571)

84. Waggett R. 1999 Capture mechanisms used by the lobate ctenophore, *Mnemiopsis leidyi*, preying on the copepod *Acartia tonsa*. *J. Plankton Res.* **21**, 2037–2052. (doi:10.1093/plankt/21.11.2037)

85. Shimeta J, Jumars PA. 1991 Physical mechanisms and rates of particle capture by suspension-feeders. *Oceanogr. Mar. Biol. Annu. Rev.* **29**, 191–257.

86. Julian D, Chang M, Judd J, Arp A. 2001 Influence of environmental factors on burrow irrigation and oxygen consumption in the mudflat invertebrate *Urechis caupo*. *Mar. Biol.* **139**, 163–173. (doi:10.1007/s002270100570)

87. Riisgård HU, Okamura B, Funch P. 2010 Particle capture in ciliary filter-feeding gymnolaemate and phylactolaemate bryozoans: a comparative study. *Acta Zool.* **91**, 416–425. (doi:10.1111/j.1463-6395.2009.00417.x)

88. LaBarbera M. 1990 Principles of design of fluid transport systems in zoology. *Science* **249**, 992–1000. (doi:10.1126/science.2396104)

89. Best BA. 1988 Passive suspension feeding in a sea pen: effects of ambient flow on volume flow rate and filtering efficiency. *Biol. Bull.* **175**, 332–342. (doi:10.2307/1541723)

90. Merritt RW, Craig DA, Wotton RS, Walker ED. 1996 Feeding behavior of aquatic insects: case studies on black fly and mosquito larvae. *Invertebr. Biol.* **115**, 206–217. (doi:10.2307/3226931)

91. McCafferty WP, Bae YJ. 1992 Filter-feeding habits of the larvae of Anthopotamus (Ephemeroptera : Potamanthidae). *Ann. Limnol. Int. J. Limnol.* **28**, 27–34. (doi:10.1051/limn/1992002)

92. Trager GC, Hwang J-S, Strickler JR. 1990 Barnacle suspension-feeding in variable flow. *Mar. Biol.* **105**, 117–127. (doi:10.1007/BF01344277)

93. Brendelberger H, Geller W. 1985 Variability of filter structures in eight Daphnia species: mesh sizes and filtering areas. *J. Plankton Res.* **7**, 473–486. (doi:10.1093/plankt/7.4.473)

94. Beninger PG, St-Jean SD, Poussart Y. 1995 Labial palps of the blue mussel *Mytilus edulis* (Bivalvia: Mytilidae). *Mar. Biol.* **123**, 293–303. (doi:10.1007/BF00353621)

95. Chen DR, Pui DYH, Liu BYH. 1995 Optimization of pleated filter designs using a finite-element numerical model. *Aerosol Sci. Technol.* **23**, 579–590. (doi:10.1080/02786829508965339)

96. Riisgård HU, Ivarsson NM. 1990 The crown-filament pump of the suspension-feeding polychaete *Sabella penicillus*: filtration, effects of temperature, and energy cost. *Mar. Ecol. Prog. Ser.* **62**, 249–257.

97. Holland ND, Strickler JR, Leonard AB. 1986 Particle interception, transport and rejection by the feather star *Oligometra serripinna* (Echinodermata: Crinoidea), studied by frame analysis of videotapes. *Mar. Biol.* **93**, 111–126. (doi:10.1007/BF00428660)

98. Wallace JB, Malas D, Athens G. 1976 The significance of the elongate, rectangular mesh found in capture nets of fine particle filter feeding Trichoptera larvae. *Arch. Hydrobiol.* **77**, 205–212.

99. Kuzmina TV, Malakhov VV. 2007 Structure of the brachiopod lophophore. *Paleontol. J.* **41**, 520–536. (doi:10.1134/S0031030107050073)

100. Chang-Feng D, Ming-Chao L. 1993 The effects of flow on feeding of three gorgonians from southern Taiwan. *J. Exp. Mar. Biol. Ecol.* **173**, 57–69. (doi:10.1016/0022-0981(93)90207-5)

101. Leonard AB, Strickler JR, Holland ND. 1988 Effects of current speed on filtration during suspension feeding in *Oligometra serripinna* (Echinodermata: Crinoidea). *Mar. Biol.* **97**, 111–125. (doi:10.1007/BF00391251)

102. McClatchie S, Boyd CM. 1983 Morphological study of sieve efficiencies and mandibular surfaces in the Antarctic krill, *Euphausia superba*. *Can. J. Fish. Aquat. Sci.* **40**, 955–967. (doi:10.1139/f83-122)

103. Asadzadeh SS, Larsen PS, Riisgård HU, Walther JH. 2019 Hydrodynamics of the leucon sponge pump. *J. R. Soc. Interface* **16**, 20180630. (doi:10.1098/rsif. 2018.0630)

104. Paig-Tran EWM, Summers AP. 2014 Comparison of the structure and composition of the branchial filters in suspension feeding elasmobranchs. *Anat. Rec.* **297**, 701–715. (doi:10.1002/ar.22850)

105. Cohen KE, Hernandez LP. 2018 The complex trophic anatomy of silver carp, *Hypophthalmichthys molitrix*, highlighting a novel type of epibranchial organ. *J. Morphol.* **279**, 1615–1628. (doi:10.1002/jmor. 20891)

106. Riisgård HUU. 2002 Methods of ciliary filter feeding in adult *Phoronis muelleri* (phylum Phoronida) and in its free-swimming actinotroch larva. *Mar. Biol.* **141**, 75–87. (doi:10.1007/s00227-002-0802-0)

107. Riisgård HU, Nielsen C, Larsen PS. 2000 Downstream collecting in ciliary suspension feeders: the catch-up principle. *Mar. Ecol. Prog. Ser.* **207**, 33–51. (doi:10. 3354/meps207033)

108. Riisgård HU, Funch P, Larsen PS. 2015 The mussel filter-pump: present understanding, with a re-examination of gill preparations. *Acta Zool.* **96**, 273–282. (doi:10.1111/azo.12110)

109. Strathmann RR, Jahn TL, Fonseca JRC. 1972 Suspension feeding by marine invertebrate larvae: clearance rate of particles by ciliated bands of a rotifer, pluteus, and trochophore. *Biol. Bull.* **142**, 505–519. (doi:10.2307/1540326)

110. Costello JH, Colin SP. 1994 Morphology, fluid motion and predation by the scyphomedusa *Aurelia aurita*. *Mar. Biol.* **121**, 327–334. (doi:10.1007/ BF00346741)

111. Pennachetti CA. 1984 Functional morphology of the branchial basket of ascidia paratropa (Tunicata, Ascidiacea). *Zoomorphology* **104**, 216–222. (doi:10. 1007/BF00312033)

112. Katija K, Troni G, Daniels J, Lance K, Sherlock RE, Sherman AD, Robison BH. 2020 Revealing enigmatic mucus structures in the deep sea using DeepPIV. *Nature* **583**, 78–82. (doi:10.1038/s41586-020-2345-2)

113. Jørgensen C. 1983 Fluid mechanical aspects of suspension feeding. *Mar. Ecol. Prog. Ser.* **11**, 89–103. (doi:10.3354/meps011089)

114. Randall D, Burggren W, French K. 2001 *Animal physiology: mechanisms and adaptions*, 5th edn. New York, NY: W.H. Freeman and Company.

115. Labarbera M. 1978 Particle capture by a pacific brittle star: experimental test of the aerosol suspension feeding model. *Science* **201**, 1147–1149. (doi:10.1126/science.201.4361.1147)

116. Flood PR, Fiala-Medioni A. 1981 Ultrastructure and histochemistry of the food trapping mucous film in benthic filter-feeders (Ascidians). *Acta Zool.* **62**, 53–65. (doi:10.1111/j.1463-6395.1981. tb00616.x)

117. Pales Espinosa E, Perrigault M, Allam B. 2010 Identification and molecular characterization of a mucosal lectin (MeML) from the blue mussel *Mytilus edulis* and its potential role in particle capture. *Comp. Biochem. Physiol. A Mol. Integr. Physiol.* **156**, 495–501. (doi:10.1016/j.cbpa. 2010.04 .004)

118. Beninger PG, St-Jean SD. 1997 The role of mucus in particle processing by suspension-feeding marine bivalves: unifying principles. *Mar. Biol.* **129**, 389–397. (doi:10.1007/s002270050179)

119. Sutherland KR, Madin LP, Stocker R. 2010 Filtration of submicrometer particles by pelagic tunicates. *Proc. Natl Acad. Sci. USA* **107**, 15 129–15 134. (doi:10.1073/pnas.1003599107)

120. Brown SA, Ruxton GD, Humphries S. 2004 Physical properties of *Hydropsyche siltalai* (Trichoptera) net silk. *J. North Am. Benthol. Soc.* **23**, 771–779. (doi:10.1899/0887-3593(2004)023<0771:ppohst>2. 0.co;2)

121. Wallace JB, Merritt RW. 1980 Filter-feeding ecology of aquatic insects. *Annu. Rev. Entomol.* **25**, 103–135.

122. Gerritsen J, Porter KG. 1982 The role of surface chemistry in filter feeding by zooplankon. *Science* **4**, 1225–1228. (doi:10.1126/science.216.4551.1225)

123. Werth AJ, Rita D, Rosario MV, Moore MJ, Sformo TL. 2018 How do baleen whales stow their filter? A comparative biomechanical analysis of baleen bending. *J. Exp. Biol.* **221**, jeb189233. (doi:10.1242/ jeb.189233)

124. Szewciw LJ, De Kerckhove DG, Grime GW, Fudge DS. 2010 Calcification provides mechanical reinforcement to whale baleen α-keratin. *Proc. R. Soc. B* **277**, 2597–2605. (doi:10.1098/ rspb.2010.0399)

125. Mascitti V, Osvaldo Kravetz F. 2002 Bill morphology of South American flamingos. *Condor* **104**, 73. (doi:10.1650/0010-5422(2002)104[0073:bmosaf]2.0. co;2)

126. Kooloos JGM, Kraaijeveld AR, Langenbach GEJ, Zweers GA. 1989 Comparative mechanics of filter feeding in *Anas platyrhynchos*, *Anas clypeata* and *Aythya fuligula* (Aves, Anseriformes). *Zoomorphology* **108**, 269–290. (doi:10.1007/BF00312160)

127. Colin SP, Costello JH, Hansson LJ, Titelman J, Dabiri JO. 2010 Stealth predation and the predatory success of the invasive ctenophore *Mnemiopsis leidyi*. *Proc. Natl Acad. Sci. USA* **107**, 17 223–17 227. (doi:10.1073/pnas.1003170107)

128. Collard F, Gilbert B, Eppe G, Roos L, Compère P, Das K, Parmentier E. 2017 Morphology of the filtration apparatus of three planktivorous fishes and relation with ingested anthropogenic particles. *Mar. Pollut. Bull.* **116**, 182–191. (doi:10.1016/j.marpolbul.2016. 12.067)

129. Silvester NR. 1983 Some hydrodynamic aspects of filter feeding with rectangular-mesh nets. *J. Theor. Biol.* **103**, 265–286. (doi:10.1016/0022-5193(83)90028-0)

130. Loudon C, Alstad DN. 1990 Theoretical mechanics of particle capture: predictions for hydropsychid caddisfly distributional ecology. *Am. Nat.* **135**, 360–381. (doi:10.1086/285051)

131. Brown SA, Ruxton GD, Pickup RW, Humphries S. 2005 Seston capture by *Hydropsyche siltalai* and the accuracy of capture efficiency estimates. *Freshw. Biol.* **50**, 113–126. (doi:10.1111/j.1365-2427.2004. 01311.x)

132. Witte U, Brattegard T, Graf G, Springer B. 1997 Particle capture and deposition by deep-sea sponges from the Norwegian-Greenland Sea. *Mar. Ecol. Prog. Ser.* **154**, 241–252. (doi:10.3354/ meps154241)

133. Cohen KE, Hernandez LP. 2018 Making a master filterer: ontogeny of specialized filtering plates in silver carp (*Hypophthalmichthys molitrix*). *J. Morphol.* **279**, 925–935. (doi:10.1002/ jmor.20821)

134. Sponaugle S. 1991 Flow patterns and velocities around a suspension-feeding gorgonian polyp: evidence from physical models. *J. Exp. Mar. Biol. Ecol.* **148**, 135–145. (doi:10.1016/0022-0981(91)90152-M)

135. Riisgård HU, Larsen PS. 2000 Comparative ecophysiology of active zoobenthic filter feeding, essence of current knowledge. *J. Sea Res.* **44**, 169–193. (doi:10.1016/S1385-1101(00)00054-X)

136. Paig-Tran EWM, Kleinteich T, Summers AP. 2013 The filter pads and filtration mechanisms of the devil rays: variation at macro and microscopic scales. *J. Morphol.* **274**, 1026–1043. (doi:10.1002/jmor. 20160)

137. Lampert W, Brendelberger H. 1996 Strategies of phenotypic low-food adaptation in Daphnia: filter screens, mesh sizes, and appendage beat rates. *Limnol. Ocean.* **41**, 216–223.

138. Werth AJ. 2013 Flow-dependent porosity and other biomechanical properties of mysticete baleen. *J. Exp. Biol.* **216**, 1152–1159. (doi:10.1242/jeb. 078931)

139. Ripperger S, Altmann J. 2002 Crossflow microfiltration: state of the art. *Sep. Purif. Technol.* **26**, 19–31. (doi:10.1016/S1383-5866(01)00113-7)

140. Gerritsen J, Porter KG, Strickler JR. 1988 Not by sieving alone: observations of suspension feeding in Daphnia. *Bull. Mar. Sci.* **43**, 366–376.

141. Taghon GL, Greene RR. 1992 Utilization of deposited and suspended particulate matter by benthic 'interface' feeders. *Limnol. Oceanogr.* **37**, 1370–1391. (doi:10.4319/lo.1992.37.7.1370)

142. Vogel S. 1996 *Life in moving fluids: the physical biology of flow*, 2nd edn. Princeton, NJ: Princeton University Press.

143. Riisgård H. 2001 On measurement of filtration rate in bivalves—the stony road to reliable data: review and interpretation. *Mar. Ecol. Prog. Ser.* **211**, 275–291. (doi:10.3354/meps211275)

144. Ayling AM. 1976 The strategy of orientation in the barnacle *Balanus trigonus*. *Mar. Biol.* **36**, 335–342.

145. Marchinko KB, Palmer AR. 2003 Feeding in flow extremes: dependence of cirrus form on wave-exposure in four barnacle species. *Zoology* **106**, 127–141. (doi:10.1078/0944-2006-00107)

146. Werth AJ. 2004 Models of hydrodynamic flow in the bowhead whale filter feeding apparatus. *J. Exp. Biol.* **207**, 3569–3580. (doi:10.1242/jeb.01202)

147. Goldbogen JA, Cade DE, Calambokidis J, Friedlaender AS, Potvin J, Segre PS, Werth AJ. 2017 How baleen whales feed: the biomechanics of

engulfment and filtration. *Ann. Rev. Mar. Sci.* **9**, 367–386. (doi:10.1146/annurev-marine-122414-033905)

148. Morris CC, Deibel D. 1993 Flow rate and particle concentration within the house of the pelagic tunicate *Oikopleura vanhoeffeni*. *Mar. Biol.* **115**, 445–452. (doi:10.1007/BF00349843)

149. Ludeman DA, Reidenbach MA, Leys SP. 2017 The energetic cost of filtration by demosponges and their behavioural response to ambient currents. *J. Exp. Biol.* **220**, 995–1007. (doi:10.1242/jeb.146076)

150. Palmer MR, Nepf HM, Pettersson TJR, Ackerman JD. 2004 Observations of particle capture on a cylindrical collector: implications for particle accumulation and removal in aquatic systems. *Limnol. Oceanogr.* **49**, 76–85. (doi:10.4319/lo.2004.49.1.0076)

151. Humphries S. 2009 Filter feeders and plankton increase particle encounter rates through flow regime control. *Proc. Natl Acad. Sci. USA* **106**, 7882–7887. (doi:10.1073/pnas.0809063106)

152. Labarbera M. 1984 Feeding currents and particle capture mechanisms in suspension feeding animals. *Integr. Comp. Biol.* **24**, 71–84. (doi:10.1093/icb/24.1.71)

153. Cheer AYL, Koehl MAR. 1987 Paddles and rakes: fluid flow through bristled appendages of small organisms. *J. Theor. Biol.* **129**, 17–39. (doi:10.1016/S0022-5193(87)80201-1)

154. Braimah SA. 1987 Pattern of flow around filter-feeding structures of immature *Simulium bivittatum* Malloch (Diptera: Simuliidae) and *Isonychia campestris* McDunnough (Ephemeroptera: Oligoneuriidae). *Can. J. Zool.* **65**, 514–521. (doi:10.1139/z87-080)

155. Sutherland KR, Costello JH, Colin SP, Dabiri JO. 2014 Ambient fluid motions influence swimming and feeding by the ctenophore *Mnemiopsis leidyi*. *J. Plankton Res.* **36**, 1310–1322. (doi:10.1093/plankt/fbu051)

156. LaBarbera M. 1981 Water flow patterns in and around three species of articulate brachiopods. *J. Exp. Mar. Biol. Ecol.* **55**, 185–206. (doi:10.1016/0022-0981(81)90111-8)

157. Starkweather PLPL. 1995 Near-coronal fluid flow patterns and food cell manipulation in the rotifer *Brachionus calyciflorus*. *Hydrobiologia* **313–314**, 191–195. (doi:10.1007/BF00025950)

158. Mayer S. 1994 Particle capture in the crown of the ciliary suspension feeding polychaete *Sabella penicillus*: videotape recordings and interpretations. *Mar. Biol.* **119**, 571–582. (doi:10.1007/BF0035432)

159. Riisgård HU, Larsen PS. 2007 Viscosity of seawater controls beat frequency of water-pumping cilia and filtration rate of mussels *Mytilus edulis*. *Mar. Ecol. Prog. Ser.* **343**, 141–150. (doi:10.3354/meps06930)

160. Gibson BM, Furbish DJ, Rahman IA, Schmeeckle MW, Laflamme M, Darroch SAF. 2021 Ancient life and moving fluids. *Biol. Rev.* **96**, 129–152. (doi:10.1111/brv.12649)

161. Brooks H, Haines GE, Lin MC, Sanderson SL. 2018 Physical modeling of vortical cross-step flow in the American paddlefish, *Polyodon spathula*. *PLoS ONE* **13**, e0193874. (doi:10.1371/journal.pone.0193874)

162. Werth AJ, Potvin J. 2016 Baleen hydrodynamics and morphology of cross-flow filtration in balaenid whale suspension feeding. *PLoS ONE* **11**, e0150106. (doi:10.1371/journal.pone.0150106)

163. Eckman JEJE, Okamura B. 1998 A model of particle capture by bryozoans in turbulent flow: significance of colony form. *Am. Nat.* **152**, 861–880. (doi:10.1086/286214)

164. Du Clos KT, Jones IT, Carrier TJ, Brady DC, Jumars PA. 2017 Model-assisted measurements of suspension-feeding flow velocities. *J. Exp. Biol.* **220**, 2096–2107. (doi:10.1242/jeb.147934)

165. Leys SP, Eerkes-Medrano DI. 2006 Feeding in a calcareous sponge: particle uptake by pseudopodia. *Biol. Bull.* **211**, 157–171. (doi:10.2307/4134590)

166. Riisgård H, Manríquez P. 1997 Filter-feeding in fifteen marine ectoprocts (Bryozoa): particle capture and water pumping. *Mar. Ecol. Prog. Ser.* **154**, 223–239. (doi:10.3354/meps154223)

167. Bone Q, Carré C, Chang P. 2003 Tunicate feeding filters. *J. Mar. Biol. Assoc. U.K.* **83**, 907–919. (doi:10.1017/S002531540300804Xh)

168. Lasker H. 1981 Comparison of the particulate feeding abilities of three species of gorgonian softCoral. *Mar. Ecol. Prog. Ser.* **5**, 61–67. (doi:10.3354/meps005061)

169. Finelli CM, Hart DD, Merz RA. 2002 Stream insects as passive suspension feeders: effects of velocity and food concentration on feeding performance. *Oecologia* **131**, 145–153. (doi:10.1007/s00442-001-0852-x)

170. Zweers G, de Jong F, Berkhoudt H. 1995 Filter feeding in flamingos (*Phoenicopterus ruber*). *Condor* **97**, 297–324. (doi:10.2307/1369017)

171. Skieresz-Szewczyk K, Jackowiak H. 2016 Morphofunctional study of the tongue in the domestic duck (*Anas platyrhynchos f. domestica*, Anatidae): LM and SEM study. *Zoomorphology* **135**, 255–268. (doi:10.1007/s00435-016-0302-2)

172. Goldbogen JA, Pyenson ND, Shadwick RE. 2007 Big gulps require high drag for fin whale lunge feeding. *Mar. Ecol. Prog. Ser.* **349**, 289–301. (doi:10.3354/meps07066)

173. Werth AJ. 2001 How do mysticetes remove prey trapped in baleen? *Bull. Museum Comp. Zool.* **156**, 189–204.

174. Sutherland K. 2008 *Filters and filtration handbook*, 5th edn. Oxford, UK: Elsevier.

175. Werth AJ. 2019 Variable porosity of throughput and tangential filtration in biological and 3D printed systems. In *Advances in engineering research* (ed. VM Petrova), pp. 571–582. New York, NY: Nova Science.

176. Gao J *et al.* 2020 Bio-inspired antibacterial cellulose paper-poly(amidoxime) composite hydrogel for highly efficient uranium(vi) capture from seawater.

Chem. Commun. **56**, 3935–3938. (doi:10.1039/c9cc09936k)

177. Liu Y, Ren J, Ling S. 2019 Bioinspired and biomimetic silk spinning. *Compos. Commun.* **13**, 85–96. (doi:10.1016/j.coco.2019.03.004)

178. DeMott WR. 1989 Optimal foraging theory as a predictor of chemically mediated food selection by suspension-feeding copepods. *Limnol. Oceanogr.* **34**, 140–154. (doi:10.4319/lo.1989.34.1.0140)

179. Stephens DW. 1985 Optimal foraging theory. *Annu. Rev. Ecol. Syst.* **15**, 2561–2566. (doi:10.1016/B978-008045405-4.00026-4)

180. Dölger J, Kiørboe T, Andersen A. 2019 Dense dwarfs versus gelatinous giants: the trade-offs and physiological limits determining the body plan of planktonic filter feeders. *Am. Nat.* **194**, E30–E40. (doi:10.1086/703656)

181. Vincent JFV. 2002 Survival of the cheapest. *Mater. Today* **5**, 28–41. (doi:10.1016/s1369-7021(02)01237-3)

182. Anlauf H. 2019 Towards mitigation of particle/liquid separation problems by evolutionary technological progress. *J. Taiwan Inst. Chem. Eng.* **94**, 10–17. (doi:10.1016/j.jtice.2017.09.043)

183. Soucek DJ, Dickinson A, Cropek DM. 2010 Effects of millimeter wave carbon fibers on filter-feeding freshwater invertebrates. *Ecotoxicol. Environ. Saf.* **73**, 500–506. (doi:10.1016/j.ecoenv.2009.10.015)

184. Cid N, Ibáñez C, Palanques A, Prat N. 2010 Patterns of metal bioaccumulation in two filter-feeding macroinvertebrates: exposure distribution, inter-species differences and variability across developmental stages. *Sci. Total Environ.* **408**, 2795–2806. (doi:10.1016/j.scitotenv.2010.03.030)

185. Iyare PU, Ouki SK, Bond T. 2020 Microplastics removal in wastewater treatment plants: a critical review. *Environ. Sci. Process. Impacts* **6**, 2664–2675. (doi:10.1039/d0ew00397b)

186. Woodall LC *et al.* 2014 The deep sea is a major sink for microplastic debris. *R. Soc. Open Sci.* **1**, 140317. (doi:10.1098/rsos.140317)

187. Mead T, Jeanrenaud S. 2016 The elephant in the room: biomimetics and sustainability? *Bioinspired Biomim. Nanobiomaterials* **6**, 113–121. (doi:10.1680/jbibn.16.00012)

188. Cohen YH, Reich Y. 2016 *Biomimetic design method for innovation and sustainability*. Cham, Switzerland: Springer International Publishing.

189. Bach D, Schmich F, Masselter T, Speck T. 2015 A review of selected pumping systems in nature and engineering—potential biomimetic concepts for improving displacement pumps and pulsation damping. *Bioinspir. Biomim.* **10**, 051001. (doi:10.1088/1748-3190/10/5/051001)

190. Jørgensen C, Kørboe T, Møhlenberg F, Riisgård H. 1984 Ciliary and mucus-net filter feeding, with special reference to fluid mechanical characteristics. *Mar. Ecol. Prog. Ser.* **15**, 283–292. (doi:10.3354/meps015283)

191. Vincent JFV, Bogatyreva OA, Bogatyrev NR, Bowyer A, Pahl AK. 2006 Biomimetics: its practice and theory. *J. R. Soc. Interface* **3**, 471–482. (doi:10.1098/rsif.2006.0127)

192. Wessling M. 2019 Smart filters. *Ger. Res.* **41**, 6–11. (doi:10.1002/germ.201970303)

193. Kang DH, Kim NK, Kang HW. 2021 Hybrid structure of a ZnO nanowire array on a PVDF nanofiber membrane/nylon mesh for use in smart filters: photoconductive PM filters. *Appl. Sci.* **11**, 8006. (doi:10.3390/app11178006)

194. Griffith KA, Newberry AT. 2008 Effect of flow regime on the morphology of a colonial cnidarian. *Invertebr. Biol.* **127**, 259–264. (doi:10.1111/j.1744-7410.2008.00127.x)

195. Sponaugle S, LaBarbera M. 1991 Drag-induced deformation: a functional feeding strategy in two species of gorgonians. *J. Exp. Mar. Biol. Ecol.* **148**, 121–134. (doi:10.1016/0022-0981(91)90151-L)

196. Gralow M, Weigand F, Herzog D, Wischeropp T, Emmelmann C. 2020 Biomimetic design and laser additive manufacturing—a perfect symbiosis? *J. Laser Appl.* **32**, 021201. (doi:10.2351/1.5131642)

197. Krick J, Ackerman JD. 2015 Adding ecology to particle capture models: numerical simulations of capture on a moving cylinder in crossflow. *J. Theor. Biol.* **368**, 13–26. (doi:10.1016/j.jtbi.2014.12.003)

198. Hamann L, Blanke A. 2022 Suspension feeders: diversity, principles of particle separation and biomimetic potential. Figshare.

2

3   Supplementary Information: Suspension Feeders - Diversity, Principles of Particle

4   Separation, and Biomimetic Potential

5

6   Leandra Hamann, Alexander Blanke

7

8   Institute of Evolutionary Biology and Animal Ecology, University of Bonn, An der Immenburg

9   1, 53121 Bonn, Germany

10

11   Table SI-1: Selection of literature identified through the four search approaches with the SFs

12   mentioned in them. The original spelling of the reference was adopted. (*) indicates that

13   species were grouped under a higher taxonomic category.

1. Scientific reviews on the biology and ecology of suspension feeders			
Title	**Ref**	**Book/Journal**	**Found suspension feeders**
Biology of suspension feeding	[1]	Book	*Porifera, Coelenterata, Rotatoria, Brachiopoda, Echiuroidea, Polychaeta, Crustacea, Insecta, Gastropoda, Bivalvia, Echinodermata, Tunicata, Acrania, Entoprocta, Polyzoa (Bryozoa), Phoronida, hemichordate Pterobranchia, Pogonophora; vertebrate suspension feeders: ammocoetes larvae of lamprey, basking shark, teleosts, anuran tadpoles
A revised classification of suspension feeders	[2]	Tuatara: Journal of the Biological Society	Impingement Feeders: Lophophorata, some rotifers, some ciliates, Pelecypoda; Ciliary feeders: entoprocts, serpulimorph polychaetes, mollusc veligers, Pelecypods, Conochilus (Rotifera); Filter feeders: sponges, Chaetopterus, Nereis, Urechis, some gastropods, ascidians, cephalochordates, larvaceans, crustaceans, pelecypods; Collision feeders: some vermetid gastropods, radiolarians, planktonic foraminiferans, some echinoderms, plankton feeding coelenterates
Comparative physiology of suspension feeding	[3]	Annual Review Physiology	*Bivalves, zooplankton crustaceans, ascidians
Convergent and alternative designs for vertebrate suspension feeding	[4]	Book	*Fishes, tadpoles, whales, birds, elasmobranchs, ammocoetes
Benthic suspension feeders and flow	[5]	Book	*Corals, hydrozoans, bryozoans, brachiopods, some polychaetes, bivalve molluscs, some echinoderms, some crustaceans
Comparative ecophysiology of active zoobenthic filter feeding, essence of current knowledge	[6]	Journal of Sea Research	*Sponges, cnidarians, bryozoans, copepods, polychaetes, bivalves, ascidians, gastropods, lancelets, brachiopods
Suspension feeders	[7]	Book (Encyclopaedia of Ecology)	*Protists, *Porifera, *Cnidaria, *Ctenophora, *Rotifera, *Entoprocta, *Cycliophora, *Sipuncula, *Echiura, *Annelida, *Mollusca, *Arthropoda, *Bryozoa, *Phoronida, *Brachiopoda, *Echinodermata, *Hemichordata, *Chordata
2. Scientific reviews on suspension-feeding mechanisms			

Title	Ref	Book/ Journal	Found Suspension Feeders
The mechanics of filter feeding: some theoretical considerations	[8]	The American Naturalist	Mussels, oysters, scallops, copepods, echinoderm larvae, gorgonian corals, zoanthids, brittle star, rotifers, sea anemone
Some hydrodynamic aspects of filter feeding with rectangular-mesh nets	[9]	Journal of Theoretical Biology	Lamellibranch bivalves, *Urechis caupo*, Stentor, Vorticella, Artemia, various insect larvae, barnacles
Ciliary and mucus-net filter feeding, with special reference to fluid mechanical characteristics	[10]	Marine Ecology Progress Series	Sabellid polychaetes, brachiopods, bivalves, gastropods, ascidians
Physical mechanisms and rates of particle capture by suspension feeders	[11]	Oceanopr. Mar. Biol. Annu. Rev.	Protozoans, anemones, corals, barnacles, copepods, crinoids, sea pens, insect larvae, daphnia, bivalves, polychaetes, sea cucumbers, phoronids, gorgonians, bryozoans, echinoderms, rotifers
Filter-feeding in marine macro-invertebrates: pump characteristics, modelling and energy cost	[12]	Biololgical Reviews of the Cambridge Philosophical Society	Sponges, polychaetes, bivalves, ascidians
Some aspects of water filtering activity of filter-feeders	[13]	Hydrobiologia	*Eudiaptomus gracilis* (copepod), *Brachionus calyciflorus*, *Dreissena polymorpha*, *Sphaerium corneum*, brachiopods, bivalves, *Crassostrea gigas*, *Ceriodaphnia cf. dubia*
Particle capture mechanisms in suspension-feeding invertebrates	[14]	Marine Ecology Progress Series	Sponges, bivalves, polychaetes, ascidians, bryozoans, crustaceans, cnidarians, ctenophores, cladocerans, suspension feeding insects, phoronids, brachiopods, gastropods, salps, appendicularians, lancelets, larvae of echinoderms, jellyfish, anthozoans

3.	**Scientific literature regarding biomimetics**		
Title	**Ref**	**Book/ Journal**	**Found suspension feeders**
Naturorientierte Lösungsfindung (in German)	[15]	Book	Baleen whales, barnacles, whale sharks, gorgonians, sea lilies, sponges, caddisfly larvae, oyster
Biomimetics - Biologically Inspired Technologies	[16]	Book	Aquatic insect larvae (e.g., flies)
Comparative Biomechanics	[17]	Book	Sponges, anemones, jellyfish, bryozoans, annelids, bivalve molluscs, barnacles, microcrustaceans, aquatic insect larvae, brittle stars, fish, amphibian tadpoles, a few birds, baleen whales

4.	**Online biomimetic databases**		
Transfer Tool	**Link**	**Search term**	**Found suspension feeders**
AskNature	asknature.org	filter; filtration	Paddlefish (*Polyodon spathula*), basking shark (*Cetorhinus maximus*), Venus' flower basket (*Euplectella aspergillum*), peacock worm (*Sabella pavonina*), sea cucumber (Cucumaria), salps (*Pegea confoederata),* blue whale (*Balaenoptera musculus*); Andean flamingo (Phoenicopterus), fiddler crab (*Uca spp.*), ascidians (Ascidiacea), common water flea (Daphnia)

14

15

2

Table SI-2: Short description of the SFMs and higher taxa. Numbers refer to Figure 1.

Taxa	#	SF	Description
Porifera	1	Porifera	Most sponges are SFs, sometimes in combination with other feeding methods. The fluid flow through the body can vary depending on asconoid, syconoid, or leuconoid forms, but the basic principle is the same. The water streams into the body through the pores and incurrent canals, passes the flagellated chambers, and exits through the excurrent canals and osculum. Larger particles are retained within the channels, by choanocytes in the flagellated chambers with their collar, or particles adhere to the choanocyte's surface to be phagocytosed [18,19].
Cnidaria			Within the cnidarians, polyp forms as well as medusan forms are able to suspension feed. Aside from many SF corals (Anthozoa), this has been observed particularly in gorgonians (Alcyonacea), sea pens (Pennatulacea), and some medusan species such as the moon jelly (*Aurelia aurita*).
	2	Alcyonacea	Gorgonians (Alcyonacea) are soft corals that grow planar and oriented perpendicular to flow. The colonial polyps on the branches have tentacles with pinnules. The water current streams through the gorgonian and food particles are retained by the tentacles of the polyps [20]. Another SF group within the Octocorallia are the sea pens (Pennatulacea), in which a primary polyp is branched into secondary polyps with pinnate tentacles [21].
	3	*Aurelia aurita*	During the jet propulsion to move forwards, water is driven towards the bell margin and subumbrellar surfaces. Particles are retained by mucus on these surfaces or by the sieving tentacles and transported by cilia towards the gut [22].
Ctenophora	4	*Mnemiopsis leidyi*	A well described lobate species is *Mnemiopsis leidyi*. Cilia on the lobes create a laminar feeding current to transport non-motile prey to the tentillae [23] and inner lobes, where the prey adheres to mucus on the inner surfaces, whereas motile prey impinges on the surface. Afterwards, prey is transferred to ciliated oral groves and transported to the mouth [24].
Entoprocta	5	Entoprocta	The mouth is surrounded by tentacles. The cilia on the tentacles induce a current and direct particles towards cilia closer at the mouth, which transport the particle into the mouth [25].
Brachiopoda	6	Brachiopoda	Brachiopods filter the water within the mantle cavity with the lophophore, which consists of one or two rows of tentacles covered with cilia. Lateral cilia produce a feeding current to retain particles between the tentacles and cilia. Fine layers of mucus on the ciliary surfaces accumulate and transport the particles [10,26] .
Phoronida	7	Phoronida	Phoronids extrude a lophophore with ciliated tentacles from their tubes in the sediments. The cilia stream water into the lophophore, where particles are retained by the screen formed by tentacles and cilia or by tentacles flicking particles towards the mouth [27].
Bryozoa	8	Bryozoa	Each individuum of the colony (zooid) has a lophophore, which can be retracted into the housing. The lophophore is organised in a ring of ciliated tentacles with the mouth in the centre of its base. The cilia induce a water current towards the mouth and out between the tentacles. The tentacles act as a sieve or actively flick a particle towards the mouth [28].
Rotifera	9	Rotifera	With two bands of cilia at the head (corona), SF rotifers induce a current and sweep particles towards the buccal region. Particles are transported to the mouth by cilia [29,30].
Annelida			Within the annelids, several SFMs evolved, especially within the Polychaeta. Two main mechanism can be distinguished: filtration with the gill crown, e.g., in the tube dwelling sabellid worms (Sabellidae) or filtration with mucus nets in burrows in the sediment, which can be found in spionids (Polychaeta), *Nereis diversicolor* (Polychaeta) or *Urechis caupo* (Echiura) [31–35].
	10	Sabellidae	When feeding, the gill crown surrounding the mouth is expanded outside the tube. The filaments of the gill grown have two rows of side branches, i.e. pinnules. Cilia on the pinnules create a feeding current towards the crown, where particles are retained by the cilia [36].
	11	*Urechis caupo*	The innkeeper worm lives in U-shaped burrows in the sediment. A mucus net is secreted and attached to the wall of the burrow. By peristaltic movement of the worm, water is drawn into the burrow and through the net, where particles are retained. The net is eaten with the particles [35].
Mollusca			Bivalves are a large group of filter feeders with similar SFMs within the molluscs [37]. The best studied representative is the blue mussel *Mytilus edulis*. Within the gastropods, only some species have adapted SF, e.g., *Dendropoma maximum*.
	12	*Mytilus edulis*	Lateral cilia on the gill filaments induce a current into the mantle cavity and through the gill filaments. Particles are retained by cirri between the filaments and transported by cilia towards the mouth. The water exists through the exhalant chamber [37].
	13	*Dendropoma maximum*	*Dendropoma maximum*, a wormlike snail (Gastropoda), lives in tubes and secretes a mucus net to retain particles. The net with the particles is ingested afterwards [38].
Crustacea			SFs can be found in all major groups of crustaceans: Branchiopoda, Maxillopoda, and Malacostraca. The feeding strategies can differ, but all use their head or thorax appendages. One example of each group will be described, daphnids

3

Taxa	#	SF	Description
			(Branchiopoda), barnacles (Cirripedia, Maxillopoda) and *Euphausia superba* (Malacostraca).
	14	Daphnia	The 3rd and 4th thoracal limbs have setae with setulae and form filter combs. With stroking movements, the limbs induce a water current towards the food groove inside the carapace to retain particles with the filter combs and other limbs [39].
	15	*Euphausia superba*	Six long limbs form the filter basket. The setae with setulae on the limbs close it on all sides and form a mesh. While swimming, the legs stream water into the basket through coarse filtering elements and is expelled through fine filtering elements [40].
	16	Cirripedia	Six pairs of long and short cirri with setae on head and thorax are involved in SF. The long cirri are extended into the water current and form a mesh between the setae. Different feeding strategies have been described depending on water flow and particle concentration: active movement and passive. The short cirri form an additional net across the entrance of the mantle cavity and clean the particles from the long cirri [41].
Hexapoda			Because of the great diversity, only the most common and best-described SFMs in the aquatic larvae of Ephemeroptera, Trichoptera, and Diptera are described [42].
	17	Ephemeroptera	The most common SFM in mayflies is with the help of filtering setae and setulae on appendages, e.g., on forelegs or mouthparts. Depending on the species, SF can be supported by constructed burrows, silk-like material, induced flows, or secondary hairs on the filtering setae [42]. Collected particles are removed by bringing the setae close to the mouth for feeding.
	18	Trichoptera	Most species in Trichoptera spin silken nets to retain particles from the flow. The larvae of Hydropsychidae uses the nets to build shelters, which can include organic and mineral particles. Macronema larvae build cases (caddis), which are lined with silk. Particles can adhere to the silk when flowing through the caddis. Depending on the species, forelegs or mouthparts are used to remove the particles for ingestion [42].
	19	Diptera	In Diptera, there are five families that include SF species: Simuliidae, Culicidae, Dixidae, Chaoboridae, and Chironomidae. Black flies have modified mouthparts, i.e., cephalic fans, which are deployed passively in the water current to retain particles. Cleaning is done by mouthparts when the fans are retracted towards the oral cavity. Most Culicidae, Dixidae, and Chaoboridae use also fan-like brushes or hairs on modified mouthparts to retain particles [42]. Chironomids build small burrows, where a silk-net is spun across the opening. The larvae move within the burrow through the net. Particles together with the net are ingested and a new net is spun [42].
Echinodermata			SF can be observed in crinoids feeding with their tentacle crown and some sea cucumber, especially Dendrochirotida. In other groups, few species from Ophiuroidea or Clypeasteroida within the Echinoidea have also been described as SFs [43,44].
	20	Crinoidea	Crinoids spreads their arms into the water current. The arms branch out in pinnules, covered with tube feet catching particles. By flicking of the tube feet, the particles are transported into the pinnule's food groove and towards the mouth [45].
	21	Dendrochirotida	The sea cucumbers of Dendrochirotida have ten to thirty branched tentacles around the mouth, which are hold upwards to retain particles. Papillae on the tentacles are likely to secrete adhesive substances to increase particle retention. One by one tentacle is inserted into the mouth and particles are scraped off [46].
Hemichordata	22	Enteropneusta	The two main groups of hemichordates are both able to SF: Pterobranchia and Enteropneusta [47]. Because enteropneusts are better studied thus far, their SFM will be described exemplarily for both groups. In addition to deposit feeding, enteropneusts are able to SF. Buried in burrows, water is drawn into the branchial pharynx, where particles are trapped in the branchial pores. Particles are accumulated in mucus and transported by cilia towards the oesophagus [47].
Cephalo-chordata	23	Amphioxi-formes	When feeding, cephalochordates lie buried in the sand and the mouth facing upwards, exposed to the water. The mouth is surrounded by movable and sticky cirri to retain larger particles. A mucus net is produced by the endostyle and covers the pharyngeal basket where particles are retained. The mucus with the particles is transported towards the gut [48].
Tunicata			All tunicates are SFs. Ascidians (Ascidiacea) are sessile, while salps (Thaliacea) and larvaceans (Larvacea) are pelagic. They all use mucus nets to retain particles [49]. While the SFMs of ascidians and salps are very similar and a mucus net is built within the branchial basket [50], larvaceans built external filter housings [51].
	24	Ascidiacea	Ascidians pass a feeding current through the inhalant siphon, into the branchial basket, and out of the exhalant siphon. The branchial basket is lined with a mucus net, produced by the endostyle in which particles are retained. Cilia produce the feeding current and transport the mucus net from towards the oesophagus [52,53].
	25	Larvacea	Larvaceans built an external filter housing from secreted mucus. By movement of the tail, water is pumped through the filter. A coarse filter retains larger particles at the water inlet, while smaller particles are concentrated inside and propelled towards the mouth [54].
Petromy-zontida	26	Petromy-zontiformes	In contrast to the predatory adults, the lamprey larvae (ammocoetes) live as SFs, buried in the sediments. With rhythmic muscular contractions, the larvae pump water into their mouth. Cirri on the mouth opening prevent larger particles to enter,

4

Taxa	#	SF	Description
			smaller particles get stuck in bands of mucus behind the gill lamellae within the pharynx [55,56].
Chondrich-thyes			Within the Chondrichthyes, four elasmobranchs are SFs. In all four, the filtering structures are formed by branchial arches and gill rakers [57]. The SFMs of mobulid rays (Mobulidae) and whale sharks (*Rhincodon typus*) are similar and well understood. Little is known about basking sharks (*Cetorhinus maximus*) and megamouth sharks (*Megachasma pelagios*) and their SFMs have not been fully understood yet [58,59].
	27	Mobulidae	When feeding, mobulid rays swim with their mouth open to stream water into the buccal cavity, between the gill rakers, and out through the gill slits. The gill rakers are modified into parallel arrays of filter lobes. The lobes are oriented in shape of wings or spoilers towards the water flow in such a way, that the particles bounce off and are directed towards the oesophagus. This filtration method is called ricochet separation [60].
	28	*Rhincodon typus*	Either through forward swimming or by suction while being stationary, whale sharks stream water into the buccal cavity, through the filtering pads and out of the gill slits. Each filtering pad is composed of lobes with connective tissue forming a mesh with irregular holes to retain particles. The SFM is described as cross-flow filtration [61].
Actinopterygii			More than 70 species within the Actinopterygii are known to be SFs [62]. The pelagic living fish can be distinguished based on their filtration mechanisms in pump or suction feeding (e.g., *Hypophthalmychthys molitrix*) and ram feeding (e.g., *Clupea harengus*) [4,62].
	29	*Hypophthalmyc hthys molitrix*	While swimming, silver carps pump water into their mouth. Particles are retained by the mesh of filtering plates (fused gill rakers) and transported towards the oesophagus by shear forces along the epibranchial organ [63].
	30	*Clupea harengus*	Similar to other ram feeding fish, like anchovy, mackerels or sardines, herrings live and feed in shoals. While swimming, herrings open their mouth and extend their gill arch system with elongated gill rakers forming a mesh. The water stream into the mouth, between the gill rakers, over the gill filaments, and exits through the gill slits under the operculum. Particles are retained by the mesh of the gill rakers [4].
Amphibia	31	Anura	Tadpoles, the anuran larvae, are able to SF either facultative or obligate. A buccal pump sucks water into the branchial basket. Depending on the particle size, they are directed either towards the oesophagus or into the pharynx, where they are retained in the branchial food traps covered with mucus [4].
Aves			Well known SF birds are flamingos (Phoenicopteriformes) and SF ducks (Anatidae). Less studied are prions or shearwaters. All SF birds feed with their beak [64].
	32	Phoenicopteri-formes	Flamingos stand in shallow water with their head down, moving it side to side while feeding, the tongue acting as a piston to draw water inside. The margins of the bill are lined with lamellae, forming a sieve between the upper and lower bill, where particles are retained. The spiny tongue moves the particles towards the oesophagus [65].
	33	Anatidae	While feeding, the tongue acts like a piston to suck water into the bill. Inside the elongated bill, the margins of upper and lower bill are lined with lamellae. When closed, the lamellae oppose each other and act as a sieve to retain particles. The spiny tongue moves particles towards the oesophagus [66].
Cetacea			Within the whales, only the baleen whales (Mysticeti) are SFs. Similar to SF fish, baleen whales can be distinguished in ram feeding in balaenid whales (e.g., *Balaena mysticetus*) and suction feeding or lunge feeding in rorqual whales (e.g., *Balaenoptera physalus*). The separation medium is comprised by the baleen plates hanging from the upper jaw [4,67,68].
	34	*Balaena mysticetus*	Bowhead whales swim with their mouth opened to continuously force water along the paired racks of baleen, passing it through the baleen plates where particles are retained. Water exits the buccal cavity at the posterior end of the lips [69].
	35	*Balaenoptera physalus*	Fin whales swim towards their prey, e.g., fish shoals, open their mouth to expand the buccal cavity, and engulf the fish in a single pulse. Afterwards, the mouth is closed, and the water is expelled out of the mouth, through the baleen fringes, where particles are retained inside [70].

17

18

5

19   Table SI-3: Overview of selected biological and technical parameters as described in the text

20   and used in Table SI-4 and Table SI-5. The bold parameters are used in Table 1.

Parameter			Description
Biological parameters	Ecology	Habitat	Marine, freshwater, terrestrial;
		Aquatic life	Pelagic, benthic
		Foraging type	Active or passive
		Motility	Motile or sessile
		Organism size	Size of organism
	Food type	**Particle size**	Sizes of seston, i.e., phytoplankton, zooplankton, bacterioplankton, detritus
Technical parameters		Separation mechanism	General description of SFM
	Separation medium	**Geometry**	Flat or funnel-shaped, enclosed or open
		Filter area/ effective area	Total area of a suspension feeder which is actually exposed to the suspension to retain particles
		Material of separation medium	Biological material the separation medium is made of
		Mesh design	Organisation of mesh forming structures; (i.e. flat surface, level of organisation, spongy, branching etc.)
		Mesh size/pore size	Size of apertures in the separation medium
	Fluid dynamics	**Flow past separation medium**	Non-FF versus FF (including dead-end and cross-flow filtration)
		Driving force	The force which is needed to cause a fluid to pass by or through a particle separating medium
		Water velocity	Fluid velocity in cm/s
		Flow regime	Fluid flow around the particle separating medium: creeping (Re < 1), laminar (Re 1-50), or turbulent (Re >50)
	Cleaning	**Working mode**	continuous or discontinuous
		Cleaning technique	Removal of particles from the particle separation medium

21

22

6

23 Table SI-4: References for ecological parameters including habitat, foraging type, motility, organism size, food size, and food to body ratio of each

24 SFMs referred to in Figure 1.

	Taxa	Habitat	Aquatic life	Ref	Foraging type	Ref	Motility	Ref	Organism size (adult)	Ref	Food size (min-max)	Ref	Food to body size (1: X)	Uptake of microplastics
1	Porifera	freshwater /marine	benthic	[71]	active	[71]	sessile	[71]	Varies strongly, up to 1 m	[71]	0.1 µm up to 8 µm within flagellated chambers	[1,14]	na	[72]
2	Alcyonacea (Octocorallia)	marine	benthic	[71]	passive	[71]	sessile	[71]	up to 1.8 m high (colonies), polyps 1-5 mm height	[71,73]	3 µm - 700 µm	[74]	na	[75]
3	*Aurelia aurita* (Scyphozoa)	marine	pelagic	[71]	active (SF coupled to forward motion)	[22]	motile	[71]	up to 40 cm in diameter	[71]	50 µm, up to 5 mm	[1,76]	32	[77,78]
4	*Mnemiopsis leidyi*	marine	pelagic	[71]	active	[71]	motile	[71]	10 cm	[71]	50 µm - 3 mm	[79]	100	na
5	Entoprocta	marine (2 freshwater species)	benthic	[71]	active (movement of cilia)	[71]	sessile	[71]	0,1 mm - 7 mm (single zooids)	[71]	2 - 12 µm (90 µm when predatory)	[80]	na	na
6	Brachiopoda	marine	benthic	[71]	active (lophophore with cilia)	[71]	sessile	[71]	1 mm - 80 mm	[71]	2 - 200 µm	[81]	400	na
7	Phoronida	marine	benthic	[71]	active (lophophore with cilia)	[71]	sessile	[71]	6 mm - 200 mm	[71]	> 5 µm	[71]	1030	na
8	Bryozoa	freshwater / marine	benthic	[71]	active (lophophore with cilia)	[71]	sessile	[71]	2 - 25 cm (colony), 0.5 mm zooids	[71]	5 - 50 µm	[82,83]	na	na
9	Rotifera	mainly freshwater / few marine	pelagic, benthic	[7]	active (movement of wheel organ)	[71]	mainly motile	[71]	40 µm to 3 mm	[71]	1.3 µm, up to 20 µm	[1,29]	82	[84]
10	Sabellidae	marine	benthic	[71]	active (pinnules)	[71]	sessile	[71]	6 mm up to 30 cm high	[71]	1 µm - >8 µm	[10]	20000	[85]

7

	Taxa	Habitat	Aquatic life	Ref	Foraging type	Ref	Motility	Ref	Organism size (adult)	Ref	Food size (min-max)	Ref	Food to body size (1: X)	Uptake of microplastics
11	*Urechis caupo*	marine	benthic	[71]	active (pump mechanism)	[71]	stationary	[71]	15-18 cm	[71]	> 4 nm	[35]	na	na
12	*Mytilus edulis*	marine	benthic	[71]	active (movement of cilia)	[71]	sessile	[71]	around 9 cm	[71]	1 µm - 35 µm	[86]	450	[87,88]
13	*Dendropoma maximum*	marine	benthic	[89]	passive	[89]	sessile	[89]	around 8 cm	[89]	na	na	na	na
14	Daphnia	mainly freshwater / few marine	benthic, pelagic	[71]	active (movement of legs)	[71]	motile	[71]	0,26 - 6 mm	[71]	0.5 µm - 5 µm (at least)	[39,90]	600	[91]
15	*Euphausia superba*	marine	pelagic	[71]	active (pumping with filter basket)	[40]	motile	[71]	6 cm	[71]	2.5 µm - 35 µm	[1,40]	3000	[92]
16	Cirripedia	marine	benthic	[71]	active and passive	[71]	sessile	[71]	stalked up to 30 cm, non-stalked 10-60 mm	[71]	1 µm - 300 µm	[93]	na	[94]
17	Ephemeroptera	freshwater / some brackish water	benthic	[71]	passive (and active)	[95]	motile	[95]	up to 20 mm	[71]	<1 - 64 µm	[96,97]	667	[98]
18	Trichoptera	freshwater / some brackish water	benthic	[99]	passive	[99]	Motile (stationary)	[99]	3-40 mm	[99]	1 - 70 µm	[100]	na	[98]
19	Diptera	freshwater	pelagic, benthic	[101,102]	passive/ active	[102]	motile/sessile	[101,102]	1-3 mm	[101]	> 0.09	[103]	na	na
20	Crinoidea	marine	benthic	[71]	passive (active, movement of tube feet)	[71]	sessile, motile	[71]	10 cm - 60 cm	[71]	11 µm up to 1000 µm, up to 300 µm	[71,104]	1000	[105]
21	Dendrochirotida	marine	benthic	[71]	passive	[46]	mainly sessile	[71]	ca 10-30 cm	[71]	0.1 - 6.1 mm	[46]	67	[106]

8

	Taxa	Habitat	Aquatic life	Ref	Foraging type	Ref	Motility	Ref	Organism size (adult)	Ref	Food size (min-max)	Ref	Food to body size (1: X)	Uptake of microplastics
22	Enteropneusta	marine	benthic	[47]	active	[47]	stationary	[47]	9-45 cm, single species up to 2 m	[47]	0.2 - 28.4 µm	[47]	10000	na
23	Amphioxiformes	marine	benthic	[71]	active (wheel organ)	[71]	stationary	[71]	up to 60 mm	[71]	0.2 µm - 300 µm, 0.062 - 100 µm	[48,107]	300	na
24	Ascidiacea	marine	benthic	[71]	active (cilia, muscular pump) and passive	[71][108]	sessile	[71]	0,5 cm - 30 cm	[71]	>0.3 µm, <50 µm	[53]	6000	na
25	Larvacea	marine	pelagic	[71]	active (movement of tail)	[71]	motile	[71]	animal up to 5 mm and filter housing up to 5 cm, 1-10 cm	[54,71]	10 - 600 µm, 0.2-30 µm	[54,109]	17	[77]
26	Petromyzontiformes	freshwater /marine	benthic	[56]	active (pump mechanism)	[56]	stationary	[56]	4-20 cm	[4,110]	5 - 340 µm most common	[56]	588	na
27	Mobulidae	marine	pelagic	[111]	active (forward swimming)	[111]	motile	[111]	1,3 - 9 m breadth	[4]	51 - 500 (>500 µm)	[60]	4000	na
28	Rhincodon typus	marine	pelagic	[61]	active (pumping and forward motion)	[61]	motile	[61]	up to 18 m	[112]	0,34 - 10,74 mm	[61]	1000	[113,114]
29	Hypophthalmychthys molitrix	freshwater	pelagic	[115]	active (forward swimming)	[115]	motile	[115]	60-100 cm	[115]	4 - 85 µm	[115]	16000	na
30	Clupea harengus	marine	pelagic	[112]	active (forward swimming)	[4]	motile	[4]	5-34 cm	[4]	< 2.1 mm	[116]	200	[117]
31	Anura	freshwater	pelagic	[112]	active	[4]	motile	[4]	1-10 cm	[4]	< 10 µm, 0,2 µm -200 µm	[12,96][118]	100	[119]
32	Phoenicopteriformes	terrestrial	terrestrial	[64]	active	[64]	motile	[64]	80 - 145 cm	[4]	Greater flamingos 1 - 10 mm (P. minor 0,02 - 0,1 mm)	[4]	2000	na

	Taxa	Habitat	Aquatic life	Ref	Foraging type	Ref	Motility	Ref	Organism size (adult)	Ref	Food size (min-max)	Ref	Food to body size (1: X)	Uptake of microplastics
33	Anatidae	terrestrial	terrestrial	[64]	active	[64]	motile	[64]	35 - 80 cm	[4]	0,2 µm - 4,4 mm,	[4]	400	[120]
34	Balaena mysticetus	marine	pelagic	[4]	active (forward swimming)	[4]	motile	[4]	14 - 18 m	[4]	0,3 - 3 mm	[4]	15000	[121]
35	Balaenoptera physalus	marine	pelagic	[4]	active (forward swimming)	[4]	motile	[4]	18 - 24 m	[4]	3- 15 cm	[4]	2000	[121]

25

10

Table SI-5: Literature guide for the data presented in Figure 1 and Table 1. (x) indicates that no information was available, (-) indicates that this

parameter is not applicable to the SFMs.

	#	SF	Separation mechanism	Particle size	Material	Mesh/ pore size	Mesh design	Geometry	Filter area	Driving force	Water velocity	Flow regime	Working mode	Cleaning technique
Porifera	1	Porifera	[18]	[14]	[18]	[14] [122]	[18]	[18] [19]	[18]	[122] [19]	[123] [122]	[19]	[18]	[18]
Cnidaria	2	Alcyonacea	[20][21]	[74]	[20]	[21]	[124] [21]	[125] [21]	[73,124]	[124] [21]	[124] [21]	[124] [21]	[20]	[20]
	3	*Aurelia aurita*	[22]	[76]	[22]	-	-	[22]	x	[22]	[22]	[22]	[22]	[22]
Ctenophora	4	*Mnemiopsis leidyi*	[23] [126]	[79]	[79]	-	-	-	x	[126]	[79]	[126]	[24]	[24]
Entoprocta	5	Entoprocta	[25][127]	[80]	[25,80]	-	-	[25]	x	[25]	x	x	x	[25]
Brachiopoda	6	Brachiopoda	[10] [26]	[81]	[128] [26]	[26]	[26]	[26]	[129]	[129]	[129]	[129]	[128]	[128]
Phoronida	7	Phoronida	[27]	[27]	[130]	[27]	[27]	[130] [131]	[27]	[27]	[27]	x	[27]	[27]
Bryozoa	8	Bryozoa	[82] [132] [133]	[83]	[134]	[82]	[82]	[82] [133]	[135] [133]	[82] [133]	[82] [133]	[83] [135]	[82]	[82]
Rotifera	9	Rotifera	[29]	[29]	[29]	-	-	-	-	[29]	[136]	[136]	[29]	[29]
Annelida	10	Sabellidae	[36]	[10]	[137]	-	-	[36]	x	[138]	[138]	[138]	[137]	[138][137]
	11	*Urechis caupo*	[35] [139]	[139]	[35] [139]	[139]	[139]	[139]	x	[35]	[140]	x	[139]	[35]
Mollusca	12	*Mytilus edulis*	[37] [141][142]	[86]	[37]	[141] [142]	[37]	[143]	[144]	[37]	[145]	[145] [141]	[37]	[37] [141]
	13	*Dendropoma maximum*	[89]	x	[146]	x	x	x	[89]	[89]	x	x	[146] [89]	[146] [89]
Arthropoda (Crustacea)	14	Daphnia	[39]	[90]	[147]	[148] [39]	[147]	[147]	[148][147]	[39]	[148]	[39]	[41]	[39]
	15	*Euphausia superba*	[40]	[40]	[40]	[40]	[40]	[40]	[40]	[40]	[40]	[40]	x	x
	16	Cirripedia	[41]	[93]	[41]	x	[41]	[41]	[149]	[41]	[41]	[149]	[41]	[41]
Arthropoda (Hexapoda)	17	Ephemeroptera	[42][99]	[96][97]	[96]	[96] [97]	[95] [96]	[95]	x	[96]	[96]	[150]	[95]	[95]
	18	Trichoptera	[42][151]	[100]	[152]	[151]	[151]	[151]	[151]	[153]	[153]	x	[151]	[42]
	19	Diptera	[42] [101][103]	[103]	[101]	[42]	[101]	[101]	[154]	[154]	[154] [103]	[101][155] [150]	[156]	[156] [101]
Echinodermata	20	Crinoidea	[104] [45]	[104]	[45]	[45]	[45]	[45]	x	[45]	[104] [157]	[45]	[157]	[157] [45]
	21	Dendrochirotida	[46]	[46]	[46]	x	[46]	[46]	x	x	x	x	[46]	[46]
Hemichordata	22	Enteropneusta	[47]	[47]	[47]	[47]	[47]	[47]	x	[158]	[47]	[158] [47]	[47]	[47]
Cephalochordata	23	Amphioxiformes	[48]	[48] [107]	[48]	[159]	[48]	[48]	[159]	[159]	[159]	x	[48]	[48] [159]

	#	SF	Separation mechanism	Particle size	Material	Mesh/pore size	Mesh design	Geometry	Filter area	Driving force	Water velocity	Flow regime	Working mode	Cleaning technique
Tunicata	24	Ascidiacea	[52] [49]	[53]	[160][161]	[52] [161]	[52] [160] [161]	[52] [49]	[52]	[52]	[49]	[52][162]	[52] [49]	[52] [49]
	25	Larvacea	[54] [51]	[54]	[54]	[54] [51]	[54]	[54]	x	[54] [51]	[54] [51] [163]	[163]	[54]	[54] [51]
Petromyzontida	26	Petromyzontiformes	[4] [55]	[55]	[55]	x	x	x	x	[4] [56]	x	x	[55]	[55]
Chondrichthyes	27	Mobulidae	[60]	[60]	[57]	[111]	[57] [111]	[111]	[111]	[111] [60]	[60] [111]	[60] [111]	[60]	[60] [111]
	28	*Rhincodon typus*	[61]	[61]	[61]	[61]	[61] [57]	[61]	[61]	[61]	[61]	[61]	[61]	[61]
Actinopterygii	29	*Hypophthalmychthys molitrix*	[63]	[63] [164]	[63]	[63]	[63]	[63]	[63]	[4]	[63]	[63]	[63]	[63] [165]
	30	*Clupea harengus*	[166] [4]	[116]	[117] [166]	[117] [166]	[117] [166]	[117] [166]	[117] [166]	[4]	[167] [168]	[167]	[169]	[169]
Amphibia	31	Anura	[4]	[4]	[4]	[170]	[170]	[4]	[4]	[4]	x	x	[4]	[170]
Aves	32	*Phoenicopteriformes*	[65]	[4]	[171]	[171]	[171] [65]	[171] [65]	x	[4]	x	x	[65]	[65]
	33	Anatidae	[66]	[4]	[66]	[66]	[66]	[66]	[66]	[4]	x	[66]	[172]	[172]
Cetacea	34	*Balaena mysticetus*	[69] [68]	[4]	[173]	[174] [175]	[173]	[173]	[67]	[4] [176]	[176] [69] [67] [174]	[176] [67]	[176] [69]	[174]
	35	*Balaenoptera physalus*	[70] [68]	[4]	[177]	[70]	[68]	[68]	[70] [67]	[4]	[70] [67]	[70] [67]	[70]	[178]

28

12

Table SI-6: Previous publications with definitions and classifications based on included SFs.

Ref	Definition of SF	Classification of SF	Included SFs
[179]	Suspension feeders – animals which feed by selecting from the surrounding water the suspended micro-organisms and detritus.	None	Bottom fauna
[180] p. 25	No definition of suspension feeders. SF organisms are assigned to "true particle feeders" (German "reine Partikelfresser", translation by Yonge 1928).	1) Filterers 2) Mucus entanglers 3) Those with tasting appendages a) Mobile b) Sessile	Metazoans
[181] p. 25	No definition of suspension feeders. SF organisms are assigned to "mechanisms for dealing with small particles".	1) Pseudopodial 2) Ciliary 3) Tentacular 4) Mucoid 5) Muscular 6) Setous	Protozoans + invertebrates
[1]	"Mechanisms for extracting on a mass scale small particles suspended in the surrounding water has been developed by numerous aquatic organisms: the suspension feeders." (p. viii) Suspension feeders are typically non-selective feeders, which clear the surrounding water of particles at rates that are independent of the concentration of the particles below certain levels and of their value as food, and which feed continuously when undisturbed. (p. 134) Filter feeders are defined by "feeding by passing the surrounding water though structures that retain particles mainly according to size and shape". (p. xxi)	Filter feeders as a subgroup of SF	Invertebrates
[2] p. 1	"These suspension feeders have evolved a variety of devices with which to separate particles from the sea."	1) Impingement feeding 2) Ciliary feeding 3) Filter feeding 4) Collision feeding	Protozoans + invertebrates
[182] p. 89	"The terms 'suspension feeding' or 'filter feeding' have been coined to designate feeding in aquatic animals that have evolved special structures to process the surrounding water and to retain small suspended particles, including food particles such as phytoplankton cells."	None	Ciliates, flagellates, invertebrates
[4] p. 37	"Suspension-feeding aquatic animals capture planktonic prey as water flows past the feeding apparatus."	1) Continuous ram feeders 2) Intermittent ram feeders 3) Continuous suction feeders 4) Intermittent suction feeders	Vertebrates
[5]	Suspension feeders feed by capturing seston. Suspension feeding includes feeding, assimilation, growth, and elimination. Filtration refers to only the first two.	1) Active SF 2) Passive SF 3) Facultative active SF 4) Combined passive-active SF 5) Deposit SF	Marine, benthic macrofauna
[7]	"Suspension feeding is the capture and ingestion of food particles that are suspended in water" Filter feeders are active SF that "pump water through a structure that function as a filter, removing particles from suspension".	1) Active 2) Passive	Marine protozoans, invertebrates and vertebrates
[14]	Suspension feeders have specialized in grazing on phytoplankton or predation on, e.g., small zooplankton organisms by evolving different mechanisms for particle retention to solve the same basic problem of extracting a sufficient amount of food from a dilute environment.	1) Collar sieving 2) Cirri trapping 3) Ciliary sieving 4) Ciliary downstream collecting 5) Mucus-net filter-feeding 6) Setal filter-feeding 7) Non-filtering ciliary-feeding	Invertebrates, except insect larvae

		8) Ciliary spike suspension-feeding 9) Tube-feet suspension-feeding 10) Cnidae prey-capture mechanisms 11) Colloblast prey-capture	

30

31

14

Table SI-7: Particles sizes found in seston including plankton and detritus compared to size

ranges of particles found in waste water and microplastics.

Size range of plankton	Seston (marine) [5,183,184]			Size range	Waste water particles [185,186]	Microplastics [187]
	Plankton		**Detritus** [188]			
			Truly dissolved material	< 1 nm	Dissolved ions, Na+, Cl-	Nanoplastics
			Colloidal organic matter (dissolved organic matter, DOM)	1 - 10 nm	Fine colloids	
20 – 200 nm	Femto-plankton	Marine viruses		10 - 100 nm	Colloids	
200 nm – 2 µm	Pico-plankton	Small protists, bacteria, Chrysophyta		100 nm - 1 µm	Small virus, large colloids	
2 µm – 20 µm	Nano-plankton	Nanoflagellates, small diatoms	Suspended particulate organic material (POM)	1 mm - 10 µm	Small bacteria, large virus, fine pigments	Microplastics
20 µm – 200 µm	Micro-plankton	Small copepods, foraminifera, ciliates, most phytoplankton		10 - 100 µm	Large bacteria, protozoans, clay particles	
200 µm – 20 mm	Meso-plankton	Amphipods, appendicularians, copepods, cladocerans		100 µm - 1 mm	Fine sand, hard dirt, starch, amoeba	
20 – 200 mm	Macro-plankton	Comb jellies, larval fish, solitary salps, euphausiids, cephalopods	Marine snow	1 - 10 mm	Coarse sand, tomato pops, worm eggs	Mesoplastics
> 200 mm	Mega-plankton	Jelly fish, colonial salps, cephalopods, amphipods		> 10 mm	Matches, toilet paper, worms	Macroplastics

34

35

REFERENCES

1.   Jørgensen CB. 1966 *Biology of Suspension Feeding*. Oxford: Pergamon Press.

2.   Bullivant JS. 1968 A Revised Classification of Suspension Feeders. *Tuatara* **16**.

3.   Jorgensen CB. 1975 Comparative Physiology of Suspension Feeding. *Annu. Rev. Physiol.* **37**, 57–79. (doi:10.1146/annurev.ph.37.030175.000421)

4.   Sanderson SLL, Wassersug RJ. 1993 Convergent and Alternative Designs for Vertebrate Suspension Feeding. In *The skull* (eds J Hanken, BK Hall), pp. 37–112. Chicago and London: University of Chicago Press.

5.   Wildish D, Kristmanson DD. 1997 *Benthic suspension feeders and flow*. Cambridge University Press.

6.   Riisgård HU, Larsen PS. 2000 Comparative ecophysiology of active zoobenthic filter feeding, essence of current knowledge. *J. Sea Res.* **44**, 169–193. (doi:10.1016/S1385-1101(00)00054-X)

7.   Hentschel BT, Shimeta J. 2008 Suspension Feeders. In *Encyclopedia of Ecology*, pp. 3437–3442. Amsterdam: Elsevier Science Ltd. (doi:10.1016/B978-008045405-4.00548-6)

8.   Rubenstein DI, Koehl MAR. 1977 The Mechanisms of Filter Feeding: Some Theoretical Considerations. *Am. Nat.* **111**, 981–994. (doi:10.1086/283227)

9.   Silvester NR. 1983 Some hydrodynamic aspects of filter feeding with rectangular-mesh nets. *J. Theor. Biol.* **103**, 265–286. (doi:10.1016/0022-5193(83)90028-0)

10. Jørgensen C, Kørboe T, Møhlenberg F, Riisgård H. 1984 Ciliary and mucus-net filter feeding, with special reference to fluid mechanical Characteristics. *Mar. Ecol. Prog. Ser.* **15**, 283–292. (doi:10.3354/meps015283)

11. Shimeta J, Jumars PA. 1991 Physical mechanisms and rates of particle capture by suspension- feeders. *Oceanogr. Mar. Biol. an Annu. Rev.* **29**, 191–257.

12. Riisgård HU, Larsen PS. 1995 Filter-Feeding in Marine Macro-Invertebrates: Pump Characteristics, Modellung and Energy Cost. *Biol. Rev.* **70**, 67–106. (doi:10.1111/j.1469-185X.1995.tb01440.x)

16

64   13.   Ostroumov SA. 2005 Some aspects of water filtering activity of filter-feeders. , 275–

65   286. (doi:10.1007/s10750-004-1875-1)

66   14.   Riisgård H, Larsen P. 2010 Particle capture mechanisms in suspension-feeding

67   invertebrates. *Mar. Ecol. Prog. Ser.* **418**, 255–293. (doi:10.3354/meps08755)

68   15.   Hill B. 1999 Naturorientierte Innovationsstrategie — Entwickeln und Konstruieren nach

69   biologischen Vorbildern. In *Bionik*, pp. 313–322. Berlin/Heidelberg: Springer-Verlag.

70   (doi:10.1007/3-540-26948-7_18)

71   16.   Bar-Cohen Y. 2006 *Biomimetics - Biologically Inspired Technologies*.

72   17.   Vogel S. 2013 *Comparative Biomechanics - Life's Physical Worls*. Oxfordshire:

73   Princeton University Press.

74   18.   Leys SP, Eerkes-Medrano DI. 2006 Feeding in a calcareous sponge: Particle uptake

75   by pseudopodia. *Biol. Bull.* **211**, 157–171. (doi:10.2307/4134590)

76   19.   Asadzadeh SS, Larsen PS, Riisgård HU, Walther JH. 2019 Hydrodynamics of the

77   leucon sponge pump. *J. R. Soc. Interface* **16**, 20180630. (doi:10.1098/rsif.2018.0630)

78   20.   Lasker H. 1981 Comparison of the Particulate Feeding Abilities of Three Species of

79   Gorgonian Soft Coral. *Mar. Ecol. Prog. Ser.* **5**, 61–67. (doi:10.3354/meps005061)

80   21.   Best BA. 1988 Passive Suspension Feeding in a Sea Pen: Effects of Ambient Flow on

81   Volume Flow Rate and Filtering Efficiency. *Biol. Bull.* **175**, 332–342.

82   (doi:10.2307/1541723)

83   22.   Costello JH, Colin SP. 1994 Morphology, fluid motion and predation by the

84   scyphomedusa Aurelia aurita. *Mar. Biol.* **121**, 327–334. (doi:10.1007/BF00346741)

85   23.   Costello JH, Coverdale R. 1998 Planktonic Feeding and Evolutionary Significance of

86   the Lobate Body Plan Within the Ctenophora. *Biol. Bull.* **195**, 247–248.

87   (doi:10.2307/1542863)

88   24.   Waggett R. 1999 Capture mechanisms used by the lobate ctenophore, Mnemiopsis

89   leidyi, preying on the copepod Acartia tonsa. *J. Plankton Res.* **21**, 2037–2052.

90   (doi:10.1093/plankt/21.11.2037)

91   25.   Nielsen C. 2002 The phylogenetic position of Entoprocta, Ectoprocta, Phoronida, and

     17

92   Brachiopoda. *Integr. Comp. Biol.* **42**, 685–691. (doi:10.1093/icb/42.3.685)

93 26. Kuzmina T V., Malakhov V V. 2007 Structure of the brachiopod lophophore. *Paleontol.*

94   *J.* **41**, 520–536. (doi:10.1134/S0031030107050073)

95 27. Riisgård HUU. 2002 Methods of ciliary filter feeding in adult Phoronis muelleri (phylum

96   Phoronida) and in its free-swimming actinotroch larva. *Mar. Biol.* **141**, 75–87.

97   (doi:10.1007/s00227-002-0802-0)

98 28. Riisgård H, Goldson A. 1997 Minimal scaling of the lophophore filter-pump in

99   ectoprocts (Bryozoa) excludes physiological regulation of filtration rate to nutritional

100   needs. Test of hypothesis. *Mar. Ecol. Prog. Ser.* **156**, 109–120.

101   (doi:10.3354/meps156109)

102 29. Strathmann RR, Jahn TL, Fonseca JRC. 1972 Suspension feeding by marine

103   invertebrate larvae: clearance rate of particles by ciliated bands of a rotifer, pluteus,

104   and trochophore. *Biol. Bull.* **142**, 505–519. (doi:10.2307/1540326)

105 30. Wallace RL, Snell TW. 2010 Rotifera. *Ecol. Classif. North Am. Freshw. Invertebr.* ,

106   173–235. (doi:10.1016/B978-0-12-374855-3.00008-X)

107 31. Riisgård HU. 1989 Properties and energy cost of the muscular piston pump in the

108   suspension feeding polychaete Chaetopterus variopedatus. *Mar. Ecol. Prog. Ser.* **70**,

109   9.

110 32. Riisgård H. 1991 Suspension feeding in the polychaete Nereis diversicolor. *Mar. Ecol.*

111   *Prog. Ser.* **70**, 29–37. (doi:10.3354/meps070029)

112 33. Riisgård HU. 1994 Filter-feeding in the polychaete Nereis diversicolor: a review.

113   *Netherlands J. Aquat. Ecol.* **28**, 453–458. (doi:10.1007/BF02334216)

114 34. Bock MJ, Miller DC. 1996 Fluid flow and suspended particulates as determinants of

115   polychaete feeding behavior. *J. Mar. Res.* **54**, 565–588.

116   (doi:10.1357/0022240963213547)

117 35. Osovitz CJ, Julian D. 2002 Burrow irrigation behavior of Urechis caupo, a filter-feeding

118   marine invertebrate, in its natural habitat. *Mar. Ecol. Prog. Ser.* **245**, 149–155.

119   (doi:10.3354/meps245149)

18

120　36.　Riisgård HU, Ivarsson NM. 1990 The crown-filament pump of the suspension-feeding

121　　　polychaete Sabella penicillus: filtration, effects of temperature, and energy cost. *Mar.*

122　　　*Ecol. Prog. Ser.* **62**, 249–257.

123　37.　Riisgård HU, Funch P, Larsen PS. 2015 The mussel filter-pump - present

124　　　understanding, with a re-examination of gill preparations. *Acta Zool.* **96**, 273–282.

125　　　(doi:10.1111/azo.12110)

126　38.　Gagern A, Schürg T, Michiels NK, Schulte G, Sprenger D, Anthes N. 2008

127　　　Behavioural response to interference competition in a sessile suspension feeder. *Mar.*

128　　　*Ecol. Prog. Ser.* **353**, 131–135. (doi:10.3354/meps07204)

129　39.　Gerritsen J, Porter KG, Strickler JR. 1988 Not by sieving alone: observations of

130　　　suspension feeding in Daphnia. *Bull. Mar. Sci.* **43**, 366–376.

131　40.　McClatchie S, Boyd CM. 1983 Morphological Study of Sieve Efficiencies and

132　　　Mandibular Surfaces in the Antarctic Krill, Euphausia superba. *Can. J. Fish. Aquat.*

133　　　*Sci.* **40**, 955–967. (doi:10.1139/f83-122)

134　41.　Trager GC, Hwang J-S, Strickler JR. 1990 Barnacle suspension-feeding in variable

135　　　flow. *Mar. Biol.* **105**, 117–127. (doi:10.1007/BF01344277)

136　42.　Yee DA, Kaufmann MG. 2019 Insect Mouthparts. In *Insect Mouthparts* (ed HW Krenn),

137　　　pp. 101–125. Cham: Springer International Publishing. (doi:10.1007/978-3-030-29654-

138　　　4)

139　43.　Davoult D, Gounin F. 1995 Suspension-feeding activity of a dense Ophiothrix fragilis

140　　　(Abildgaard) population at the water-sediment interface: Time coupling of food

141　　　availability and feeding behaviour of the species. *Estuar. Coast. Shelf Sci.* **41**, 567–

142　　　577. (doi:10.1016/0272-7714(95)90027-6)

143　44.　Dong Y, Li Y, He P, Wang Z, Fan S, Zhang Z, Zhang X, Xu Q. 2021 Gut Microbial

144　　　Composition and Diversity in Four Ophiuroid Species: Divergence Between

145　　　Suspension Feeder and Scavenger and Their Symbiotic Microbes. *Front. Microbiol.*

146　　　**12**, 1–14. (doi:10.3389/fmicb.2021.645070)

147　45.　Holland ND, Strickler JR, Leonard AB. 1986 Particle interception, transport and

19

148   rejection by the feather star Oligometra serripinna (Echinodermata: Crinoidea), studied

149   by frame analysis of videotapes. *Mar. Biol.* **93**, 111–126. (doi:10.1007/BF00428660)

150 46.   Roberts D, Gebruk A, Levin V, Manship BAD. 2000 Feeding and digestive strategies

151   in deposit-feeding Holothurians. *Oceanogr. Mar. Biol. an Annu. Rev.* **38**, 257–310.

152 47.   Cameron CBCB. 2002 Particle retention and flow in the pharynx of the enteropneust

153   worm Harrimania planktophilus: The filter-feeding pharynx may have evolved before

154   the chordates. *Biol. Bull.* **202**, 192–200. (doi:10.2307/1543655)

155 48.   Nielsen SE, Bone Q, Bond P, Harper G. 2007 On particle filtration by amphioxus

156   (Branchiostoma lanceolatum). *J. Mar. Biol. Assoc. United Kingdom* **87**, 983–989.

157   (doi:10.1017/S0025315407053519)

158 49.   Bone Q, Carré C, Chang P. 2003 Tunicate feeding filters. *J. Mar. Biol. Assoc. United*

159   *Kingdom* **83**, 907–919. (doi:10.1017/S002531540300804Xh)

160 50.   Sutherland KR, Madin LP, Stocker R. 2010 Filtration of submicrometer particles by

161   pelagic tunicates. *Proc. Natl. Acad. Sci. U. S. A.* **107**, 15129–15134.

162   (doi:10.1073/pnas.1003599107)

163 51.   Conley KR, Gemmell BJ, Bouquet JM, Thompson EM, Sutherland KR. 2018 A self-

164   cleaning biological filter: How appendicularians mechanically control particle adhesion

165   and removal. *Limnol. Oceanogr.* **63**, 927–938. (doi:10.1002/lno.10680)

166 52.   Petersen JK. 2007 Ascidian suspension feeding. *J. Exp. Mar. Bio. Ecol.* **342**, 127–137.

167   (doi:10.1016/j.jembe.2006.10.023)

168 53.   Sumerel AN, Finelli CM. 2014 Particle size, flow speed, and body size interactions

169   determine feeding rates of a solitary ascidian Styela plicata: A flume experiment. *Mar.*

170   *Ecol. Prog. Ser.* **495**, 193–204. (doi:10.3354/meps10571)

171 54.   Katija K, Troni G, Daniels J, Lance K, Sherlock RE, Sherman AD, Robison BH. 2020

172   Revealing enigmatic mucus structures in the deep sea using DeepPIV. *Nature* **583**,

173   78–82. (doi:10.1038/s41586-020-2345-2)

174 55.   Moore JW, Mallatt JM. 1980 Feeding of Larval Lamprey. *Can. J. Fish. Aquat. Sci.* **37**,

175   1658–1664. (doi:10.1139/f80-213)

176   56.   Mallatt J. 1982 Pumping rates and particle retention efficiencies of the larval lamprey,

177   an unusual suspension feeder. *Biol. Bull.* **163**, 197–210. (doi:10.2307/1541509)

178   57.   Paig-Tran EWM, Summers AP. 2014 Comparison of the Structure and Composition of

179   the Branchial Filters in Suspension Feeding Elasmobranchs. *Anat. Rec.* **297**, 701–

180   715. (doi:10.1002/ar.22850)

181   58.   Sims DW. 2000 Filter-feeding and cruising swimming speeds of basking sharks

182   compared with optimal models: They filter-feed slower than predicted for their size. *J.*

183   *Exp. Mar. Bio. Ecol.* **249**, 65–76. (doi:10.1016/S0022-0981(00)00183-0)

184   59.   Watanabe YY, Papastamatiou YP. 2019 Distribution, body size and biology of the

185   megamouth shark Megachasma pelagios. *J. Fish Biol.* **95**, 992–998.

186   (doi:10.1111/jfb.14007)

187   60.   Divi R V., Strother JA, Paig-Tran EWM. 2018 Manta rays feed using ricochet

188   separation, a novel nonclogging filtration mechanism. *Sci. Adv.* **4**, eaat9533.

189   (doi:10.1126/sciadv.aat9533)

190   61.   Motta PJ *et al.* 2010 Feeding anatomy, filter-feeding rate, and diet of whale sharks

191   Rhincodon typus during surface ram filter feeding off the Yucatan Peninsula, Mexico.

192   *Zoology* **113**, 199–212. (doi:10.1016/j.zool.2009.12.001)

193   62.   Storm TJ, Nolan KE, Roberts EM, Sanderson SL. 2020 Oropharyngeal morphology

194   related to filtration mechanisms in suspension-feeding American shad (Clupeidae). *J.*

195   *Exp. Zool. Part A Ecol. Integr. Physiol.* **333**, 493–510. (doi:10.1002/jez.2363)

196   63.   Cohen KE, Hernandez LP, Crawford CH, Flammang BE. 2018 Channeling vorticity:

197   Modeling the filter-feeding mechanism in silver carp using µcT and 3D PIV. *J. Exp.*

198   *Biol.* **221**. (doi:10.1242/jeb.183350)

199   64.   Rico-Guevara A, Sustaita D, Gussekloo S, Olsen A, Bright J, Corbin C, Dudley R.

200   2019 Feeding in Birds: Thriving in Terrestrial, Aquatic, and Aerial Niches. pp. 643–

201   693. (doi:10.1007/978-3-030-13739-7_17)

202   65.   Zweers G, de Jong F, Berkhoudt H. 1995 Filter Feeding in Flamingos (Phoenicopterus

203   ruber). *Condor* **97**, 297–324. (doi:10.2307/1369017)

21

204   66.   Kooloos JGM, Kraaijeveld AR, Langenbach GEJ, Zweers GA. 1989 Comparative

205   mechanics of filter feeding in Anas platyrhynchos, Anas clypeata and Aythya fuligula

206   (Aves, Anseriformes). *Zoomorphology* **108**, 269–290. (doi:10.1007/BF00312160)

207   67.   Werth AJ, Potvin J, Shadwick RE, Jensen MM, Cade DE, Goldbogen JA. 2018

208   Filtration area scaling and evolution in mysticetes: Trophic niche partitioning and the

209   curious cases of sei and pygmy right whales. *Biol. J. Linn. Soc.* **125**, 264–279.

210   (doi:10.1093/BIOLINNEAN/BLY121)

211   68.   Goldbogen JA, Cade DE, Calambokidis J, Friedlaender AS, Potvin J, Segre PS, Werth

212   AJ. 2017 How Baleen Whales Feed: The Biomechanics of Engulfment and Filtration.

213   *Ann. Rev. Mar. Sci.* **9**, 367–386. (doi:10.1146/annurev-marine-122414-033905)

214   69.   Werth AJ. 2004 Models of hydrodynamic flow in the bowhead whale filter feeding

215   apparatus. *J. Exp. Biol.* **207**, 3569–3580. (doi:10.1242/jeb.01202)

216   70.   Goldbogen JA, Pyenson ND, Shadwick RE. 2007 Big gulps require high drag for fin

217   whale lunge feeding. *Mar. Ecol. Prog. Ser.* **349**, 289–301. (doi:10.3354/meps07066)

218   71.   Westheide W, Rieger G. 2013 *Spezielle Zoologie. Teil 1: Einzeller und Wirbellose*

219   *Tiere*. Berlin, Heidelberg: Springer Berlin Heidelberg.

220   72.   Modica L, Lanuza P, García-Castrillo G. 2020 Surrounded by microplastic, since

221   when? Testing the feasibility of exploring past levels of plastic microfibre pollution

222   using natural history museum collections. *Mar. Pollut. Bull.* **151**, 110846.

223   (doi:10.1016/j.marpolbul.2019.110846)

224   73.   Chang-Feng D, Ming-Chao L. 1993 The effects of flow on feeding of three gorgonians

225   from southern Taiwan. *J. Exp. Mar. Bio. Ecol.* **173**, 57–69. (doi:10.1016/0022-

226   0981(93)90207-5)

227   74.   Ribes M, Coma R, Gili J-M. 1999 Heterogeneous feeding in benthic suspension

228   feeders: The natural diet and grazing rate of the temperate gorgonian Paramuricea

229   clavata (Cnidaria: Octocorallia) over a year cycle. *Mar. Ecol. Prog. Ser.* **183**, 125–137.

230   (doi:10.3354/meps183125)

231   75.   Angiolillo M *et al.* 2015 Distribution and assessment of marine debris in the deep

22

232   Tyrrhenian Sea (NW Mediterranean Sea, Italy). *Mar. Pollut. Bull.* **92**, 149–159.

233   (doi:10.1016/j.marpolbul.2014.12.044)

234   76.   Stoecker DK, Michaels AE, Davis LH. 1987 Grazing by the jellyfish, Aurelia aurita, on

235   microzooplankton. *J. Plankton Res.* **9**.

236   77.   Cole M, Lindeque P, Fileman E, Halsband C, Goodhead R, Moger J, Galloway TS.

237   2013 Microplastic ingestion by zooplankton. *Environ. Sci. Technol.* **47**, 6646–6655.

238   (doi:10.1021/es400663f)

239   78.   Costa E, Gambardella C, Piazza V, Vassalli M, Sbrana F, Lavorano S, Garaventa F,

240   Faimali M. 2020 Microplastics ingestion in the ephyra stage of Aurelia sp. triggers

241   acute and behavioral responses. *Ecotoxicol. Environ. Saf.* **189**, 109983.

242   (doi:10.1016/j.ecoenv.2019.109983)

243   79.   Colin SP, Costello JH, Hansson LJ, Titelman J, Dabiri JO. 2010 Stealth predation and

244   the predatory success of the invasive ctenophore Mnemiopsis leidyi. *Proc. Natl. Acad.*

245   *Sci. U. S. A.* **107**, 17223–17227. (doi:10.1073/pnas.1003170107)

246   80.   Emschermann P. 1993 Lime-Twig Glands: A Unique Invention of an Antarctic

247   Entoproct. *Biol. Bull.* **185**, 97–108. (doi:10.2307/1542133)

248   81.   Mccammon HM. 1969 The Food of Articulate Brachiopods. *J. Paleontol.* **43**, 976–985.

249   82.   Riisgård H, Manríquez P. 1997 Filter-feeding in fifteen marine ectoprocts

250   (Bryozoa):particle capture and water pumping. *Mar. Ecol. Prog. Ser.* **154**, 223–239.

251   (doi:10.3354/meps154223)

252   83.   Grünbaum D. 1995 A Model of Feeding Currents in Encrusting Bryozoans shows

253   Interference between Zooids within a Colony. *J. Theor. Biol.* **174**, 409–425.

254   84.   Setälä O, Fleming-Lehtinen V, Lehtiniemi M. 2014 Ingestion and transfer of

255   microplastics in the planktonic food web. *Environ. Pollut.* **185**, 77–83.

256   (doi:10.1016/j.envpol.2013.10.013)

257   85.   Piazzolla D, Cafaro V, Mancini E, Scanu S, Bonamano S, Marcelli M. 2020 Preliminary

258   Investigation of Microlitter Pollution in Low-Energy Hydrodynamic Basins Using

259   Sabella spallanzanii (Polychaeta: Sabellidae) Tubes. *Bull. Environ. Contam. Toxicol.*

23

260   **104**, 345–350. (doi:10.1007/s00128-020-02797-x)

261   86.   Strohmeier T, Strand T, Alunno-Bruscia M, Duinker A, Cranford PJ. 2012 Variability in

262   particle retention efficiency by the mussel Mytilus edulis. *J. Exp. Mar. Bio. Ecol.* **412**,

263   96–102. (doi:10.1016/j.jembe.2011.11.006)

264   87.   von Moos N, Burkhardt-Holm P, Köhler A. 2012 Uptake and Effects of Microplastics on

265   Cells and Tissue of the Blue Mussel Mytilus edulis L. after an Experimental Exposure.

266   *Environ. Sci. Technol.* **46**, 11327–11335. (doi:10.1021/es302332w)

267   88.   Farrell P, Nelson K. 2013 Trophic level transfer of microplastic: Mytilus edulis (L.) to

268   Carcinus maenas (L.). *Environ. Pollut.* **177**, 1–3. (doi:10.1016/j.envpol.2013.01.046)

269   89.   Ribak G, Heller J, Genin A. 2005 Mucus-net feeding on organic particles by the

270   vermetid gastropod Dendropoma maximum in and below the surf zone. *Mar. Ecol.*

271   *Prog. Ser.* **293**, 77–87. (doi:10.3354/meps293077)

272   90.   Gophen M, Geller W. 1984 Filter mesh size and food particle uptake by Daphnia.

273   *Oecologia* **64**, 408–412. (doi:10.1007/BF00379140)

274   91.   Jemec A, Horvat P, Kunej U, Bele M, Kržan A. 2016 Uptake and effects of microplastic

275   textile fibers on freshwater crustacean Daphnia magna. *Environ. Pollut.* **219**, 201–209.

276   (doi:10.1016/j.envpol.2016.10.037)

277   92.   Dawson AL, Kawaguchi S, King CK, Townsend KA, King R, Huston WM, Bengtson

278   Nash SM. 2018 Turning microplastics into nanoplastics through digestive

279   fragmentation by Antarctic krill. *Nat. Commun.* **9**, 1001. (doi:10.1038/s41467-018-

280   03465-9)

281   93.   Barnes H. 1959 Stomach Contents and Microfeeding of Some Common Cirripedes.

282   **37**. (doi:https://doi.org/10.1139/z59-027)

283   94.   Xu X-Y, Wong CY, Tam NFY, Liu HM, Cheung SG. 2020 Barnacles as potential

284   bioindicator of microplastic pollution in Hong Kong. *Mar. Pollut. Bull.* **154**, 111081.

285   (doi:10.1016/j.marpolbul.2020.111081)

286   95.   McCafferty WP, Bae YJ. 1992 Filter-feeding habits of the larvae of Anthopotamus

287   (Ephemeroptera : Potamanthidae). *Ann. Limnol. - Int. J. Limnol.* **28**, 27–34.

24

288   (doi:10.1051/limn/1992002)

289   96.   Soluk DA, Craig DA. 1988 Vortex feeding from pits in the sand: A unique method of

290   suspension feeding used by a stream invertebrate. *Limnol. Oceanogr.* **33**, 638–645.

291   (doi:10.4319/lo.1988.33.4.0638)

292   97.   Wallace JB, O'hop J. 1979 Fine Particle Suspension-Feeding Capabilities of Isonychia

293   spp. (Ephemeroptera: Siphlonuridae) 1.

294   98.   Windsor FM, Tilley RM, Tyler CR, Ormerod SJ. 2019 Microplastic ingestion by riverine

295   macroinvertebrates. *Sci. Total Environ.* **646**, 68–74.

296   (doi:10.1016/j.scitotenv.2018.07.271)

297   99.   Wallace JB, Merritt RW. 1980 Filter-feeding ecology of aquatic insects. *Annu. Rev.*

298   *Entomol.* **25**, 103–135. (doi:Filter-feeding ecology of aquatic insects)

299   100.   Brown SA, Ruxton GD, Pickup RW, Humphries S. 2005 Seston capture by

300   Hydropsyche siltalai and the accuracy of capture efficiency estimates. *Freshw. Biol.*

301   **50**, 113–126. (doi:10.1111/j.1365-2427.2004.01311.x)

302   101.   Merritt RW, Craig DA, Wotton RS, Walker ED. 1996 Feeding behavior of aquatic

303   insects: Case studies on black fly and mosquito larvae. *Invertebr. Biol.* **115**, 206–217.

304   (doi:10.2307/3226931)

305   102.   Brackenbury J. 2001 Locomotion through use of the mouth brushes in the larva of

306   Culex pipiens (Diptera: Culicidae). *Proc. R. Soc. B Biol. Sci.* **268**, 101–106.

307   (doi:10.1098/rspb.2000.1336)

308   103.   Craig DA, Chance MM. 1982 Filter feeding in larvae of Simuliidae (Diptera:

309   Culicomorpha): aspects of functional morphology and hydrodynamics. *Can. J. Zool.*

310   **60**, 712–724. (doi:10.1139/z82-100)

311   104.   Leonard AB. 1989 Functional response in Antedon mediterranea (Lamarck)

312   (Echinodermata: Crinoidea): the interaction of prey concentration and current velocity

313   on a passive suspension-feeder. *J. Exp. Mar. Bio. Ecol.* **127**, 81–103.

314   (doi:10.1016/0022-0981(89)90210-4)

315   105.   Zhang D, Liu X, Huang W, Li J, Wang C, Zhang D, Zhang C. 2020 Microplastic

25

316   pollution in deep-sea sediments and organisms of the Western Pacific Ocean.

317   *Environ. Pollut.* **259**, 113948. (doi:10.1016/j.envpol.2020.113948)

318 106. Graham ER, Thompson JT. 2009 Deposit- and suspension-feeding sea cucumbers

319   (Echinodermata) ingest plastic fragments. *J. Exp. Mar. Bio. Ecol.* **368**, 22–29.

320   (doi:10.1016/j.jembe.2008.09.007)

321 107. Ruppert EE, Nash TR, Smith AJ. 2000 The size range of suspended particles trapped

322   and ingested by the filter-feeding lancelet Branchiostoma floridae (Cephalochordata:

323   Acrania). *J. Mar. Biol. Assoc. United Kingdom* **80**, 329–332.

324   (doi:10.1017/S0025315499001903)

325 108. Knott NA, Davis AR, Buttemer WA. 2004 Passive flow through an unstalked intertidal

326   ascidian: Orientation and morphology enhance suspension feeding in Pyura

327   stolonifera. *Biol. Bull.* **207**, 217–224. (doi:10.2307/1543210)

328 109. Conley KR, Lombard F, Sutherland KR. 2018 Mammoth grazers on the ocean's

329   minuteness: a review of selective feeding using mucous meshes. *Proc. R. Soc. B Biol.*

330   *Sci.* **285**, 20180056. (doi:10.1098/rspb.2018.0056)

331 110. Evans TM, Bauer JE. 2016 Identification of the nutritional resources of larval sea

332   lamprey in two Great Lakes tributaries using stable isotopes. *J. Great Lakes Res.* **42**,

333   99–107. (doi:10.1016/j.jglr.2015.11.010)

334 111. Paig-Tran EWM, Kleinteich T, Summers AP. 2013 The filter pads and filtration

335   mechanisms of the devil rays: Variation at macro and microscopic scales. *J. Morphol.*

336   **274**, 1026–1043. (doi:10.1002/jmor.20160)

337 112. Westheide W, Rieger G. 2015 *Spezielle Zoologie. Teil 2: Wirbel- oder Schädeltiere.*

338   Berlin, Heidelberg: Springer Berlin Heidelberg. (doi:10.1007/978-3-642-55436-0)

339 113. Abreo NAS, Blatchley D, Superio MD. 2019 Stranded whale shark (Rhincodon typus)

340   reveals vulnerability of filter-feeding elasmobranchs to marine litter in the Philippines.

341   *Mar. Pollut. Bull.* **141**, 79–83. (doi:10.1016/j.marpolbul.2019.02.030)

342 114. Fossi MC, Baini M, Panti C, Galli M, Jiménez B, Muñoz-Arnanz J, Marsili L, Finoia

343   MG, Ramírez-Macías D. 2017 Are whale sharks exposed to persistent organic

26

344   pollutants and plastic pollution in the Gulf of California (Mexico)? First ecotoxicological

345   investigation using skin biopsies. *Comp. Biochem. Physiol. Part - C Toxicol.*

346   *Pharmacol.* **199**, 48–58. (doi:10.1016/j.cbpc.2017.03.002)

347 115. Cohen KE, Hernandez LP. 2018 Making a master filterer: Ontogeny of specialized

348   filtering plates in silver carp (Hypophthalmichthys molitrix). *J. Morphol.* **279**, 925–935.

349   (doi:10.1002/jmor.20821)

350 116. Last JM. 1989 The food of herring, Clupea harengus, in the North Sea, 1983–1986. *J.*

351   *Fish Biol.* **34**, 489–501. (doi:10.1111/j.1095-8649.1989.tb03330.x)

352 117. Collard F, Gilbert B, Eppe G, Roos L, Compère P, Das K, Parmentier E. 2017

353   Morphology of the filtration apparatus of three planktivorous fishes and relation with

354   ingested anthropogenic particles. *Mar. Pollut. Bull.* **116**, 182–191.

355   (doi:10.1016/j.marpolbul.2016.12.067)

356 118. Seale DB, Hoff K, Wassersug R. 1982 Xenopus laevis larvae (Amphibia, Anura) as

357   model suspension feeders. *Hydrobiologia* **87**, 161–169. (doi:10.1007/BF00015196)

358 119. Hu L, Su L, Xue Y, Mu J, Zhu J, Xu J, Shi H. 2016 Uptake, accumulation and

359   elimination of polystyrene microspheres in tadpoles of Xenopus tropicalis.

360   *Chemosphere* **164**, 611–617. (doi:10.1016/j.chemosphere.2016.09.002)

361 120. Ryan PG. 2008 Seabirds indicate changes in the composition of plastic litter in the

362   Atlantic and south-western Indian Oceans. *Mar. Pollut. Bull.* **56**, 1406–1409.

363   (doi:10.1016/j.marpolbul.2008.05.004)

364 121. Fossi MC, Coppola D, Baini M, Giannetti M, Guerranti C, Marsili L, Panti C, de Sabata

365   E, Clò S. 2014 Large filter feeding marine organisms as indicators of microplastic in

366   the pelagic environment: The case studies of the Mediterranean basking shark

367   (Cetorhinus maximus) and fin whale (Balaenoptera physalus). *Mar. Environ. Res.* **100**,

368   17–24. (doi:10.1016/j.marenvres.2014.02.002)

369 122. Leys SP, Yahel G, Reidenbach MA, Tunnicliffe V, Shavit U, Reiswig HM. 2011 The

370   Sponge Pump: The Role of Current Induced Flow in the Design of the Sponge Body

371   Plan. *PLoS One* **6**, e27787. (doi:10.1371/journal.pone.0027787)

372   123. Ludeman DA, Reidenbach MA, Leys SP. 2017 The energetic cost of filtration by

373   demosponges and their behavioural response to ambient currents. *J. Exp. Biol.* **220**,

374   995–1007. (doi:10.1242/jeb.146076)

375   124. Sponaugle S, LaBarbera M. 1991 Drag-induced deformation: a functional feeding

376   strategy in two species of gorgonians. *J. Exp. Mar. Bio. Ecol.* **148**, 121–134.

377   (doi:10.1016/0022-0981(91)90151-L)

378   125. Sponaugle S. 1991 Flow patterns and velocities around a suspension-feeding

379   gorgonian polyp: evidence from physical models. *J. Exp. Mar. Bio. Ecol.* **148**, 135–

380   145. (doi:10.1016/0022-0981(91)90152-M)

381   126. Sutherland KR, Costello JH, Colin SP, Dabiri JO. 2014 Ambient fluid motions influence

382   swimming and feeding by the ctenophore Mnemiopsis leidyi. *J. Plankton Res.* **36**,

383   1310–1322. (doi:10.1093/plankt/fbu051)

384   127. Riisgård HU, Nielsen C, Larsen PS. 2000 Downstream collecting in ciliary suspension

385   feeders: The catch-up principle. *Mar. Ecol. Prog. Ser.* **207**, 33–51.

386   (doi:10.3354/meps207033)

387   128. Thayer CW. 1986 Are brachiopods better than bivalves? Mechanisms of turbidity

388   tolerance and their interaction with feeding in articulates. *Paleobiology* **12**, 161–174.

389   (doi:10.1017/S0094837300013634)

390   129. LaBarbera M. 1981 Water flow patterns in and around three species of articulate

391   brachiopods. *J. Exp. Mar. Bio. Ecol.* **55**, 185–206. (doi:10.1016/0022-0981(81)90111-

392   8)

393   130. Temereva EN, Malakhov V V. 2010 Filter feeding mechanism in the phoronid

394   Phoronopsis harmeri (Phoronida, Lophophorata). *Russ. J. Mar. Biol.* **36**, 109–116.

395   (doi:10.1134/S1063074010020057)

396   131. Temereva EN, Malakhov V V. 2009 On the organization of the lophophore in

397   phoronids (Lophophorata: Phoronida). *Russ. J. Mar. Biol.* **35**, 479–489.

398   (doi:10.1134/S1063074009060054)

399   132. Tamberg Y, Shunatova N. 2016 Feeding behavior in freshwater bryozoans: function,

28

400   form, and flow. *Invertebr. Biol.* **135**, 138–149. (doi:10.1111/ivb.12124)

401   133.   Riisgård HU, Okamura B, Funch P. 2010 Particle capture in ciliary filter-feeding

402   gymnolaemate and phylactolaemate bryozoans - a comparative study. *Acta Zool.* **91**,

403   416–425. (doi:10.1111/j.1463-6395.2009.00417.x)

404   134.   Nielsen C. 2002 Ciliary filter-feeding structures in adult and larval gymnolaemate

405   bryozoans. *Invertebr. Biol.* **121**, 255–261.

406   135.   Eckman JEJE, Okamura B. 1998 A model of particle capture by bryozoans in turbulent

407   flow: Significance of colony form. *Am. Nat.* **152**, 861–880. (doi:10.1086/286214)

408   136.   Starkweather PLPL. 1995 Near-coronal fluid flow patterns and food cell manipulation

409   in the rotifer Brachionus calyciflorus. *Hydrobiologia* **313**–**314**, 191–195.

410   (doi:10.1007/BF00025950)

411   137.   Dubois S, Barillé L, Cognie B, Beninger P. 2006 Feeding mechanism of the

412   polychaete Sabellaria alveolata revisited: reply to Riisgård & Nielsen (2006). *Mar.*

413   *Ecol. Prog. Ser.* **328**, 307–311. (doi:10.3354/meps328307)

414   138.   Mayer S. 1994 Particle capture in the crown of the ciliary suspension feeding

415   polychaete Sabella penicillus: videotape recordings and interpretations. *Mar. Biol.* **119**,

416   571–582. (doi:10.1007/BF0035432)

417   139.   MacGinitie GE. 1945 The size of the mesh opening in mucous feeding nets of marine

418   animals. *Biol. Bull.* **88**, 107–111. (doi:10.2307/1538038)

419   140.   Julian D, Chang M, Judd J, Arp A. 2001 Influence of environmental factors on burrow

420   irrigation and oxygen consumption in the mudflat invertebrate Urechis caupo. *Mar.*

421   *Biol.* **139**, 163–173. (doi:10.1007/s002270100570)

422   141.   Ward JE, Sanford LP, Newell RIE, MacDonald BA. 1998 A new explanation of particle

423   capture in suspension-feeding bivalve molluscs. *Limnol. Oceanogr.* **43**, 741–752.

424   (doi:10.4319/lo.1998.43.5.0741)

425   142.   Jørgensen C. 1996 Bivalve filter feeding revisited. *Mar. Ecol. Prog. Ser.* **142**, 287–302.

426   (doi:10.3354/meps142287)

427   143.   Beninger PG, St-Jean SD, Poussart Y. 1995 Labial palps of the blue mussel Mytilus

     29

428   edulis (Bivalvia: Mytilidae). *Mar. Biol.* **123**, 293–303. (doi:10.1007/BF00353621)

429   144.   Jones HD, Richards OG, Southern TA. 1992 Gill dimensions, water pumping rate and

430   body size in mussel Mytilus edulis L. *Mar. Biol. EcoL.* **155**.

431   145.   Riisgård HU, Larsen PS. 2007 Viscosity of seawater controls beat frequency of water-

432   pumping cilia and filtration rate of mussels Mytilus edulis. *Mar. Ecol. Prog. Ser.* **343**,

433   141–150. (doi:10.3354/meps06930)

434   146.   Hughes RN, Lewis AH. 2009 On the spatial distribution, feeding and reproduction of

435   the vermetid gastropod Dendropoma maximum. *J. Zool.* **172**, 531–547.

436   (doi:10.1111/j.1469-7998.1974.tb04383.x)

437   147.   Brendelberger H, Geller W. 1985 Variability of filter structures in eight Daphnia

438   species: mesh sizes and filtering areas. *J. Plankton Res.* **7**, 473–486.

439   (doi:10.1093/plankt/7.4.473)

440   148.   Lampert W, Brendelberger H. 1996 Strategies of phenotypic low-food adaptation in

441   Daphnia: Filter screens, mesh sizes, and appendage beat rates. *Limnol. Ocean.* **41**.

442   149.   Nishizaki MT, Carrington E. 2014 Temperature and water flow influence feeding

443   behavior and success in the barnacle Balanus glandula. *Mar. Ecol. Prog. Ser.* **507**,

444   207–218. (doi:10.3354/meps10848)

445   150.   Braimah SA. 1987 Pattern of flow around filter-feeding structures of immature

446   Simulium bivittatum Malloch (Diptera: Simuliidae) and Isonychia campestris

447   McDunnough (Ephemeroptera: Oligoneuriidae). *Can. J. Zool.* **65**, 514–521.

448   (doi:10.1139/z87-080)

449   151.   Wallace JB, Malas D, Athens G. 1976 The Significance of the Elongate, Rectangular

450   Mesh Found in Capture Nets of Fine Particle Filter Feeding Trichoptera Larvae. *Arch.*

451   *fur Hydrobiol.* **77**, 205–212.

452   152.   Brown SA, Ruxton GD, Humphries S. 2004 Physical properties of Hydropsyche siltalai

453   (Trichoptera) net silk. *J. North Am. Benthol. Soc.* **23**, 771–779. (doi:10.1899/0887-

454   3593(2004)023<0771:ppohst>2.0.co;2)

455   153.   Hemphill N. 1988 Competition between two stream dwelling filter-feeders,

30

456   Hydropsyche oslari and Simulium virgatum. *Oecologia* **77**, 73–80.

457   (doi:10.1007/BF00380928)

458   154. Zhang Y. 2006 Balancing food availability and hydrodynamic constraint: Phenotypic

459   plasticity and growth in Simulium noelleri blackfly larvae. *Oecologia* **147**, 39–46.

460   (doi:10.1007/s00442-005-0243-9)

461   155. Cheer AYL, Koehl MAR. 1987 Fluid flow through filtering appendages of insects. *Math.*

462   *Med. Biol.* **4**, 185–199. (doi:10.1093/imammb/4.3.185)

463   156. Finelli CM, Hart DD, Merz RA. 2002 Stream insects as passive suspension feeders:

464   Effects of velocity and food concentration on feeding performance. *Oecologia* **131**,

465   145–153. (doi:10.1007/s00442-001-0852-x)

466   157. Leonard AB, Strickler JR, Holland ND. 1988 Effects of current speed on filtration

467   during suspension feeding in Oligometra serripinna (Echinodermata: Crinoidea). *Mar.*

468   *Biol.* **97**, 111–125. (doi:10.1007/BF00391251)

469   158. Vo M, Mehrabian S, Étienne S, Pelletier D, Cameron CB. 2019 The hemichordate

470   pharynx and gill pores impose functional constraints at small and large body sizes.

471   *Biol. J. Linn. Soc.* **127**, 75–87. (doi:10.1093/biolinnean/blz005)

472   159. Riisgård HU, Svane I. 1999 Filter Feeding in Lancelets (Amphioxus), Branchiostoma

473   lanceolatum. *Invertebr. Biol.* **118**, 423. (doi:10.2307/3227011)

474   160. Pennachetti CA. 1984 Functional morphology of the branchial basket of ascidia

475   paratropa (Tunicata, Ascidiacea). *Zoomorphology* **104**, 216–222.

476   (doi:10.1007/BF00312033)

477   161. Flood PR, Fiala-Medioni A. 1981 Ultrastructure and Histochemistry of the Food

478   Trapping Mucous Film in Benthic Filter-Feeders (Ascidians). *Acta Zool.* **62**, 53–65.

479   (doi:10.1111/j.1463-6395.1981.tb00616.x)

480   162. Du Clos KT, Jones IT, Carrier TJ, Brady DC, Jumars PA. 2017 Model-assisted

481   measurements of suspension-feeding flow velocities. *J. Exp. Biol.* **220**, 2096–2107.

482   (doi:10.1242/jeb.147934)

483   163. Morris CC, Deibel D. 1993 Flow rate and particle concentration within the house of the

31

484   pelagic tunicate Oikopleura vanhoeffeni. *Mar. Biol.* **115**, 445–452.

485   (doi:10.1007/BF00349843)

486 164. Smith DW. 1989 The feeding selectivity of silver carp, Hypophthalmichthys molitrix

487   Val. *J. Fish Biol.* **34**, 819–828. (doi:10.1111/j.1095-8649.1989.tb03366.x)

488 165. Cohen KE, Hernandez LP. 2018 The complex trophic anatomy of silver carp,

489   Hypophthalmichthys molitrix, highlighting a novel type of epibranchial organ. *J.*

490   *Morphol.* **279**, 1615–1628. (doi:10.1002/jmor.20891)

491 166. Gibson RNN. 1988 Development, morphometry and particle retention capability of the

492   gill rakers in the herring, Clupea harengus L. *J. Fish Biol.* **32**, 949–962.

493   (doi:10.1111/j.1095-8649.1988.tb05438.x)

494 167. Cheer A, Cheung S, Hung T-C, Piedrahita RH, Sanderson SL. 2012 Computational

495   Fluid Dynamics of Fish Gill Rakers During Crossflow Filtration. *Bull. Math. Biol.* **74**,

496   981–1000. (doi:10.1007/s11538-011-9709-6)

497 168. Paig-Tran EWM, Bizzarro JJ, Strother JA, Summers AP. 2011 Bottles as models:

498   Predicting the effects of varying swimming speed and morphology on size selectivity

499   and filtering efficiency in fishes. *J. Exp. Biol.* **214**, 1643–1654.

500   (doi:10.1242/jeb.048702)

501 169. Sanderson SL, Cheer AY, Goodrich JS, Graziano JD, Callan WT. 2001 Crossflow

502   filtration in suspension-feeding fishes. *Nature* **412**, 439–441. (doi:10.1038/35086574)

503 170. Wassersug R. 1972 The mechanism of ultraplanktonic entrapment in anuran larvae. *J.*

504   *Morphol.* **137**, 279–287. (doi:10.1002/jmor.1051370303)

505 171. Mascitti V, Osvaldo Kravetz F. 2002 Bill morphology of South American flamingos.

506   *Condor* **104**, 73. (doi:10.1650/0010-5422(2002)104[0073:bmosaf]2.0.co;2)

507 172. Skieresz-Szewczyk K, Jackowiak H. 2016 Morphofunctional study of the tongue in the

508   domestic duck (Anas platyrhynchos f. domestica, Anatidae): LM and SEM study.

509   *Zoomorphology* **135**, 255–268. (doi:10.1007/s00435-016-0302-2)

510 173. Werth AJ, Rita D, Rosario M V., Moore MJ, Sformo TL. 2018 How do baleen whales

511   stow their filter? A comparative biomechanical analysis of baleen bending. *J. Exp. Biol.*

32

512   **221**, jeb189233. (doi:10.1242/jeb.189233)

513   174.   Werth AJ, Potvin J. 2016 Baleen hydrodynamics and morphology of cross-flow

514   filtration in balaenid whale suspension feeding. *PLoS One* **11**.

515   (doi:10.1371/journal.pone.0150106)

516   175.   Werth AJ. 2013 Flow-dependent porosity and other biomechanical properties of

517   mysticete baleen. *J. Exp. Biol.* **216**, 1152–1159. (doi:10.1242/jeb.078931)

518   176.   Simon M, Johnson M, Tyack P, Madsen PT. 2009 Behaviour and kinematics of

519   continuous ram filtration in bowhead whales (Balaena mysticetus). *Proc. R. Soc. B*

520   *Biol. Sci.* **276**, 3819–3828. (doi:10.1098/rspb.2009.1135)

521   177.   Szewciw LJ, De Kerckhove DG, Grime GW, Fudge DS. 2010 Calcification provides

522   mechanical reinforcement to whale baleen α-keratin. In *Proceedings of the Royal*

523   *Society B: Biological Sciences*, pp. 2597–2605. (doi:10.1098/rspb.2010.0399)

524   178.   Werth AJ. 2001 How do mysticetes remove prey trapped in baleen? *Bull. Museum*

525   *Comp. Zool.* **156**, 189–204.

526   179.   Hunt OD. 1925 The Food of the Bottom Fauna of the Plymouth Fishing Grounds. *J.*

527   *Mar. Biol. Assoc. United Kingdom* **13**, 560–599. (doi:10.1017/S0025315400008079)

528   180.   Jordan HJ, Hirsch GC. 1927 Einige vergleichend — physiologische Probleme der

529   Verdauung bei Metazoen. In *Verdauung und Verdauungsapparat* (eds BP Babkin, G

530   v. Bergmann, M Bergmann, H Bluntschli, A Eckstein, L Elek, H Eppinger, R Feulgen,

531   H Full, O Goetze, et al.), Berlin, Heidelberg: Springer Berlin Heidelberg.

532   (doi:10.1007/978-3-642-48565-7)

533   181.   Yonge CM. 1928 Feeding Mechanisms in the Invertebrates. *Biol. Rev.* **3**, 21–76.

534   (doi:10.1111/j.1469-185X.1928.tb00882.x)

535   182.   Jørgensen C. 1983 Fluid mechanical aspects of suspension feeding. *Mar. Ecol. Prog.*

536   *Ser.* **11**, 89–103. (doi:10.3354/meps011089)

537   183.   Alcaraz M, Calbet A. 2003 Zooplankton Ecology. In *Encyclopedia of Life Support*

538   *Systems*,

539   184.   Makoto O, Tsutomu I. 1992 *Methods in Marine Zooplankton Ecology*. Krieger.

     33

540   185.   Levine AD, Tchobanoglous G, Asano T, Levine AD, Tchobanoglous G, Asano T. 1985

541   Characterization of the size distribution of contaminants in wastewater : treatment and

542   reuse implications. *Water Pollut. Control Fed.* **57**, 805–816.

543   186.   Turrell WR. 2020 Estimating a regional budget of marine plastic litter in order to advise

544   on marine management measures. *Mar. Pollut. Bull.* **150**, 110725.

545   (doi:10.1016/j.marpolbul.2019.110725)

546   187.   Hartmann NB *et al.* 2019 Are We Speaking the Same Language? Recommendations

547   for a Definition and Categorization Framework for Plastic Debris. *Environ. Sci.*

548   *Technol.* **53**, 1039–1047. (doi:10.1021/acs.est.8b05297)

549   188.   Hara S, Koike I. 2000 Dynamics of Organic Marine Aggregates Nanometer-Colloids to

550   Marine Snow. In *Dynamics and Characterization of Marine Organic Matter* (eds N

551   Handa, E Tanoue, T Hama), p. 560.

552

553

554

555

10.2.2. Manuscript II

Retention of Microplastics by Biofilms and Ingestion by Protists

Leandra Hamann[1,2][*][§], Jennifer Werner[1][*], Felicia Haase[1,3,4], Massimo Thiel[1], Anja Scherwaß[1],

Christian Laforsch[5], Martin G.J. Löder[5], Alexander Blanke[2], Hartmut Arndt[1][§]

*shared first authorship

§ corresponding author: Hartmut.Arndt@uni-koeln.de, lhamann@evolution.uni-bonn.de

[1] Institute of Zoology, University of Cologne, Cologne, Germany

[2] Institute of Evolutionary Biology and Animal Ecology, University of Bonn, Bonn, Germany

[3] Coastal and Marine Research Centre, Griffith University, Southport, QLD 4215, Australia

[4] School of Environment and Science, Griffith University, Southport, QLD 4215, Australia

[5] Department Animal Ecology I and BayCEER, University of Bayreuth, Universitätsstraße 30,

95447 Bayreuth, Germany

1

Highlights

- Riverine biofilms contain up to 10 x more microplastics than ambient water

- Between 70 % and 78 % of microplastics are smaller than 50 µm

- Biofilms retain 6 - 12 x more microplastics than surfaces without biofilms

- The ciliate *Stentor coeruleus* ingests microplastics in feeding experiments

Abstract (300 words)

Microplastics (MPs) are released into the environment through diverse, mainly terrestrial, human activities and rivers transport MPs from land to sea. Biofilms cover the surfaces of all aquatic ecosystems, including rivers and may play an essential role in the fate of MPs. Biofilms are a habitat for microzoobenthos such as bacteria, flagellates, ciliates, and other protists, which potentially could ingest MPs and thereby enable a transfer to macrozoobenthic organisms. In order to study if biofilms retain and accumulate MPs, we analysed natural biofilms grown on clay tiles in the River Rhine in field and laboratory studies. The results of our field studies show that natural biofilms contained up to 10 x more MPs after 6, 12, and 18 months than the controls that show the concentration in the surrounding water. Between 70 % and 78 % of MPs were smaller than 50 µm, and between 11 % and 36 % were between 5.9 µm and 11 µm in biofilm and river water samples. Additionally, we exposed biofilms grown on clay tiles, other substrates, and the ciliate *Stentor coeruleus* to artificial MP in laboratory experiments. The results show that 6 - 12 times more MPs were found in biofilms compared to clay tiles without biofilms with a dependency on flow velocity. MP ingestion in *Stentor coeruleus* was dependent on the surrounding concentration, with higher ingestion rates for higher MP concentrations. We assume that biofilm morphology, the properties of the extracellular polymeric substances and the incorporated microorganisms are responsible for MP retention and accumulation in biofilms. High MP concentration of small sizes (<50 µm) as reported here might have been underestimated until now, even though this size class seems particularly relevant for the ingestion by protists and the transfer to higher trophic levels.

55 Furthermore, the effects of MP retention in biofilms might be relevant for particle transport

56 models in riverine systems, risk assessment of MP exposure, and effects on micro- and

57 macroorganisms.

58

59 **Keywords:** biofilms, protists, microplastics, particle retention, rivers, uptake experiments

60

61 Define Abbreviations in a footnote on the first page

62 MPs = microplastic particles (including fibres)

3

1. Introduction

Small plastic particles, so-called microplastics (MPs), are released into the environment due to a broad range of human activities, such as the use of cosmetics, abrasion from synthetic clothing, loss of virgin plastic pellets, tyre wear, or fragmentation from larger plastic objects (Auta, Emenike & Fauziah, 2017; Boucher & Friot, 2017; Falco *et al.*, 2019). As a results, all environmental compartments contain MPs, from the atmosphere (Evangeliou et al., 2020) to soil (Horton et al., 2017), and marine and freshwater environments. In marine systems, MPs are present in surface waters (Moore *et al.*, 2001) to the deep sea (Woodall *et al.*, 2014), from sediments (Van Cauwenberghe *et al.*, 2015) to arctic ice (Peeken *et al.*, 2018). However, relatively little is known about the fate and effects in freshwater systems compared to marine ecosystems (Wagner *et al.*, 2014; Horton *et al.*, 2017; Li, Liu & Chen, 2018a). MPs enter riverine systems via point sources, e.g., sewage treatment plants, sewer overflow, effluents of factories, and non-point sources, e.g., by precipitation and land runoff (Wagner *et al.*, 2014; Siegfried *et al.*, 2017).

Riverine ecosystems play a significant role in transporting and distributing MPs and plastic litter from inland to shores and oceans as their final sink (Lebreton *et al.*, 2017). In the River Yangtze (Asia), on average 4137 MPs per m^3 were found with 90 % of particles in a range of 0.5 to 5 mm (Zhao *et al.*, 2014), the River Nile (Africa) contained up 1718 MPs per m^3 in surface waters (Shabaka *et al.*, 2022), and in the River Rhine (Europe), 0.5 up to over 20 MPs per m^3 were measured in a size range from 300 µm to 5 mm at 11 locations (Mani *et al.*, 2016). However, rivers per se are also vulnerable ecosystems that can be affected by MPs and can act as at least temporary sinks as they are retained and accumulated in sediments, shorelines and floodplains (Wagner *et al.*, 2014; Dris *et al.*, 2015; Nizzetto *et al.*, 2016; Besseling *et al.*, 2017; Siegfried *et al.*, 2017; Hoellein *et al.*, 2019; Rolf *et al.*, 2022). Sediments at the shore of the River Rhine contained 228 to 3,763 MPs per kg sediment in the size of 63 to 5000 µm (Klein, Worch & Knepper, 2015), and in the river's floodplains, concentrations of 25,502 up to 84,824 MP per kg dry soil were found in the size range of 11 to 5000 µm (Rolf *et al.*, 2022).

4

90 Hence, substrates and surfaces seem to play an important role in the environmental fate of

91 MPs in rivers.

92 Biofilms are microbial communities of bacteria, algae, and protists living in a matrix consisting

93 of extracellular polymeric substances (EPS) on organic and inorganic substrates (Branda *et*

94 *al.*, 2005; Böhme, Risse-Buhl & Küsel, 2009), such as stones, leaf litter, macrophytes, animals,

95 artificial substrates (Arndt *et al.*, 2003) and MPs: Models of riverine transport of MPs show that

96 the growth of a biofilm on the surface of MPs influences the settling behaviour of MPs and thus

97 their distribution in the river water column (Besseling *et al.*, 2017; Hoellein *et al.*, 2019), similar

98 to marine environments (Lobelle & Cunliffe, 2011; Zettler, Mincer & Amaral-Zettler, 2013;

99 Yokota *et al.*, 2017). Biofilm formation is initiated by bacteria living in the ambient water that

100 settle on substrates and excrete EPS, which in turn supports attachment of algae, protozoans,

101 and metazoans with maturing (Costerton, Irvin & Cheng, 1981; Vasudevan, 2014). With

102 ongoing growth, seasonality and the entrapping of different species, biofilms form a three-

103 dimensional structure with varying thicknesses (Vasudevan, 2014). Within river ecosystems,

104 biofilms influence the food chain (Vasudevan, 2014), nutrient cycling (Chen *et al.*, 2020), and

105 degradation of herbicides (Bighiu & Goedkoop, 2021).

106 Although the importance of biofilms on MPs regarding their transport behaviour and distribution

107 has been proven, the retention of MPs within biofilms that cover substrates is largely unknown

108 and is not considered in current retention models. However, as it has been observed for other

109 kinds of suspended particles in streams (Arnon *et al.*, 2009; Böhme *et al.*, 2009; Battin *et al.*,

110 2016), biofilms might act as a temporary sink for MPs and thereby foster the incorporation of

111 MPs into microbial and macrobial food webs. MPs ingestion by biofilm-associated

112 microorganisms has seldomly been studied, and the literature is restricted almost exclusively

113 to the marine realm (Cole *et al.*, 2013; Setälä, Fleming-Lehtinen & Lehtiniemi, 2014; Langlet

114 *et al.*, 2020). Ciliates are estimated to ingest 10 % of the natural particles retained in biofilms

115 from ambient water (Roche *et al.*, 2017).

116 Because biofilms cover every surface in aquatic environments and have a permanent

117 exchange to the bulk water through the permeable EPS and active microbial community, we

5

118 assume that biofilms play a crucial role in the retention and accumulation of MPs riverine

119 systems. Therefore, we analysed the MPs concentration in biofilms of the River Rhine,

120 focusing on particles <100 μm, which might be of particular relevance to subsequent negative

121 health effects. In laboratory experiments, we compared the retention of artificial MPs by

122 naturally-grown biofilms with other substrates to estimate the accumulation potential by

123 biofilms. Additionally, we tested the ingestion rate of artificial MPs with varying concentrations

124 by a typical biofilm inhabiting ciliate in feeding experiments to determine the role of protists

125 within biofilms and the possible transfer to higher trophic levels.

2. Methods

126

2.1. Study site: River Rhine at Cologne

127

128 The River Rhine flows from its origin in Switzerland northwards through the west side of

129 Germany and ends in the Dutch North Sea. The stretch of the River Rhine at Cologne,

130 Germany, is characterized as the Lower Rhine (Preusser, 2008) with a flow velocity of 1.5 m s^{-1}

131 ^{1}. The study was conducted at the Ecological Rhine Station boat of the University of Cologne,

132 permanently anchored in Cologne-Bayenthal (Rhine-km 684.5). Behind the boat, a float with

133 channels is attached in the downstream direction, allowing biofilms to grow on different

134 substrates under natural conditions. These channels have a depth of 0.5 m, and the water

135 current of the River Rhine is slowed down to 0.8 m s^{-1} on average, representing the conditions

136 of the neighbouring groyne fields (Ackermann *et al.*, 2011).

137

2.2. Field experiment: natural microplastic concentration in biofilms

138

2.2.1. Sample exposition in the River Rhine

139

140 In total 96 clay tiles (4.9 x 4.9 x 0.5 cm) were deposited in the float channels of the

141 Ecological Rhine Station in the River Rhine in February 2020. After 6 months (September

142 2020), biofilms were carefully removed from 12 tiles with a wooden brush with natural fibres,

143 filled up to 40 ml with unfiltered River Rhine water, and stored in glass bottles covered with

6

144   aluminium foil in a -18 °C freezer. The operators were careful not to contaminate the samples

145   with MPs from clothes or atmospheric plastic particles while taking the samples. In addition,

146   three control samples of River Rhine water were taken in the same manner, including stirring

147   with the brush but without the biofilms, and stored under the same conditions. The procedure

148   was repeated after 12 months (February 2021) and 18 months (September 2021).

149

150   ### 2.2.2.   Sample analysis

151   The samples were analysed in a laboratory at the University of Bayreuth. To prevent

152   contamination, all samples were handled in laminar flow boxes (Laminar Flow Box FBS,

153   Spetec GmbH). Furthermore, the laboratory was equipped with an air purifier (DustBox

154   withHEPA H14 filter, Möcklinghoff LufttechnikGmbH). All tools and devices were cleaned twice

155   before and after each usage by rinsing with filtered deionized water and filtered 35% ethanol

156   (2 and 0.2 µm, respectively). All chemicals, solutions, and liquids were filtered before use.

157   Cotton lab coats were worn during the sample preparation and analysis. Prior to analysis with

158   Micro-Fourier transform infrared spectroscopy (µFTIR), the samples were purified with an

159   enzymatic-oxidative purification protocol based on the method (Löder et al. (2017)). Organic

160   matter was destroyed with sequential incubation in sodium dodecyl sulphate and protease,

161   followed by density separation in zinc chloride solution (density 1.7 - 1.8 g cm^{-3}) to remove

162   mineral particles. Dependent on the amount of material left, samples were subdivided (a

163   minimum ¼ was used) as described by Rolf et al. (2022) and finally filtered onto Anodisc filters

164   (mesh size 0.2 µm, 25 mm diameter Anodisc, Whatman GE Healthcare) for µFTIR imaging.

165   The samples were measured with a LUMOS II µFTIR spectrometer (Bruker Optics GmbH &

166   Co. KG, Ettlingen, Germany) equipped with a 32x32 detector pixel focal plane array (FPA)

167   detector.

168   We measured the whole sample filters in transmission mode in a wave number range from

169   3600 to 1250 cm^{-1} with a resolution of 8 cm^{-1} and an accumulation of 2 scans. The background

170   was measured with an accumulation of 36 scans on the pure Anodisc filter. The focal plane

171   array detector combined with the IR objective results in a spatial resolution of 5.9 µm per pixel.

7

172 The data was converted to the ENVI file format in the Bruker OPUS Software (version 7.5)

173 imported in the Epina ImageLab software (version 3.47) and the polymer type of each particle

174 identified by a random forest decision classifier software tool for MPs

175 ('BayreuthParticleFinder'). This classifier can identify 22 different polymers automatically and

176 enables an extremely rapid analysis within 0.5 h per filter. Each automatically identified MPs

177 particle was manually double-checked against reference spectra according to a four-eye

178 principle by experienced staff for quality assurance. Subsequently, the particle sizes were

179 measured and shapes recorded from the photographs of the Anodisc filters. The largest

180 dimension was considered as the particle size.

181 To be able to compare the MPs size distribution to the study of Rolf et al. (2022), we adapted

182 their size classes and added an additional size class at the lowest size spectrum because we

183 were particularly interested in small MPs. Thus, we used the following nine size classes: <11

184 μm, 11–50 μm, 51–100 μm, 101–150 μm, 151–300 μm, 301–500 μm, 501–1000 μm, 1001–

185 5000 μm and > 5000 μm. Additionally, we assigned the particles to three shape categories,

186 namely fragments, fibres and pixels. Pixels describe particles with only one pixel in diameter

187 and thus an undetermined shape but with an IR spectrum of MPs.

188 ### 2.3. Laboratory experiments: Biofilms and protists

189 #### *2.3.1. Microplastic particles for laboratory experiments*

190 For all laboratory experiments, Fluoresbrite® polystyrene monodispersed microspheres

191 (Polysciences Europe GmbH, Hirschberg an der Bergstrasse, Germany) internally dyed with

192 phyco-erythrin ('polychromatic red', 525-565 nm excitation, Ø 1 μm and Ø 6 μm) and

193 fluorescein ('yellow-green', 441-485 nm excitation, Ø 10 μm) produced by Polysciences, Inc.,

194 were used as MP model particles. As the MPs came in suspension, we diluted the MPs

195 concentration to our desired concentration of 500 particles ml^{-1} of 6 μm-sized particles in the

196 first experiment and 1 μm, 6 μm, and 10 μm-sized particles each in the second experiment.

197 The MPs concentration for the experiments was chosen to be similar to previous exposure

198 experiments (GESAMP, 2016).

2.3.2. Experimental setup in endless flow channels

Prior to the experiments, biofilms were grown under natural conditions in the direct flow of the River Rhine for 30 days on clay tiles (4.9 x 4.9 x 0.5 cm) attached to concrete holders in the flow channels of the Ecological Rhine Station in December 2018 and March 2019, respectively. The retention of MPs by biofilms on rough clay tiles was compared to other surfaces without biofilms in an experiment using four endless flow channels (Figure 1, for details of the flow channel, see Schössow, Arndt & Becker, 2016). The oval-shaped flow channels were equipped with paddle wheels connected to an electromotor by which the flow velocity can be adjusted manually. For the experiments, the channels were filled with 10 L of filtered River Rhine (Whatman® GF/C filters, pore size: 1.2 µm, Whatman plc, Maidstone, Kent, United Kingdom) and 10 L of regular tap water. Frames help the samples in place and were installed on the opposite side of the paddle wheels (Figure 1). The clay tiles with biofilms were inserted 24 h before the experiments in two of the four channels to ensure that the biofilms could acclimate to the water temperature, light conditions, and flow velocities in the setup.

In the first experiment, four types of substrate were exposed in the experimental flow channels for comparison in addition to the biofilm samples on the rough clay tiles. Rough and smooth acrylic glass tiles, and rough and smooth clay tiles (4.9 x 4.9 x 0.5 cm) without biofilms were exposed to the MPs suspension to determine the retention effects of the surface properties (Figure 1). In experiment 2, only rough clay tiles with and without biofilms were compared (for experimental details and the number of replicates, see supplementary information Table SI-1 and Table SI-2.)

In both experiments, the substrates were exposed for 24 h to the artificial MPs particles. Afterwards, the substrate surfaces were taken as samples using a brush and rinsing with filtered River Rhine water (10 ml for tiles without biofilms, and 25 ml for tiles with biofilms to allow repeated rinsing) and transferred into 50 ml screw-cap tubes (Sarstedt, Germany). To determine the concentration of the suspended MPs, water samples were taken in three replicates per sample spot in front, above, and behind the frames using a syringe with a broad

227   opening, and filled into 15 ml graduated centrifuge tubes (Sarstedt, Germany). All samples

228   were stored in the dark at 4 °C.

229   MPs concentration of samples were quantitatively analysed using an Axiostar Plus

230   Fluorescence (FL) microscope (Carl Zeiss Jena GmbH, 07740 Jena, Germany), which was

231   connected to an external lightning unit (HXP-120, Zeiss, Germany) for fluorescence excitation

232   and excitation light of the filter set 38 HE as recommended by the MPs manufacturer (see

233   2.3.2., excitation BP470/40, beam Splitter FT 495, emission BP 525/50, Zeiss, Germany).

234   Concentrations of MPs in biofilms and the water column were determined by counting the

235   fluorescent MPs particles in a defined sample volume (2 µl for biofilms and 5 µl for water

236   samples) placed on glass objectives with three replicates. MPs counts per cm² of substrate

237   were calculated by means of the three replicates multiplied by the dilution through rinsing

238   divided by the tiles' surface area. We assumed an average biofilm depth of 100 µm.

239   The hydrodynamic conditions were calculated based on Arnon *et al.* (2009). The mean flow

240   rate was calculated with $Q = U * w * d$ for each flow velocity U of 0.1 m s^{-1} and 0.2 m s^{-1}, the

241   tank width *w* of 0.14 m and water column depth *d* of 0.1 m. Froude number was calculated with

242   Fr = U / $\sqrt{g * d}$, with *g* as the gravitational constant 9.81 m s^{-2} and the water column depth *d*.

243   The Reynolds number was calculated for the three particle sizes and two flow velocities to be

244   between 0.0996 and 1.992, thus, Stokes' Law was applied to calculate the settling velocities

245   of the particles:

246    $v = \frac{2\,(\rho_p - \rho_w)}{9 * \mu} * g * r^2$, with ρ_p as the density of the particles (polystyrene, 1050 kg m^{-3}), ρ_w

247   of the fluid, µ as the dynamic viscosity of water (at 10°C as this was measured for the first

248   Experiment) and *r* as the particle radius (Table 1).

249

250

251   ***2.3.3. Microplastic uptake by protists***

252   The uptake of MPs was studied for the biofilm-associated ciliate *Stentor coeruleus*

253   (Stentoridae), which is a stalked, omnivorous filter-feeder (Fenchel, 1987). *S. coeruleus* was

254　chosen for the experiments because of its occurrence in the River Rhine at Cologne and its

255　large size of 250 µm to 1.5 mm (Ackermann *et al.*, 2011), which facilitates optical analysis of

256　MPs uptake. Cultures of *S. coeruleus* were obtained from Helbig (Prien am Chiemsee,

257　Germany) and stored at 20 °C under laboratory conditions. The cultures were fed with

258　*Chlorococcum sp.* (Chlorococcaceae; "Lebendkulturen Helbig", Prien am Chiemsee,

259　Germany) and *Chlamydomonas asymmetrica* (Chlamydomonadaceae; Culture collection of

260　algae of the University of Cologne (CCAC)) on every third to fourth day.

261　The ingestion of MPs by *S. coeruleus* was studied for 6 µm and 10 µm particles with varying

262　MPs concentrations (500 p ml^{-1}, 1250 p ml^{-1}, 2500 p ml^{-1}, 5000 p ml^{-1}). The MPs suspension

263　was vortexed prior to the experiment to avoid aggregation. Before each experiment, 70 ml of

264　the ciliate medium with particles and 15 ml of the *S. coeruleus* cultures were transferred into

265　120 ml tubes. Experiments were run in three replicates for one hour for each concentration of

266　500 p ml^{-1}, 1250 p ml^{-1}, 2500 p $ml^{-1,}$ and 5000 p ml^{-1} and controls without MPs. To prevent

267　sedimentation of particles, experimental tubes were attached to a plankton wheel (2.39 rpm).

268　For counting, 1 ml was taken from the 120 ml tubes and immediately transferred to a

269　Sedgewick-Rafter cell. All *S. coeruleus* specimens were then immediately examined alive and

270　individually for MPs uptake under the microscope (10x magnification with fluorescent light,

271　Axiophot Fluorescent Microscope, ZEISS), because fixation methods might have led to

272　egestion and underestimation of the ingested MP amount (Pace & Bailiff, 1987).

273

274　**2.1.　Statistical analyses**

275　The data of the field and laboratory experiment were analysed in the R programming

276　environment (version 3.5.2, R Core Group 2018, packages: ggplot, dunn.test) to identify

277　significant differences between MPs concentrations in biofilms and River Rhine water as

278　controls, the influence of different substrate on MPs concentration and influence of ambient

279　MPs concentration on the ingestion of MPs by ciliates. Before data analysis, the data structure

280　was checked for normality, heteroscedasticity and outliers (Zuur, Ieno & Elphick, 2010). Mean

11

281 concentrations between samples were tested for significance using ANOVA as a parametric

282 test or alternatively a Kruskal-Wallis-Test as a non-parametric test. Data is reported as mean

283 with standard deviation. The control groups, in which no MP particles were used, were zero in

284 all experiments and thus were not included in the statistical tests.

285

3. Results and Discussion

3.1.   Natural microplastic concentrations in biofilms in the River Rhine

288 After 6 months in the River Rhine, biofilms on the tiles, which equal 40 ml of Rhine water plus

289 biofilm from one tile, contained a mean value of 240 ± 143 MPs per tile (n = 5, Figure 2A),

290 corresponding to 10 MPs cm^{-2} of biofilms. This value was significantly higher than in the control

291 samples with the same amount of river water (24 ± 30 MPs per 40 ml, n = 4, p < 0.5, Kruskall-

292 Wallis and post-hoc Dunn test (method 'holm')). In the 12-month-old biofilms, the average

293 concentration was 147 ± 88 MPs per tile (n = 4). While in the 18-month-old biofilms, the

294 concentration was 93 MPs per tile (n = 4) which was not significantly different from the

295 corresponding controls with 48 ± 18 MPs per ml (Kruskall-Wallis and post-hoc Dunn test

296 (method 'holm'), n = 3). During the transportation of the frozen samples by a transportation

297 company to the University of Bayreuth for analysis, several samples were destroyed, which

298 led to varying number of replicates and the total loss of the control samples after 12 months.

299 Converting the MPs concentration of biofilm samples to area, the average MPs abundance

300 ranges between 4 and 10 MPs cm^{-2} of biofilm covered surface in the size range of 5.9 to 5000

301 μm. The thickness of biofilms in river water can vary between 140 - 160 μm after 40 days

302 (Roche *et al.*, 2017) to several mm (Zhang & Bishop, 1994; Arnon *et al.*, 2009). Assuming that

303 biofilms have an average thickness of 1 mm with a density close to water, the calculated

304 concentration per weight ranges between 38,734 and 99,958 MP kg^{-1} depending on duration.

305 Currently, no data on MPs concentration in aquatic biofilms is available for comparison, and

306 also comparison to MPs concentration in surface water or sediments is limited due to different

307 physical and chemical properties of the environmental compartments, and methodological and

12

308 analytical procedures. For floodplains, Rolf *et al.* (2022) reported a concentration of 25,502 to

309 51,119 MP kg^{-1} in 0 - 5 cm depth and 25,616 - 84,824 MP kg^{-1} in 5 - 20 cm depth. Mani *et al.*

310 (2016) analysed the MPs profile along the River Rhine and reported around 2 to 6 MPs m^{-3} of

311 Rhine water ranging from 300 µm to 5 mm in size in the area of Cologne, while Schrank et al.

312 (2022) found 0.7 to 354.9 MPs m^{-3} in the size range of 20 µm to 5000 µm on different sample

313 spots of surface waters along the river Rhine. Our river water controls contained 32 ± 27 MPs

314 per 40 ml, which equals around 800,000 MPs m^{-3}. One reason for this high number on

315 comparison to the other studies might be that we analysed MPs down to a size 5.9 µm.

316 Compared to the controls, the biofilm samples show a high standard deviation of MPs

317 concentration, especially taken after 6 months (Figure 2A). One factor could be the retention

318 of MPs agglomerations in single sample, another might be biofilm morphology. Biofilms grow

319 heterogeneous even on small areas that lead to differences in coverage, thickness, and

320 composition (Figure 1B, and e.g. Walker, Sargison & Henderson, 2013), which in turn influence

321 MPs concentrations in the samples. One reason for the heterogeneous growth are seasonal

322 changes that influence the morphology and composition of biofilms. For example, ciliates like

323 peritrichs are likely to occur during colder months, whereas heterotrichs have been found

324 during warmer periods, where the algae as the main food source for this group peaks

325 (Ackermann *et al.*, 2011). However, this should mean that the samples taken after 6 and 18

326 months should have similar concentrations or, due to the accumulation of MPs, increasing

327 concentrations, of which both is not the case. Weather data for the 14 days before sample

328 extraction indicate that temperature and rain fall were similar in September of 2020 and 2021

329 (Supplementary Figure SI-1). Daily sunshine duration was longer in 2020, which might have

330 increased algae abundance and biofilm growth. Hence, mature biofilms with developed surface

331 morphology might have retained more MPs in this year. If biofilms incorporate MPs for longer

332 periods, it might also be the case that the biofilms have been exposed to a high MPs

333 concentration before the sampling date. On the sampling date, MPs concentration in the

334 biofilms were still increased, while the control concentration showed the current concentration

335 being low again. Local MP concentration in rivers is influenced by population density, the

13

336   amount of drainage systems from wastewater treatment plants leading into the river, and heavy

337   rainfalls that wash of litter and MPs from roads and urban surfaces (Zhao *et al.*, 2014; Mani *et*

338   *al.*, 2016; Siegfried *et al.*, 2017).

339   MPs size distribution is similar in all biofilms and control samples after 6, 12, and 18 months

340   (Figure 2B). Between 70 % and 78 % of MPs are smaller than 50 µm, and between 11 % and

341   36 % are smaller than 11 µm in biofilms and control samples (Supplementary Table SI-2). This

342   means that the particle size distribution of MPs in biofilms represents the conditions in the

343   ambient water and that there is likely no size selectivity during particle retention in biofilms.

344   Only 8 % and 25 % and of the particles are larger than 300 µm in the biofilm samples. The

345   river water control samples showed no particles larger than 300 µm.

346   A similar size distribution was found in the study by Rolf *et al.* (2022), who reported that 75 %

347   of MPs are in size of 11 - 150 µm for the year 2019 in the Cologne area. For 2021 (6-month

348   duration) and 2022 (18-month duration), we found a similar size distribution with 72 % to 78 %

349   particles between 11 - 150 µm. Overall, our results also confirm that with decreasing size the

350   amount of MPs increases, except for particles between 5.9 -11 µm. In contrast to Rolf *et al.*

351   (2022), we found most particles in size of 11 - 50 µm and not between 101 - 150 µm. This

352   coincides more with MPs found in the River Elbe (Germany), in which 96 % of MPs in the water

353   column were smaller than 20 µm with the smallest analysed diameter of 4 µm (Triebskorn *et*

354   *al.*, 2019). However, these small particle sizes are at the resolution limit of µFTIR used for MPs

355   identification, and might therefore affect data quality. The analysis of small MPs size has

356   always been difficult, especially in the early years of MP investigations. For along time, a mesh

357   size of 330 µm, which is typical for plankton sampling, was selected as lower cut-off point to

358   analyse particle sizes, not only in rivers (Mani *et al.*, 2016), but also in marine environments

359   (Moore *et al.*, 2001; Botterell *et al.*, 2020). More recent studies like this one or by Rolf *et al.*,

360   (2022) increasingly try to include smaller MPs sizes and can show that MPs concentrations

361   are often underestimated because of differences in the cut-off point (Huvet *et al.*, 2016).

362

363 MPs properties regarding shape and material are also similar in biofilms compared to the Rhine

364 water controls (Figure 2C). Fragments accounted for the majority of MPs shape in our study,

365 ranging between 76.3 % and 84.3 % in the samples, while pixels range between 12.8 % and

366 22.6 %, and fibres between 1.1 % and 2.8 % in the biofilm samples. In the control samples,

367 61.1 % and 86.1 % were fragments, 11.1 % and 30.5 % were pixels and 2.8 % and 8.3 % were

368 fibres similar to previous studies with 65 % of the particles in floodplain soils being fragments

369 (Rolf *et al.*, 2022). In total, 16 different polymer types were identified (Figure 2D). The most

370 frequent polymers were Polyethylene (PE), Polypropylene (PP), and Polystyrene (PS). This is

371 similar to MPs found in the floodplains in the River Rhine (Rolf *et al.*, 2022) and the water

372 column of the River Elbe in Germany (Triebskorn *et al.*, 2019; Schrank *et al.*, 2022). These

373 three polymers especially are used for packaging (Geyer, Jambeck & Law, 2017). PE and PP

374 have a density lower than water, whereas PS has a higher density. Thus, retention seems not

375 to be dependent on polymer density (Rolf *et al.*, 2022). Only PE is noticeably more abundant

376 in the control samples than the other materials. Again, we assume that slight variations

377 between MPs in biofilms and the Rhine water controls regarding particle size, shape, and

378 material are probably due to temporal changes in MPs concentration and the ability of biofilms

379 to "store" MPs over some time. Additionally, it was shown for natural particles that the

380 concentrations within the biofilms can vary depending on particles size, particle material, and

381 fluid velocity (de Beer et al., 1996; Arnon et al., 2010; Walker, Sargison & Henderson, 2013;

382 Roche *et al.*, 2017).

383

384 **3.2.   Retention of microplastics by biofilms in flow channels**

385 In the lab experiments, it was possible to identify and count all three sizes of the fluorescent

386 MPs in the samples, i.e., on smooth and rough clay tiles, smooth and rough acrylic tiles, and

387 in the biofilms grown on rough clay tiles (Figure 3A). The retention of MPs by different

388 substrates shows significant differences in biofilms compared to the other substrates (Figure

389 3B). The trapped amount of MPs in biofilms was with 6 - 8 times (velocity of 0.1 m s^{-1}) and

15

390 9 - 12 times (velocity of 0.2 m s^{-1}) significantly larger than on rough and smooth clay tiles, which

391 resemble for example natural stone surfaces (Kruskal-Wallis-Test (* = p < 0.05), post-hoc

392 Dunn-Test with method 'holm'). The highest numbers of MPs retained by biofilms were found

393 at the 0.2 m s^{-1} flow velocity with a mean concentration of 10,899 MP per cm². For acrylic tiles,

394 only the flow velocity of 0.1 m s^{-1} was tested, with 370 MPs m^{-2} for rough and 305 MPs cm^{-2} for

395 smooth acrylic tiles. There were no significant differences of MPs retention between the two

396 flow velocities (0.1 m s^{-1}, 0.2 m s^{-1}) for each of these substrates.

397 Particle size significantly influenced the amount of MPs particles retained in the biofilms and

398 thus the number of the particles trapped in the biofilm increased with increasing particle size

399 (p < 0.001; Figure 3C). The concentration of the retained particles was at least twice as high

400 for the 10 μm particles as for the 1 μm particles. The highest concentrations of particles in the

401 biofilms were found for the 10 μm particle size and it differed significantly between the two flow

402 velocities with 12,639 MPs cm^{-2} for 0.1 m s^{-1} and 16,164 MP cm^{-2} for 0.2 m s^{-1} (p < 0.05, Figure

403 3C). There were no significant differences in the numbers of MPs in the biofilms between the

404 two flow velocities for the MP sizes 1 μm and 6 μm, resp. (Figure 3C). Similar to our results,

405 biofilms recirculating laboratory flumes retained more MPs of 5 μm than 1 μm in size and higher

406 flow velocities (Arnon *et al.*, 2009). It is assumed that larger particles are retained through

407 sedimentation, particle interception and surface straining (Arnon *et al.*, 2009) and an increased

408 flow velocity pushes particles deeper into the three-dimensional structure of the biofilms where

409 they are entrapped (Reynolds & Carling, 1991; De Beer, Stoodley & Lewandowski, 1996;

410 Risse-Buhl & Küsel, 2009). Our results of the field studies (flow velocity 0.8 m s^{-1}) cannot

411 confirm this as we can see no differences in the density distribution of particle sizes retained

412 in the biofilms and the bulk water of the River Rhine. Additionally, the flow channel experiments

413 in this study and by Arnon *et al.* (2009) used only a small fraction of particle size. For larger

414 particles, the particle properties in combination with flow velocity might cause a different

415 encounter behavior than in smaller particles (Rubenstein & Koehl, 1977; Shimeta & Jumars,

416 1991).

16

417   The mean volume flow rate for the flow tank during the experiments was around 0.0014 m³ s⁻

418   ¹ for 0.1 m s⁻¹ and 0.0028 m³ s⁻¹ for 0.2 m s⁻¹ (Table 1). The Froude number is indicating slow

419   flow (Fr <1) of 0.1 and 0.2, which is typical for rivers (Boavida *et al.*, 2011; Kuriqi & Ardiçliolu,

420   2018). The particle settling velocities were calculated for the duration of the experiment as

421   0.59 m 24h⁻¹, 2.07 m 24h⁻¹ and 58.63 m 24h⁻¹ for 1 μm, 6 μm, and 10 μm particles, respectively.

422   This means that the particles could have sedimented to the bottom of the tank within the

423   experimental duration.

424   The particle recovery was calculated for experiment 2 by the sum of the particles in biofilms

425   and bulk water divided by the number of particles at the beginning of the experiment (500 p ml⁻

426   ¹). On average for all particle sizes, 42.64 ± 15.4 % (27.8-70 %) were recovered, slightly less

427   than Arnon et al. (2009) presented with a 50 - 70 % recovery.

428   Bases on the low MPs retention of acrylic tiles (Figure 2B), the tank's material of the flow

429   channel has only a small influence in the results.

430

431   3.3.   Microplastic uptake by *protists*

432   We could identify and count the 6 μm and 10 μm MPs particles in the cell body of *Stentor*

433   *coeruleus* (Figure 4C) after one hour of exposure at different MPs concentrations (0 p ml⁻¹, 500

434   p ml⁻¹, 1250 p ml⁻¹, 2500 p ml⁻¹, 5000 p ml⁻¹). At the initial concentration of 10000 p ml⁻¹, it was

435   too difficult to identify individual particles inside the cells. The results show that the amount of

436   MPs ingested by the ciliate increases with increasing exposure concentration: Almost every

437   increase in the exposure concentration led to a significant increase in particle concentration in

438   *S. coeruleus* for 6 μm and 10 μm particles (Figure 4E). The maximum amount of ingested MPs

439   was counted at an exposure concentration of 5000 p ml⁻¹ with a mean of 21 MPs Ind⁻¹ for the

440   6 μm and 10 μm particles. There were no significant differences related to particle sizes; both

441   were ingested in the same amount.

442   The ingestion of MPs strongly depends on the feeding types of the protist species (Fenchel,

443   1987). As a non-selective suspension feeder that prefers bacteria and algae of 7 - 22 μm in

444 size (Wenzel & Liebsch, 1975; Foissner, Berger & Kohmann, 1992), *S. coeruleus* shows the

445 expected MPS ingestion in the size of 6 μm and 10 μm. We therefore assume that all non-

446 selective, suspension-feeding and filter-feeding protists in biofilms also ingest MPs. *Oxyrrhis*

447 *marina*, a heterotrophic dinoflagellate, was found to ingest MPs of 7.3 μm, but no larger

448 particles in laboratory studies (Cole *et al.*, 2013). The pelagic ciliate *Tintinnopsis lobiancoi* was

449 tested for MPs (10 μm) uptake with varying concentrations (1,000, 2,000, 10,000 p ml^{-1}) under

450 laboratory conditions. Between 55 to 85 MPs were found per cell and thus were higher than

451 MPs uptake by other zooplankton taxa testet,under the same conditions such as copepoda,

452 cladocera, polychaeta, rotifera, or mysida (Setälä *et al.*, 2014). Two holotrich ciliates isolated

453 from South African streams ingested MPs particles at the same rate as microbial prey with up

454 to 3870 MPs h^{-1} (Bulannga & Schmidt, 2022). Other feeding types, such as raptorial feeding

455 amoeba, are likelier to feed on particles attached to the biofilms (Arndt *et al.*, 2003; Böhme *et*

456 *al.*, 2009). Smaller protists, e.g., flagellates of sizes 1 - 450 μm (Jeuck & Arndt, 2013), are likely

457 to ingest even smaller MPs.

458

459 Besides the more recent interest in MPs and protozoans, researchers have used artificial

460 particles already in the 60th, 70[th,] and 80th to study feeding types, clearance rate, bacterivory,

461 or cyclosis in ciliates, flagellates and amoeba (examples are Mueller, Röhlich & Törö, 1965;

462 Weisman & Korn, 1967; Batz & Wunderlich, 1976; Fenchel, 1980; Borsheim, 1984; Jonsson,

463 1986; McManus & Fuhrman, 1986; Sherr, Sherr & Fallon, 1987). Heterotrophic flagellates

464 (Pace & Bailiff, 1987) and pelagic protists (Batz & Wunderlich, 1976; Jonsson, 1986; McManus

465 & Fuhrman, 1986) show a steady state of particle ingestion and egestion after a while. In a

466 study by Eisenmann *et al.* (2001), the ciliate *Epystilis* ingested up to 1,000 particles per

467 individual after 3.5 hours of the 24 h experiment with biofilms. After this peak, the number of

468 ingested particles per ciliate decreased rapidly until they did not contain any particles at the

469 end of the experiment. Instead, particles were rather attached to the stalks of the ciliates

470 (Eisenmann *et al.*, 2001). Regarding a potential selectivity of MPs, Sherr *et al.* (1987)

471 compared the uptake of fluorescent-labelled bacteria and fluorescent latex particles by ciliates

18

472   and flagellates, which showed that the uptake ratios were 10:1 (bacteria vs. latex particles) for

473   the ciliates and 6:1 for the flagellates, thus bacteria were preferred over the plastic particles

474   for both groups. These results indicates an ability of protists to distinguish between different

475   particle types and suggest a slight discrimination of particles of bad food quality, which was

476   shown in other studies (Sherr *et al.*, 1987). Similar observations were made for flagellates

477   (McManus & Fuhrman, 1986) and for amoeba (Bowser and Olszweski, 1983; Winiecka-

478   Krusnell et al., 2009). Fenchel (1980) showed particle discrimination by size in suspension-

479   feeding protozoans due to the functionality of the mouth apparatus, but no discrimination for

480   particle type (Fenchel, 1980). However, subsequent studies showed that particle uptake by

481   ciliates correlates with particle concentration and particle size, the ladder depending also on

482   cell size of the protozoans (Jonsson, 1986).

483   Our results of the experiments with *Stentor coeruleus* and previous studies prove that many

484   protists can ingest MPs. This raises the question: What happens after ingestion, and which

485   effects have MPs on protists? None of the early studies specifically investigated further

486   ecological effects. In more recent studies, the benthic foraminiferan *Haynesina germanica* was

487   exposed to virgin polypropylene pellets for 10 hours, which showed no lethal or short-term

488   effects on locomotion or metabolism (Langlet *et al.*, 2020). It seems as if protists handle MPs

489   like other inert and indigestible items, resulting in a seemingly harmless expulsion of particles.

490   Surface properties are essential for predatory ciliates to identify their prey (Kersnowska, Peck

491   & Haller, 1988) and can influence their clearance rate (Sanders, 1988). For nanomaterials,

492   surface charges affect bioavailability (Zhu *et al.*, 2013) in addition to abundance, size, shape,

493   aggregation, age, colour, density, and selectivity of species (Botterell *et al.*, 2020). Similarily,

494   the absorption of organic matter that forms a so called eco-corona (Shi *et al.*, 2023),the

495   settlement of microbial organisms and the formation of biofilms on plastic litter and MPs is

496   suspected to alter physical and biological properties, influences biofilm composition and thus

497   the availability to grazing and predatory organisms on higher trophic levels (Yokota *et al.*, 2017;

498   Büks, Schaik & Kaupenjohann, 2020; Michler-Kozma, Neu & Gabel, 2022). Another effect

499   might be posed by plastic additives that leach during the degradation processes of litter. MPs

19

leachates did not have lethal or adverse effects on the activity in benthic foraminiferans (Langlet *et al.*, 2020) but caused oxidative stress when ingested into cells-based bioassays used for ecotoxicological effects (Rummel *et al.*, 2019).

3.4. Conclusion

MPs are retained by biofilms and lead to higher concentrations within biofilms than the ambient water or on other surfaces. Environmental factors, like MPs concentration and size, seasonal changes or flow velocity influence particles retention, as does the biofilm morphology and the presence of protists. The complex three-dimensional structure wih pits, grooves, and caves increases the surface and entraps particles (Mikos & Peppas, 1990; Drury, Characklis & Stewart, 1993; Okabe, Yasuda & Watanabe, 1997; Böhme *et al.*, 2009; Roche *et al.*, 2017). During growth, mature biofilms often reach a thickness that cannot withstand the forces of river flow velocities and parts of the biofilms can tear off, also called sloughing (Wanner & Gujer 1986; Okabe *et al.*, 1997), which might lead to MPs redistribution (Drury *et al.*, 1993). MPs can be found in the depth of biofilms within 90 min and can remain there for 20 days or longer (Stoodley, DeBeer & Lewandowski, 1994; Okabe *et al.*, 1997). The relation of the temporal, spatial and biological characteristics of biofilms make it difficult to estimate the "storage potential" of MPs within biofilms and the ecological effects. As pores become significantly smaller towards the substrate, the biofilm becomes increasingly dense (Zhang & Bishop, 1994) and might become clogged with MP altering the flow field around biofilms that is essential for mass transfer and oxygen flux (De Beer *et al.*, 1996; Reichert & Wanner, 1997). The presence of MPs down to a size of 5.9 µm and the ingestion of these MPs by protists prove that plastics are likely to enter the food web in lower trophic levels than suggested. These small have a higher relevance on ecological effects, as shown for < 20 µm, especially for particles < 1µm (Triebskorn *et al.*, 2019). To date, research has mostly focused on vertebrates and invertebrates (de Sá *et al.*, 2018), and there is a lack of information on the exposition and effects of MP in biofilms and protists (Rillig & Bonkowski, 2018; Langlet *et al.*, 2020). More

20

527   research is required to test the effects of MPs and various polymer types, shapes, and sizes

528   on single protists and microbial communities, similar as it has yet been investigated for

529   metazoans. This helps estimate ecological risks in aquatic environments and might establish

530   biofilms as assessable MPs sink or monitoring system (More *et al.*, 2014; Li *et al.*, 2018b).

531

532

533

4. Acknowledgments

5. Funding

6. References

Ackermann B., Esser M., Scherwaß A. & Arndt H. (2011). Long-Term Dynamics of Microbial Biofilm Communities of the River Rhine with Special References to Ciliates. *International Review of Hydrobiology* **96**, 1–19. https://doi.org/10.1002/iroh.201011286

Arndt H., Schmidt-Denter K., Auer B. & Weitere M. (2003). Protozoans and Biofilms. *Fossil and Recent Biofilms* **189**, 161–179. https://doi.org/10.1007/978-94-017-0193-8_10

Arnon S., Marx L.P., Searcy K.E. & Packman A.I. (2009). Effects of overlying velocity, particle size, and biofilm growth on stream-subsurface exchange of particles. *Hydrological Processes* **20**, n/a-n/a. https://doi.org/10.1002/hyp.7490

Auta H.S., Emenike C.U. & Fauziah S.H. (2017). Distribution and importance of microplastics in the marine environmentA review of the sources, fate, effects, and potential solutions. *Environment International* **102**, 165–176. https://doi.org/10.1016/j.envint.2017.02.013

Battin T.J., Besemer K., Bengtsson M.M., Romani A.M. & Packmann A.I. (2016). The ecology and biogeochemistry of stream biofilms. *Nature Reviews Microbiology* **14**, 251–263.

22

560   https://doi.org/10.1038/nrmicro.2016.15

561   Batz W. & Wunderlich F. (1976). Structural transformation of the phagosomal membrane in

562   Tetrahymena cells endocytosing latex beads. *Archives of Microbiology* **109**, 215–220.

563   https://doi.org/10.1007/BF00446631

564   De Beer D., Stoodley P. & Lewandowski Z. (1996). Liquid flow and mass transport in

565   heterogeneous biofilms. *Water Research* **30**, 2761–2765. https://doi.org/10.1016/S0043-

566   1354(96)00141-8

567   Besseling E., Quik J.T.K., Sun M. & Koelmans A.A. (2017). Fate of nano- and microplastic in

568   freshwater systems: A modeling study. *Environmental Pollution* **220**, 540–548.

569   https://doi.org/10.1016/j.envpol.2016.10.001

570   Bighiu M.A. & Goedkoop W. (2021). Interactions with freshwater biofilms cause rapid removal

571   of common herbicides through degradation-evidence from microcosm studies.

572   *Environmental Science: Processes and Impacts* **23**, 66–72.

573   https://doi.org/10.1039/d0em00394h

574   Boavida I., Santos J.M., Pinheiro A.N. & Ferreira M.T. (2011). Fish habitat availability

575   simulations using different morphological variables. *Limnetica* **30**, 393–404

576   Böhme A., Risse-Buhl U. & Küsel K. (2009). Protists with different feeding modes change

577   biofilm morphology. *FEMS Microbiology Ecology* **69**, 158–169.

578   https://doi.org/10.1111/j.1574-6941.2009.00710.x

579   Borsheim K.Y. (1984). Clearance reates of bacteria-sized particles by freshwater ciliates

580   measured with monodisperse fluorescent latex beads. *Oecologia* **63**, 286–288

581   Botterell Z.L.R., Beaumont N., Dorrington T., Steinke M., Thompson R.C. & Lindeque P.K.

582   (2020). Bioavailability and effects of microplastics on marine zooplankton : *Environmental*

583   *Pollution* **245**, 98–110

584   Boucher J. & Friot D. (2017). *Primary microplastics in the oceans: A global evaluation of*

585   *sources.* IUCN International Union for Conservation of Nature, Gland, Switzerland.

586   Branda S.S., Vik Å., Friedman L. & Kolter R. (2005). Biofilms: The matrix revisited. *Trends in*

587   *Microbiology* **13**, 20–26. https://doi.org/10.1016/j.tim.2004.11.006

23

588   Büks F., Schaik N.L. Van & Kaupenjohann M. (2020). What do we know about how the

589   terrestrial multicellular soil fauna reacts to microplastic? 245–267

590   Bulannga R.B. & Schmidt S. (2022). Uptake and accumulation of microplastic particles by two

591   freshwater ciliates isolated from a local river in South Africa. *Environmental Research*

592   **204**. https://doi.org/https://doi.org/10.1016/j.envres.2021.112123

593   Van Cauwenberghe L., Devriese L., Galgani F., Robbens J. & Janssen C.R. (2015).

594   Microplastics in sediments: A review of techniques, occurrence and effects. *Marine*

595   *Environmental Research* **111**, 5–17. https://doi.org/10.1016/j.marenvres.2015.06.007

596   Chen X., Chen X., Zhao Y., Zhou H., Xiong X. & Wu C. (2020). Effects of microplastic biofilms

597   on nutrient cycling in simulated freshwater systems. *Science of the Total Environment*

598   **719**. https://doi.org/10.1016/j.scitotenv.2020.137276

599   Cole M., Lindeque P., Fileman E., Halsband C., Goodhead R., Moger J., *et al.* (2013).

600   Microplastic ingestion by zooplankton. *Environmental Science and Technology* **47**, 6646–

601   6655. https://doi.org/10.1021/es400663f

602   Costerton J.W., Irvin R.T. & Cheng K.J. (1981). The bacterial glycocalyx in nature and disease.

603   *Annual review of microbiology* **35**, 299–324.

604   https://doi.org/10.1146/annurev.mi.35.100181.001503

605   Dris R., Imhof H., Sanchez W., Gasperi J., Tassin B., Laforsch C., *et al.* (2015). Beyond the

606   ocean: Contamination of freshwater ecosystems with (micro-) plastic particles.

607   https://doi.org/https://doi.org/10.1071/EN14172

608   Drury W.J., Characklis W.G. & Stewart P.S. (1993). Interactions of 1 µm latex particles with

609   pseudomonas aeruginosa biofilms. *Water Research* **27**, 1119–1126.

610   https://doi.org/10.1016/0043-1354(93)90003-Z

611   Eisenmann H., Letsiou I., Feuchtinger A., Beisker W., Mannweiler E., Hutzler P., *et al.* (2001).

612   Interception of Small Particles by Flocculent Structures, Sessile Ciliates, and the Basic

613   Layer of a Wastewater Biofilm. *Applied and Environmental Microbiology* **67**, 4286–4292.

614   https://doi.org/10.1128/AEM.67.9.4286-4292.2001

615   Evangeliou N., Grythe H., Klimont Z., Heyes C., Eckhardt S., Lopez-Aparicio S., *et al.* (2020).

616   Atmospheric transport is a major pathway of microplastics to remote regions. *Nature*

617   *Communications* **11**, 3381. https://doi.org/10.1038/s41467-020-17201-9

618 Falco F. De, Pace E. Di, Cocca M. & Avella M. (2019). The contribution of washing processes

619   of synthetic clothes to microplastic pollution. *Scientific Reports*, 1–11.

620   https://doi.org/10.1038/s41598-019-43023-x

621 Fenchel T. (1987). *Ecology of Protozoa*, 1st edn. Springer Berlin Heidelberg, Berlin,

622   Heidelberg.

623 Fenchel T. (1980). Suspension feeding in ciliated protozoa: Functional response and particle

624   size selection. *Microbial Ecology* **6**, 1–11. https://doi.org/10.1007/BF02020370

625 Foissner W., Berger H. & Kohmann F. (1992). *Taxonomische und ökologische Revision der*

626   *Ciliaten des Saprobiensystems – Band II: Peritrichia, Heterotrichida, Odontostomatida*.

627   München.

628 GESAMP (2016). *Sources, fate and effects of microplastics in the marine environment: part 2*

629   *of a global assessment*.

630 Geyer R., Jambeck J.R. & Law K.L. (2017). Production, use, and fate of all plastics ever made.

631   *Science Advances* **3**, e1700782. https://doi.org/10.1126/sciadv.1700782

632 Hoellein T.J., Shogren A.J., Tank J.L., Risteca P. & Kelly J.J. (2019). Microplastic deposition

633   velocity in streams follows patterns for naturally occurring allochthonous particles.

634   *Scientific Reports* **9**, 3740. https://doi.org/10.1038/s41598-019-40126-3

635 Horton A.A., Walton A., Spurgeon D.J., Lahive E. & Svendsen C. (2017). Microplastics in

636   freshwater and terrestrial environments: Evaluating the current understanding to identify

637   the knowledge gaps and future research priorities. *Science of The Total Environment* **586**,

638   127–141. https://doi.org/10.1016/j.scitotenv.2017.01.190

639 Huvet A., Paul-Pont I., Fabioux C., Lambert C., Suquet M., Thomas Y., *et al.* (2016).

640   Quantifying the smallest microplastics is the challenge for a comprehensive view of their

641   environmental impacts. *Proceedings of the National Academy of Sciences of the United*

642   *States of America* **113**, E4123–E4124. https://doi.org/10.1073/pnas.1607221113

643 Jeuck A. & Arndt H. (2013). A Short Guide to Common Heterotrophic Flagellates of Freshwater

25

644   Habitats Based on the Morphology of Living Organisms. *Protist* **164**, 842–860.

645   https://doi.org/10.1016/j.protis.2013.08.003

646 Jonsson P. (1986). Particle size selection, feeding rates and growth dynamics of marine

647   planktonic oligotrichous ciliates (Ciliophora: Oligotrichina). *Marine Ecology Progress*

648   *Series* **33**, 265–277. https://doi.org/10.3354/meps033265

649 Kersnowska M., Peck R.K. & Haller G.D.E. (1988). Cell to Cell Recognition Between the Ciliate

650   Pseudomicrothorax dubius and Its Food Organisms : the Role of Surface Charges. 93–

651   100

652 Klein S., Worch E. & Knepper T.P. (2015). Occurrence and spatial distribution of microplastics

653   in river shore sediments of the rhine-main area in Germany. *Environmental Science and*

654   *Technology* **49**, 6070–6076. https://doi.org/10.1021/acs.est.5b00492

655 Kuriqi A. & Ardiçliolu M. (2018). Investigation of hydraulic regime at middle part of the loire

656   river in context of floods and low flow events. *Pollack Periodica* **13**, 145–156.

657   https://doi.org/10.1556/606.2018.13.1.13

658 Langlet D., Bouchet V.M.P., Delaeter C. & Seuront L. (2020). Motion behavior and metabolic

659   response to microplastic leachates in the benthic foraminifera Haynesina germanica.

660   *Journal of Experimental Marine Biology and Ecology* **529**, 151395.

661   https://doi.org/10.1016/j.jembe.2020.151395

662 Lebreton L.C.M., Van Der Zwet J., Damsteeg J.W., Slat B., Andrady A. & Reisser J. (2017).

663   River plastic emissions to the world's oceans. *Nature Communications* **8**, 1–10.

664   https://doi.org/10.1038/ncomms15611

665 Li J., Liu H. & Chen J.P. (2018a). Microplastics in freshwater systems : A review on occurrence

666   , environmental effects , and methods for microplastics detection. *Water Research* **137**,

667   362–374. https://doi.org/10.1016/j.watres.2017.12.056

668 Li L., Xu G., Yu H. & Xing J. (2018b). Dynamic membrane for micro-particle removal in

669   wastewater treatment: Performance and influencing factors. *Science of the Total*

670   *Environment* **627**, 332–340. https://doi.org/10.1016/j.scitotenv.2018.01.239

671 Lobelle D. & Cunliffe M. (2011). Early microbial biofilm formation on marine plastic debris.

26

672   *Marine Pollution Bulletin* **62**, 197–200. https://doi.org/10.1016/j.marpolbul.2010.10.013

673   Löder M.G.J., Imhof H.K., Ladehoff M., Löschel L.A., Lorenz C., Mintenig S., *et al.* (2017).

674   Enzymatic Purification of Microplastics in Environmental Samples. *Environmental*

675   *Science and Technology* **51**, 14283–14292. https://doi.org/10.1021/acs.est.7b03055

676   Mani T., Hauk A., Walter U. & Burkhardt-Holm P. (2016). Microplastics profile along the Rhine

677   River. *Scientific Reports* **5**, 17988. https://doi.org/10.1038/srep17988

678   McManus G.B. & Fuhrman J.A. (1986). Bacterivory in seawater studied with the use of inert

679   fluorescent   particles.   *Limnology   and   Oceanography*   **31**,   420–426.

680   https://doi.org/10.4319/lo.1986.31.2.0420

681   Michler-Kozma D.N., Neu T.R. & Gabel F. (2022). Environmental conditions affect the food

682   quality of plastic associated biofilms for the benthic grazer Physa fontinalis. *Science of*

683   *The Total Environment* **816**, 151663. https://doi.org/10.1016/j.scitotenv.2021.151663

684   Mikos A.G. & Peppas N.A. (1990). Bioadhesive analysis of controlled-release systems. IV. An

685   experimental method for testing the adhesion of microparticles with mucus. *Journal of*

686   *Controlled Release* **12**, 31–37. https://doi.org/10.1016/0168-3659(90)90180-2

687   Moore C.., Moore S.., Leecaster M.. & Weisberg S.. (2001). A Comparison of Plastic and

688   Plankton in the North Pacific Central Gyre. *Marine Pollution Bulletin* **42**, 1297–1300.

689   https://doi.org/10.1016/S0025-326X(01)00114-X

690   More T.T., Yadav J.S.S., Yan S., Tyagi R.D. & Surampalli R.Y. (2014). Extracellular polymeric

691   substances of bacteria and their potential environmental applications. *Journal of*

692   *Environmental Management* **144**, 1–25. https://doi.org/10.1016/j.jenvman.2014.05.010

693   Mueller M., Röhlich P. & Törö I. (1965). Studies on Feeding and Digestion in Protozoa. VII.

694   Ingestion of Polystyrene Latex Particles and its Early Effect on Acid Phosphatase in

695   Paramecium   multimicronucleatum   and   Tetrahymena   pyriformis.   *The   Journal   of*

696   *Protozoology* **12**, 27–34. https://doi.org/10.1111/j.1550-7408.1965.tb01807.x

697   Nizzetto L., Bussi G., Futter M.N., Butterfield D. & Whitehead P.G. (2016). A theoretical

698   assessment of microplastic transport in river catchments and their retention by soils and

699   river sediments. *Environmental Science: Processes and Impacts* **18**, 1050–1059.

700   https://doi.org/10.1039/c6em00206d

701   Okabe S., Yasuda T. & Watanabe Y. (1997). Uptake and release of inert fluorescence particles

702   by mixed population biofilms. *Biotechnology and Bioengineering* **53**, 459–469.

703   https://doi.org/10.1002/(SICI)1097-0290(19970305)53:5<459::AID-BIT3>3.0.CO;2-G

704   Pace M. & Bailiff M. (1987). Evaluation of a fluorescent microsphere technique for measuring

705   grazing rates of phagotrophic microorganisms. *Marine Ecology Progress Series* **40**, 185–

706   193. https://doi.org/10.3354/meps040185

707   Peeken I., Primpke S., Beyer B., Gütermann J., Katlein C., Krumpen T., *et al.* (2018). Arctic

708   sea ice is an important temporal sink and means of transport for microplastic. *Nature*

709   *Communications* **9**, 1505. https://doi.org/10.1038/s41467-018-03825-5

710   Preusser F. (2008). Characterisation and evolution of the River Rhine system. *Geologie en*

711   *Mijnbouw/Netherlands Journal of Geosciences* **87**, 7–19.

712   https://doi.org/10.1017/S0016774600024008

713   Reichert P. & Wanner O. (1997). Movement of solids in biofilms: Significance of liquid phase

714   transport. *Water Science and Technology* **36**, 321–328. https://doi.org/10.1016/S0273-

715   1223(97)00339-9

716   Reynolds C.S. & Carling P.A. (1991). Flow in river channels: new insights into hydraulic

717   retention. *Archiv fur Hydrobiologie* **121**, 171–179.

718   https://doi.org/https://doi.org/10.1127/0003-9136/91/0121-0171

719   Rillig M.C. & Bonkowski M. (2018). Microplastic and soil protists: A call for research.

720   *Environmental Pollution* **241**, 1128–1131. https://doi.org/10.1016/j.envpol.2018.04.147

721   Risse-Buhl U. & Küsel K. (2009). Colonization dynamics of biofilm-associated ciliate

722   morphotypes at different flow velocities. *European Journal of Protistology* **45**, 64–76.

723   https://doi.org/10.1016/j.ejop.2008.08.001

724   Roche K.R., Drummond J.D., Boano F., Packman A.I., Battin T.J. & Hunter W.R. (2017).

725   Benthic biofilm controls on fine particle dynamics in streams. *Water Resources Research*

726   **53**, 222–236. https://doi.org/10.1002/2016WR019041

727   Rolf M., Laermanns H., Kienzler L., Pohl C., Möller J.N., Laforsch C., *et al.* (2022). Flooding

28

728   frequency and floodplain topography determine abundance of microplastics in an alluvial

729   Rhine soil. *Science of the Total Environment* **836**, 155141. https://doi.org/10.1016/j.scitotenv.2022.155141

730

731 Rubenstein D.I. & Koehl M.A.R. (1977). The Mechanisms of Filter Feeding: Some Theoretical

732   Considerations. *The American Naturalist* **111**, 981–994. https://doi.org/10.1086/283227

733 Rummel C.D., Escher B.I., Sandblom O., Plassmann M.M., Arp H.P.H., Macleod M., *et al.*

734   (2019). Effects of Leachates from UV-Weathered Microplastic in Cell-Based Bioassays.

735   https://doi.org/10.1021/acs.est.9b02400

736 de Sá L.C., Oliveira M., Ribeiro F., Rocha T.L. & Futter M.N. (2018). Studies of the effects of

737   microplastics on aquatic organisms: What do we know and where should we focus our

738   efforts in the future? *Science of the Total Environment* **645**, 1029–1039.

739   https://doi.org/10.1016/j.scitotenv.2018.07.207

740 Sanders R.W. (1988). Feeding by Cyclidium sp. (Ciliophora , Scuticociliatida) on particles of

741   different sizes and surface properties. **43**, 446–457

742 Schössow M., Arndt H. & Becker G. (2016). Response of gastropod grazers to food conditions,

743   current velocity, and substratum roughness. *Limnologica* **58**, 49–58.

744   https://doi.org/10.1016/j.limno.2016.02.003

745 Schrank I., Löder M.G.J., Imhof H.K., Moses S.R., Heß M., Schwaiger J., *et al.* (2022). Riverine

746   microplastic contamination in southwest Germany: A large-scale survey. *Frontiers in*

747   *Earth Science* **10**, 1–17. https://doi.org/10.3389/feart.2022.794250

748 Setälä O., Fleming-Lehtinen V. & Lehtiniemi M. (2014). Ingestion and transfer of microplastics

749   in the planktonic food web. *Environmental Pollution* **185**, 77–83.

750   https://doi.org/10.1016/j.envpol.2013.10.013

751 Shabaka S., Moawad M.N., Ibrahim M.I.A., El-Sayed A.A.M., Ghobashy M.M., Hamouda A.Z.,

752   *et al.* (2022). Prevalence and risk assessment of microplastics in the Nile Delta estuaries:

753   "The Plastic Nile" revisited. *Science of The Total Environment* **852**, 158446.

754   https://doi.org/https://doi.org/10.1016/j.scitotenv.2022.158446

755 Sherr B.F., Sherr E.B. & Fallon R.D. (1987). Use of Monodispersed, Fluorescently Labeled

29

Bacteria to Estimate In Situ Protozoan Bacterivory †. *Applied and Environmental Microbiology* **53**, 958–965. https://doi.org/10.1128/AEM.53.5.958-965.1987

Shi X., Chen Z., Wei W., Chen J. & Ni B. (2023). Soil & Environmental Health Toxicity of micro / nanoplastics in the environment : Roles of plastisphere and. *Soil & Environmental Health* **1**, 100002. https://doi.org/10.1016/j.seh.2023.100002

Shimeta J. & Jumars P.A. (1991). Physical mechanisms and rates of particle capture by suspension- feeders. *Oceanography and marine biology: an annual review* **29**, 191–257

Siegfried M., Koelmans A.A., Besseling E. & Kroeze C. (2017). Export of microplastics from land to sea. A modelling approach. *Water Research* **127**, 249–257. https://doi.org/10.1016/j.watres.2017.10.011

Stoodley P., DeBeer D. & Lewandowski Z. (1994). Liquid flow in biofilm systems. *Applied and Environmental Microbiology* **60**, 2711–2716. https://doi.org/10.1128/aem.60.8.2711-2716.1994

Triebskorn R., Braunbeck T., Grummt T., Hanslik L., Huppertsberg S., Jekel M., *et al.* (2019). Relevance of nano- and microplastics for freshwater ecosystems: A critical review. *TrAC - Trends in Analytical Chemistry* **110**, 375–392. https://doi.org/10.1016/j.trac.2018.11.023

Vasudevan R. (2014). Biofilms : microbial cities of scientific significance. **1**, 84–98. https://doi.org/10.15406/jmen.2014.01.00014

Wagner M., Scherer C., Alvarez-Muñoz D., Brennholt N., Bourrain X., Buchinger S., *et al.* (2014). Microplastics in freshwater ecosystems: what we know and what we need to know. *Environmental Sciences Europe* **26**, 1–9. https://doi.org/10.1186/s12302-014-0012-7

Walker J.M., Sargison J.E. & Henderson A.D. (2013). Turbulent boundary-layer structure of flows over freshwater biofilms. *Experiments in Fluids* **54**, 1628. https://doi.org/10.1007/s00348-013-1628-x

Weisman R.A. & Korn E.D. (1967). Phagocytosis of Latex Beads by Acanthamoeba. I. Biochemical Properties*. **6**. https://doi.org/10.1021/bi00854a017

Wenzel F. & Liebsch H. (1975). Quantitative Untersuchungen zur Nahrungsaufnahme von

784   Stentor coeruleus Ehrenberg. *Ehrenberg. Zool. Anz. Jena* **195**

785   Woodall L.C., Sanchez-Vidal A., Canals M., Paterson G.L.J., Coppock R., Sleight V., *et al.*

786   (2014). The deep sea is a major sink for microplastic debris. *Royal Society Open Science*

787   **1**, 140317. https://doi.org/10.1098/rsos.140317

788   Yokota K., Waterfield H., Hastings C., Davidson E., Kwietniewski E. & Wells B. (2017). Finding

789   the missing piece of the aquatic plastic pollution puzzle: Interaction between primary

790   producers and microplastics. *Limnology and Oceanography Letters* **2**, 91–104.

791   https://doi.org/10.1002/lol2.10040

792   Zettler E.R., Mincer T.J. & Amaral-Zettler L.A. (2013). Life in the "Plastisphere": Microbial

793   Communities on Plastic Marine Debris. *Environmental Science & Technology* **47**, 7137–

794   7146. https://doi.org/10.1021/es401288x

795   Zhang T.C. & Bishop P.L. (1994). Density, porosity, and pore structure of biofilms. *Water*

796   *Research* **28**, 2267–2277. https://doi.org/10.1016/0043-1354(94)90042-6

797   Zhao S., Zhu L., Wang T. & Li D. (2014). Suspended microplastics in the surface water of the

798   Yangtze Estuary System, China: First observations on occurrence, distribution. *Marine*

799   *Pollution Bulletin* **86**, 562–568. https://doi.org/10.1016/j.marpolbul.2014.06.032

800   Zhu M., Nie G., Meng H., Xia T., Nel A. & Zhao Y. (2013). Physicochemical properties

801   determine nanomaterial cellular uptake, transport, and fate. *Accounts of Chemical*

802   *Research* **46**, 622–631. https://doi.org/10.1021/ar300031y

803   Zuur A.F., Ieno E.N. & Elphick C.S. (2010). A protocol for data exploration to avoid common

804   statistical problems. *Methods in Ecology and Evolution* **1**, 3–14.

805   https://doi.org/10.1111/j.2041-210x.2009.00001.x

806

807

i. Tables

809

810   Table 1: Average hydrodynamic conditions in the experiments. Mean flow rate and Froude

811   number are calculated for the two flow velocities tested (0,1 and 0,2 m sec $^{-1}$). The particle

812   settling velocities are calculated for all particle sizes and given in m s^{-1} and for the total duration

813   (24h) of the experiment. (one column)

Flow tank width	w (m)	0.14	
Water column depth	d (m)	0.1	
Flow tank velocity	U (m s^{-1})	0.1	0.2
Mean volume flow rate	Q (m³ s^{-1})	0.0014	0.0028
Froude number	Fr	0.10096	0.20193
Particle settling velocity		m s^{-1}	m 24h^{-1}
for 1 µm	v	1.13 x 10^{-7}	0.59
for 6 µm	v	3.994 x 10^{-7}	2.07
for 10 µm	v	1.131 x 10^{-5}	58.63

814

815

816   **ii. captions**

817
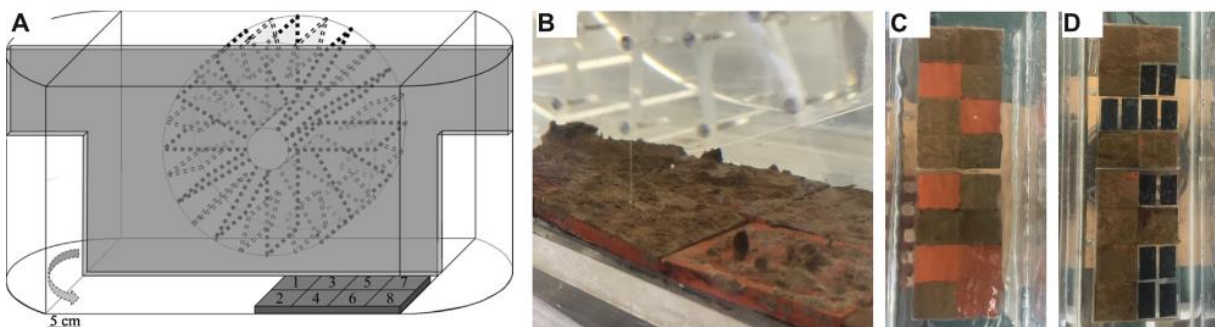
818

819   Figure 1: Experimental set-up for the biofilm studies in the laboratory. A: Endless flow channel

820   with a paddle wheel to induce a current and a frame for tiles in the opposite side (picture

821   adjusted from Schössow et al., 2016). B: Natural grown biofilms on clay tiles in the endless

822   flow channel. C+D: Clay tiles with biofilms, either in combination with empty clay tiles (C) or

823   empty acrylic tiles (D, Experiment 1).

824

825
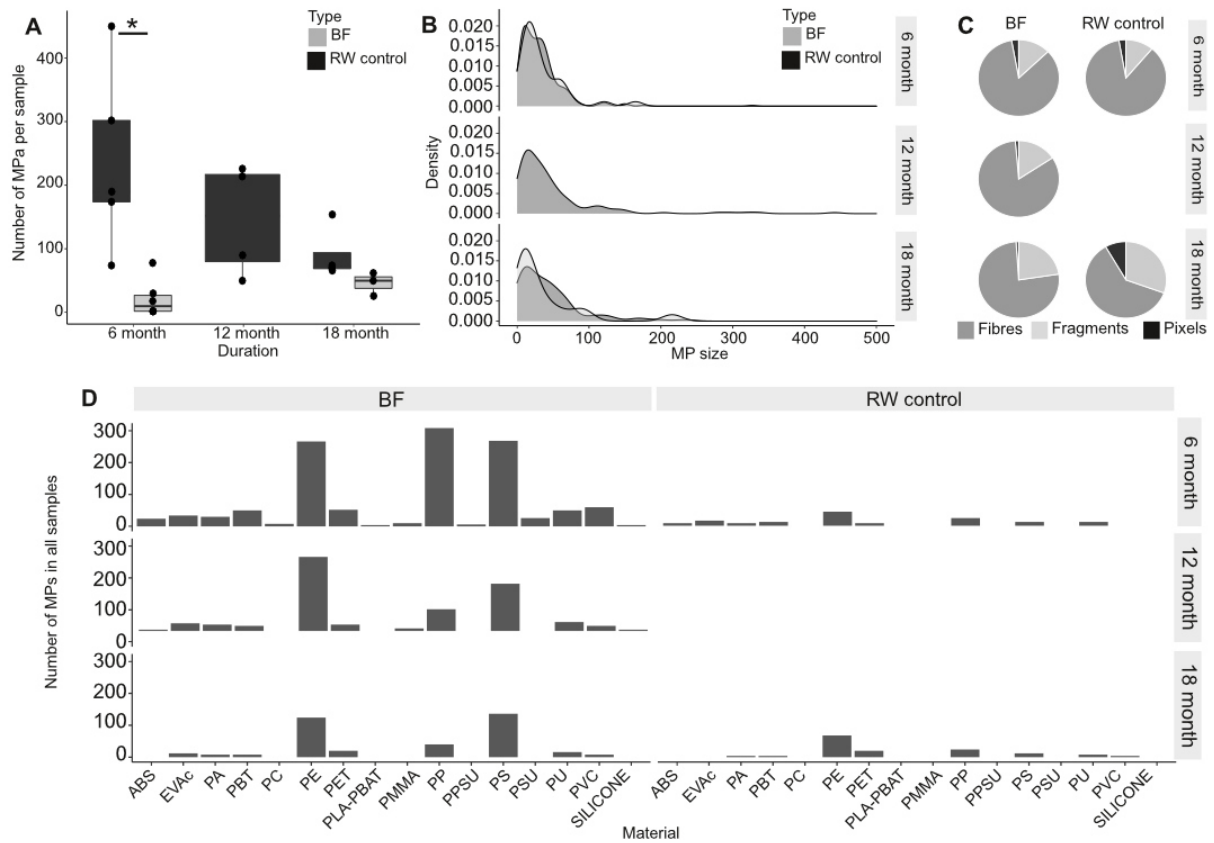
Figure 2: MPs found in the field samples of biofilms and controls across the duration of the experiment after 6 months, 12 months, and 18 months growth in the River Rhine. **A**. Number of MP particles found in each sample (black points) for biofilms and the river water (RW) controls, which are samples taken from the ambient water. Significances (* <0.05) were identified with Kruskall-Wallis and post-hoc Dunn test (method 'holm'). **B**. Density plot of the particle sizes found in biofilms and RW controls for each duration for particles <500 µm. **C**. Relative share of particle shapes distinguished for fragments, fibres and pixels found (pixel indicate particles of a size that is one pixel, thus, no shape could be determined, see text). **D**. Total number of MPs particles across all samples for each plastic material across all samples of biofilms and RW controls, respectively.

836

837
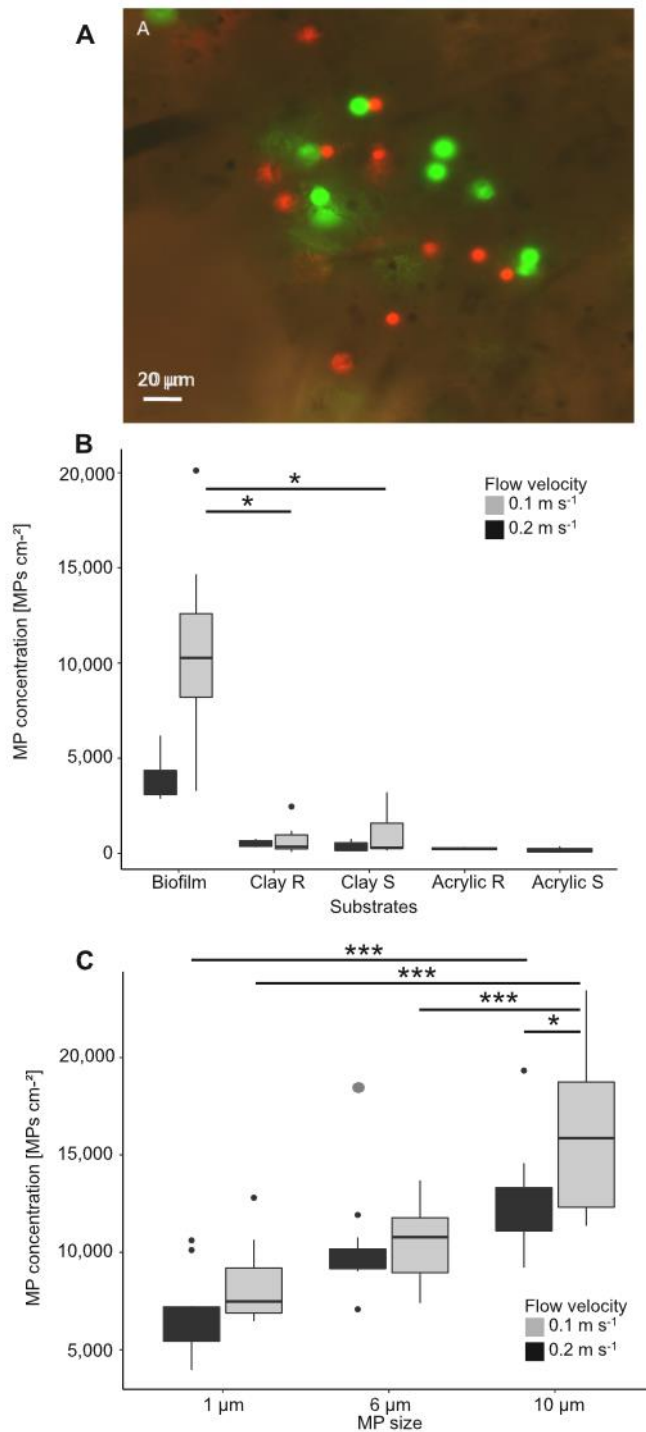
Figure 3: Laboratory experiments in flow tanks with biofilms grown in the River Rhine and fluorescent MPs. **A**. Fluorescent microplastics of 6 µm (red) and 10 µm (green) in biofilm samples (Fluorescent microscope picture, x20 magnification). **B**. Comparison of the particle retention of the 6 µm particle size by the substrates biofilm, rough clay tiles (R), smooth clay tiles (S), rough acrylic (R) and smooth acrylic (S) for two different flow velocities (0.1 m s^{-1} (black) and 0.2 m s^{-1} (grey)) after exposition for 24 hours. Kruskal-Wallis-Test (* = p < 0.05),

34

844   post-hoc Dunn-Test with method 'holm'. **C**. Concentration of microplastics (MP cm^{-2}) in the

845   biofilms compared for the three MP sizes (1 µm, 6 µm, 10 µm) for two flow velocities (0.1 m s^{-1}

846   ^{1} (black) and 0.2 m s^{-1} (grey)) after 24 hours. One outlier was removed from statistics (grey

847   circle), ANOVA $p < 0.05$, post-hoc TukeyHSD. *< 0.05, ***< 0.001.

848
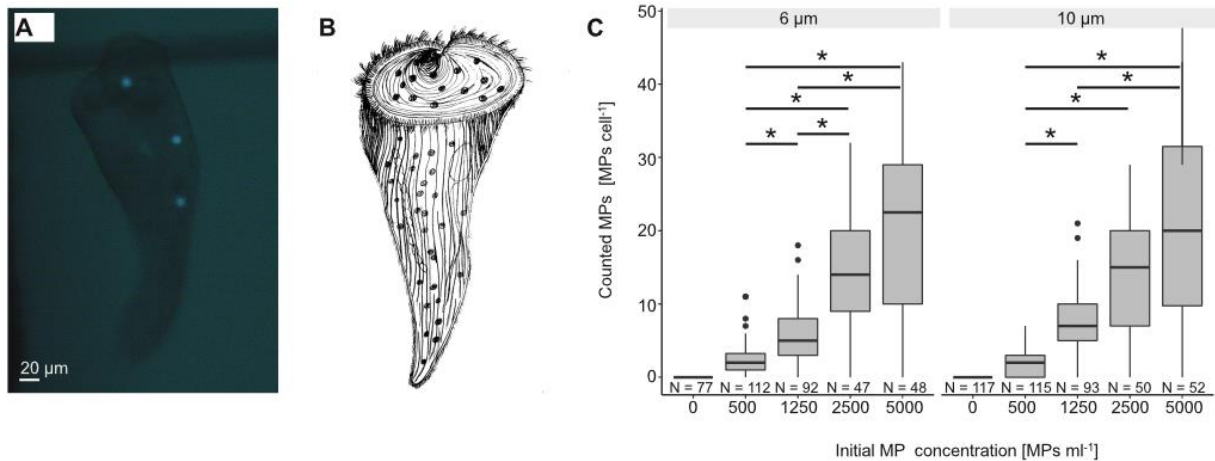
849

850   Figure 4: Uptake of microplastic particles by the ciliate *Stentor coeruleus*. **A**. *S. coeruleus* with

851   10 µm green plastic particles (epifluorescent microscope). **B**. Schematic drawing of *Stentor*

852   (by J. Werner). **C**. Ingestion of MP (MP cell^{-1}) for the particle sizes of 6 µm and 10 µm by *S.*

853   *coeruleus* in presence of varying concentrations (MP ml^{-1}). Kruskal-Wallis-Test, post-hoc

854   Dunn-Test (*= $p < 0.05$). The control (concentration of 0 MP ml^{-1}) was significantly different

855   from all other groups (not indicated).

856

35

Supplementary

Retention of Microplastics by Biofilms and Ingestion by Protists

Leandra Hamann[1,2*§], Jennifer Werner[1*], Felicia Haase[1,3,4], Massimo Thiel[1], Anja Scherwaß[1],

Christian Laforsch[5], Martin G.J. Löder[5], Alexander Blanke[2], Hartmut Arndt[1§]

*shared first authorship

§ corresponding author: Hartmut.Arndt@uni-koeln.de, lhamann@evolution.uni-bonn.de

[1] Institute of Zoology, University of Cologne, Cologne, Germany

[2] Institute of Evolutionary Biology and Animal Ecology, University of Bonn, Bonn, Germany

[3] Coastal and Marine Research Centre, Griffith University, Southport, QLD 4215, Australia

[4] School of Environment and Science, Griffith University, Southport, QLD 4215, Australia

[5] Department Animal Ecology I and BayCEER, University of Bayreuth, Universitätsstraße 30,

95447 Bayreuth, Germany

18 Table SI-1: Setups of experiment 1 (December 2018) and 2 (March 2019) with the combination

19 of substrata, MP size, MP concentration, and flow velocity for each channel. The temperature

20 in the circular flow tanks was 10.65 °C in the first and 12.3 °C in the second experiment at the

21 start. This was similar to the temperatures of the River Rhine (Table 2). The temperature

22 dropped on average by 1.8 °C in the first and 1.4 °C in the second experiment after 24 hours.

	Channel 1	Channel 2	Channel 3	Channel 4
EXPERIMENT 1 (December 2018)				
Substrata	BF on rough clay (n = 10) rough acrylic (n = 3) smooth acrylic (n = 3)	Smooth clay (n = 4) Rough clay (n = 4)	BF on rough clay (n = 10) Smooth clay (n = 3) Rough clay (n = 3)	Smooth clay (n = 4) Rough clay (n = 4)
Microplastics	6 µm	6 µm	6 µm	6 µm
Concentration	500 p ml^{-1}	500 p ml^{-1}	500 p ml^{-1}	500 p ml^{-1}
Flow velocity	0.1 m s^{-1}	0.1 m s^{-1}	0.2 m s^{-1}	0.2 m s^{-1}
EXPERIMENT 2 (March 2019)				
Substrata	BF on rough clay (n = 10)	Rough clay (n = 10)	BF on rough clay (n = 10)	Rough clay (n = 10)
Microplastics	1 µm, 6 µm, 10 µm	1 µm, 6 µm, 10 µm	1 µm, 6 µm, 10 µm	1 µm, 6 µm, 10 µm
Concentration	500 p ml^{-1}	500 p ml^{-1}	500 p ml^{-1}	500 p ml^{-1}
Flow velocity	0.1 m s^{-1}	0.1 m s^{-1}	0.2 m s^{-1}	0.2 m s^{-1}

23

24

2

Table SI-2: Additional data from the field studies: accumulated absolute and relative number

of MPs across all samples in biofilms (A) and controls (B) after 6 month, 12 month, and 18

month regarding size classes.

A) BIOFILM	6 month		12 month		18 month	
Size class	Number of MPs	%	Number of MPs	%	Number of MPs	%
<11 µm	220	18,33	100	17,01	88	23,66
11-50 µm	706	58,83	312	53,06	176	47,31
51-100 µm	144	12,00	104	17,69	68	18,28
101-150 µm	20	1,67	44	7,48	24	6,45
151-300 µm	6	0,50	16	2,72	16	4,30
301-500 µm	4	0,33	12	2,04	0	0,00
>500 µm	100	8,33	0	0,00	0	0,00
sum	1200	100	588	100	372	100

B) CONTROL	6 month		12 month		18 month	
Size class	Number of MPs	%	Number of MPs	%	Number of MPs	%
<11 µm	16	11,11	na	na	52	36,11
11-50 µm	96	66,67	na	na	56	38,89
51-100 µm	24	16,67	na	na	28	19,44
101-150 µm	4	2,78	na	na	0	0,00
151-300 µm	4	2,78	na	na	8	5,56
301-500 µm	0	0,00	na	na	0	0,00
>500 µm	0	0,00	na	na	0	0,00
sum	144	100	0	0	144	100

28

29

30

31

32

33

34
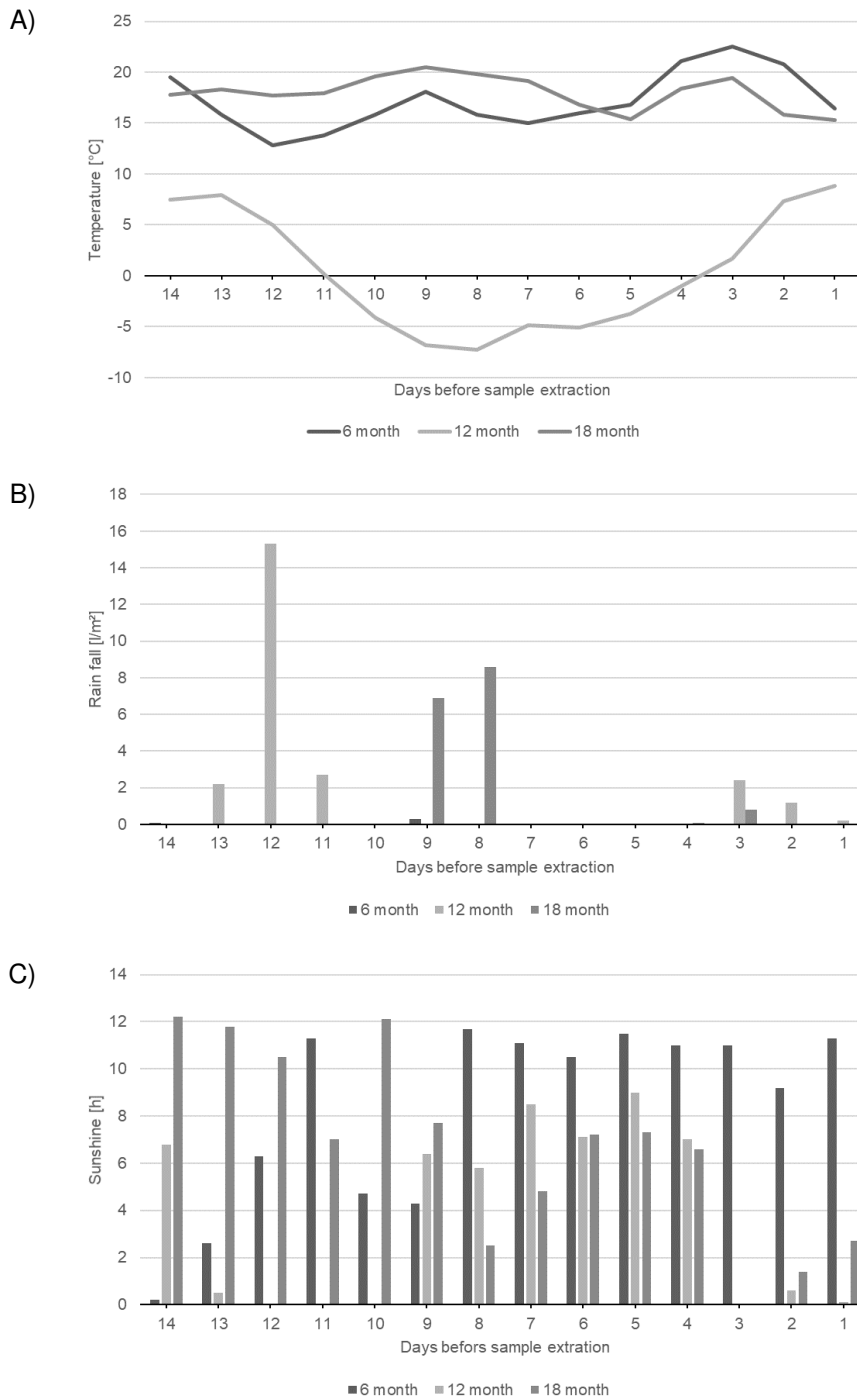
Figure SI-1: Weather data for the 14 days prior to sample extraction (6 months: 04.09.2020-17.09.2020; 12 months: 04.02.2021-17.02.2021; 18 months: 04.09.2021-17.09.2021) from the Rhine River in the area of Cologne: A) Temperature, B) rain fall, and C) duration of sunshine. Source: www.wetterkontor.de

10.2.3. Manuscript III

1   **Morphological Diversity of Filter-Feeding Structures in Five Ram-Feeding**

2   **Fish Species (Clupeidae, Scombridae)**

3   Leandra Hamann[1], Jan Hagenmeyer[1, 2], Santiago Eduardo[1, 3], Tobias Spanke[4], Alexander

4   Blanke[1]

5   [1] Institute of Evolutionary Biology and Animal Ecology, University of Bonn, An der Immenburg

6   1, 53121 Bonn, Germany

7   [2] Ruhr-University Bochum, Universitätsstraße 150, 44801 Bochum, Germany

8   [3] Otto-von-Guericke-Universität Magdeburg, Universitätsplatz 2, 39106 Magdeburg, Germany

9   [4] Leibniz Institute for the Analysis of Biodiversity Change, Adenauerallee 127, 53113 Bonn,

10   Germany

11 **ABSTRACT (300 words)**

12 Ram-feeding fish, such as anchovies, herrings, or mackerels, feed on plankton using cross-

13 flow filtration. During cross-flow filtration, a suspension flows parallel to a porous filter medium

14 thereby transporting particles along the surface which avoids clogging. In order to identify

15 cross-flow filtration in five ram-feeding fish species, we employ a combination of

16 morphometrics, micro-CT, and video analysis to describe the gill arch system and calculate

17 relevant filtration parameters. Our results show three morphotypes, which differ in geometry,

18 mesh size, surface structures, and the presence of mucus. *Scomber scombrus* and

19 *Rastrelliger kanagurta* (Scombriformes) have denticles and hair that are directed into the

20 buccal cavity forming surface structures and secrete mucus as adhesive material. The clupeid

21 species have a mechanical separation mechanism with a smooth filter medium formed by the

22 gill raker and lateral directed denticles. Geometric differences, such as gill arch system length

23 and symmetry further separate *Clupea harengus* and *Sardina pilchardus* from *Engraulis*

24 *encrasicolus* (Clupeiformes). The gill arch system in all five species is cone or ellipsoid with

25 the anterior part parallel to flow and the posterior part perpendicular to flow. Therefore, we

26 conclude that these species use a combination of cross-flow and dead-end filtration to retain

27 food particles.

1. INTRODUCTION

Suspension-feeding is an aquatic feeding strategy to separate food particles from water (Jørgensen, 1966). Suspension feeders such as sponges, mussels, crustaceans, flamingos, or baleen whales influence nutrient fluxes, local flow fields, and bio-chemical processes on a local and global level. Within the suspension-feeder category are filter-feeding fish of particular interest to humans. Pilchards, anchovies, and herrings, belong to the most commonly fished species for human consumption (Alder *et al.*, 2008). Silver carp and bighead carp were considered for waste water treatment to remove and recycle nutrients and algae and improve water quality (Hernderson, 1983). Bio-inspired filter modules were developed that mimic the filter-feeding mechanism (Hung & Piedrahita, 2014; Schroeder *et al.*, 2019). Filter-feeding fish also ingest microplastics (Phillips & Bonner, 2015; Ory *et al.*, 2018; Ribeiro *et al.*, 2020) so that their filter-feeding mechanisms are relevant for ecology, fishery, filtration technologies, and environmental protection.

The particle separation mechanism in filter-feeding fishes was described as cross-flow filtration (CFF). Water streams parallel to the gill arches (GA) that bear elongated gill rakers (GR) each covered with denticles thus forming a mesh-like configuration (Figure 1) (Sanderson *et al.*, 2001). The parallel flow transports the particles along the separation medium towards the oesophagus while at the same time cleared water exits through the gill arches system (Sanderson *et al.*, 2001). More than 70 filter-feeding species from 21 families are known, which divide into ram-feeding and pump-feeding species. Ram feeders use their forward motion to stream water into the mouth, while pump feeders suck water into their mouth through rhythmic contractions of pharyngeal structures (Sanderson & Wassersug, 1993; Storm *et al.*, 2020).

Although CFF in filter-feeding fishes is known, many details of their filtration mechanism were not assessed so far. For example, the gill arch system (GAS) morphology varies strongly between species. Gill rakers are long blade-shaped (Gibson, 1988), bushy (Friedland *et al.*, 2006), short with an oval cross-section (Langeland & Nost, 1995), or even fused as in the silver carp (Cohen & Hernandez, 2018). Pump-feeding cichlids have microbranchiospines, dermal

3

ossifications on the external faces of the GA whose function is yet unclear (Goodrich *et al.*, 2000), whereas breams (*Abramis brama*) have a palatal organ within the oral cavity (Hoogenboezem *et al.*, 1993). Intraspecific variability of CFF morphology was observed in *Sardina pilchardus* with variations in the number of gill rakers and gill raker gaps (Garrido & van der Lingen, 2014), which may indicate adaption to local prey characteristics and different feeding environments (Costalago, Garrido, & Palomera, 2015). Differences in morphology lead to the identification of new variations of cross-flow filtration. In the so-called cross-step filtration d-type ribs formed by the gill arches and rakers in the paddlefish induce characteristic vortices (Sanderson *et al.*, 2016). Due to the differences in morphology, we suspect that even more variations of cross-flow filtration might be present.

This study analyses the morphology of the gill arch system (GAS) and identifies details of CFF in five ram-feeding fish from the groups Scombridae and Clupeidae. Because endoscopic live data from inside the oral cavity is difficult to obtain (Cheer, Ogami, & Sanderson, 2001) we used digital microscopy to describe the three-dimensional arrangement of the GAS and conducted a video analysis of filter-feeding fish in aquaria and the wild to observe feeding behaviour. We were thus able to describe the morphology in detail and calculate filtration parameters, such as mesh size, open area ratio, and fluid exit ratio. Parameters such as leakiness or volume flow through the gill arch system enabled us to infer the flow regime within the buccal cavity and identify geometric traits that induce CFF.

2. MATERIAL AND METHODS

2.1. Study Organisms

We analysed seven Atlantic mackerels (*Scomber scombrus,* Linnaeus 1758), seven Indian mackerels (*Rastrelliger kanagurta,* Cuvier 1816), seven Atlantic herrings (*Clupea harengus,* Linnaeus 1758), eleven Atlantic pilchards or sardines (*Sardina pilchardus,* Walbaum 1792), and eleven Atlantic anchovys (*Engraulis encrasicolus,* Linnaeus 1758) (Figure 1) to account for potential variation in the GAS. All species are ram-feeding filter feeders (Sanderson & Wassersug, 1993; Storm *et al.*, 2020). The fish were ordered from "FrischeParadies" (Cologne,

82   Germany) and caught fresh from fishing grounds in the North East Atlantic, West Indian Ocean,

83   Mediterranean, and Black Sea (Figure 1) one day before they were picked up at the shop. The

84   fish were round, not decapitated or gutted, and cooled on ice during transport. After being

85   visually inspected for damages, they were immediately frozen at -18°C at the University.

86   ## 2.2.   Morphometrics based on digital microscopy

87   Before dissection, the fish were thawed in cold water for one hour. Each specimen was

88   weighed and photographed with their mouth closed and open. The head was cut off, dissection

89   was begun on the left side of the GAS, and proceeded from larger to smaller structures, i.e.,

90   head, gill arches, gill rakers, and denticles. Larger structures were photographed with a Nikon

91   D850 equipped with an AF-S Micro NIKKOR 60 mm 1:2.8G ED. Smaller structures were

92   analysed with a Keyence VHX-700F (Ver 2.3.8.2 with lens VH-Z20R RZx20-x200, System Ver

93   1.93) at the University of Cologne. Photos were taken by one operator and analysed by two

94   operators using ImageJ. In total, 20 parameters were measured (Figure 2A). Open mouth

95   position for parameters 3 to 10 was held with pins and needles so that the jaw was opened

96   with the GAS fully expanded and the GRs closing the gap between the GAs as established in

97   previously (Sanderson & Wassersug, 1993; Storm *et al.*, 2020). We are aware that

98   measurements on soft and moveable structures are difficult to analyse. However, the open

99   mouth position is an essential feature in ram-feeding fish. We therefore compared the open

100   mouth position to measurements extracted from our video analysis to ensure that the angle

101   represented a natural feeding position. The GAS is described with anatomical terminology

102   along the anterior-posterior axis, the dorso-ventral axis, and the medial-lateral axis (Storm *et*

103   *al.*, 2020). Based on the branchial bones, each of the five GAs is subdivided into three

104   branchials: epibranchial, ceratobranchial, and hypobranchial. In some species it was difficult

105   to distinguish between ceratobranchial and hypobranchial, thus they were measured together.

106   GA length (parameter 12) was determined as the sum of the epi-, cerato- and hypobranchial,

107   respectively. The length of the pharyngobranchials was measured separately and not

108   accounted into GA length. Length of the GR (parameter 13) was measured for five GR on each

109   branchial at the dorsal and ventral ends of the epibranchial and hypobranchial where they are

shortest, and close to the epibranchial-ceratobranchial joint at the ceratobranchial where they are longest (Magnuson & Heitz, 1971). GR width, distance, and height was measured at their base close to the GA (parameter 14-16). Vertical position of the denticles was measured from the intrapharyngeal side of the GR to the base of the denticles (parameter 17). Length and distance between denticles (parameter 18 and 19) were measured on GR close at the base. Measurements on structures were taken five times for different GR and ten times for different denticles. The open area ratio (parameter 20) was determined in a black-white image by measuring the area occupied by GR and denticles compared to the open area where water can flow through.

Not all parameters apply to all species. If all measurements were possible, 766 measurements were taken per individual. Dissections and measurements on the fresh samples were carried out within eight hours and were kept in water at all times to prevent artefacts from drying. After dissection, the GAs were fixed in 5% formaldehyde and dehydrated in increasing ethanol concentration up to 70 % ethanol for long-term fixation.

2.3. MicroCT scanning

One individual for each of the five selected ram-feeding species, was selected for MicroCT scanning to visualise the three-dimensional arrangement of the GAS in an open-mouth position. The head was cut off from the body and pinned upwards in an open-mouth position onto Styrofoam. The samples were then fixed in 5 % formaldehyde, dehydrated in increasing ethanol concentrations up to 70 %, and stained with PTA. Afterwards, each head was scanned with the Bruker SkyScan 1173 (around 54 kV, 142 µA, 500 ms exposure time, no filter) at the Zoological Research Museum Alexander Koenig in Bonn, Germany. The scans were reconstructed with NRecon (Version 1.7.5.9), and volume renders were created with Drishti (Version 2.6.4). Virtual cross-sections of the fish heads were made in the sagittal plane along the hyoid bone and in the frontal plane close to the epi-ceratobranchial joint on GA1 with view on the dorsal side of the GAS.

2.4. Video analysis

Public aquaria across Europe were contacted to film feeding behaviour and determine swimming speed before and during feeding. Fishes were filmed for several minutes prior to and during feeding with the camera and LED light positioned on tripods outside the tanks. The fishes were given their usual food but it was crushed and decreased in size to increase the chances of filter-feeding (Crowder, 1985; Garrido *et al.*, 2007). *S. scombrus* were fed with a mixture of small crustaceans, shrimps, and blue mussels, which were crushed by hand to decrease size. *C. harengus* were fed with small crustaceans and pellets, *S. pilchardus* were fed with pellets crushed in a blender. Due to travel restrictions during the Covid-19 pandemic video footage for *E. encrasicolus* was taken by the aquarium curator with a GoPro in a quarantine tank and sent to the authors. Because of quality issues, only swimming speed was measured. *R. kanagurta* is not held in captivity, so field footage was organised from dives in the Red Sea by amateur divers.

The footage was analysed in ImageJ. Measurements were taken only in frames where the fishes were parallel to the camera and the total length visible. Head length, jaw angle, and branchiostegal height were measured relative to standard length of each individual (parameters 1, 2, 4, 5 in Figure 2A). Assuming isometric allometry in adult fish of these species, the measurements were multiplied by the mean standard length of each species gained from the dissected individuals to be able to compare the data to the dissected species. The swimming speed was determined by using the Manual Particle Tracing Module in ImageJ. Sequences of at least ten frames were measured by following the eye of the fish and dividing the travelled distance by the standard length. Feeding behaviour was determined based on whether the mouth was continuously held open. Cleaning behaviour was only observed in *S. scombrus* and *R. kanagurta* and recognisable by quick closing and opening of the mouth after ram-feeding. Due to the aquaria holding conditions, it is possible that the same individuals of the shoal were measured several times.

2.5. Calculation of filtration parameters

164 The calculation of the total filtration area (TA) of each GA of the left side is based on the

165 averaged GR length multiplied by the GA length for the upper (U) and lower (L) GA individually,

166 similar to Magnuson & Heitz, 1971. As we only measured five GR on every branchial, we

167 changed the formula accordingly and calculated the average GR length per branchial and

168 multiplied it with GR number and the average GR distance (D), as shown here for the anterior

169 side of GA1:

$$170 \qquad TA_{GA1} = UA_{GA1} + LA_{GA1}$$

$$171 \qquad = \left(\frac{\overline{GR_{L,E}} + \overline{GR_{L,C}}}{2} * \frac{\overline{GR_{D,E}} + \overline{GR_{D,C}}}{2} * n_{U,GR} \right)$$

$$172 \qquad + \left(\frac{\overline{GR_C} + \overline{GR_H}}{2} * \frac{\overline{GR_{D,C}} + \overline{GR_{D,E}}}{2} * n_{L,GR} \right)$$

173 We assume that the GR length decreases linearly from the longest GR at the ceratobranchial

174 towards the distal ends of the epibranchial and hypobranchial, respectively (Figure 2B). The

175 same calculation was used to calculate the posterior area if present. The total filtration area is

176 the sum of the area between the GA and the area between the first GA and the operculum.

177 Finally, the area was doubled to include the filtration area of the right side of the fish. The

178 symmetry of the GAS is determined by the ratio of upper area (UA), formed by the GR of the

179 epibranchial, to lower area (LA), formed by the GR of the cerato- and hypobranchial of each

180 GA.

$$181 \qquad Symmetry = \frac{UA_{GA1}}{LA_{GA1}}$$

182 The closed area (the area that is covered by the GR and denticles) and open area (open space

183 through which the water can flow) were measured in pictures taken at the anterior

184 ceratobranchial of each GA. The open area ratio is calculated as the ratio of open area to the

185 sum of open and closed area:

$$186 \qquad Open\ Area\ Ratio = \frac{Open\ Area}{Open\ Area + Closed\ Area}$$

187   Because the open area ratio remained similar from GA 1-5 in the clupeiform species, the mean

188   open area ratio at the cerato branchial of GA1 was used to calculate the open area of all GA

189   based on the total filtration area. It was not possible to measure the open and closed area on

190   GA 2-4 in the scombriform species because of the high density of denticles and calculated the

191   open area ratio in the same way as for the Clupeiformes.

192   The leakiness for each GA (Figure 2B) describes the relative amount of flow through the open

193   area of one GA to the total open area (Cheer *et al.*, 2012).

194
$$Leakiness\ [\%] = \frac{Open\ area_{GA1}\ [mm^2]}{Open\ area\ [mm^2]}$$

195   The fluid exit ratio (Brooks *et al.*, 2018) is calculated as the ratio of the total open filtration area

196   to the open mouth area:

197
$$Fluid\ Exit\ Ratio = \frac{open\ filtration\ area\ [mm^2]}{open\ mouth\ area\ [mm^2]}$$

198   Depending on the position of the opposing GR and denticles, the mesh size can be calculated

199   as minimum or maximum mesh size (Figure 2B) and also be understood as the minimum size

200   of particles that are retained (Collard *et al.*, 2017). The minimum mesh size (MS_{min}) is formed

201   if denticles between two GR are alternating, so it is calculated as the product of denticle

202   distance and denticle length:

203
$$MS_{min} = D_{distance} * D_{length}$$

204   The maximum mesh size (MS_{max}) is formed if denticles between two GR are directly opposite

205   of each other, so it is calculated as the product of the denticle distance and the gap between

206   the two GR:

207
$$MS_{max} = D_{distance} * GR_{distance}$$

208   A decrease or increase in mesh size from anterior to posterior can be determined by the ratio

209   of the mesh size from GA1 to GA4. The mesh size ratio was based on the mean of the minimum

210   and maximum mesh size.

211 The Reynolds number describes the ratio of inertial to viscous forces and describes the local

212 flow regime. It is an important indicator to indentify the type of particle encounter with the filter

213 medium, e.g., hydrosol filtration theory (Rubenstein & Koehl, 1977), and draw comparisons to

214 the fluid dynamics in other suspension feeders as it is a dimensionless number (Hamann &

215 Blanke, 2022). It was calculated as:

216
$$Re = \frac{\rho * l * v}{\mu}$$

217 With the density ρ as 1.027×10^3 kg m^{-3} and the dynamic viscosity μ as 0.00141 kg /(m^{-1} s^{-1})

218 for seawater at 10°C. The flow velocity v was measured in the videos during feeding as

219 standard length per second multiplied by the standard length of the dissected species. The

220 Reynolds number was calculated around the fish (standard length), at the mouth opening

221 (based on the equivalent spherical diameter of open mouth height and width), and around the

222 denticles (based on denticle width on the anterior GR of GA1) with the mean swimming velocity

223 for each species. In contrast to other studies (Motta *et al.*, 2010; Brooks *et al.*, 2018), we did

224 not apply a reduction of flow velocity at the mouth and around the denticles. Therefore, our

225 calculations are likely to show the maximum possible Reynolds numbers. The volume flow

226 rate through the mouth was calculated by the open mouth area multiplied by the flow velocity

227 v.

2.6. Statistics

229 The results were analysed and visualised using R Studio (Version 3.6.3., package ggplot2)

230 and Scribus (Version 1.5.6.1). Descriptive statistics of untransformed data were calculated for

231 all measured and calculated parameters. Measurements are reported as mean with standard

232 deviations. Ratios were calculated based on means and reported without standard deviation.

233 In Order to investigate the relationship of morphological traits, we used principle component

234 analysis (PCA) based on 19 parameters, including ten absolute values and nine relative values

235 (Table 1). Variables were not included if they were binary or partly binary (i.e., number of

236 posterior GR, position of denticles, mucus, teeth, additional structures), angles (i.e., lip angle,

237   jaw angle), or they were used to calculate filtration parameters and therefore not independent.

238   To limit the number of variables, only data concerning the GA1 were included, e.g., GR

239   number, open area ratio, or mesh sizes. Of the included 817 data points, 46 were missing,

240   which were imputed for the PCA by the mean of each variable for each species, respectively

241   (Dray & Josse, 2015). Afterwards, we performed a regression of each log-transformed variable

242   with the log-transformed standard length to extract the residuals and correct for size. The PCA

243   with the residuals was based on a correlation matrix (scale = TRUE, center = TRUE). A

244   threshold of 75% was chosen to select the principle components (PCs) that explain most of

245   the variance. The loadings of these PCs were extracted and ranked respectively based on

246   their absolute values (or modulus) to identify essential contributors. The same dataset was

247   used to calculate a correlation matrix. Because some of the data was not normal distributed,

248   we used the Spearman rank test to calculate the correlation coefficient. The comparison of the

249   jaw angle in the dissected individuals and the videos, as well as the comparison of the

250   swimming speed before and during feeding was done with a Kruskal-Wallis rank sum test (chi-

251   squared) with a posthoc dunn test (method 'Holm').

252   3. RESULTS

253   3.1.   Morphometrics and filtration parameters

254   *S. scombrus* is the largest species analysed with 169.4 ±4 mm as standard length, followed by

255   *C. harengus* (248.2 ±7.3 mm), *R. kanagurta* (210.1 ±12.4 mm), *S. pilchardus* (118.7 ±6.4 mm),

256   and *E. encrasicolus* (97.9 ±2.4 mm; Table 1). The standard length increased by 1% or 2%

257   when the mouth is held open in feeding position except for *E. encrasicolus* were it decreased

258   by 2%. *S. scombrus* is the only species with little teeth on the lip. The mouth height to width

259   ratio ranges from 1.2 to 1.8, which indicates an oval opening along the ventral-dorsal axis. The

260   jaw angle of the open spanned heads ranges from 45° *S. scombrus* to 74° in *E. encrasicolus*

261   (Table 1). The branchiostegal height is largest in *R. kanagurta* and smallest in *E. encrasicolus*

262   ranging between 3.5 to 13.0 mm. The angle of the protruded lips is 95° up to 180°, closing the

263   mouth opening at the sides. The head makes up around 19.8% in *C. harengus* and maximum

264   27% in *R. kanagurta* of the standard length. The epibranchial of GA1 begins at around two

265   thirds into the buccal cavity, except in *E. encrasicolus* in which the epibranchial starts already

266   in the first third (Table 1).

267   Gill arch length decreases from anterior to posterior (Figure 3A). Only in *S. pilchardus* is the

268   second GA longer than the first. The GA ratio describing the decrease in length from GA1 to

269   GA5 is largest in *R. kanagurta* with 0.38 and smallest in *C. harengus* and *E. encrasicolus* with

270   0.21, meaning that GA5 is only 38% and 21% of the length of GA1, respectively (Table 1). The

271   same trend can also be seen in the number of GR on each GA (Figure 3B). Here, *S. pilchardus*

272   has more GR on GA2 and GA3 than on the first, while GR distance remains similar. The two

273   mackerel species *S. scombrus* and *R. kanagurta* have anterior and posterior GR, of which the

274   number of posterior GR is only little less. For example, in *R. kanagurta* the number of GR on

275   the anterior side of GA1 is on average 53 and on the posterior side 43 with similar GR distance.

276   GA5 has no GR in the two mackerel species. *C. harengus* and *E. encrasicolus* have posterior

277   GR only on GA4 and GA5, especially on the GA3 they are less in number. *S. pilchardus* has

278   posterior GR only on GA4, of which only one individual had posterior GR on GA2 and GA3,

279   counting 7 and 3 in number (Figure 3B).

280   The total filtration area is largest in *R. kanagurta* with 2157.4 ±277.4 mm² and smallest in *E.*

281   *encrasicolus* with 344.8 ±52.6 mm² (Table1, Figure 3C). The symmetry of upper to lower GA

282   area is in all species smaller than 0.4, meaning that the area created by the GR on the

283   epibranchial is smaller than the area on cerato and hypobranchial of each GA (Table 1, Figure

284   3H). The open area ratio of GA1 ranges between 0.51 and 0.57 in *S. scombrus*, *R. kanagurta*,

285   *C. harengus* and *S. pilchardus*. In *E. encrasicolus* the open area ratio is 0.71 (Table 1). In *S.*

286   *scombrus* and *R. kanagurta*, the leakiness is highest at the first gap with 76.1% and 78.8%. In

287   the posterior gaps between the GAs, the amount of water that flows through the open area

288   ranges between 8% down to around 6% at the fourth gap formed by the posterior GR of GA3

289   and anterior GR of GA4. In the three clupeid species, the leakiness at the first gap ranges

290   between 50.3% and 61.2%, at the second gap between 21.1% and 22.9%, at the third gap

12

between 11.8% and 14.7%, and at the fourth gap between 5.9% and 12.1% (Table 1). The fluid exit ratio is in all five species larger than 1, which means that the filtration area is larger than the open mouth area. It is smallest in *R. kanagurta* with 1.28 and largest in *S. pilchardus* with 3.57 (Table 1).

GR are longest on GA1 in all five species (Figure 3D). In Scombriformes, the length of the GR is abruptly shorter in GA2 to GA4, GA5 has no GR. In Clupeiformes, the length decreases more evenly from first to last GA. Within one GA, GR length is largest on the ceratobranchial and smallest and the distal ends of epi and hypobranchial. The GAS length, determined by the sum of the mean GR length at the ceratobranchial of all GA, is longest in *R. kanagurta* with 32.5 ± 2.5 mm and smallest in *E. encrasicolus* with 10.6 ± 0.8 mm (Table1). The mean of the length to width ratio of the anterior GR on GA1 varies between 46.3 and 114.1 (Table 1, Figure 3F). The length to width ratio of the posterior GR in *S. scombrus* and *R. kanagurta* range around 10 and 25. The height to width ratio of the GR on GA1 ranges between 3.5 and 8 (Figure 3F)

The denticles in *S. scombrus* and *R. kanagurta* sit on top of the anterior, blade-shaped GR on GA1. They are spaced at regular intervals, thin (Figure 4), and measure around 0.59 mm in length (Table 1). The denticles on the ceratobranchial of the GR on GA1 are longer than on the epi- and hypobranchial (Figure 3H). On the shorter, posterior GR of GA1 and GR on GR2, GR3, and GR4, the denticles vary strongly in size (Figure 3G) but are irregularly arranged and closer together (Figure 4). Other scombrids were described to bear patches of tiny teeth on most GA (Collette & Gillis, 1992). Based on the outer appearance, it is difficult to tell denticles and teeth apart (Figure 4), which might explain the high variance in length. We assume that structures originating from the GAs are teeth and structures originating from GR are denticles. Because GA5 has no GR, we assume that the measured structures are teeth. These teeth are generally longer, ranging in length around 1.5 mm (Figure 3G), and appear thicker and sturdier. Additionally, part of the five GA in the two species of Scombriformes are four pharyngobranchials, of which the third and fourth are visible within the oral cavity and bear

318   teeth (Figure 1, Figure 5), as described for *R. kanagurta* (Gnanamuttu, 1966). On each side,

319   the pharyngobranchials are located dorsally, between the epibranchials of GA3 and GA4, and

320   opposite GA5 (Figure 5). The first visible, more anterior pharyngobranchial is small, slender

321   with small teeth, and the second one is rectangular and has more pronounced teeth. For other

322   species within the Scombridae, e.g., *Grammatorcynus bicainatus*, the pharyngobranchials

323   were also described as pharyngeal tooth patches (Collette & Gillis, 1992).

324   The denticles of *C. harengus*, *S. pilchardus,* and *E. encrasicolus* are at regular distances at

325   the sides of the GR blades of GA1 at about a relative distance of 0.17, 0.27 and 0.23 of the

326   height measured from the interior face of the GR (Table 1). They are short, vary in shape

327   between the three species (Figure 4), and were described as conical, diabolo-shaped, and

328   sickle-shaped (Collard *et al.*, 2017). The denticle length remains similar across all GA and is

329   0.098 ±0.015 mm in *C. harengus*, 0.091 ±0.013 mm in *S. pilchardus,* and 0.085 ±0.018 mm in

330   *E. encrasicolus* (Table 1, Figure 3F). The denticle length is similar across the branchials on

331   GA 1 (Figure 3H).

332   The calculated minimum and maximum mesh sizes are smallest in *S. pilchardus* with 0.007

333   mm^2 and 0.014 mm^2 and largest in *S. scombrus* with 0.113 mm^2 and 0.148 mm^2. In the clupeid

334   species, the minimum mesh size is smaller than the maximum mesh size on all GA. In the

335   scombrid species, this is only true for the anterior and posterior GR on GA1 and the posterior

336   GR on GR2 (Figure 3I). Otherwise, the minimum mesh size is larger than the maximum mesh

337   size. The mesh size ratio based on the mean mesh size of GA1 to GA4 shows that the mesh

338   size becomes smaller from anterior to posterior in *S. scombrus*, *R. kanagurta*, *S. pilchardus*,

339   and *E. encrasicolus*. Only in *C. harengus*, the mesh size is smaller in GA1 compared to GA4

340   (Table 1)

341   During the dissection of the fish, mucus formation was noticed close to the oesophagus in *S.*

342   *scombrus* and *R. kanagurta*. The investigation of GA5 and the second additional structure

343   showed a high amount of dark pigmented areas between the denticles and in the groove

344   between the pharyngobranchials (Figure 6). These pigments are arranged on structures that

345   we termed 'mucus villi' because they remind of intestinal villi.

346   ## 3.2.   Principle component analysis (PCA) and correlation matrix

347   The first three PCs explain 78,5% of the variance in the data (Figure 7). Based on the ranking

348   of the loadings (Table 2), PC1 relates to overall geometry and size (highest loadings in

349   descending order: GAS length, GR length on GA1, the length ratio of GA1 to GA5 (GA1-5

350   ratio), the GR height to width ratio, the filtration area, and the head length), whereas PC2

351   relates to the filter medium, and the fluid flow (highest loadings: GR number, mesh size max,

352   mesh size min, the leakiness of GA1 and the MO ratio), and PC3 represents the symmetry

353   (highest loadings: symmetry, mesh size ratio, fluid exit ratio, weight, and leakiness at GA1). In

354   all of the combinations of the PCs, the individuals of one species cluster into distinct groups

355   with little overlap between groups. While in PC1 groups are evenly distributed, PC2 results in

356   two groups that consist of *R. kanagurta*, *S. scombrus,* and *E. encrasicolus* on the one hand,

357   and *C. harengus* and *S. pilchardus* on the other hand, thus not representing the two taxonomic

358   groups Scombridae and Clupeiformes. PC3 shows a higher spread of the individuals within

359   each group and separates the two scombrids, *R. kanagurta* and *S. scombrus*, with the clupeid

360   species in between them.

361   Most variables in the correlation matrix correlate positively with each other (Figure 8). Due to

362   the high number of combinations, only the significant correlations with a correlation coefficient

363   of $\rho >0.7$ are described (see supplement information S-1 and Figure SI-1). For example: weight

364   correlates positively with GAS length ($\rho = 0.7$), GAS length positively correlated with GR length

365   of GA1 ($\rho = 0.92$), and head length correlates positively with denticle length ($\rho = 0.83$). This

366   shows that despite the correction for standard length, size play a significant in the feeding

367   morphology. Additionally, the longer the GAS, the larger is the filtration area ($\rho = 0.7$) and the

368   more cone-shaped and not cyindrical is the GAS ($\rho = 0.81$). The shape of the mouth opening

369   is more oval shaped in *C. harengus* and *S. pilchardus* and more round in the other three

370   species. The more oval the mouth shape, the higher is the number of GR on GA1 ($\rho = 0.73$).

371 GR number on GA1 negatively correlates with minimum (ρ = -0.74) and maximum mesh size

372 (ρ = -0.80).

3.3. MicroCT scans

374 The MicroCT scans of the fish heads show the three-dimensional arrangement of the GAS

375 within the buccal cavity in an open mouth position (Figure 1). In *S. scombrus* (Figure 1A) and

376 *R. kanagurta* (Figure 1B), GA1 is very prominent in the anterior part of the buccal cavity. GA5

377 and the fourth pharyngobranchial narrow down the buccal cavity towards the oesophagus

378 However, the GR in *R. kanagurta* only touch the operculum with their distal tip, whereas the

379 GR in *S. scombrus* are directed inwards. Even though the jaw angle of the head in this *S.*

380 *scombrus* specimen is 56.3° and lays within the range of jaw angles during feeding (Figure 9),

381 we assume that the mouth was not fully opened sideways, so the opercula did not open, and

382 the GAS could not expand to a natural feeding position.

383 In the lateral view of *C. harengus* (Figure 1C) and *S. pilchardus* (Figure 1D), the buccal cavity

384 has a narrow, cylindrical shape that bends upwards towards the oesophagus. In the frontal

385 cross-section with the view on the dorsal side, the buccal cavity starts narrow and opens up at

386 the GAS. In *S. pilchardus*, GA1 is in contact with the inner sides of the opercula, which again

387 might indicate that the GAS is not fully expanded. The buccal cavity, the opercula, and the

388 GAS in *E. encrasicolus* (**Fehler! Verweisquelle konnte nicht gefunden werden.**E) are

389 shorter in an anterior-posterior direction compared to the other species. From both views, the

390 GAS has a conical, symmetric shape.

3.4. Video analysis: behaviour while ram-feeding

392 The jaw angle and the swimming velocity was measured in 20 *S. scombrus*, five *R. kanagurta*,

393 nine *C. harengus*, 15 *S. pilchardus,* and 24 *E. encrasicolus* during feeding with an open mouth

394 position (Table 1). Comparison of the jaw angles of the manually opened mouth in the

395 dissected individuals to the filter-feeding individuals in the videos shows no significant

396 differences (Figure 9A). The mean swimming velocity ranges between 0.34 m/s in *C. harengus*

397 up to 0.5 m/s in *S. scombrus* (Table 1). In *S. scombrus*, *C. harengus*, and *E. encrasicolus*, the

398   swimming velocity is higher during feeding than during non-feeding (Figure 9B). There is only

399   a significant difference in the swimming speed for *S. pilchardus* before and while feeding

400   (Kruskal-Wallis rank sum test (chi-squared), posthoc dunn test (method 'Holm') p = 0.0009).

401   Based on the SL, the Reynolds number around the fishes ranges between 35,000 in *E.*

402   *encrasicolus* and 137,000 in *S. scombrus*. At the mouth opening, the Reynolds number ranges

403   between 4,100 in *S. pilchardus* and 15,600 in *R. kanagurta* and around the denticles, the

404   Reynolds number ranges between 30 in *E. encrasicolus* and 300 in *S. scombrus* (Table 1).

405   With an open mouth position, the volume flow rates range between 1.9 l/min in *S. pilchardus*

406   and up to 23.5 l/min in *R. kanagurta* (Table 1).

407   The feeding behaviour was observed in six individuals each of *S. scombrus*, *R. kanagurta*, *C.*

408   *harengus*, and *S. pilchardus* (Figure 9C). *C. harengus* and *S. pilchardus* show frequent mouth

409   opening and closing with an average opening time of 0.17s and 0.27s, respectively. The

410   average opening time in *S. scombrus* and *R. kanagurta* is 0.53s and 3.7s. In both species,

411   cleaning was observed after the mouth was held open. Cleaning lasted 0.25s in *S. scombrus*

412   and 0.71s in *R. kanagurta*.

413

4. DISCUSSION

415   There are three morphotypes of the GAS and buccal cavity (Figure 10). Within the clupeid

416   species, *S. pilchardus* and *C. harengus* are similar with an oval-shaped mouth opening and a

417   narrow buccal cavity leading towards the GAS (Figure 10A), while in *E. encrasicolus*, the mouth

418   is wide open with a short distance from the round mouth opening to the shorter and cone-

419   shaped GAS (Figure 10B). The two scombrid species have a round mouth opening, and the

420   distance to the GAS is longer than in *E. encrasicolus* (Figure 10C). The MicroCT scans show

421   that GR length is sufficient to bridge the gap towards the next anterior GA, or in the case of

422   GA1, the GR reach the inner side of the buccal cavity in an open-mouth position (Magnuson

423   & Heitz, 1971; Storm *et al.*, 2020). All GR in the three clupeid species are blade-shaped,

424 whereas, in the two scombrid species, only the anterior GR on GA1 are blade shaped; all other

425 anterior and posterior GR are shorter and thicker. Posterior GR are as long and evenly

426 distributed as the anterior GR in the two scombrid species, while the GR in *C. harengus* on

427 GA3 and GA4 or *S. pilchardus* on GA2, GA3 and GA4 are only few and short. *E. encrasicolus*

428 has no anterior GR.

429 While the denticles on the blade-shaped GR are all thin, of similar length, and arranged at a

430 regular distance in two rows, the denticles on the short GR are densely packed, demonstrate

431 high variability in length, and are directed inwards into the buccal cavity. In the scombrid

432 species, long teeth, which are oriented into the buccal cavity, sit on the inner side of the GA

433 and two visible pharyngobranchials. Additionally, mucus was found in front of the oesophagus.

434 Within the clupeid species, the GA, GR, and denticles in the two morphotypes form a smooth

435 filtration surface with regular meshes, however, the geometry of the open mouth, the pipe

436 length, and the cone-shaped GAS is different in *S. pilchardus* and *C. harengus* to the

437 morphotype of *E. encrasicolus*. The change in morphology from GA1 to the posterior GA, the

438 'brushy' surface structure formed by denticles and teeth, and the presence of mucus

439 characterise the morphotype of the scombrid species.

440 In all three morphotypes, the GAS system is cone-shaped and angled towards the incoming

441 flow, a typical characteristic for cross-flow filtration in ram-feeders (Cheer *et al.*, 2001; Paig-

442 Tran *et al.*, 2011; Hamann & Blanke, 2022). However, as the water flows posteriorly and exits

443 through the permeable filtration medium, the angle of the GAS becomes more perpendicular,

444 which suggests a transition to dead-end filtration (Brainerd, 2001). Based on the morphology

445 of the GAS we hypothesise that these ram-feeding fish use a combination of cross-flow and

446 dead-end-filtration, which was also suggested for the ram-feeding American shad (Storm *et*

447 *al.*, 2020). Our results therefore contrast the idea that ram-feeders solely feed by the

448 mechanism of cross-flow filtration.

449 During the behavioural studies of the experiment, we observed frequent cleaning, which further

450 supports the hypothesis that cross-flow filtration is not the only filtration mechanism present in

the fish mouth. Clogging reduces filtration performance; therefore, cleaning is an important step in any filtration process (Hamann & Blanke, 2022). Cross-flow filtration in technical applications is characterised by a time-dependent, steady-state particle distribution and a prolonged occurrence of clogging (Ripperger & Altmann, 2002; Makabe *et al.*, 2021). In the case of filter-feeding organisms, cross-flow filtration was assumed to reduce clogging (Brooks *et al.*, 2018), avoid clogging (Storm *et al.*, 2020), or that it is prevented by periodic swallowing (Paig-Tran *et al.*, 2011). Therefore, it is crucial to consider the time-dependent behaviour in our studies to identify cross-flow filtration. However, our ability to interpret these results is limited due to the available environment of the aquaria. Another observed factor was the size of the fed particles, which seem to influence swimming speed and feeding type. For example, while we measured 0.5 m/s for *S. scombrus* in the aquarium, it was reported that the swimming speed of *S. scombrus* in the Norwegian Sea ranged between 1.1 and 1.8 m/s measured with sonar (Nøttestad *et al.*, 2016). Most ram-filter-feeding fish species can also do particulate-feeding, and can be differentiated based on swimming speed, mouth opening time, and cleaning frequency (Batty, Blaxter, & Libby, 1986; Pepin, Koslow, & Pearre, 1988; James & Findlay, 1989). However, within the current literature, there are no established criteria to identify these feeding types. Flter-feeding was either identified when the mouth was opened longer than 0.5 s (Pepin *et al.*, 1988), 0.2 s, 0.5 s, or 1-3 s. in *S. scombrus* (Macy, Sutherland, & Durbin, 1998), 1-3 s in *Scomber japonicus* (O'Connell & Zweifel, 1972), or >0.4 to 3 s in *Engraulis capensis* (James & Findlay, 1989). Additionally, the occurrence of filter-feeding depends on particle concentration (O'Connell & Zweifel, 1972; Gibson & Ezzi, 1985) and particle size (Garrido *et al.*, 2007), especially in relation to fish size (Crowder, 1985). For the Gizzard shad, particle selectivity was also based on nutrient content (Heidman *et al.*, 2012). Therefore, we cannot clearly identify filter-feeding in the aquaria experiments. However, during the observations of *R. kanagurta* in the field, we were able to measure open-mouth durations of up to 12 s with cleaning activity in between, thus, we identify this as ram-feeding.

4.1. FILTRATION MACHANISM IN RAM-FEEDING FISH

In all five species, the lips protrude forwards, and the branchiostegal rays stretch outwards when the jaw opens for filter-feeding. Through the forward motion of ram-feeding, the water flows into the buccal cavity and out from the operculum and the branchiostegal rays. The protruded lips and the open operculum form a pipe-like structure to guide the water towards and through the cone-shaped GAS system (Figure 10). Because of the cone shape and the closed end, we assume that most of the water exists at the anterior opening of the cone (largest circumference), given the distribution of the calculated leakiness. Besides the anterio-posterior geometry, the GAS is asymmetric in its dorsoventral orientation. The area formed by the upper GA is in all species smaller than the lower area, hence, more water is exiting laterally from the operculum and ventrally at the branchiostegal rays. This "pipe length" correlates positively with a long, cone-shaped GAS, but negatively with mesh size and open area ratio, so we assume that this might influence the flow in such a way that it becomes laminar as indicated by the calculated Reynolds number. Around the denticles, the ratio between inertial and viscous forces ranges between Re ~30 in the smaller species and Re ~300 in the larger species, which is in line with results of other studies (Rykaczewski, 2009; Brooks *et al.*, 2018).

Another adaptation to reduce hydrodynamic drag and, therefore, energy expenditure, is the blade shape of the GR. All GR in the clupeid species and the GR on GA1 in the scombrid species are blade-shaped with length-to-width and height-to-width ratios that are similar to other filter-feeding species (Gibson, 1988; Storm *et al.*, 2020). The height-to-width ratio of the GR cross-section is also described as the fineness ratio in hydrodynamics and describes the geometry of streamlined bodies to minimise drag (Vogel, 1996). Bodies of organisms that are exposed to fluids usually have fineness ratios between 2 and 8 (Blake, 1983; Williams & Kooyman, 1985; Ahlborn, Blake, & Chan, 2009). The fineness ratio of the GR on GA1 in the selected species is between 2.6 and 7.2 and lies within the optimal range for streamlined bodies.

503   A high open area ratio and large filtration area reduce the resistance to flow (Sutherland, 2008).

504   The filtration area is larger than the mouth opening area (fluid exit ratio), which indicates that

505   there is no increased drag within the mouth that would lead to the formation of a pronounced

506   bow wave in front of the mouth (Brooks *et al.*, 2018). However, we did not include the drag

507   posed by the gill filaments during gas exchange as each GA has two rows of gill filaments

508   (Strother, 2013), or the friction drag along surfaces, which become more relevant at lower

509   Reynolds numbers and should be included in more complex models (Cheer *et al.*, 2001).

510   In both cross-flow and dead-end filtration, the particles are retained on the surface of the filter

511   medium. Additionally, cross-flow filtration uses the tangential flow to transport particles along

512   the surface, which is facilitated by a smooth surface. This can be seen in the three clupeid

513   species where the denticles extend laterally from the GR to form small meshes (Rykaczewski,

514   2009; Collard *et al.*, 2017). It is unclear if the differences in denticle shape influence mesh size

515   or have other functions. Mesh size is calculated based on the assumption of evenly distributed,

516   rectangular, stiff meshes (Sutherland, 2008; Collard *et al.*, 2017). However, denticles from

517   neighbouring GR do not touch and form closed meshes, and might bend in the oncoming flow.

518   Therefore, GR might be more relevant in mesh formation, as demonstrated by the positive

519   correlation of GR number and minimum mesh size, even though minimum mesh size is

520   calculated based on denticle length and width only. Still, it is unclear how mesh size influences

521   particle retention because, e.g., removing GR and microbranchiospines in Galilee Saint Peter's

522   fish (*Tilapia galilaea*) did not affect particle ingestion rate and selectivity (Drenner *et al.*, 1987).

523   However, this species is a pump-feeding fish, and its GR are not as long as the ones of ram-

524   feeding fish in our study. GR length and GR gap might thus be indicators for different filter-

525   feeding types, as shown for *Scomber japonicus* (Molina, Manrique, & Velasco, 1996). The

526   calculated mesh size and the role of denticles is even more unclear in the two scombrid

527   species. Their denticles and teeth are directed into the buccal cavity, differ in length, and are

528   not evenly spaced, except on GR on GA1. Therefore, particles might be retained within this

529   brushy structure, which is more typical for depth filtration. Alternatively, the surface structures

530   and mucus might form vortices, thereby inducing particle capture in a more similar manner to

531 cross-step filtration in paddlefish (Sanderson *et al.*, 2016) or ricochet filtration in manta rays

532 (Divi, Strother, & Paig-Tran, 2018).

4.2. ECOLOGICAL IMPLICATIONS

534 All five analysed species are large shoal, pelagic fish at an intermediate trophic level and widely

535 distributed (Bullen, 1912; Garrido & van der Lingen, 2014). As shown for filter-feeding and

536 particulate-feeding anchovies, pilchards (Garrido & van der Lingen, 2014), or Tilapia

537 (Dempster, Baird, & Beveridge, 1995), plasticity in feeding behaviour allows dietary

538 opportunism on plankton as it is a heterogenous food source. Based on our results, the

539 dimensions of the GAS are a significant factor in selecting particle size. Even when the

540 morphometric data is corrected for standard length, weight, GR length, and denticle length,

541 they positively correlate with one another. In the size-corrected data, *C. harengus* and *S.*

542 *pilchardus* have similar mesh sizes. They often cluster together, probably using very similar

543 mechanisms, even though the standard length of *C. harengus* is around twice as long as of *S.*

544 *pilchardus*. Particle size selection based on GAS dimensions was also reported: A large fish

545 with small GR gap retains smaller particles than an overall smaller fish (Magnuson & Heitz,

546 1971). Adaption to different food sizes allows the co-occuring of several species within one

547 habitat, as observed for anchovy and sardine species (Garrido & van der Lingen, 2014).

548 Because of the interaction of environmental conditions, feeding behaviour, the variety in filter-

549 feeding morphology, and food particle characteristics (Cheer *et al.*, 2012), it is challenging to

550 predict filtration efficiency. Looking at gut content, S. *scombrus* and *R. kanagurta* feed mainly

551 on copepods, cladocerans, diatoms, peridinians, and larvae of adult decapoda, but also

552 appendicularians, polychaeta larvae, post-larvae bivalves, pteropods, cirripede nauplii, small

553 hydromedusae, and fish eggs and larvae (Bullen, 1912; Bhimachar & George, 1952; Runge,

554 Pepin, & Silvert, 1987), which shows a high retention ability for a diversity of particle types and

555 sizes. One study showed that the gut content of *R. kanagurta* was the same as the ambient

556 plankton, indicating non-selectivity (Rao & Rao, 1957). This is also supported by the fact that

557 ram-feeding fish ingest microplastics: 40 to 50% of *C. harengus*, *S. pilchardus*, *E. encrasicolus*

558 had microplastics in their stomachs in sizes between 0.13 mm to 22.4 mm (Collard *et al.*, 2017).

559 Microplastics were found in the flesh and excised organs of dried *R. kanagurta* purchased from

560 food markets in Malaysia (Karami *et al.*, 2017). Comparison of different types of planktivorous

561 fish, including *S. scombrus* and S*. pilchardus*, showed that the larger mackerels had more

562 microplastics ingested than the smaller sardines (Lopes *et al.*, 2020). Exposure tests in the

563 pump-filter-feeding silver carp showed that the ingestion of microplastics of low concentration

564 passes through the digestive tracts and is excreted, and fish can recover, whereas in high

565 concentration, microplastics cause irreparable damage to gills and intestines (Zhang *et al*.,

566 2021).

ACKNOWLEDGEMENTS

FINANCIAL REPORT

REFERENCES

AHLBORN, B.K., BLAKE, R.W. & CHAN, K.H.S. (2009) Optimal fineness ratio for minimum drag in large whales. *Canadian Journal of Zoology* **87**, 124–131.

ALDER, J., CAMPBELL, B., KARPOUZI, V., KASCHNER, K. & PAULY, D. (2008) Forage Fish: From Ecosystems to Markets. *Annual Review of Environment and Resources* **33**, 153–166.

BATTY, R.S.S., BLAXTER, J.H.S.H.S. & LIBBY, D.A.A. (1986) Herring (Clupea harengus) filter-feeding in the dark. In *Marine Biology* p.

BHIMACHAR, B.S. & GEORGE, P.C. (1952) Observations on the food and feeding of the Indian mackerel,Rastrelliger canagurta (Cuvier). *Proceedings of the Indian Academy of Sciences*, 105–118.

BLAKE, R.W. (1983) Functional design and burst-and-coast swimming in fishes. *Canadian*

591   *Journal of Zoology* **61**, 2491–2494.

592   BRAINERD, E.L. (2001) Ichthyology: Caught in the crossflow. *Nature* **412**, 387–388.

593   BROOKS, H., HAINES, G.E., LIN, M.C. & SANDERSON, S.L. (2018) Physical modeling of vortical

594   cross-step flow in the American paddlefish, Polyodon spathula. *PLOS ONE* **13**,

595   e0193874.

596   BULLEN, G.E. (1912) Some notes upon the feeding habits of mackerel and certain clupeoids in

597   the english channel. *Journal of the Marine Biological Association of the United Kingdom*

598   **9**, 394–403.

599   CHEER, A., CHEUNG, S., HUNG, T.-C., PIEDRAHITA, R.H. & SANDERSON, S.L. (2012)

600   Computational Fluid Dynamics of Fish Gill Rakers During Crossflow Filtration. *Bulletin of*

601   *Mathematical Biology* **74**, 981–1000.

602   CHEER, A.Y., OGAMI, Y. & SANDERSON, S.L. (2001) Computational fluid dynamics in the oral

603   cavity of ram suspension-feeding fishes. *Journal of Theoretical Biology* **210**, 463–474.

604   COHEN, K.E. & HERNANDEZ, L.P. (2018) Making a master filterer: Ontogeny of specialized

605   filtering plates in silver carp (Hypophthalmichthys molitrix). *Journal of Morphology* **279**,

606   925–935.

607   COLLARD, F., GILBERT, B., EPPE, G., ROOS, L., COMPÈRE, P., DAS, K. & PARMENTIER, E. (2017)

608   Morphology of the filtration apparatus of three planktivorous fishes and relation with

609   ingested anthropogenic particles. *Marine Pollution Bulletin* **116**, 182–191.

610   COLLETTE, B.B. & GILLIS, G.B. (1992) Morphology, systematics, and biology of the double-lined

611   mackerels (Grammatorcynus, Scombridae). *Fishery Bulletin* **90**, 13–53.

612   COSTALAGO, D., GARRIDO, S. & PALOMERA, I. (2015) Comparison of the feeding apparatus and

613   diet of European sardines Sardina pilchardus of Atlantic and Mediterranean waters:

614   Ecological implications. *Journal of Fish Biology* **86**, 1348–1362.

615   CROWDER, L.B. (1985) Optimal foraging and feeding mode shifts in fishes. *Environmental*

616   *Biology of Fishes* **12**, 57–62.

617   DEMPSTER, P., BAIRD, D.J. & BEVERIDGE, M.C.M. (1995) Can fish survive by filter-feeding on

618   microparticles? Energy balance in tilapia grazing on algal suspensions. *Journal of Fish*

619   *Biology* **47**, 7–17.

620   DIVI, R. V., STROTHER, J.A. & PAIG-TRAN, E.W.M. (2018) Manta rays feed using ricochet

621   separation, a novel nonclogging filtration mechanism. *Science Advances* **4**, eaat9533.

622   DRAY, S. & JOSSE, J. (2015) Principal component analysis with missing values: a comparative

623   survey of methods. *Plant Ecology* **216**, 657–667.

624   DRENNER, R.W., HAMBRIGHT, K.D., VINYARD, G.L. & GOPHEN, M. (1987) Particle Ingestion by

625   Tilapia galilaea is Not Affected by Removal of Gill Rakers and Microbranchiospines.

626   *Transactions of the American Fisheries Society* **116**, 272–276.

627   FRIEDLAND, K.D., AHRENHOLZ, D.W., SMITH, J.W., MANNING, M. & RYAN, J. (2006) Sieving

628   functional morphology of the gill raker feeding apparatus of atlantic menhaden. *Journal of*

629   *Experimental Zoology Part A: Comparative Experimental Biology* **305**, 974–985.

630   GARRIDO, S. & VAN DER LINGEN, C.D. (2014) Feeding Biology and Ecology. In *Biology and*

631   *Ecology of Sardines and Anchovies* (ed K. GANIAS), pp. 122–189. CRC Press.

632   GARRIDO, S., MARÇALO, A., ZWOLINSKI, J. & VAN DER LINGEN, C. (2007) Laboratory

633   investigations on the effect of prey size and concentration on the feeding behaviour of

634   Sardina pilchardus. *Marine Ecology Progress Series* **330**, 189–199.

635   GIBSON, R.N. & EZZI, I.A. (1985) Effect of particle concentration on filter- and particulate-

636   feeding in the herring Clupea harengus. *Marine Biology* **88**, 109–116.

637   GIBSON, R.N.N. (1988) Development, morphometry and particle retention capability of the gill

638   rakers in the herring, Clupea harengus L. *Journal of Fish Biology* **32**, 949–962.

639   GNANAMUTTU, B.Y.J.C. (1966) Osteology of the Indian Mackerel, Rastrelliger kanagurta

640   (Cuvier). *Indian Journal of Fisheries* **13**, 1–26.

641 GOODRICH, J.S.S., SANDERSON, S.L.L., BATJAKAS, I.E.E. & KAUFMAN, L.S.S. (2000) Branchial
642   arches of suspension-feeding Oreochromis esculentus: Sieve or sticky filter? *Journal of*
643   *Fish Biology* **56**, 858–875.

644 HAMANN, L. & BLANKE, A. (2022) Suspension feeders: diversity, principles of particle separation
645   and biomimetic potential. *Journal of The Royal Society Interface* **19**.

646 HEIDMAN, M., HOLLEY, L., CHAMBERS, R. & SANDERSON, S. (2012) Selective feeding on nutrient-
647   rich particles by gizzard shad Dorosoma cepedianum does not involve mechanical
648   sorting. *Aquatic Biology* **17**, 129–139.

649 HERNDERSON, S. (1983) An Evaluation of Filter Feeding Fishes for Removing Excessive
650   Nutrients and Algae from Wastewater. *United States Environmental Protection Agency*.

651 HOOGENBOEZEM, W., LAMMENS, E.H.R.R.H.R.R., MACGILLAVRY, P.J.J. & SIBBING, F.A.A. (1993)
652   Prey retention and sieve adjustment in filter-feeding bream (Abramis brama) (Cyprinidae).
653   *Canadian Journal of Fisheries and Aquatic Sciences* **50**, 465–471.

654 HUNG, T. & PIEDRAHITA, R.H. (2014) Experimental validation of a novel bio-inspired particle
655   separator. *Aquacultural Engineering* **58**, 11–19.

656 JAMES, A. & FINDLAY, K. (1989) Effect of particle size and concentration on feeding behaviour,
657   selectivity and rates of food ingestion by the Cape anchovy Engraulis capensis. *Marine*
658   *Ecology Progress Series* **50**, 275–294.

659 JØRGENSEN, C.B. (1966) *Biology of Suspension Feeding*. Pergamon Press, Oxford.

660 KARAMI, A., GOLIESKARDI, A., HO, Y. BIN, LARAT, V. & SALAMATINIA, B. (2017) Microplastics in
661   eviscerated flesh and excised organs of dried fish. *Scientific Reports* **7**, 5473. Nature
662   Publishing Group.

663 LANGELAND, A. & NOST, T. (1995) Gill raker structure and selective predation on zooplankton
664   by particulate feeding fish. *Journal of Fish Biology* **47**, 719–732.

665 LOPES, C., RAIMUNDO, J., CAETANO, M. & GARRIDO, S. (2020) Microplastic ingestion and diet

666   composition of planktivorous fish. *Limnology and Oceanography Letters* **5**, 103–112.

667   MACY, W.K., SUTHERLAND, S.J. & DURBIN, E.G. (1998) Effects of zooplankton size and

668   concentration and light intensity on the feeding behavior of Atlantic mackerel Scomber

669   scombrus. *Marine Ecology Progress Series* **172**, 89–100.

670   MAGNUSON, J.J. & HEITZ, J.G. (1971) Gill raker apparatus and food selectivity among

671   mackerels, tunas, and dolphins. *Fishery Bulletin* **69**, 361–370.

672   MAKABE, R., AKAMATSU, K., TATSUMI, R., KOIKE, O. & NAKAO, S. ICHI (2021) Numerical

673   simulations of lift force and drag force on a particle in cross-flow microfiltration of colloidal

674   suspensions to understand limiting flux. *Journal of Membrane Science* **621**, 118998.

675   Elsevier B.V.

676   MOLINA, R., MANRIQUE, F. & VELASCO, H. (1996) Filtering apparatus and feeding of the Pacific

677   Mackerel (Scomber japonicus) in the Gulf of California. In *PACIFIC MACKEREL*

678   *FILTERING APPARATUS AND FEEDING CalCOFI Rep* p.

679   MOTTA, P.J., MASLANKA, M., HUETER, R.E., DAVIS, R.L., DE LA PARRA, R., MULVANY, S.L.,

680   HABEGGER, M.L., STROTHER, J.A., MARA, K.R., GARDINER, J.M., TYMINSKI, J.P. & ZEIGLER,

681   L.D. (2010) Feeding anatomy, filter-feeding rate, and diet of whale sharks Rhincodon

682   typus during surface ram filter feeding off the Yucatan Peninsula, Mexico. *Zoology* **113**,

683   199–212.

684   NØTTESTAD, L., DIAZ, J., PENÃ, H., SØILAND, H., HUSE, G. & FERNÖ, A. (2016) Feeding strategy

685   of mackerel in the Norwegian Sea relative to currents, temperature, and prey. *ICES*

686   *Journal of Marine Science* **73**, 1127–1137.

687   O'CONNELL, C.P. & ZWEIFEL, J.R. (1972) A laboratory study of particulate and filter feeding of

688   the pacific mackerel, Scomber japonicus. *Fishery Bulletin* **70**, 973–981.

689   ORY, N., CHAGNON, C., FELIX, F., FERNÁNDEZ, C., FERREIRA, J.L., GALLARDO, C., GARCÉS

690   ORDÓÑEZ, O., HENOSTROZA, A., LAAZ, E., MIZRAJI, R., URBINA, M.A. & THIEL, M. (2018)

691   Low prevalence of microplastic contamination in planktivorous fish species from the

692   southeast Pacific Ocean. *Marine Pollution Bulletin* **127**, 211–216.

693   PAIG-TRAN, E.W.M., BIZZARRO, J.J., STROTHER, J.A. & SUMMERS, A.P. (2011) Bottles as

694   models: Predicting the effects of varying swimming speed and morphology on size

695   selectivity and filtering efficiency in fishes. *Journal of Experimental Biology* **214**, 1643–

696   1654.

697   PEPIN, P., KOSLOW, J.A. & PEARRE, S. (1988) Laboratory study of foraging by Atlantic mackerel,

698   Scomber scombrus, on natural zooplankton assemblages. *Canadian Journal of Fisheries*

699   *and Aquatic Sciences* **45**, 879–887.

700   PHILLIPS, M.B. & BONNER, T.H. (2015) Occurrence and amount of microplastic ingested by

701   fishes in watersheds of the Gulf of Mexico. *Marine Pollution Bulletin* **100**, 264–269.

702   RAO, K.V.N. & RAO, K.P. (1957) Differences in the Food of the Young and the Adult Indian

703   Mackerel, Rastrelliger kanagurta (Cuv.). *Nature* **180**, 711–712.

704   RIBEIRO, F., OKOFFO, E.D., O'BRIEN, J.W., FRAISSINET-TACHET, S., O'BRIEN, S., GALLEN, M.,

705   SAMANIPOUR, S., KASERZON, S., MUELLER, J.F., GALLOWAY, T. & THOMAS, K. V. (2020)

706   Quantitative Analysis of Selected Plastics in High-Commercial-Value Australian Seafood

707   by Pyrolysis Gas Chromatography Mass Spectrometry. *Environmental Science &*

708   *Technology* **54**, 9408–9417.

709   RIPPERGER, S. & ALTMANN, J. (2002) Crossflow microfiltration - State of the art. *Separation and*

710   *Purification Technology* **26**, 19–31.

711   RUBENSTEIN, D.I. & KOEHL, M.A.R. (1977) The Mechanisms of Filter Feeding: Some

712   Theoretical Considerations. *The American Naturalist* **111**, 981–994.

713   RUNGE, J.A., PEPIN, P. & SILVERT, W. (1987) Feeding behavior of the Atlantic mackerel

714   Scomber scombrus on the hydromedusa Aglantha digitale. *Marine Biology* **94**, 329–333.

715   RYKACZEWSKI, R.R. (2009) Influence of Oceanographic Variability on the Planktonic Prey and

716   Growth of Sardine and Anchovy in the California Current Ecosystem. University of

717   California.

718   SANDERSON, S.L., ROBERTS, E., LINEBURG, J. & BROOKS, H. (2016) Fish mouths as engineering

719   structures for vortical cross-step filtration. *Nature Communications* **7**, 11092. Nature

720   Publishing Group.

721   SANDERSON, S.L.L., CHEER, A.Y.A.Y., GOODRICH, J.S.J.S., GRAZIANO, J.D.J.D. & CALLAN,

722   W.T.T. (2001) Crossflow filtration in suspension-feeding fishes. *Nature* **412**, 439–441.

723   SANDERSON, S.L.L. & WASSERSUG, R.J. (1993) Convergent and Alternative Designs for

724   Vertebrate Suspension Feeding. In *The skull* (eds J. HANKEN & B.K. HALL), pp. 37–112.

725   University of Chicago Press, Chicago and London.

726   SCHROEDER, A., MARSHALL, L., TREASE, B., BECKER, A. & SANDERSON, S.L.L. (2019)

727   Development of helical, fish-inspired cross-step filter for collecting harmful algae.

728   *Bioinspiration & Biomimetics* **14**, 056008.

729   STORM, T.J., NOLAN, K.E., ROBERTS, E.M. & SANDERSON, S.L. (2020) Oropharyngeal

730   morphology related to filtration mechanisms in suspension-feeding American shad

731   (Clupeidae). *Journal of Experimental Zoology Part A: Ecological and Integrative*

732   *Physiology* **333**, 493–510.

733   STROTHER, J.A. (2013) Hydrodynamic resistance and flow patterns in the gills of a tilapine fish.

734   *Journal of Experimental Biology* **216**, 2595–2606.

735   SUTHERLAND, K. (2008) *Filters and Filtration Handbook* Fifth Edit. Elsevier.

736   VOGEL, S. (1996) *Life in Moving Fluids: The Physical Biology of Flow - Revised and Expanded*

737   *Second Edition*. Princeton University Press, Princeton.

738   WILLIAMS, T.M. & KOOYMAN, G.L. (1985) Swimming Performance and Hydrodynamic

739   Characteristics of Harbor Seals Phoca vitulina. *Physiological Zoology* **58**, 576–589.

740   ZHANG, C., WANG, J., PAN, Z., WANG, S., ZHANG, L., WANG, Q., YE, Q., ZHOU, A., XIE, S., ZENG,

741   F., XU, G. & ZOU, J. (2021) A dosage-effect assessment of acute toxicology tests of

742   microplastic exposure in filter-feeding fish. *Fish & Shellfish Immunology* **113**, 154–161.

743   **TABLES**

744   Table 1: Measurements for the analysed species divided into: habitus and head, gill arches,

745   gill raker and denticles, filtration parameters, and feeding behaviour and fluid dynamics. (*)

746   Swimming speed and Reynold's numbers were calculated based on the standard length of the

747   dissected species. Bold parameters are included in the principal component analysis.

		S. scombrus	*R. kanagurta*	*C. harengus*	*S. pilchardus*	*E. encrasicolus*
	N	7	7	7	11	11
HABITUS AND HEAD	**Weight [g]**	197.9 ±22.4	168.0 ±40.4	193.6 ±16.6	23.0 ±3.4	9.3 ±0.7
	Standard length [mm]	269.4 ±4.0	210.1 ±12.4	248.2 ±7.3	118.7 ±6.4	97.9 ±2.4
	Oral teeth	yes	no	no	no	no
	MO Ratio (height/ width)*	1.2	1.4	1.3	1.8	1.3
	MO Area measured [mm²]	333.1 ±162.9	831.4 ±169.4	292.0 ±154.7	77.0 ±31.9	158.1 ±24.3
	Lip angle [°]	97.2 ±30.4	133.5 ±10.3	168.0 ± 36.0	163.2 ± 28.2	94.8 ± 11.3
	Jaw angle [°]	43.8 ± 9.9	63.1 ± 5.2	58.5 ± 15.1	52.9 ± 12.5	70.0 ± 8.3
	Branchiostegal height [mm]	9.5 ± 4.2	13.0 ± 1.6	10.2 ± 4.9	5.7 ± 2.8	3.4 ± 1.3
	Head length [%]*	24.0 ± 0.9	27.0 ± 0.8	19.8 ± 1.5	24.6 ± 1.3	25.4 ± 0.8
	Lip-Epi [%]*	65.0 ± 3.7	63.6 ± 3.5	59.0 ± 4.2	59.4 ± 2.6	39.7 ± 7.3
GILL ARCHES, GILL RAKER, DENTICLES	**GA 5-1 ratio***	0.35 ± 0.03	0.38 ± 0.04	0.21 ± 0.03	0.33 ± 0.03	0.21 ± 0.03
	GAS length [mm]	25.4 ± 1.1	32.5 ± 2.5	21.2 ± 1.3	15.8 ± 0.8	10.6 ± 0.8
	GR length GA1 [mm]	14.5 ± 0.6	18.6 ± 1.6	11.0 ± 0.9	6.7 ± 0.5	4.6 ± 0.2
	GR distance GA1 cerato anterior [mm]	0.765 ± 0.148	0.659 ± 0.083	0.302 ± 0.034	0.187 ± 0.025	0.248 ± 0.055
	GR number GA1	44.6 ± 1.7	53 ± 2.8	67.1 ± 1.2	91 ± 3.6	64.8 ± 2.3
	GR shape (length to width)*	50.4	106.8	52	114.1	46.3
	Fineness ratio of GR on GA1 (height/width)*	4.8	7.2	2.5	6	3.6
	Denticle length at GA1 (anterior, cerato)	0.592 ±0.155	0.593 ±0.158	0.098 ±0.015	0.091 ±0.013	0.085 ±0.018
	Denticle width					
	Position of denticles, cerato GA1 (rel)*	0	0	0.17	0.27	0.23
	Mucus	yes	yes	no	no	no
	pharyngobranchials	yes	yes	no	no	no
FILTRATION PARAMETERS	**Total filtration area [mm²]**	1830.0 ± 314.9	2157.4 ±277.4	1077.8 ±125.3	450.6 ±102.3	344.8 ±52.6
	Symmetry at GA1*	0.28	0.3	0.32	0.35	0.4
	Open area ratio at cerato GA1*	0.574	0.566	0.518	0.567	0.714
	Open area [mm²]	895.6 ±305.3	1067.1 ±383.2	563.5 ±132.3	274.6 ±48.0	262.4 ±65.5
	Leakiness GA1 [%]*	76.1	78.8	58.9	50.3	61.2
	Leakiness GA2 [%]*	8.5	9.5	22	22.9	21.2
	Leakiness GA3 [%]*	8.9	5.6	12.3	14.7	11.8
	Leakiness GA4 [%]*	6.4	6.1	6.7	12.1	5.9
	Fluid exit ratio*	2.69	1.28	1.93	3.57	1.66
	Mesh size min [mm²]	0.113	0.048	0.015	0.007	0.0097
	Mesh size max [mm²]	0.148	0.053	0.048	0.014	0.028
	Mesh size ratio	1.61	1.18	0.91	2.24	1.84
FEEDING BEHAVIOUR AND FLUID DYNAMICS	**Location (originator)**	Sea Life Center Oberhausen, Germany (Leandra Hamann)	Red Sea (field), Egypt (Swantje Neumeyer, Bodo Kallwitz)	Aquarium Stralsund, Germany (Leandra Hamann)	Aquarium La Rochelle, France (Leandra Hamann)	Aquarium San Sebastian, Spain (Amalia Martínez de Murguía)
	N	20	5	9	15	24
	Feeding state	feeding	feeding	feeding	feeding	feeding
	SS (SL/s)	1.85	2.24	1.36	3.48	3.58

SL of dissected species [m]	0.27	0.21	0.25	0.12	0.1
SS (m/s)	0.5	0.47	0.34	0.41	0.35
Re around fish (based on SL)	137166	101201.3	85417.3	50150.7	34995.1
Re at mouth opening (based on equivalent spherical diameter)	10487	15670	6637	4183	5074
Re around denticles at cerato GA1	302	285	34	38	30
Volume flow rate through mouth [l/min]	9.96	23.52	5.90	1.91	3.32

748

749

FIGURES

A *Scomber scombrus*
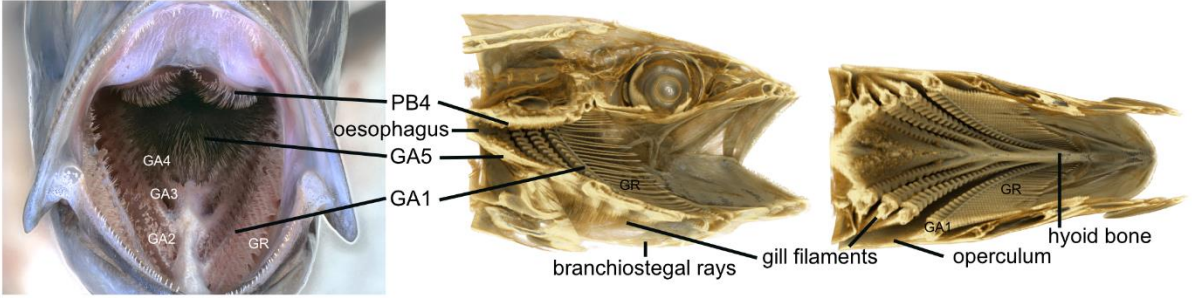
B *Rastrelliger kanagurta*
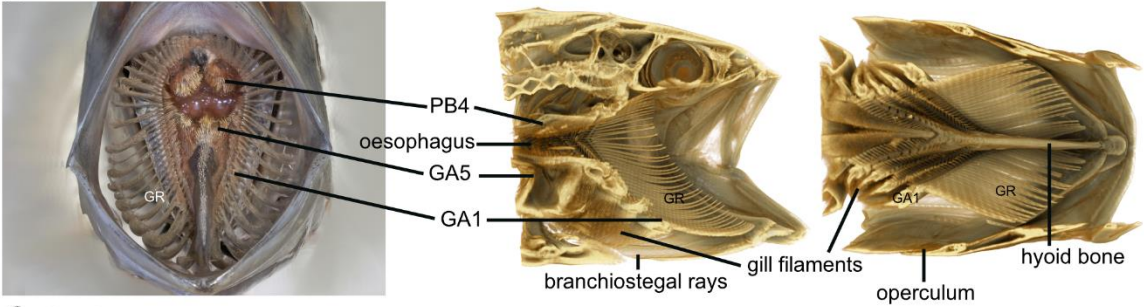
C *Clupea harengus*
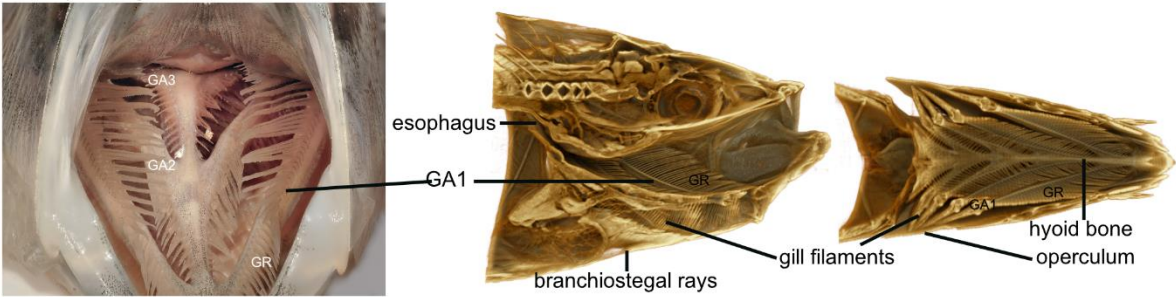
D *Sardina pilchardus*
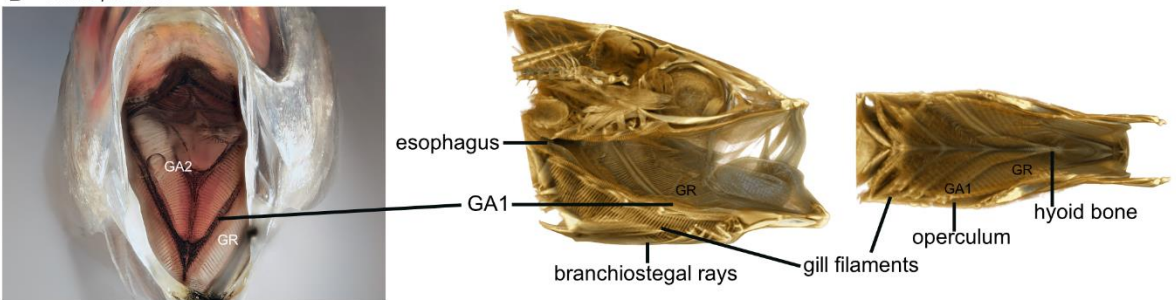
E *Engraulis encrasicolus*
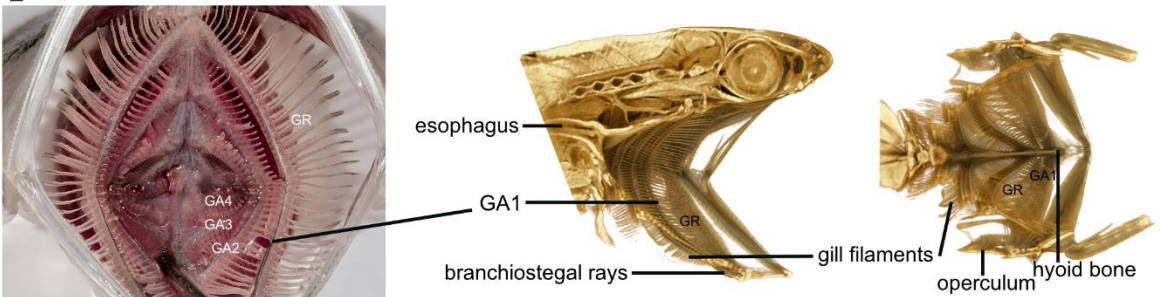
Figure 1: Stacked photographs of the frontal view, and MicroCT scnas with lateral and dorsal view on the GAS of the studied ram-feeding fish: A) Atlantic mackerel (*Scomber scombrus*, Linnaeus 1758, Fishing ground: North east Atlantic - Food and Agricultural Organisation (FAO) 27), B) Indian mackerel (*Rastrelliger kanagurta*, Cuvier 1816, West Indian Ocean - FAO 51), C) Atlantic herring (*Clupea harengus*, Linnaeus 1758, North east Atlantic - FAO 27), D) Atlantic pilchard (*Sardina pilchardus*, Walbaum 1792, Mediterranean and Black Sea - FAO 37), and E) Atlantic anchovy (*Engraulis encrasicolus*, Linnaeus 1758, Mediterranean and Black Sea - FAO 37), with GA = gill arch, GR = gill raker, PB = pharyngobranchial. Mouth opening angles approximately in physiological configuration. Images and scans not to scale.
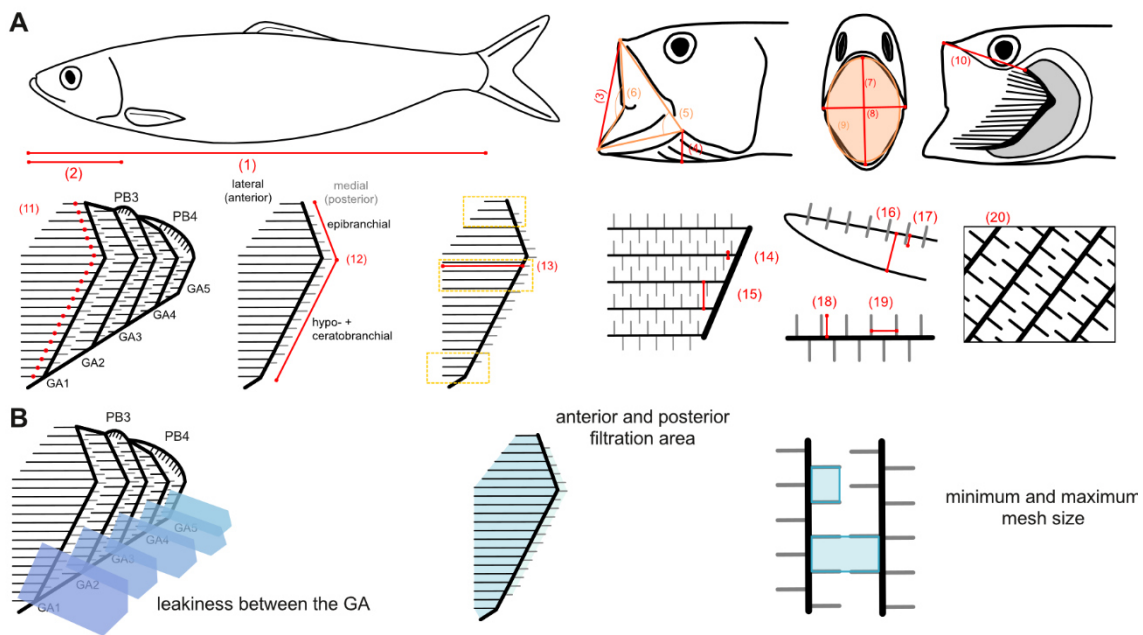
Figure 2: A) Measured parameters: 1) standard length (SL) with open and closed mouth, 2) head length, 3) open mouth height (lateral), 4) branchiostegal height, 5) jaw angle, 6) lip angle, 7) open mouth height frontal, 8) open mouth width frontal, 9) open mouth area, 10) upper lip to epibranchial, 11) number of GR, 12) length of GA and pharyngobranchials (PB, only in Scombridae), 13) length of GR, 14) width of GR, 15) distance between GR, 16) height of GR, 17) vertical position of denticles on the GR, 18) length of denticles, 19) distance between denticles, 20) open area ratio. See supplementary information XY for a description of

770   parameters on an exemplarily species. B) Calculated filtration parameters: volume flow

771   through the gaps between the GA, filtration area for each GA, minimum and maximum mesh

772   size.

773

774
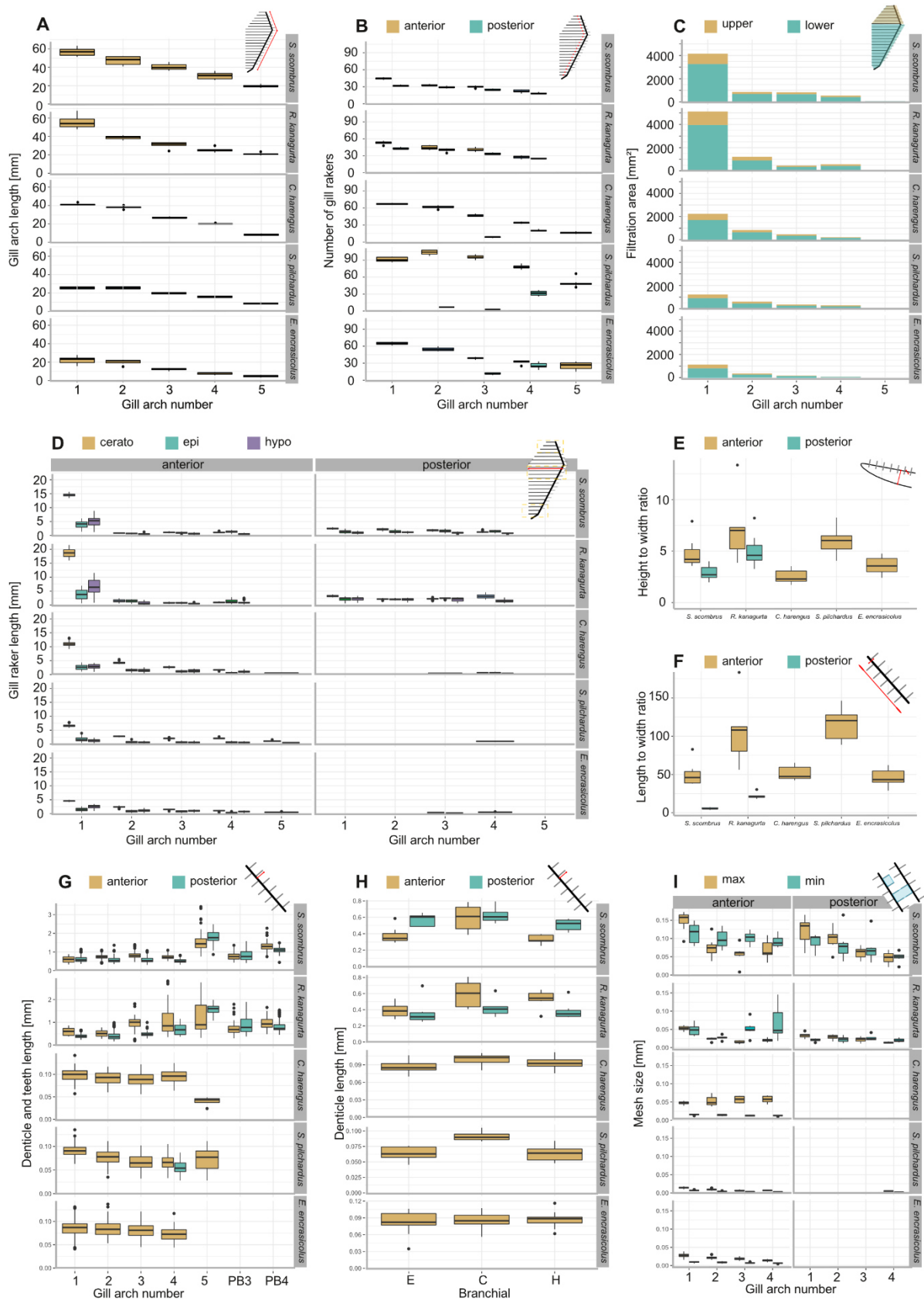
Figure 3: Morphometric measurements and filtration parameters of the studied ram-feeding

fish. Species measurements shown in different rows in each subfigure, except in E and F. A)

777   Gill arch length, B) Number of gill rakers on the anterior and posterior side of each gill arch, C)

778   Filtration area of upper (epibranchial) and lower (cerato- and hypobranchial) gill arch, D) Gill

779   raker length on epi-, cerato- and hypobranchial on the anterior and posterior side of each gill

780   arch, E) Height to width ratio of the gill rakers on the first gill arch, F) Length to width ratio of

781   the gill rakers on the first gill arch, G) Denticle length of the anterior and posterior gill raker of

782   each gill arch and on pharyngobranchial 3 and pharyngobranchial 3 in the two scombrid

783   species, H) Denticle length of the anterior and posterior gill rakers on each branchial of the first

784   gill arch, I) Minimum and maximum mesh size of the anterior and posterior sides of the first

785   four gill arches.

786
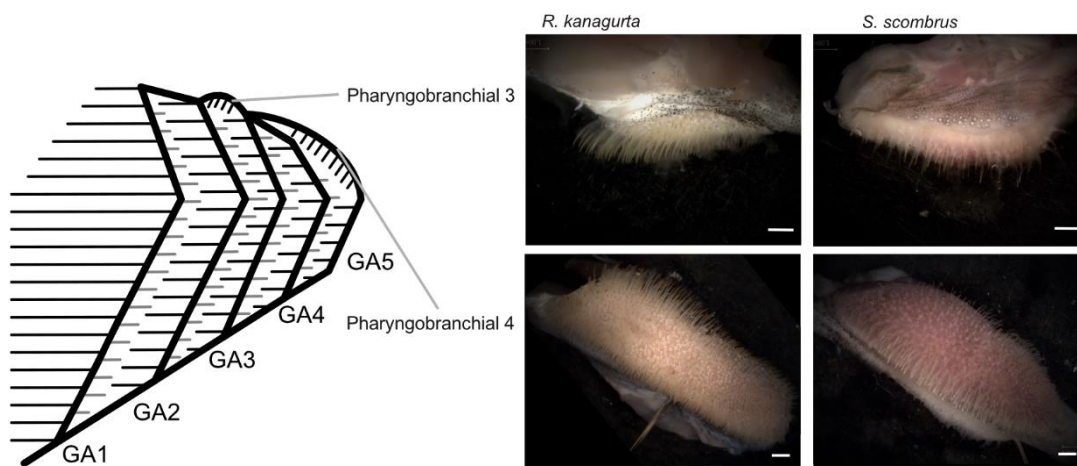
788   Figure 4: Position of pharyngobranchial 3 and pharyngobranchial 4 within the gill arch system

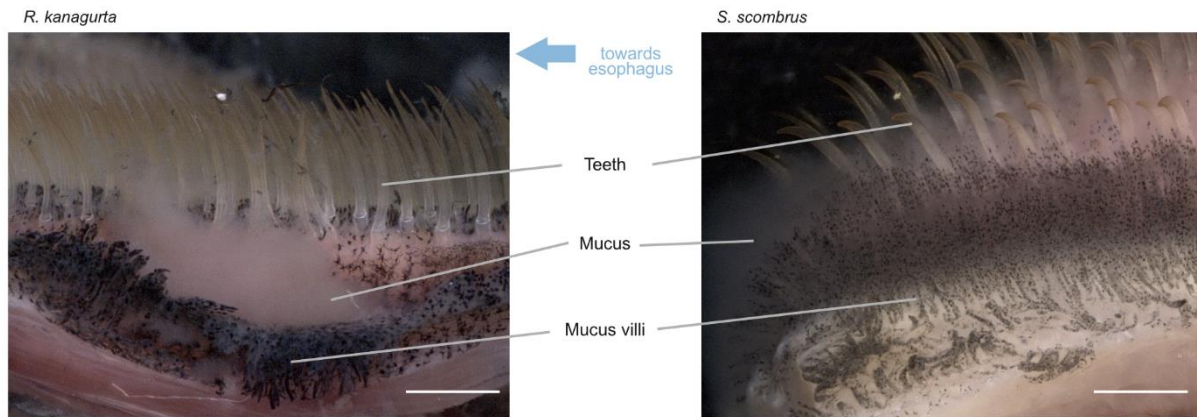789   in *R. kanagurta* and *S. scombrus*. Scale bar 1 mm

790
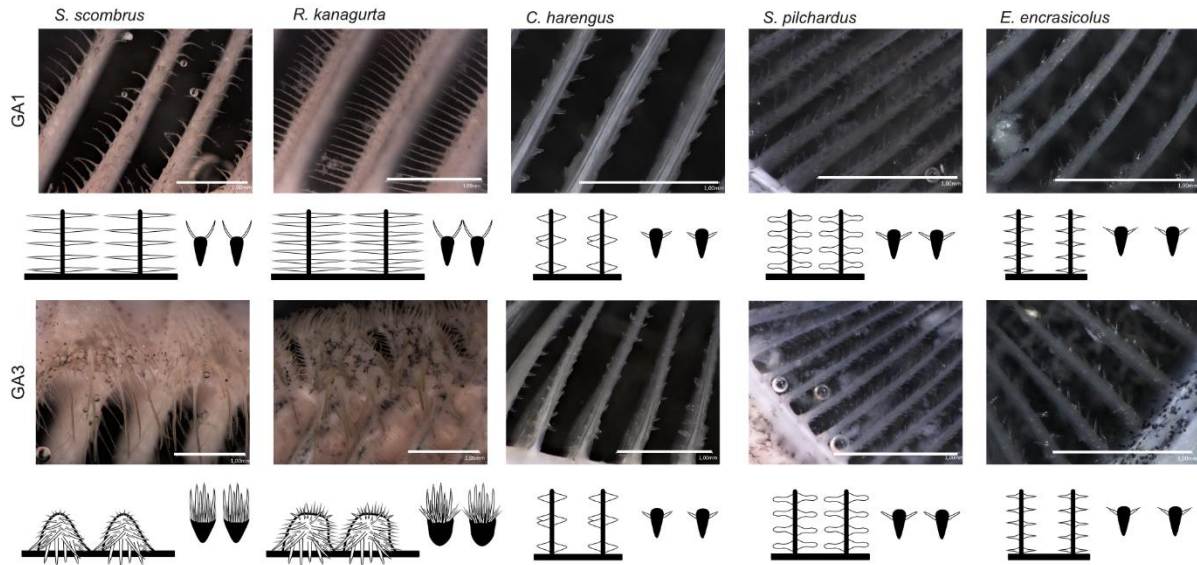
791

792   Figure 5: Denticle shape of the anterior gill rakers of first and third gill arch of each species.

793   Scale bar 1 mm, drawings not to scale to each other.

794

795

796   Figure 6: View of the food groove and medial side of GA5 in *R. kanagurta* and *S. scombrus*.

797   Water flows from right to left towards the oesophagus. Mucus was observed to originate from

798   the mucus villi, which are located between the denticles and especially densely covering the

799   food groove between the left and right GA5. Scale bar 1 mm.

800
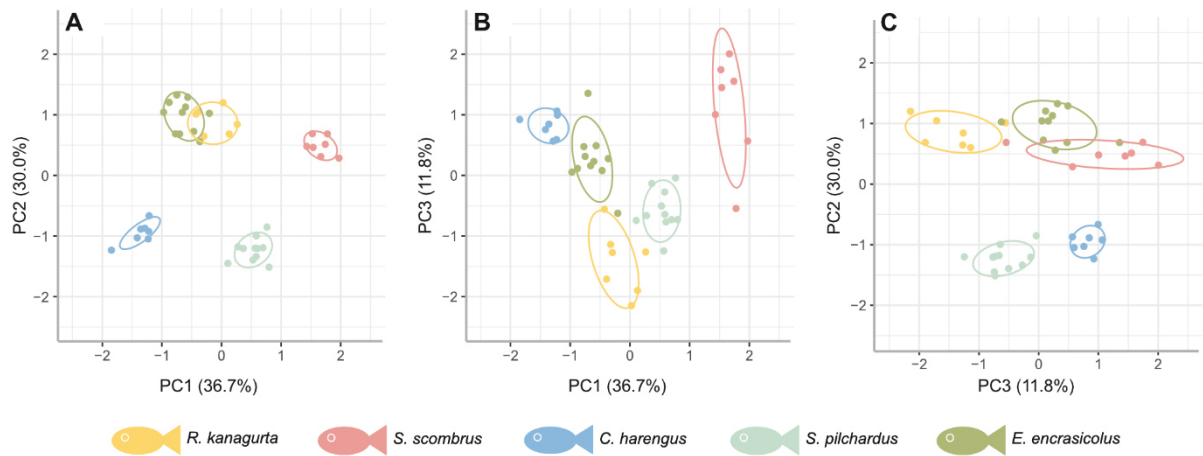
801

802   Figure 7: PCA based on the residuals to correct for allometry for five ram-feeding species

803   (colours). Principle component (PC) 1, PC2, and PC3 account for approximately 78,5% of the

804   variation.

805
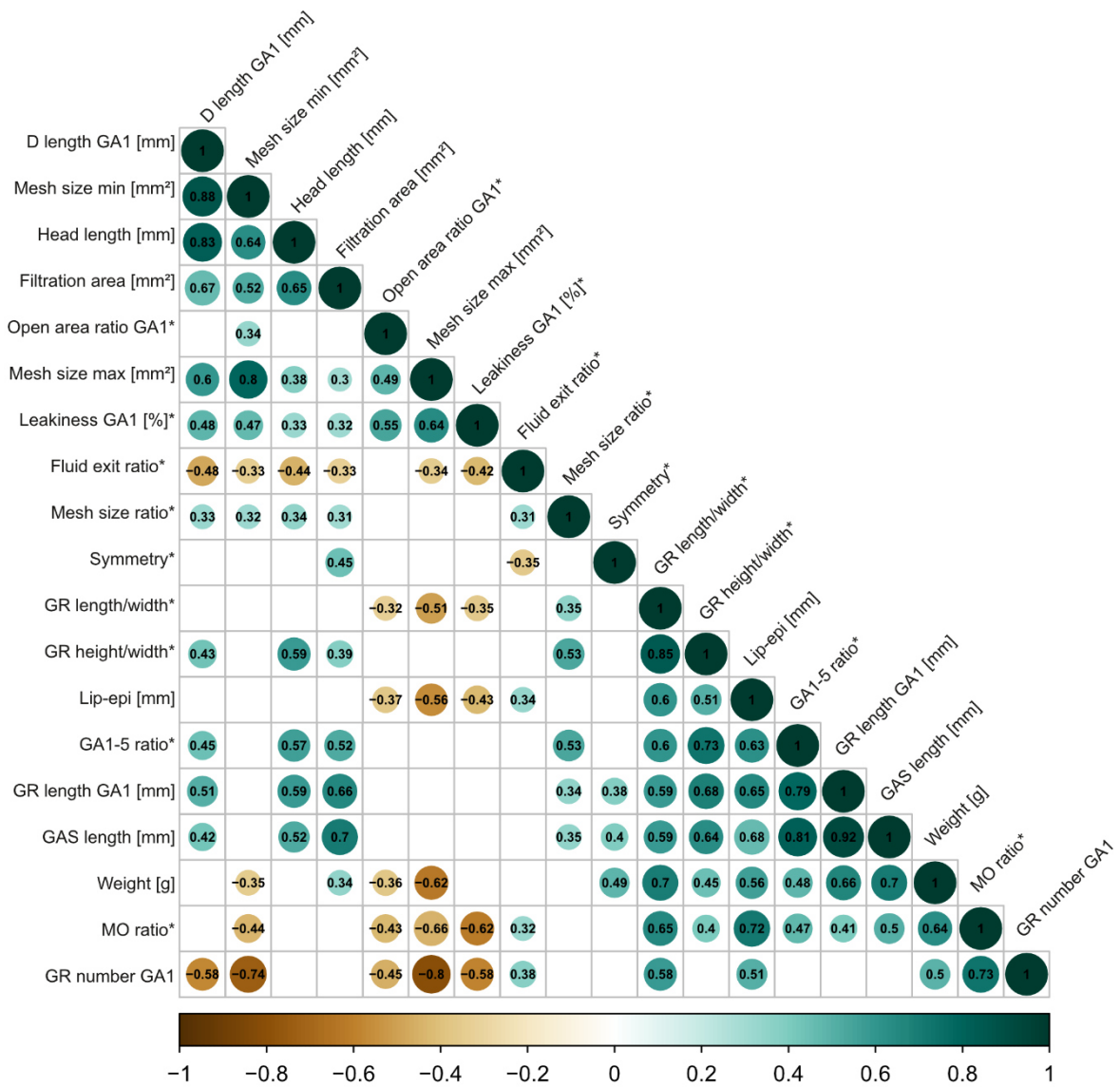
Figure 8: Correlation matrix based on Spearman rank tests with the size-corrected 19 parameters across the five ram-feeding species to describe the GAS system. Only significant correlations (p <0.05) are indicated by colour (positive correlations in green, negative correlations in brown) and the respective correlation coefficient. Relative values are indicated with an asterisk (see XX).

813
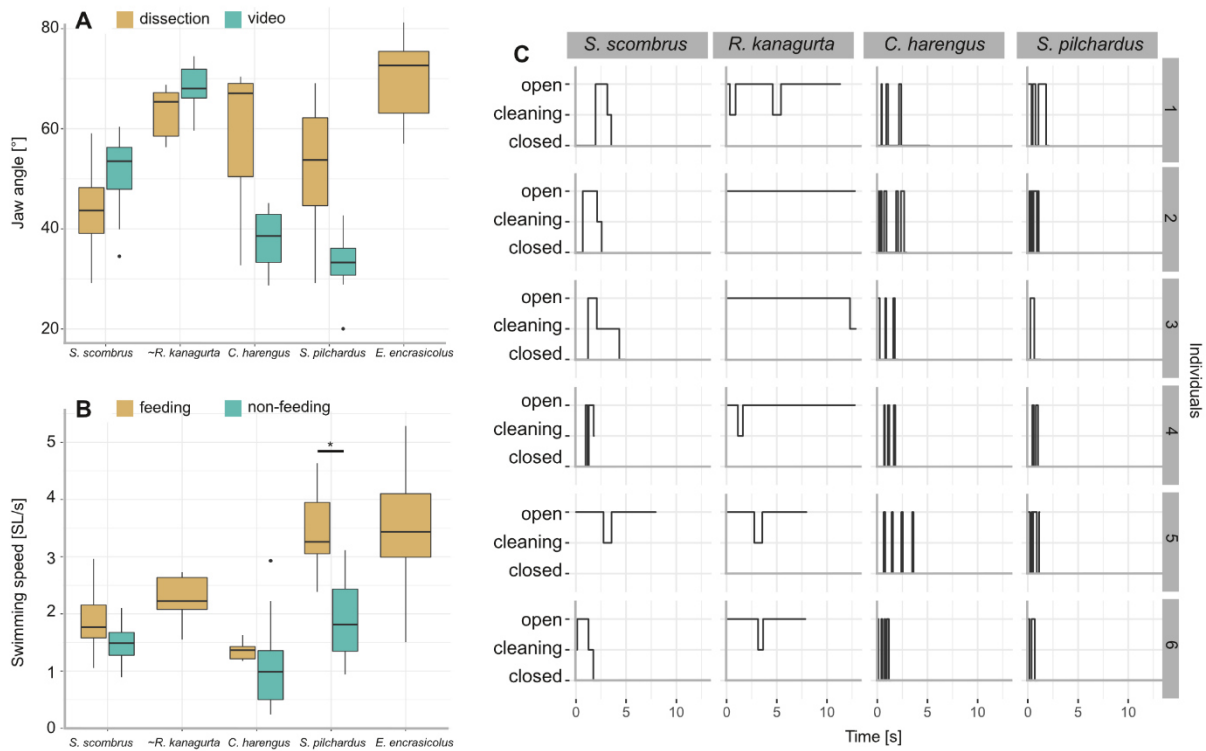
Figure 9: Results from the videography of five ram-feeding fishes during feeding. *S. scombrus*, *C. harengus*, *S. pilchardus* and *E. encrasicolus* were filmed in public aquaria. *R. kanagurta* was filmed in the field, indicated by (~). A) Comparison of the jaw angle in feeding individuals and the manually opened jaws during dissection. Due to video quality, the jaw angle in *E. encrasicolus* was not measured. Kruskal-Wallis rank sum test (chi-squared) with posthoc dunn test (method 'Holm') showed no significant difference in the comparison within each species. B) Comparison of the swimming speed before feeding (non-feeding) and during feeding. Data was not available for *R. kanagurta* and *E. encrasicolus*. Kruskal-Wallis rank sum test (chi-squared) with posthoc dunn test (method 'Holm') showed significant difference in the swimming speed for *S. pilchardus* before and while feeding (p = 0.0009). C) Feeding behaviour of six individuals described by the mouth position (closed, cleaning, open) over time.

825
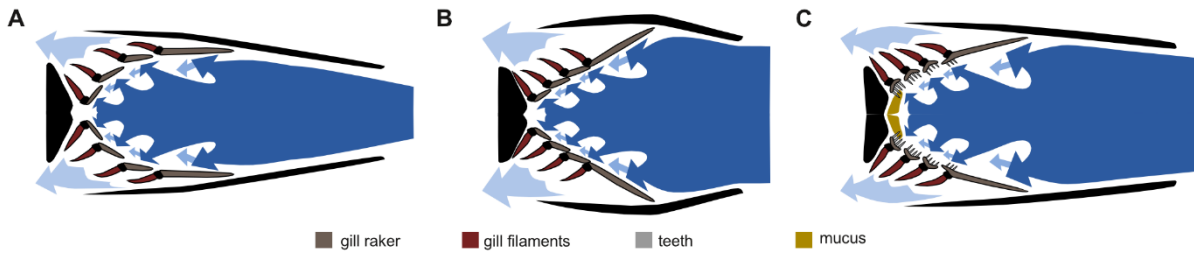
826

827 Figure 10: Schematic drawing of the flow through the three morphotypes types: A) *C. harengus*

828 and *S. pilchardus*, B) *E. encrasicolus*, and C) *S. scombrus and R. kanagurta*.

829

1   **Supplement Information**

2

3   **Morphological Diversity of Filter-Feeding Structures in Five Ram-Feeding**

4   **Fish Species (Clupeidae, Scombridae)**

5   Leandra Hamann[1], Jan Hagenmeyer[1, 2], Santiago Eduardo[1, 3], Tobias Spanke[4], Alexander

6   Blanke[1]

7   [1] Institute of Evolutionary Biology and Animal Ecology, University of Bonn, An der Immenburg

8   1, 53121 Bonn, Germany

9   [2] Ruhr-University Bochum, Universitätsstraße 150, 44801 Bochum, Germany

10   [3] Otto-von-Guericke-Universität Magdeburg, Universitätsplatz 2, 39106 Magdeburg,

11   Germany

12   [4] Leibniz Institute for the Analysis of Biodiversity Change, Adenauerallee 127, 53113 Bonn,

13   Germany

14

15

16

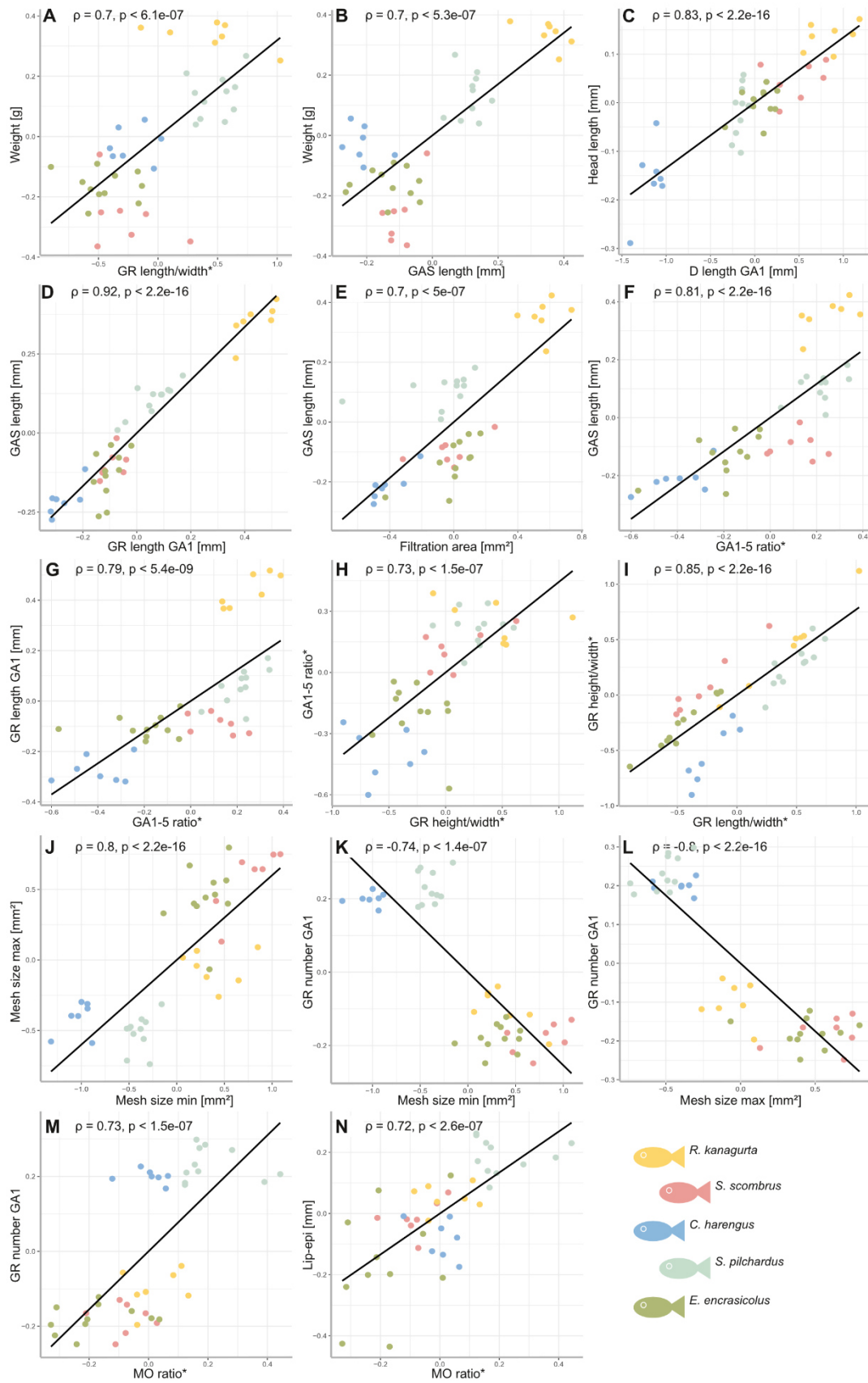**SI – 1. Description of significant correlations with a correlation coefficient of ρ >0.70**

Weight correlates positively with GR length to width ratio (Figure SI-1A, ρ = 0.70) and GAS length (Figure SI-1B, ρ = 0.7). The heavier the fish, the larger the GAS, as can be seen in *R. kanagurta*. Denticle length positively correlates with head length (Figure SI-1C, ρ = 0.83): The larger the fish, the larger the smallest structures, i.e., denticles.

GAS length positively correlates with GR length of GA1 (Figure SI-1D, ρ = 0.92). As GAS length is the sum of all GR lengths on the ceratobranchials of each GA, this indicates that not only GA1 plays an important role in the dimension of the GAS, but all other GAs do as well. The filtration area positively correlates with GAS length (Figure SI-1E, ρ = 0.7); the longer the filter, the larger the filtration area. The ratio of GA1 to GA5 describes the overall shape of the GAS; the higher the ratio, the more cone-shaped is the GAS. The ratio of GA1 to GA5 positively correlates with GAS length (Figure SI-1F, ρ = 0.81) and the GR length of GA1 (Figure SI-1G, ρ = 0.85). Hence, the more cone-shaped the GAS is, the longer is the GAS in total, especially the GR length on GA1. This can be seen particularly well in *R. kanagurta,* which differentiates from the other species with a long GR on GA1, long GAS, high filtration area, and a more cone-shaped GAS.

GR height to width ratio positively correlates with the ratio of GA1 to GA5 (Figure SI-1H, ρ = 0.73). In addition, GR length to width ratio and height to width ratio correlates positively across all species (Figure SI-1I, ρ = 0.85), the longer the GR, the higher side of the GR. Mesh size min correlates positively with mesh size max (Figure SI-1J, ρ = 0.80), but both mesh sizes correlate negatively with GR number on GA1; the larger the minimum and maximum mesh size, the lower the number of GR on GA1 (Figure SI-1K, ρ = -0.74, Figure SI-1L ρ = -0.80). In combining these parameters, the species are clustered in two groups. *C. harengus* and *S. pilchardus* have a high number of GR on GA1 with small mesh sizes, whereas R. kanagurta, S. scombrus, and *E. encrasicolus* have large mesh sizes and a lower number of GR on GR1. The same distinction between the two groups can also be seen in the positive correlation of GR number on GA1 with mouth opening ratio (Figure SI-1M, ρ = 0.73). The higher the mouth

44   opening ratio, the more oval is its shape, as seen in *C. harengus* and *S. pilchardus*. The mouth

45   opening ratio correlates positively with the distance from the dorsal tip of the lip to the

46   epibranchial of GA1 (Figure SI-1N, $\rho = 0.72$), which describes the position of the GAS within

47   the head. *E. encrasicolus* has a more round-shaped mouth opening with a short distance from

48   the mouth opening to the GAS, while *S. pilchardus* has an oval-shaped mouth opening, and

49   the GAS sits further back within the oral cavity.

50

51

Figure SI-1: Figure SI-1: Detailed presentation of significant correlations with ρ >70 based on

the Spearman rank test in the correlation matrix (Figure 8).

54 Table SI-1: Loadings for PC1, PC2, and PC3 for the 19 parameters. The ranking of parameters

55 for each PC was made based on the amount of the value (*) indicate relative values, such as

56 ratios.

Parameters	PC1	ranking	PC2	ranking	PC3	ranking
GAS length [mm]	0.360	1	-0.043	14	0.126	11
GR length GA1 [mm]	0.356	2	0.037	15	0.162	10
GA1-5 ratio*	0.324	3	-0.028	16	-0.206	7
GR height/width*	0.306	4	-0.023	17	-0.205	8
Filtration area [mm²]	0.290	5	0.172	13	0.108	14
Head length	0.288	6	0.222	9	-0.045	17
D length GA1 [mm]	0.278	7	0.257	6	-0.116	13
GR length/width*	0.274	8	-0.214	10	-0.065	16
Weight [g]	0.270	9	-0.176	12	0.307	4
Lip-epi [mm]	0.205	10	-0.246	7	-0.117	12
Symmetry*	0.176	11	0.019	18	0.500	1
MO ratio*	0.162	12	-0.313	5	-0.098	15
Mesh size ratio*	0.154	13	0.010	19	-0.472	2
Mesh size min [mm²]	0.143	14	0.346	3	-0.212	6
Open area ratio GA1*	-0.058	15	0.230	8	0.011	19
Fluid exit ratio*	-0.050	16	-0.188	11	-0.343	3
Mesh size max [mm²]	-0.050	17	0.378	2	-0.195	9
Leakiness GA1 [%]*	0.015	18	0.320	4	0.226	5
GR number GA1	-0.010	19	-0.402	1	0.016	18

57

58